Summer 2015

Inelastic Behavior and Strength of Steel Beam-Columns with Applied Torsion

Mamadou Konate
Old Dominion University

INELASTIC BEHAVIOR AND STRENGTH OF STEEL BEAM-COLUMNS WITH APPLIED TORSION

by

Mamadou Konate
B.A. May 2008, University of Colorado
M.S. August 2010, Old Dominion University

A Dissertation Submitted to the Faculty of
Old Dominion University in Partial Fulfillment of the
Requirements for the Degree of

DOCTOR OF PHILOSOPHY

CIVIL AND ENVIRONMENTAL ENGINEERING

OLD DOMINION UNIVERSITY
August 2015

Approved by:

Zia Razzaq (Director)

Duc T. Nguyen (Member)

Julie Hao (Member)

Mojtaba B. Sirjani (Member)

ABSTRACT

INELASTIC BEHAVIOR AND STRENGTH OF STEEL BEAM-COLUMNS WITH APPLIED TORSION

Mamadou Konate
Old Dominion University, 2015
Director: Dr. Zia Razzaq

This dissertation presents the outcome of an experimental and theoretical study of the inelastic behavior and strength of steel beam-columns with applied torsion. Although the international steel design specifications contain interaction relations for biaxially loaded beam-columns, the influence of applied torsion on such members has been completely ignored in the past. A series of hollow square section steel members are tested using an apparatus specially designed to apply torsion in the presence of an axial load and biaxial bending. The theoretical analysis involves formulation of a system of materially nonlinear differential equations and their solution based on a finite integral formulation. The predicted member response agreed quite well with the experiments. A set of new yield limit and strength interaction expressions are then developed which include the influence of applied torsion. In addition, beam-column interaction relations used in Australia, Canada, China, Great Britain, Japan, Russia, the U.S. and Eurocode are modified to account for applied torsion. Finally, this dissertation presents new load-moment-torsion interaction relations for possible adoption in the international steel design specifications.

This thesis is dedicated to my family back home.

ACKNOWLEDGMENTS

The author is deeply grateful to his committee chair and advisor, Dr. Zia Razzaq, for his advice and encouragement. This research would not have been possible without his guidance and help. The author would also like to thank his committee members, fellow graduate students, and staff of the Engineering Workshop for their time and support. Special gratitude is due to Dr. Isao Ishibashi, the Graduate Program Director of the CEE Department and Dr. Gary Schafran, the former Chair of the CEE Department, for their constant help and support throughout the author's graduate studies. Finally, and most importantly, the author would like to express his sincere appreciation and gratitude to his family in Mali for their moral and financial support and encouragement.

NOMENCLATURE

A	Area
B	Section width
D	Section depth
dA	Elemental area
E	Modulus of elasticity
G	Shear modulus
I_x, I_y	Moment of inertia about x-axis and y-axis
I_{xy}	Product of inertia relative to x-axis and y-axis
$I_{\omega x}, I_{\omega x}$	Warping product of inertia about x-axis and y-axis
$[K]$	Member global tangent stiffness matrix
k_{Bx}, k_{Tx}	End rotational stiffness about x axis
k_{By}, k_{Ty}	End rotational stiffness about y axis
L	Member length
m_{Bx}, m_{Tx}	Restraint moments at bottom and top end about x axis
m_{By}, m_{Ty}	Restraint moments at bottom and top end about y axis
M_{Bx}, M_{Tx}	Applied moments at bottom and top end about x axis
M_{By}, M_{Ty}	Applied moments at bottom and top end about y axis
$M_{xp}, M_{yp,}$	Bending moments due to plastification
M_{xre}, M_{yre}	Bending moments due to residual stress
M_{ze}	Torsional moment due to residual stress
M_{zp}	Torsional moment due to plastification
$\{M_v\}$	Moment vector
$\{\Delta'''\}$	Vector of the third order derivative of deflection
P	Applied axial load
P_p	Axial load due to plastified elements in the member
P_r	Axial load due to residual stress
R_x, R_y	Reaction at bottom of the beam-column

S_x, S_y	Elastic section of modulus about x-axis and y-axis
$S_{\omega x}$, $S_{\omega y}$	Warping section of modulus about x-axis and y-axis
T	Applied torque
U	Total deflection in x-direction
V	Total deflection in y-direction
u	Deflection due to load in x-direction
v	Deflection due to load in y-direction
u_o	Midspan initial member crookedness in x-direction
v_o	Midspan initial member crookedness in y-direction
u_{oi}	Initial member crookedness in x-direction
v_{oi}	Initial member crookedness in y-direction
u''	The second order derivative of u
v''	The second order derivative of v
Z_x, Z_y	Plastic section of modulus about x-axis and y-axis
β	Angle between the column and the base plate
ε	Normal strain
ε_r	Residual strain
ε_0	Average axial strain
ε_ω	Normal strain due to warping
Φ_x,Φ_y	Bending curvatures
σ_Y,	Yield normal stress
τ_Y,	Yield shear stress
σ_{rt},σ_{rc}	Compressive and tensile residual stress
ψ	Angle of twist

TABLE OF CONTENTS

Chapter Page

Chapter Page

LIST OF TABLES

Table Page

LIST OF FIGURES

Figure Page

Figure Page

Figure Page

CHAPTER 1

INTRODUCTION

1.1 Introduction

This dissertation presents the outcome of a theoretical and experimental study into the inelastic behavior of steel beam-columns subjected to nonproportional biaxial bending and torsion. The study is focused on nonsway thin-walled steel members. The study of such members is complicated due to the interaction amongst biaxial bending, axial load, and torsion in the materially nonlinear or inelastic range. Symmetric steel buildings subjected to asymmetric loading or unsymmetric steel buildings under various practical loading conditions have their members subjected to such combined loads. Combined eccentric traffic loading and lateral loads due to wind and earthquake effects on bridges can also produce biaxial bending and torsion effects on bridge structural members.

The inelastic behavior of biaxially loaded beam-columns with applied torsion is governed by a system of four coupled materially nonlinear or inelastic ordinary differential equations of equilibrium. Closed-form solutions for these equations are not possible. The four equations can, however, be reduced to three by utilizing an expression for inelastic axial strain based on the differential equation for axial load equilibrium. In this dissertation, an iterative finite integral solution to the resulting three nonlinear differential equations is developed and programmed.

To verify the validity of the theoretical predictions, laboratory tests are conducted on hollow rectangular section beam-columns under applied torsion. For the experimental study, special arrangements are made to the apparatus used by Zhao (13) allowing freedom of torsional rotation about the longitudinal axis at the test member bottom end. Although hollow rectangular steel sections are torsionally quite stiff, they can still be expected to carry torsional moments in the presence of axial load and uniaxial or biaxial bending moments. After validating the analysis, predictions are then made for the inelastic behavior and strength of steel members with larger or practical sizes under the combined action of axial compressive load, biaxial bending moments and torsional moment. The results

generated in the study are first used to formulate a set of new yield limit interaction expressions. Finally, a new dimensionless torsional moment term is added to the ultimate strength interaction expressions present in the design specifications from Australia, Canada, China, Japan, Great Britain, and Russia as well as those in the American Institute of Steel Construction Manual and Eurocode3.

1.2 Literature Review

1.2.1 Beam-Column Studies with Nonproportional Loading

A number of researchers have previously studied the behavior of steel beam-columns without any applied torsion. Ketter (1) conducted a theoretical study beyond the elastic limit of structural members subjected to a constant load with increasing moment. The author used the finite integral approach intertwined with a cross-sectional elasto-plastic tangent stiffness procedure in the analysis. Galambos and Ketter (2) formulated Newmark's procedure to determine load-deflection curves of wide-flange columns under combined bending and thrust. The theoretical solutions given in these investigations are also compared to tests conducted by Mason, Fisher, and Winter (3).

Milner (4) conducted both theoretical and experimental studies on biaxial columns under nonproportional loading. The author used iterative techniques such as the finite difference approach and a numerical integration procedure to solve the governing differential equations. Razzaq (5) and Marshall and Ellis (6) conducted an experimental and theoretical study on elastic-plastic behavior of thin-walled members with box sections subjected to biaxial bending and compression. Test results were in good agreement with the theoretical predictions.

Sakda (8) conducted an analysis of biaxially loaded columns. The limit theorems and tangent stiffness method were used to analyze the elastic-plastic behavior of the cross-section in order to obtain interaction equations. Razzaq and McVinnie (9, 10) conducted an experimental and theoretical study on hollow rectangular section nonsway beam-columns subjected to nonproportional loading. Test results revealed that twisting may be neglected for columns of hollow square or rectangular sections.

Darbhamulla (11) performed an experimental and theoretical study of the inelastic stability of nonporportionally loaded imperfect rectangular tubular nonsway steel beam-

columns. The authors presented a new set of inelastic slope-deflection equations which were derived from a system of nonlinear ordinary differential equations. Eidan (12) performed an experimental and theoretical comprehensive study of the inelastic stability of sway steel beam-columns subjected to nonproportional loads. The authors formulated a set of materially nonlinear differential equations of equilibrium for planar and biaxially loaded beam-columns including sidesway. Zhao (13) conducted an experimental and theoretical investigation on thermo-elasto-plastic behavior of biaxially loaded steel beam-columns including those from the World Trade Center towers. Thermo-elasto-plastic stiffness degradation and load-moment interaction curves were formulated for typical WTC beam-columns that were in the impacted area during the 9/11 attacks.

1.2.2 Structural Member Studies Including Torque

Many studies have been conducted on steel members under pure torsion. Donnell (18) conducted a theoretical and experimental study on the stability of thin-walled sections under torsion. The author has developed a theoretical solution for round, thin-walled tubes for which the walls become unstable under torsion. The results of the theory were compared to the experimental results. The experimental failure torque was found to be lower than the theoretical predicted buckling torque. Burgoyne and Brown (19) performed a theoretical study of nonlinear uniform torsion of prismatic members. The authors have introduced two methods for solving the governing differential equations. Chen (20) presented a simple approximate and experimental method to evaluate the increase of torsional rigidity of thin prismatic bars and tubular members due to the presence of initial twist. Test data observed were used to verify the analysis.

Ellis, Jury and Davies (21) conducted theoretical and experimental studies on torsional behavior of rectangular hollow sections. Marshall's simplified thick wall torsion theory (22) and finite element (FE) analysis were used to predict the observed torque-twist behavior in the investigation. Test results observed agreed with the predicted values in the elastic range. However, in the inelastic range test results appeared to be significantly lower. Carey (23) conducted an experimental and theoretical study of plastic strength in torsion of prismatic bars with a concentric or eccentric hole using the sand-heap analogy. The

respective circular, square, and rectangular cross sections were tested. It was concluded that the circular shaft with an interior hole had the maximum strength.

Previous studies have been published on structural steel members subjected to combined uniaxial bending moment and torsion. Abramyan (26) conducted a theory for prismatic rods of hollow rectangular sections subjected to bending and torsion. Numerical technique was used to solve the linear differential equations. Estabrooks and Grondin (27) performed an experimental and theoretical study of steel I-Shaped beams subjected to combined bending and torsion. It was concluded that many design methods did not consider the destabilizing effects of torsion, warping stresses, nor biaxial bending in the inelastic range. Nuttall and Gaydon (28) conducted a theoretical study on combined bending and twisting of beams of various sections. Upper and lower approximations were used to obtain the interaction curves for cylinders, rectangles, I-shaped and box sections.

Ishikawa (29) conducted an elasto-plastic stress analysis of a prismatic bar under combined bending and torsion. In the study, an analytical method was formulated for a compressible isotropic work hardening material exhibiting a nonlinear stress strain law. Wiener and Bathe (30) conducted a study on elastic-plastic analysis of I-beams in bending and torsion. It was concluded that the I-beam model studied in this paper could be used for general analysis. Kyungsik and Chai (31) studied the ultimate strengths of steel rectangular box beams subjected to the combined action of bending and torsion. A commercial finite element analysis program (ABAQUS) was used to verify the proposed predictor ultimate strength interaction equations.

Hill and Siebel (32) conducted a theoretical study on the combined bending and twisting of thin tubes in the plastic range. von Mises yield criterion and Reuss stress-strain relations were used in the analysis. Equations were formulated to determine the stresses and warping in a partially plastic thin tube of arbitrary cross-section. Hill and Siebel (33) conducted an experimental and theoretical investigation of plastic distortion of solid bars by combined bending and twisting. Upper and lower approximate values were used to obtain the fully-plastic state of a plastic-rigid material. However, test results were not sufficient enough to show which approximation was better.

Imegwu (34) studied, theoretically, the plastic flexure and torsion of prismatic beams loaded by terminal bending and twisting moments. The interaction curve was obtained and

compared with the lower bound curve given by Hill and Siebel, and the difference between the two curves was outlined. Onat and Shield (35) investigated the influence of the loading program on the agreement between the predictions of the Hencky and the Prandtl-Reuss stress-strain relations for a perfectly plastic material in the case of the combined bending and twisting of thin-walled tubes. Good agreement was found in the results between the developed approximate method "composite" beam and those obtained from the incremental approach.

Boulton (36) conducted an experimental and theoretical study of plastic twisting and bending of an I-section in which the warp is restricted. The lower bound theory and Tresca failure criterion were used to obtain the full-plastic twisting and bending of an I-section in which warping of the cross-section is prevented at the ends. However, close agreement could not be found between the predicted and test values. Dinno and Merchant (37) outlined a procedure for calculating the plastic collapse of I-sections under bending and torsion. Experiments showed the introduced method to be safe and suitable for the design of I-section members under torsional strength with warping restraint and on the combined action of bending and torsion.

A number of studies on the behavior of structural members subjected to combined action of biaxial bending moments and torsional moment have been published. Razzaq and Galambos (38) presented a theoretical and experimental study of biaxial bending of a beam with or without torsion. The semi-analytic method was found to be the most efficient one among the six techniques considered for solving the three simultaneous governing differential equations for bending and torsion. Trahair and Bild (39) conducted a theoretical investigation of elastic biaxial bending and torsion of thin-walled open section members. It was concluded that the classical equations developed by Timoshenko, Vlasov and others were too complex for solution by hand; therefore, numerical methods such as a finite integral were used. Strelbytska and Evseyenko (40) conducted both theoretically and experimentally an investigation of cantilever bars in biaxial bending with torsion of thin-walled bars beyond the elastic limit. Test results were in good agreement with the theoretical predictions.

Shugyo and Li (41) presented an inelastic and stability analysis of linearly tapered box columns with a hollow square section under biaxial bending and torsion. Using extended

Horne's stability criterion, the ultimate strength of the columns was obtained. The numerical results were presented in the form of interaction diagrams. Hodge and Sankaranarayanan (42) presented a theoretical study for the determination of safe loads of beams subjected to combined twisting and biaxial bending moments. The lower-bound theorem of limit analysis was used to obtain the yield criterion in terms of the stress resultants for a beam under combined twisting and biaxial moments. Iwegwu (43) conducted a theoretical study of a uniform prismatic beam of square section under combined plastic biaxial bending and torsion. Numerical solution of the second-order non-linear differential equation derived by Hill for a Levy-Mises material was used. Results showed that the moments from the interaction of bending moments and a twisting moment were found to deviate by a small amount.

The behavior of structural members under combined axial and torsional loading have been previously published. Avitzur and Pan (44) provided an upper bound technique concept to analyze a cylindrical bar under combined axial force and torsion actions. The solution from this analysis coincided with the older existing classic solution for combined loading. Mahendran and Murray (45) conducted a theoretical and experimental study on the ultimate load behavior of box-columns under combined axial and torsional loads. The theoretical results were found to be in good agreement with test results. Wang, Nie and Fan (46) analyzed the mechanical behavior of CFST columns subjected to combined axial force and torsion. A simplified formula was proposed based on the regression method. Theoretical results were found to be in good agreement with the proposed method.

Sved and Brooks (47) investigated, theoretically, the elasto-plastic behavior of a round bar subjected to axial force and torque. Numerical results showed that the effect of Poisson's ratio is relatively small. Feign (48) conducted experimental and theoretical studies on thin-walled tubes under combined tension-torsion. Test results fall between the predictions of the flow and deformation theory. Mii (49) conducted a theoretical investigation of plastic deformation of light-metal bars strained with combined tension and torsion. The deformation of the material in the strain-hardening region was assumed to obey the maximum shear stress theory in the study. Ono (50) analyzed the stress and strain in metals undergoing a plastic flow-tube wall subjected to axial pull and torque. The general procedure of analysis was outlined and demonstrated through numerical examples.

A very few studies have been conducted on steel members subjected to combined action of an axial compressive load, uniaxial or biaxial bending and torsion. Kitada and Nakai (51) conducted an experimental study on ultimate strength of thin-walled box stub or short columns subjected to the combined action of torsion in addition to axial load and uniaxial bending. Test results were compared with a computer program developed in another study but without including second-order effects. It was found that the global axial, flexural and torsional stiffnesses of the box column specimen up to the ultimate state were not affected when local buckling in a plate element occurred. Timoshenko (52) developed a theory for combined axial load, bending, and torsion for a thin-walled member; however, it is applicable only in the elastic range for open cross sections. Trahair and Pi (53) studied the behavior, analysis and design of compressed members under the combined actions of torsion and bending, but their research was also limited to the elastic range. Interaction equations were formulated and could be used for design purposes with this type of loading, assuming that the member will remain elastic.

Bleich and Bleich (54) conducted a theoretical study of bending, torsion and buckling of bars composed of thin walls in the elastic range only. Goodier (55) conducted an elastic theoretical investigation of flexural-torsional buckling of bars of open sections, under bending, eccentric thrust and induced torsional effects. Galambos (56) conducted a theoretical and experimental study on failure of steel wide-flange columns subjected to an axial force, bending moments in the plane of their strong axis, and induced torsional effects. It was concluded that at a certain critical load, these columns deflect in their weak direction accompanied by twisting about the shear center.

To the best of the author's knowledge, no experimental and theoretical study has previously been published on the inelastic behavior of steel beam-columns subjected to nonproportional biaxial bending in the presence of applied torsion.

1.3 Problem Definition

The main problem addressed in this dissertation is to develop an inelastic theoretical behavior prediction model for biaxially loaded nonsway beam-columns with applied torsion and verify it experimentally. Figure 1 shows an imperfect steel member BT with z as its longitudinal axis, subjected to a concentrated torsional moment M_z applied at the bottom end, an axial compressive or thrust load P, and bending moments M_{Bx}, M_{By}, M_{Tx}, and M_{Ty}. Subscripts B and T refer to the column bottom and top ends. The boundaries of the member have partial rotational end restraints about the x and y axes. The initial geometric imperfection is taken in the form of half-sine wave functions u_i and v_i in the xz and yz planes as shown in Figure 1 and Figure 2. The total displacement U shown in Figure 2 is the sum of u and u_i, where u is the displacement due to the applied loads. Similarly, V is the sum of v and v_i, where v is the displacement owing to the applied loads. Figure 2 also shows the angle of twist, ψ, at any location z along the member's length. Two types of cross sections are considered in the theoretical analysis, namely, a hollow rectangular section and an I-shaped section. The cross sections possess initial residual stresses due to manufacturing processes.

The theoretical challenge is to predict the behavior and strength of the member as governed by a system of four simultaneous nonlinear ordinary differential equations based on an iterative finite integral solution scheme. The experimental part of the problem involves the development of a new torsional testing method in the presence of both biaxial bending and axial compression and comparing hollow square section member behavior with that predicted theoretically. The last portion of the problem is to develop new yield limit interaction relations and to modify ultimate strength interaction expressions from eight major regions or countries of the world so that the effect of applied torsion is accounted for.

1.4 Objectives and Scope

The principal objectives of the research embodied in this dissertation are as follows:

1. Incorporate the influence of applied torsion into the governing nonlinear differential equations for the problem including both biaxial bending and axial thrust.

2. Develop and program an iterative nonlinear algorithm based on a finite integral solution for the governing differential equations.
3. Develop a torsional testing method and test assembly that can be incorporated into a previously developed biaxial bending apparatus.
4. Conduct a series of tests on hollow square section members with an axial thrust, uniaxial or biaxial bending, and torsion to understand the basic behavior as well as to validate the theoretical solutions.
5. Develop new yield limit interaction relations for members with both hollow rectangular and I-shaped cross sections.
6. Incorporate a new dimensionless torsional moment term into biaxial bending and axial thrust interaction expressions from the following eight major regions of the world:
   a) Australia (AS4100 Specification)
   b) Japan (AIJ Specification)
   c) U.S. (AISC-LFRD Specification)
   d) Great Britain (BS 5950 Specification)
   e) Canada (CSA Specification)
   f) Europe (Eurocode 3)
   g) China (GBJ Specification)
   h) Russia (SNiP Specification)

A total of 60 steel member tests are conducted on hollow square sections with dimensions $1\frac{1}{2} \times 1\frac{1}{2} \times \frac{1}{8} \times 37\frac{3}{4}\ in$. The majority of experiments are conducted with pinned boundary conditions. However, some tests included a combination of pinned and fixed boundary conditions. Nevertheless, the theory utilizes partial rotational end restraints about the x and y axes.

1.5 Assumptions and Conditions

The following are the main assumptions and conditions adopted in the study presented in this dissertation:

1. All external loads are applied at the ends of the structural member in a quasi-static manner up to its ultimate strength.

2. Small deflection theory is adopted.
3. The axial force is applied to the centroid of the cross section and retains this position until the member load-carrying capacity is reached.
4. Local buckling is not included.
5. The member material follows elastic-perfectly-plastic normal and shear stress-strain relationships.
6. The stress-strain relationships have for compression and tension the same shape.
7. A concentrated torsional moment is applied only at the bottom end of the member.
8. The influence of material unloading is ignored.

CHAPTER 2

THEORETICAL FORMULATION

Presented in this chapter is the theoretical nonlinear analysis of beam-columns with applied torsion in the inelastic range. The analysis includes cross-sectional residual stresses and member initial crookedness. The materially nonlinear ordinary differential equations of equilibrium are formulated for the problem. To obtain the solution to the nonlinear differential equations, an iterative finite integral solution scheme is developed and programmed. The material yielding is determined using von Mises yield criterion.

2.1 Nonlinear Thrust-moment-curvature Relations

Figure 3 shows a discretized hollow rectangular section with width b, depth d, wall thickness t, and a typical elemental area A_i. Figure 4 and Figure 5 show residual stress distributions for a hollow rectangular section and an I-section used in the analysis. The adopted elastic-perfectly-plastic normal stress versus strain relationship for steel is shown in Figure 6. At a point (x, y) of the cross section subjected to an axial load as well as bending moments $M_x$and M_y about the x and y axes, the normal strain ϵ is given by (57):

$$\epsilon = \epsilon_0 + \Phi_x\, y - \Phi_y\, x + \epsilon_r + \epsilon_\omega \tag{1}$$

in which ϵ_0 is the average axial strain; Φ_x and Φ_y are the bending curvatures about the x and y axes of the section; ϵ_r is the residual strain; and ϵ_ω is the warping strain. The following normal stress-strain (σ-ϵ) relations for steel are adopted in this dissertation:

$$\sigma = E\epsilon \qquad \text{for } -\epsilon_Y < \epsilon < \epsilon_Y \tag{2}$$

$$\sigma = +\sigma_Y \qquad \text{for } \epsilon \geq \epsilon_Y \tag{3}$$

$$\sigma = -\sigma_Y \qquad \text{for } \epsilon \leq -\epsilon_Y \tag{4}$$

in which E is Young's modulus; ϵ_Y is the normal yield strain; and σ_Y is the normal yield stress. In Equations 2 through 4, tensile stresses and strains are considered positive. The elastic normal stress at any point (x, y) on a cross section can be expressed as (57):

$$\sigma = \frac{P}{A} + \frac{(M_x)y}{I_x} - \frac{(M_y)x}{I_y} + \sigma_r + \sigma_\omega \tag{5}$$

where P is the axial load; M_x and M_y are the bending moments about the x and y-axes; A is the cross sectional area; I_x and I_y are the moment of inertia values of the member cross

section about the x-axis and y-axis; σ_r is the residual stress; and σ_ω is the warping normal stress. Equation 5 is obviously not applicable in the inelastic range requiring normal stresses to be determined only iteratively. Based on the elastic-perfectly-plastic stress-strain relationship shown in Figure 6, the axial load and biaxial moment equilibrium equations for a cross section can be expressed as (58):

$$P = -\int_{Ae}\sigma_e\, dA - \int_{Ap}\sigma_Y\, dA \tag{6}$$

$$M_x = \int_{Ae}\sigma_e\, y\, dA + \int_{Ap}\sigma_Y\, y\, dA \tag{7}$$

$$M_y = -\int_{Ae}\sigma_e\, x\, dA - \int_{Ap}\sigma_Y\, x\, dA \tag{8}$$

In these equations, dA is an elemental area of the cross section; σ_e is the elastic normal stress; and $\int_{Ae}$ and $\int_{Ap}$ represent integrals over elastic and plastic regions. For a partially plastified section, σ_e distribution is found iteratively and not using Equation 5. To evaluate the integrals in Equations 6-8, a given member cross section is first divided into a number of elemental areas as shown schematically in Figure 3. The integrals ($\int$) are then replaced with summations (Σ) over a given cross section while using Equations 1 through 4. In a study by Zhao (13) for a problem in the absence of torsion, 228 elemental areas per plate were found to give proper convergence. Thus, a total of 912 elemental areas were used for each cross-section in this dissertation. An iterative procedure is used until Equations 6-8 are satisfied within a specified tolerance (0.0001) between the external and internal forces. This process relates the thrust, P, and bending moments, M_x, and M_y, to the internal average axial strain ϵ_0, and the curvatures Φ_x and Φ_y appearing in Equation 1.

2.2 Nonlinear Differential Equation of Torsion

Figure 7 shows the adopted elastic-perfectly-plastic shear stress-strain relationship. The shear stress τ and shear strain Υ relationship adopted for steel is as follows:

$$\tau = G\Upsilon \qquad \text{for } -\Upsilon_Y < \Upsilon < \Upsilon_Y \tag{9}$$

$$\tau = \tau_Y \qquad \text{for } \Upsilon \geq \Upsilon_Y \tag{10}$$

where G is the shear modulus; Υ_Y is the shear yield strain; and τ_Y is the shear yield stress. The elastic shear elastic stress can be expressed as (57):

$$\tau = -\frac{R_y Q}{hI_x} - \frac{R_x Q}{hI_y} + \tau_\omega + \tau_{sv} \tag{11}$$

In this equation, R_x and R_y are the shear forces about the x-axis and y-axis; Q is a statical area moment; h is the cross-sectional plate thickness, τ_ω is the warping shear stress; and τ_{sv} is Saint Venant shear stress. In this dissertation, the internal resisting torsional moment, M_{zint}, from Reference 57 is modified to include inelastic behavior and takes the following form:

$$M_{zint} = (C_{te})\psi' - C_{\omega e}\psi''' + M_{zp} \tag{12}$$

in which C_{te} is Saint Venant torsional stiffness for the elastic portion of the cross section; ψ is the angle of twist; ψ''' is the third derivative of the angle of twist; $C_{\omega e}$ is the warping stiffness of the elastic portion of the cross section; and M_{zp} is the internal torsional moment for the plastified portion of the cross section. However, warping effects are small for hollow square and rectangular sections and can therefore be neglected. Furthermore, the following von Mises Yield criterion (59) is adopted in the present study:

$$\sigma^2 + 3\tau^2 \leq {\sigma_Y}^2. \tag{13}$$

Marshall's simplified equations for a hollow rectangular cross section, the internal resisting elasto-plastic torsional moment, M_{zint}, can be written as (22):

$$M_{zint} = \tau_Y C_{Mt} \quad \text{for yield limit} \tag{14}$$

$$M_{zint} = \tau_Y (C_{Mte} + C_{Mtp}) \quad \text{for inelastic} \tag{15}$$

$$M_{zint} = 2t\,A_E \tau_Y \quad \text{for plastic} \tag{16}$$

where:

$$C_{Mt} = \frac{h_c\, I_t}{h h_c + 2A_E} \tag{17}$$

$$C_{Mte} = \frac{(1-\beta)h_{c,elastic}\left(\frac{4hA_{E,elastic}^2}{h_{c,elastic}} + \frac{(1-\beta)^2 h^3 h_{c,elastic}}{3}\right)}{(1-\beta)h h_{c,elastic} + 2A_{E,elastic}} \tag{18}$$

$$C_{Mtp} = 2\beta h(b-\beta h)(d-\beta h) - \frac{(4-\pi)(2r_o - \beta(r_o - r_i))}{4} \tag{19}$$

in which:

$$h_c = 2(((b-h)+(d-h)) - (4-\pi)(r_o + r_i) \tag{20}$$

$$I_t = \frac{h^3 h_c}{3} + \frac{4hA_E^2}{h_c} \tag{21}$$

$$A_E = (b-h)(d-h) - \frac{(4-\pi)(r_o + r_i)^2}{4} \tag{22}$$

$$h_{c,elastic} = 2(b+d-2h-2\beta h) - (4-\pi)(r_o + r_i - \beta(r_o - r_i)) \tag{23}$$

$$A_{E,elastic} = (b - h - \beta h)(d - h - \beta h) - \frac{(4-\pi)(r_o + r_i - \beta(r_o + r_i))^2}{4} \quad (24)$$

$$\beta = \frac{1}{2} + \frac{A_E}{h h_c} - \frac{\tau_Y L}{2G\psi_M \, h} \qquad \text{for} \quad 0 \leq \beta \leq 1 \quad (25)$$

The angle of twist in Equation 25 is given by (22):

$$\psi_M = \frac{L\tau_Y C_M}{G I_t} \quad (26)$$

In Equations 14 through 26, C_{Mt} is the torsional modulus constant; I_t is the torsional inertia constant; h_c is the mean perimeter; A_E is the enclosed hatched area shown in Figure 8 and defined by the wall midline; h is the cross-sectional wall thickness; C_{Mte} is the torsional modulus constant for the elastic part of a partially plastified cross section; C_{tp} is the torsional modulus constant for the plastified portion of the cross section; β accounts for partial yielded portion of the cross-section; ψ_M is the angle of twist; C_M is equal to C_{Mt} for yield limit and equal to $(C_{Mte} + C_{Mtp})$ for the inelastic range; and the external and internal corner radii r_o and r_i account for relatively small correction for the roundness of the four corners of a rectangular hollow section. The finite integral formulation in this dissertation ignores the effect of cross sectional corner roundness.

2.3 Nonlinear Equilibrium Equations for Torsionally Loaded Beam-column

For the beam-column with applied torsion shown in Figure 1, the total deflections U and V including member initial crookedness are expressed as:

$$U = u_i + u \quad (27)$$

$$V = v_i + v \quad (28)$$

where u and v are the deflections due to the applied loads; and u_i and v_i are the initial crookedness functions in the xz and yz planes given by:

$$u_i = u_o \sin(\frac{\pi z}{L}) \quad (29)$$

$$v_i = v_o \sin(\frac{\pi z}{L}) \quad (30)$$

In these expressions, u_o and v_o are the initial mid-span amplitudes. The external bending including p-delta effects and torsional moment at any distance z from the lower end B of the member can be expressed as:

$$M_x = P\,V - m_{Bx} - M_{Bx} + \frac{z}{L}(M_{Bx} + M_{Tx} - m_{Tx} + m_{Bx}) \tag{31}$$

$$M_y = -P\,U + m_{By} - M_{By} + \frac{z}{L}(M_{By} + M_{Ty} + m_{Ty} - m_{By}) \tag{32}$$

$$M_z = M_{Rz} \tag{33}$$

In Equations 31-33, M_{Rz} is the reacting torsional moment; m_{By}, m_{Tx} and m_{Ty} are the induced bending moments at the member ends due to partial rotational end restraints and are given by:

$$m_{Bx} = k_{Bx}\,\theta_{Bx} \tag{34}$$

$$m_{By} = k_{By}\,\theta_{By} \tag{35}$$

$$m_{Tx} = -k_{Tx}\,\theta_{Tx} \tag{36}$$

$$m_{Ty} = -k_{Ty}\,\theta_{Ty} \tag{37}$$

In these equations, k_{Bx}, k_{By}, k_{Tx} and k_{Ty} are the stiffness values for the partial rotational end restraints, and θ_{Bx}, θ_{By}, θ_{Tx}, and θ_{Ty} are the corresponding end slopes defined as follows:

$$\theta_{Bx} = v'(0) \tag{38}$$

$$\theta_{By} = u'(0) \tag{39}$$

$$\theta_{Tx} = -\,v'(L) \tag{40}$$

$$\theta_{Ty} = -\,u'(L) \tag{41}$$

The moments in Equations 31 through 33 are now transferred to a new set of rectilinear coordinates ξ, η and ζ of the displaced cross section. Using the second-order approach in Reference 57, the biaxial bending and torsion equations for the problem dealt with in this dissertation take the following form:

$$M_\xi = P\,V - m_{Bx} - M_{Bx} + \frac{z}{L}(M_{Bx} + M_{Tx} - m_{Tx} + m_{Bx}) + \psi(m_{By} - M_{By} + \frac{z}{L}(M_{By} + M_{Ty} + m_{Ty} - m_{By})) - M_{Rz}u' \tag{42}$$

$$M_\eta = -P\,U + m_{By} - M_{By} + \frac{z}{L}(M_{By} + M_{Ty} - m_{Tx} + m_{Bx}) - \psi\left(-m_{Bx} - M_{Bx} + \frac{z}{L}(M_{Bx} + M_{Tx} + m_{Ty} - m_{By})\right) - M_{Rz}v' \tag{43}$$

$$M_\zeta = -\bar{K}\psi' + v'\left[m_{By} - M_{By} + \frac{z}{L}(M_{By} + M_{Ty} + m_{Ty} - m_{By}) - Px_0\right] + u'\left[-m_{Bx} - M_{Bx} + \frac{z}{L}(M_{Bx} + M_{Tx} - m_{Tx} + m_{Bx}) + Py_0\right] -$$

$$\frac{v}{L}\left(M_{By} + M_{Ty} + m_{Ty} - m_{By}\right) - \frac{u}{L}(M_{Bx} + M_{Tx} - m_{Tx} + m_{Bx}) + M_{Rz} \quad (44)$$

in which x_0 and y_0 are the coordinates of the shear center; M_ξ, M_η, and M_ζ are the moments about the new axes ξ, η, and ζ, respectively; $\bar{K}$ is Wagner term defined as (57):

$$\bar{K} = \int_A \sigma a^2 dA \quad (45)$$

in which a^2 is given as:

$$a^2 = (x_0 - x)^2 + (y_0 - y)^2 \quad (46)$$

where a is the distance between the point where σ acts and the shear center. Substituting Equation 46 into Equation 45 results in:

$$\bar{K} = -P\bar{r}^2 + \beta_x M_{Bx} - \beta_y M_{By} \quad (47)$$

where:

$$\beta_x = \frac{\int_A y(x^2+y^2)dA}{I_x} - 2y_o \quad (48)$$

$$\beta_y = \frac{\int_A x(x^2+y^2)dA}{I_y} - 2x_o \quad (49)$$

Letting the terms Φ_x, Φ_y and ϵ_ω in Equation 1 be:

$$\Phi_x = -v'' \quad (50)$$

$$\Phi_y = u'' \quad (51)$$

$$\epsilon_\omega = -\omega_n \psi'' \quad (52)$$

Equations 50 through 52 into Equation1 leads to the following form:

$$\epsilon = \epsilon_0 - v'' y - u'' x + \epsilon_r - \omega_n \psi'' \quad (53)$$

Using Equations 2-4 together with Equation 53 on the right hand side of Equations 6 through 8 results in:

$$-a_{11}\,\varepsilon_0 + a_{12}v'' + a_{13}u'' + a_{14}\psi'' - P_r - P_p = P \quad (54)$$

$$-a_{21}\,\varepsilon_0 + a_{22}v'' + a_{23}u'' + a_{24}\psi'' - M_{xre} - M_{xp} = -M_x \quad (55)$$

$$-a_{31}\,\varepsilon_0 + a_{32}v'' + a_{33}u'' + a_{34}\psi'' - M_{yre} - M_{yp} = M_y \quad (56)$$

in which the primes indicate differentiation with respect to z; P_r is the residual axial load; M_{xre} and M_{yre} are the residual bending moments about x and y; P_p is the internal plastic axial load; M_{xp} and M_{yp} are the internal plastic bending moments about the x and y axes; and the quantities a_{ij} terms are the elastic constant coefficients and defined as follows:

$$a_{11} = E\,A_e \tag{57}$$

$$a_{12} = E\,S_{xe} \tag{58}$$

$$a_{13} = E\,S_{ye} \tag{59}$$

$$a_{14} = E\,S_{\omega_{ne}} \tag{60}$$

$$a_{21} = ES_{xe} \tag{61}$$

$$a_{22} = E\,I_{xe} \tag{62}$$

$$a_{23} = E\,I_{xye} \tag{63}$$

$$a_{24} = E\,I_{\omega ye} \tag{64}$$

$$a_{31} = E\,S_{ye} \tag{65}$$

$$a_{32} = E\,I_{xye} \tag{66}$$

$$a_{33} = E\,I_{ye} \tag{67}$$

$$a_{34} = E\,I_{\omega xe} \tag{68}$$

in which:

$$A_e = \int_{Ae} dA \tag{69}$$

$$S_{xe} = \int_{Ae} y\,dA \tag{70}$$

$$S_{ye} = \int_{Ae} x\,dA \tag{71}$$

$$S_{\omega_{ne}} = \int_{Ae} \omega_n\,dA \tag{72}$$

$$I_{xe} = \int_{Ae} y^2\,dA \tag{73}$$

$$I_{ye} = \int_{Ae} x^2\,dA \tag{74}$$

$$I_{\omega xe} = \int_{Ae} \omega x\,dA \tag{75}$$

$$I_{\omega ye} = \int_{Ae} \omega y\,dA \tag{76}$$

$$I_{xye} = \int_{Ae} xy\,dA \tag{77}$$

The other terms in Equations 54-56 are defined as follows:

$$P_r = \int_{Ae} \sigma_r\,dA \tag{78}$$

$$P_p = \int_{Ap} \sigma_Y\,dA \tag{79}$$

$$M_{xre} = \int_{Ae} \sigma_r\,y\,dA \tag{80}$$

$$M_{yre} = \int_{Ae} \sigma_r\,x\,dA \tag{81}$$

$$M_{xp} = \int_{Ap} \sigma_Y\,y\,dA \tag{82}$$

$$M_{yp} = \int_{Ap} \sigma_Y \, x \, dA \tag{83}$$

Equation 54 is first used to solve for ε_0 which is then substituted into Equations 55 and 56. Thus, the resulting two flexural equilibrium equations and the torsional equilibrium equation take the following form:

$$B_{xx}\, v'' + B_{xy} u'' + B_{x\omega}\, \psi" + \left(S_{xe} P_{ep}\right) - A_e M_{xx(ep)} = -A_e M_x \tag{84}$$

$$B_{yx}\, v'' + B_{yy} u'' + B_{y\omega}\, \psi" + \left(S_{ye} P_{ep}\right) - A_e M_{yy(ep)} = A_e M_y \tag{85}$$

Also, equating the internal resisting torsional moment given by Equation 12 to the torsional moment M_z at any location z, the following torsional equilibrium equation is obtained:

$$(\, C_{te}\,)\psi' - C_{\omega e}\psi''' + M_{zzp} = M_z \tag{86}$$

where:

$$B_{xx} = \left(\frac{a_{11}a_{22} - a_{12}a_{21}}{a_{11}}\right) \tag{87}$$

$$B_{xy} = \left(\frac{a_{11}a_{23} - a_{21}a_{13}}{a_{11}}\right) \tag{88}$$

$$B_{x\omega} = \left(\frac{a_{11}a_{24} - a_{21}a_{14}}{a_{11}}\right) \tag{89}$$

$$B_{yx} = \left(\frac{a_{11}a_{32} - a_{12}a_{31}}{a_{11}}\right) \tag{90}$$

$$B_{yy} = \left(\frac{a_{11}a_{33} - a_{13}a_{31}}{a_{11}}\right) \tag{91}$$

$$B_{y\omega} = \left(\frac{a_{11}a_{34} - a_{14}a_{31}}{a_{11}}\right) \tag{92}$$

$$P_{ep} = P + P^*_{ep} \tag{93}$$

$$P^*_{ep} = P_r + P_p \tag{94}$$

$$M_{xx(ep)} = M_{xre} + M_{xp} \tag{95}$$

$$M_{yy(ep)} = M_{yre} + M_{yp} \tag{96}$$

In Equations 84-86, the M_x, M_y, and M_z moments correspond to the undeflected member. Replacing M_x, M_y, and M_z with M_ξ, M_η, and M_ζ in Equations 84-86 results in:

$$B_{xx}\, v'' + B_{xy} u'' + B_{x\omega}\, \psi" + \left(S_{xe} P_{ep}\right) - A_e M_{xx(ep)} = -A_e M_\xi \tag{97}$$

$$B_{yx}\, v'' + B_{yy} u'' + B_{y\omega}\, \psi" + \left(S_{ye} P_{ep}\right) - A_e M_{yy(ep)} = A_e M_\eta \tag{98}$$

$$(\, C_{te}\,)\psi' - C_{\omega e}\psi''' + M_{zp} = M_\zeta \tag{99}$$

In these Equations, the M_ξ, M_η, and M_ζ moments correspond to the deflected member.

Substituting Equations 42-44 into Equations 97-99, the final governing nonlinear differential equations of equilibrium are obtained as follows:

$$B_{xx}v'' + B_{xy}u'' + B_{x\omega}\psi'' - A_e M_{Rz}u' + A_e P v +$$
$$A_e\psi\left(m_{By} - M_{By} + \frac{z}{L}(M_{By} + M_{Ty} + m_{Ty} - m_{By}) - Px_o\right)$$
$$-A_e m_{Bx} + A_e\frac{z}{L}(-m_{Tx} + m_{Bx})$$
$$= \Gamma_x + \Gamma_{xr} + \Gamma_{xp} \tag{100}$$

$$B_{yx}v'' + B_{yy}u'' + B_{y\omega}\psi'' + A_e M_{Rz}v' + A_e P u +$$
$$A_e\psi\left(-m_{Bx} - M_{Bx} + \frac{z}{L}(M_{Bx} + M_{Tx} - m_{Tx} + m_{Bx}) + Px_o\right)$$
$$-A_e m_{By} - A_e\frac{z}{L}(m_{Ty} - m_{By})$$
$$= \Gamma_y + \Gamma_{yr} + \Gamma_{yp} \tag{101}$$

$$C_{\omega e}\psi''' - (C_{te} + \bar{K})\psi' + v'\left[m_{By} - M_{By} + \frac{z}{L}(M_{By} + M_{Ty} + m_{Ty} - m_{By}) - Px_0\right]$$
$$+ u'\left[-m_{Bx} - M_{Bx} + \frac{z}{L}(M_{Bx} + M_{Tx} - m_{Tx} + m_{Bx}) + Py_0\right] -$$
$$\frac{v}{L}(M_{By} + M_{Ty} + m_{Ty} - m_{By}) - \frac{u}{L}(M_{Bx} + M_{Tx} - m_{Tx} + m_{Bx})$$
$$= \Gamma_z + \Gamma_{zp} \tag{102}$$

where:

$$\Gamma_x = -A_e P v_i + A_e M_{Bx} - A_e\frac{z}{L}(M_{Bx} + M_{Tx}) - S_{xe}P \tag{103}$$
$$\Gamma_{xr} = -S_{xe}P_{re} + A_e M_{xre} \tag{104}$$
$$\Gamma_{xp} = -S_{xe}P_p + A_e M_{xp} \tag{105}$$
$$\Gamma_y = -A_e P\, u_i - A_e M_{By} + A_e\frac{z}{L}(M_{By} + M_{Ty}) - S_{ye}P \tag{106}$$
$$\Gamma_{yr} = -S_{ye}P_{re} + A_e M_{yre} \tag{107}$$
$$\Gamma_{yp} = -S_{ye}P_p + A_e M_{yp} \tag{108}$$
$$\Gamma_z = -M_{Rz} \tag{109}$$
$$\Gamma_{zp} = M_{zp} \tag{110}$$

In these equations, Γ_x, Γ_y and Γ_z contain both applied load terms in addition to other quantities as indicated; Γ_{xr} and Γ_{yr} contain both internal resisting load terms due to residual stresses and other quantities; Γ_{xp}, Γ_{yp} and Γ_{zp} contain internal plastic loads and

other quantities. In this dissertation, the materially nonlinear governing differential equations are developed for an arbitrary cross section but are applied to hollow rectangular and I-shaped sections.

2.3.1 Nonlinear Equilibrium Equations for Combined Axial Load and Torsion

If an axial compressive load and torsional moment are simultaneously applied, Equations 100-102 reduce to the following expressions:

$$B_{xx}\,v'' + B_{xy}u'' + B_{x\omega}\psi'' - M_{Rz}u' + A_eP\,(v + v_i) + A_e\psi\left(m_{By} + \frac{z}{L}(m_{Ty} - m_{By}) - Px_o\right) = A_em_{Bx} - A_e\frac{z}{L}(-m_{Tx} + m_{Bx}) - \left(S_{xe}P_{ep}\right) + A_eM_{xx(ep)} \quad (111)$$

$$B_{yx}\,v'' + B_{yy}u'' + B_{y\omega}\psi'' + M_{Rz}v' + A_eP\,(u + u_i) + A_e\psi\left(-m_{Bx} + \frac{z}{L}(-m_{Tx} + m_{Bx}) + Px_o\right) = A_em_{By} + A_e\frac{z}{L}(m_{Ty} - m_{By}) - \left(S_{ye}P_{ep}\right) + A_eM_{yy(ep)} \quad (112)$$

$$C_{\omega e}\psi''' - (C_{te} + \bar{K})\psi' + u'\left[-m_{Bx} + \frac{z}{L}(-m_{Tx} + m_{Bx}) + Py_0\right] + v'\left[m_{By} + \frac{z}{L}(m_{Ty} - m_{By}) - Px_0\right] - \frac{v}{L}(m_{Ty} - m_{By}) - \frac{u}{L}(-m_{Tx} + m_{Bx}) = -M_{Rz} + M_{zp} \quad (113)$$

Equations 111-113 are the materially nonlinear governing differential equations for a steel column of any cross section under combined axial load and torsion.

2.3.2 Nonlinear Equilibrium Equations for Combined Uniaxial Bending and Torsion Torque

In the presence of uniaxial bending moment and torsion, Equations 100-102 reduce to the following expressions:

$$B_{xx}\,v'' + B_{xy}u'' + B_{x\omega}\psi'' - M_{Rz}u' + A_e\,\psi\left(m_{By} - M_{By} + \frac{z}{L}(M_{By} + M_{Ty} + m_{Ty} - m_{By})\right) = A_em_{Bx} - A_e\frac{z}{L}(-m_{Tx} + m_{Bx}) - \left(S_{xe}P^*_{ep}\right) + A_eM_{xx(ep)} \quad (114)$$

$$B_{yx}\,v'' + B_{yy}u'' + B_{y\omega}\psi'' + A_eM_{Rz}v' + A_e\psi\left(-m_{Bx} + \frac{z}{L}(-m_{Tx} + m_{Bx})\right)$$

$$= A_e m_{By} - A_e M_{By} + A_e \frac{z}{L}\left(M_{By} + M_{Ty} + m_{Ty} - m_{By}\right) - \left(S_{ye} P_{ep}^{*}\right) + A_e M_{yy(ep)} \quad (115)$$

$$C_{\omega e}\psi''' - (C_{te} + \bar{K})\psi' + u'\left[-m_{Bx} + \frac{z}{L}(-m_{Tx} + m_{Bx})\right] +$$

$$v'\left[m_{By} - M_{By} + \frac{z}{L}\left(M_{By} + M_{Ty} + m_{Ty} - m_{By}\right)\right]$$

$$- \frac{v}{L}\left(M_{By} + M_{Ty} + m_{Ty} - m_{By}\right) - \frac{u}{L}(-m_{Tx} + m_{Bx}) = -M_{Rz} + M_{zp} \quad (116)$$

Equations 114-116 are the nonlinear governing differential equations for combined uniaxial bending and torsion.

2.3.3 Nonlinear Equilibrium Equations for Combined Biaxial Bending and Torsion

If biaxial bending moments and torsional moment are applied simultaneously, Equations 100-102 reduce to the following expressions:

$$B_{xx} v'' + B_{xy} u'' + B_{x\omega}\psi'' - A_e M_{Rz} u' +$$

$$A_e \psi\left(m_{By} - M_{By} + \frac{z}{L}\left(M_{By} + M_{Ty} + m_{Ty} - m_{By}\right)\right)$$

$$= A_e m_{Bx} + A_e M_{Bx} - A_e \frac{z}{L}(M_{Bx} + M_{Tx} - m_{Tx} + m_{Bx}) - \left(S_{xe} P_{ep}^{*}\right) + A_e M_{xx(ep)} \quad (117)$$

$$B_{yx} v'' + B_{yy} u'' + B_{y\omega}\psi'' + M_{Rz} v' +$$

$$A_e \psi\left(-m_{Bx} - M_{Bx} + \frac{z}{L}(M_{Bx} + M_{Tx} - m_{Tx} + m_{Bx})\right)$$

$$= m_{By} - M_{By} + \frac{z}{L}\left(M_{By} + M_{Ty} + m_{Ty} - m_{By}\right) - \left(S_{ye} P_{ep}^{*}\right) + A_e M_{yy(ep)} \quad (118)$$

$$C_{\omega e}\psi''' - (C_{te} + \bar{K})\psi' + u'\left[-m_{Bx} - M_{Bx} + \frac{z}{L}(M_{Bx} + M_{Tx} - m_{Tx} + m_{Bx})\right]$$

$$+ v'\left[m_{By} - M_{By} + \frac{z}{L}\left(M_{By} + M_{Ty} + m_{Ty} - m_{By}\right)\right]$$

$$- \frac{v}{L}\left(M_{By} + M_{Ty} + m_{Ty} - m_{By}\right) - \frac{u}{L}(M_{Bx} + M_{Tx} - m_{Tx} + m_{Bx})$$

$$= -M_{Rz} + M_{zp} \quad (119)$$

Equations 117-119 govern the nonlinear behavior of a member with combined biaxial bending and torsion.

2.3.4 Nonlinear Equilibrium Equations for Combined Axial Load, Uniaxial Bending and Torsion

If an axial compressive load, uniaxial bending moment, and torsional moment are applied concurrently, Equations 100-102 reduce to the following expressions:

$$B_{xx}\,v'' + B_{xy}u'' + B_{x\omega}\psi'' - M_{Rz}u' + A_eP\,(v + v_i) +$$
$$A_e\psi\left(m_{By} - M_{By} + \frac{z}{L}\left(M_{By} + M_{Ty} + m_{Ty} - m_{By}\right) - Px_o\right)$$
$$= A_em_{Bx} - A_e\frac{z}{L}(-m_{Tx} + m_{Bx}) - \left(S_{xe}P_{ep}\right) + A_eM_{xx(ep)} \tag{120}$$
$$B_{yx}\,v'' + B_{yy}u'' + B_{y\omega}\psi'' + M_{Rz}v' + A_eP\,(u + u_i) +$$
$$A_e\psi\left(-m_{Bx} + \frac{z}{L}(-m_{Tx} + m_{Bx}) + Px_o\right)$$
$$= m_{By} - M_{By} + \frac{z}{L}\left(M_{By} + M_{Ty} + m_{Ty} - m_{By}\right) - \left(S_{ye}P_{ep}\right) + A_eM_{yy(ep)} \tag{121}$$
$$C_{\omega e}\psi''' - (\,C_{te} + \bar{K})\psi' + u'\left[-m_{Bx} + \frac{z}{L}(-m_{Tx} + m_{Bx}) + Py_0\right] +$$
$$v'\left[m_{By} - M_{By} + \frac{z}{L}\left(M_{By} + M_{Ty} + m_{Ty} - m_{By}\right) - Px_0\right]$$
$$-\frac{v}{L}\left(M_{By} + M_{Ty} + m_{Ty} - m_{By}\right) - \frac{u}{L}(-m_{Tx} + m_{Bx}) = -M_{Rz} + M_{zp} \tag{122}$$

Equations 120-122 are the nonlinear governing differential equations for a steel beam-column under uniaxial bending and torsion.

2.3.5 Nonlinear Equilibrium Equations for Combined Axial Load, Biaxial Bending Moments at the Top End and Uniform Torsion

If an axial load, biaxial bending moments at the top end of the member, and a uniform torsional moment are applied simultaneously, Equations 100-102 reduce to the following expressions by neglecting warping effects:

$$B_{xx}\,v'' + B_{xy}u'' - M_{Rz}u' + A_eP\,(v + v_i) +$$
$$\psi\left(m_{By} + \frac{z}{L}\left(M_{Ty} + m_{Ty} - m_{By}\right) - Px_o\right)$$
$$= m_{Bx} - \frac{z}{L}(M_{Tx} - m_{Tx} + m_{Bx}) - \left(S_{xe}P_{ep}\right) + A_eM_{xx(ep)} \tag{123}$$
$$B_{yx}\,v'' + B_{yy}u'' + M_{Rz}v' + A_eP\,(u + u_i) +$$
$$\psi\left(-m_{Bx} + \frac{z}{L}(M_{Tx} - m_{Tx} + m_{Bx}) + Px_o\right)$$
$$= m_{By} + \frac{z}{L}\left(M_{Ty} + m_{Ty} - m_{By}\right) - \left(S_{ye}P_{ep}\right) + A_eM_{yy(ep)} \tag{124}$$

$$-(C_{te}+\bar{K})\psi'+u'\left[-m_{Bx}+\frac{z}{L}(M_{Tx}-m_{Tx}+m_{Bx})+Py_0\right]+$$

$$v'\left[m_{By}+\frac{z}{L}(M_{Ty}+m_{Ty}-m_{By})-Px_0\right]-$$

$$\frac{v}{L}(M_{Ty}+m_{Ty}-m_{By})-\frac{u}{L}(M_{Tx}-m_{Tx}+m_{Bx})$$

$$=-M_{Rz}+M_{zp} \tag{125}$$

Equations 123-125 are the materially nonlinear governing differential equations for a steel hollow rectangular section member under axial thrust, biaxial bending moments applied at the top end and uniform torsion.

2.4 Boundary Conditions

Figure 9 shows moment versus rotation relations for the partial rotational end restraints. In this figure, m_p is the spring plastic moment, and θ_p is the plastic end rotation. The m-θ relationship is expressed as:

$$m = k\,\theta \qquad \text{for } \theta < \theta_p \tag{126}$$

$$m = m_p \qquad \text{for } \theta \geq \theta_p \tag{127}$$

in which m is the typical end spring bending moment; θ is the corresponding end slope; and k is the end spring stiffness.

2.4.1 Pinned Boundary Conditions

In this research, the following geometric boundary conditions are considered for pinned end boundary conditions only:

At z = 0:

$$v(0) = 0 \tag{128}$$

$$u(0) = 0 \tag{129}$$

$$\psi'(0) = 0 \tag{130}$$

At z = L:

$$v(L) = 0 \tag{131}$$

$$u(L) = 0 \tag{132}$$

$$\psi(L) = 0 \tag{133}$$

$$\psi'(L) = 0 \tag{134}$$

The natural boundary conditions are as follows:

$$m_{Bx} = 0 \tag{135}$$

$$m_{By} = 0 \tag{136}$$

$$m_{Tx} = 0 \tag{137}$$

$$m_{Ty} = 0 \tag{138}$$

Equations 135 through 138 are used in conjunction with the governing differential equations, namely, Equations 100-102.

2.4.2 Mixed Pinned and Fixed Boundary Conditions

If the member end at z = 0 is flexurally fixed about both x and y axes, then the following geometric boundary conditions need to be enforced in addition to Equations 128-134:

$$v'(0) = 0 \tag{139}$$

$$u'(0) = 0 \tag{140}$$

Furthermore, if the member end at z = L is flexurally fixed about the y-axis, the following condition needs to be used:

$$u'(L) = 0 \tag{141}$$

Using Equations 128 through 141, Equations 123 and 124 can finally be expressed as follows:

At z = 0:

$$B_{xx}\, v''(0) + B_{xy} u''(0) - A_e \psi(0) M_{By0}$$
$$= A_e M_{Bx0} - S_{xe} P + \Gamma_{xr0} + \Gamma_{xp0} \tag{142}$$

$$B_{yx}\, v''(0) + B_{yy} u''(0) - A_e \psi(0) M_{Bx0}$$
$$= -A_e M_{By0} - S_{ye} P + \Gamma_{yr0} + \Gamma_{yp0} \tag{143}$$

At z = L:

$$B_{xx}\, v''(L) + B_{xy} u''(L)$$
$$= -A_e M_{TxL} - S_{xe} P + \Gamma_{xrL} + \Gamma_{xpL} \tag{144}$$

$$B_{yx}\, v''(L) + B_{yy} u''(L) + A_e M_{Rz} v'(L)$$
$$= A_e M_{TyL} - S_{ye} P + \Gamma_{yrL} + \Gamma_{ypL}\,. \tag{145}$$

In Equations 142-145, M_{TxL} is the applied bending moment at the member top end; and M_{Bx0}, M_{By0}, and M_{TyL} are the induced moments.

An iterative finite integral procedure is developed to solve Equations 100-102 for combined loads and is presented in the next section. The finite integral procedure is also used to numerically calculate the induced end moments using Equations 142-145.

2.5 Finite Integral Formulation

Brown and Trahair (60) used the finite integral approach to obtain numerical solutions of linear ordinary differential equations. Usami and Galambos (61) used the finite integral approach in a study of single angle beam-columns. Zhao (13) studied the behavior of biaxially loaded steel beam-columns subjected to high temperature using a finite integral formulation. The finite integral method involves converting dependent variables and their derivatives to the highest-order derivatives in a given system of differential equations. The highest-order derivatives are then substituted into governing differential equations which are then applied at a number of cross sections in the $0 \leq z \leq L$ range. The resulting system of equations for a nonlinear problem is then iteratively solved for the highest derivatives. The final solution for the dependent variables is then numerically calculated through a series of back-substitution. For the problem addressed in this dissertation, the various steps of the finite integral procedure are formulated and are summarized in Appendices A, B, and C. Consequently, Equations 100-102 for the general case of combined axial load, biaxial bending, and torsion take the following finite integral form:

$$[B_{xx}\,[N_1] + A_e P\,[N_3] - \left(1 - \tfrac{z}{L}\right) A_e k_{Bx}[N_8] + \tfrac{z}{L} A_e k_{Tx}\,[N_9]]\{v_i'''\} + [B_{xy}[N_1] - A_e M_{oz}[N_2]]\{u_i'''\} + [B_{x\omega}[N_4] + A_e\{[N_6] + [N_7]\}\,(-M_{By} + \tfrac{z}{L}(M_{By} + M_{Ty}) - Px_o)]\{\phi_i'''\} = \Gamma_x + \Gamma_{xr} + \Gamma_{xp} \quad (146)$$

$$[B_{yx}\,[N_1] + A_e M_{oz}[N_2]]\{v_i'''\} + [B_{yy}[N_1] + A_e P\,[N_3] - \left(1 - \tfrac{z}{L}\right) A_e k_{By}[N_8] + \tfrac{z}{L} k_{Ty}\, A_e[N_9]]\{u_i'''\} + [B_{y\omega}\,[N_4] + A_e\{[N_6] + [N_7]\}\,\left(-M_{Bx} + \tfrac{z}{L}(M_{Bx} + M_{Tx}) + Px_o\right)]\{\phi_i'''\} = \Gamma_y + \Gamma_{yr} + \Gamma_{yp} \quad (147)$$

$$\left[[N_2]\left(-M_{By} + \tfrac{z}{L}(M_{By} + M_{Ty}) - Px_0\right) - \tfrac{[N_3]}{L}(M_{Ty} + M_{By})\right]\{v_i'''\} + \left[[N_2](-M_{Bx} + \tfrac{z}{L}(M_{Bx} + M_{Tx}) + Py_0) - \tfrac{[N_3]}{L}(M_{Tx} + M_{Bx})\right]\{u_i'''\} + [C_{\omega e} - [N_5](C_{te} + \bar{K})]\{\phi_i'''\} = \Gamma_z + \Gamma_{zp} \quad (148)$$

in which $[N_1]$ to $[N_9]$ are defined in Appendix C. Equations 146-148 can be written as the following system of 3N simultaneous nonlinear equations and programmed.

$$[K]\{\Delta'''\} = \{\Gamma\} \tag{149}$$

in which $[K]$ represents global tangent stiffness matrix of the order 3N x 3N; the vector $\{\Delta'''\}$ contains third-order derivatives of u, v, and ψ given as:

$$\{\Delta'''\}^T = \{u_1''' u_2''' \cdots\cdots u_{(N-1)}''' u_{(N)}''' \; v_1''' v_3''' \cdots\cdots v_{(N-1)}''' \; v_{(N)}'''$$
$$\psi_1'''\psi_3''' \cdots\cdots \psi_{(N-1)}'''\psi_{(N)}''' \} \tag{150}$$

The right side vector $\{\Gamma\}$ containing the applied loads and other terms is defined as follows:

$$\{\Gamma\}= \begin{Bmatrix} \{\Gamma_x\} + \{\Gamma_{xr}\} + \{\Gamma_{xp}\} \\ \{\Gamma_y\} + \{\Gamma_{yr}\} + \{\Gamma_{yp}\} \\ \{\Gamma_z\} + \{\Gamma_{zp}\} \end{Bmatrix} \tag{151}$$

Equation 149 is iteratively solved for each set of externally applied loads until the member reaches the state of collapse. The member load-carrying capacity is attained when the determinant of the [K] matrix reaches zero. In the elastic range, the residual and plastic moment vectors are zero; however, they are iteratively computed in the inelastic range. The overall solution procedure is presented in the next section.

2.6 Solution Procedure for Biaxially Loaded Beam-Columns with Applied Torsion

A finite-integral algorithm for solving the nonlinear governing Equation 149 is developed and presented herein. The solution scheme is given below:

1. Define geometric and material properties for the member.
2. Specify external loads.
3. Formulate $\{\Gamma\}$ vector.
4. Generate the global member stiffness matrix [K].
5. Solve for $\{\Delta'''\}$ using Equation 149.
6. Using back substitutions, calculate $\{\Delta''\}$, $\{\Delta'\}$, and $\{\Delta\}$ using the finite integral expressions in Appendices A, B and C, and $\{\epsilon_o\}$ using Equation 54.
7. Discretize each of the N cross sections along the member length, and compute the total elemental area normal strain $\epsilon_{i,j}$ and normal stress $\sigma_{i,j}$ values, where i, j refer to elemental area coordinate locations in the x and y coordinate system.

8. Compute $\tau_{i,j}$ and $\sigma_{pi,j}$ while invoking von Mises yield criterion for each of the N cross sections, where σ_p is given by $\sigma_p = \sqrt{\sigma_Y{}^2 - \tau^2}$.
9. If $|\sigma_{i,j}| < |\sigma_{pi,j}|$ for all cross sections of the member, the member is elastic. In this case, go to Step 10; otherwise, go to Step 12.
10. Increase the external loads, and go to Step 3.
11. If |[K] |is close to zero, go to Step 13; otherwise, go to Step 10.
12. Calculate inelastic coefficients and go to Step 3 if the current {Δ} vector is within $\mp$ 0.01 percent of the previous {Δ} vector and if the external and internal loads are also in equilibrium within $\mp$ 0.01; otherwise, recompute inelastic coefficients, and go to Step 3.
13. Stop.

The above iterative algorithm is programmed to obtain numerical results presented in Chapter 4. A complete listing of the program is given in Appendix D.

2.7 Load Paths

The following different load paths are adopted for the torsionally loaded beam-columns.

P: The axial load P is applied incrementally until the load carrying capacity of the member is reached.

U: The uniaxial end moment M_{Tx} is applied incrementally until the strength limit is reached.

B: The biaxial end moments M_{Tx} and M_{Ty} are applied incrementally until the member fails.

T: The torsional moment T is applied incrementally until the failure occurs.

TP: The axial load P is first applied incrementally and then held constant, followed by gradually increasing torsional moment until the load carrying capacity of the member is reached.

UT: The uniaxial end moment M_{Tx} is first applied incrementally and then held constant, followed by gradually increasing torsional moment until the strength limit is reached.

BT: The biaxial end moments M_{Tx} and M_{Ty} are first applied incrementally and then held constant, followed by gradually increasing torsional moment until the member fails.

PUT: The axial load P and uniaxial end moment M_{Tx} are first applied incrementally and then held constant, followed by gradually increasing torsional moment until the failure occurs.

PBT: The axial load P and biaxial end moments M_{Tx} and M_{Ty} are first applied incrementally and then held constant, followed by gradually increasing torsional moment until the load carrying capacity of the member is reached.

TP: The torsional moment T corresponding to the load-carrying capacity obtained in T are first applied incrementally and then held constant, followed by gradually increasing axial load P until the failure occurs.

TU: The torsional moment T corresponding to the load-carrying capacity obtained in T are first applied and then held constant, followed by gradually increasing uniaxial end moment M_{Tx} until the member fails.

TB: The torsional moment T_P corresponding to the load-carrying capacity obtained in T is first applied and then held constant, followed by gradually increasing biaxial end moments M_{Tx} and M_{Ty} until the load-carrying capacity is reached.

TBP: The maximum torsional moment T_P obtained in T and 0.7 of the biaxial bending moments M_{Tx} and M_{Ty} obtained in TB are first applied and then held constant, followed by gradually increasing P until the load-carrying capacity is reached.

CHAPTER 3

EXPERIMENTAL INVESTIGATION

This chapter presents the outcome of an experimental study of the behavior of steel beam-columns with applied torsion up to the collapse condition. The objective of the experimental study is not only to study the member behavior but also to validate the theoretical study presented in this dissertation.

3.1. Test Equipment and Procedure

Razzaq and McVinnie (10) developed an apparatus for testing biaxially loaded steel beam-columns. A similar apparatus was used by both Sanders (62) and Zhao (13) at Old Dominion University. The axial load test setup is shown in Figure 10. The figure shows lower and upper end gimbals at the ends of the test specimen as well as a steel casing with Hydraulic Jack A and Load Cell A. The lower end gimbal is shown in Figure 11. It consists of a four-sided steel gimbal outer box. The gimbal inner box is supported by a pair of inner bearings and a shaft along the x-axis. The inner bearings are housed in two opposite walls of the gimbal outer box. The opposing walls of the gimbal outer box have a pair of shafts and outer bearings along the y-axis. As shown in Figure 12, the lower end gimbal is attached to Steel Plate 1, which has a gliding steel chamber below it. The gliding steel chamber rides on the outer surface of a steel casing that houses a 50-kip capacity compression Load Cell A mounted on Hydraulic Jack A. The steel casing is welded to a floor steel plate which in turn is anchored to the laboratory test bed. The upper end gimbal is identical to the lower end gimbal; however, it is mounted in an upside down position. The upper end gimbal is attached to a steel cross-beam which is bolted at its ends to steel columns. The end columns are anchored to the laboratory test bed thus forming a large reaction frame while the cross-beam supports the upper end gimbal. The axial load is applied using Hydraulic Jack A and measured with Load Cell A. Load Cell A pushes Steel Plate 1 which in turn transmits the axial load to the lower gimbal outer box through a pair of outer bearings and shafts. The load is finally transferred to the test specimen through the gimbal inner box. The combined axial and bending test setup is shown in Figure 13.

The bending moment is applied at the top end of the member by means of a moment arm bolted to the upper gimbal inner box as shown in Figure 14. The moment arm is a 1.0 x 2.0 x 24.0 in. solid rectangle steel section. Load W is applied through two 0.75-in. diameter tie rods. These rods are 75 inches long each and separated by 12-inch long 0.5-in thick steel plates forming a closed ring at the top and bottom. By means of ball and socket arrangement, the Top Plate B sits on the machined arm. Using a similar arrangement, the Bottom Plate B is attached to a 5-kip capacity compression Load Cell B. Load Cell B is mounted on Hydraulic Jack B, which is bolted to a small reaction frame in an upside down position as illustrated in Figure 15. The small steel reaction frame is mounted to the laboratory test bed. Load W can finally be produced by manually controlling Hydraulic Jack B. The uniaxial bending moment is applied by adopting an angle of 0° between the moment arm and the x axis of the gimbal as shown in Figure 16(a). The biaxial bending moments M_x and M_y are generated by applying a resultant bending moment M about the x' axis shown in Figure 16(b). With an angle $\beta = 45°$, the biaxial bending moments M_{Tx} and M_{Ty} are each equal to M (sin45°).

The combined axial, bending and torsion test setup is shown in Figure 17. The torsional moment is applied at the bottom end by means of an eccentric force F applied with Hydraulic Jack C and transmitted to the member by means of a chain shown more clearly in Figure 18. The bottom-end gimbal rests on a steel plate as shown in Figure 19 and rides on solid steel spheres arranged in a circle as schematically shown in Figure 20. The torsional moment value equals F times the eccentricity e. Figure 21 shows the schematic of the apparatus modified to include torsional loading capability. The modified Steel Plate 1 and the additional Steel Plate 2 are shown in Figure 22. A shaft is welded to Steel Plate 2 that fits into the center of the circular bearing on Steel Plate 1 as shown in Figure 23. The shaft connects the two plates so that Steel Plate 2 can rotate freely on Steel Plate 1.

A 1.5 x 1.5 x $\frac{1}{8}$ in. hollow square steel section is used for the experimental study. As schematically shown in Figure 24, each test member has a clear length of 34 inches. However, the distance between the centerlines of the end gimbals, that is, including both the actual member length and the solid portions of the end fixtures, is 37.75 inches, which is the length adopted in the analysis. The axial load and both bending and torsional moments are applied slowly and incrementally with regular stops to manually record the

output data in the elastic range. However, in the inelastic range deflection increments are used rather than load increments. The member load-carrying capacity is observed when the applied load starts dropping while at the same time the deformations keep increasing.

3.2 Material properties

Based on ASTM tension tests, the following values of Young's modulus, E, and the normal yield stress, σ_Y, for the steel specimens were obtained:

$E = 29,599$ ksi

$\sigma_Y = 58.999$ ksi

The shear modulus, G, and the shear yield stress, τ_Y, for the steel were found using a torsion test conducted on a segment of a 1.5x1.5x0.125 in. hollow square section. The values were found to be as follows:

$G = 11{,}200$ ksi

$\tau_Y = 32.301$ ksi

In this dissertation, the above material properties mentioned are used in the analysis.

3.3 Experimental Results

A total of 60 tests are conducted on a member with hollow square sections with pinned boundary conditions and a combination of pinned and fixed boundary conditions.

3.3.1 Yield Limit Loading Test Results

The yield limit loading is defined as the set of external loads that cause initiation of yielding at any point in a member. For yield limit tests, the member boundary conditions are given in Section 2.4.1. The yield load values used are dimensionless and are defined as follows:

$$p = \frac{P}{P_c} \tag{152}$$

$$m_x = \frac{M_x}{M_{cx}} \tag{153}$$

$$m_y = \frac{M_y}{M_{cy}} \tag{154}$$

$$t = \frac{T}{T_c} \tag{155}$$

where:

$$P_c = A(\sigma_Y - \sigma_r) \tag{156}$$

$$M_{cx} = S_x(\sigma_Y - \sigma_r) \tag{157}$$

$$M_{cy} = S_y(\sigma_Y - \sigma_r) \tag{158}$$

$$T_c = 2A_E t(\tau_c) \tag{159}$$

$$\sigma_c = (\sigma_Y - \sigma_r) \tag{160}$$

$$\tau_c = \sqrt{\frac{(\sigma_y^2 - \sigma_r^2)}{3}} \tag{161}$$

In these expressions, P_c, M_{cx}, M_{cy} and T_c are the yield limit axial load, bending moment about the x and y axes, and torsional moment, respectively; S_x and S_y are sections of modulie about the x and y axes, respectively; the residual stress term σ_r is defined in Equation 5; σ_c is the yield limit normal stress; τ_c is the yield limit shear stress. In the present study, σ_r is taken as σ_{rc} in Equation 156. However, σ_r is taken as σ_{rt} in Equations 157 through 159. The dimensionless axial normal strain is expressed as:

$$e = \frac{(\epsilon_{a1,2} \pm \epsilon_r)}{\epsilon_Y} \tag{162}$$

In Equation 162, $\epsilon_{a1,2}$ is the normal strain due to the applied load and represents ϵ_{a1} and ϵ_{a2}, respectively; ϵ_r and ϵ_Y are defined in Equations 1 and 2. In Equation 162, the minus sign is used when only an axial compressive load is applied in which case $\epsilon_r = -\epsilon_{rc}$. However, when a bending moment is applied, the positive sign is used in which case $\epsilon_r = \epsilon_{rt}$. Also, with reference to Figure 16c showing strain gauge locations SG1 and SG2, the following specific definitions of e are needed.

For the Axial compressive test:

$$e_1 = \frac{(\epsilon_{a1} + 0.2\epsilon_Y)}{\epsilon_Y} \tag{163}$$

$$e_2 = \frac{(\epsilon_{a2} + 0.2\epsilon_Y)}{\epsilon_Y} \tag{164}$$

where ϵ_{a1} and ϵ_{a2} are the midspan strains measured with gages SG1 and SG2, respectively. If corner strains are measured with reference to Figure 4 showing the corner residual stresses, the following expressions of e are needed:

$$e_3 = \frac{(\epsilon_{a3} + 0.5\epsilon_Y)}{\epsilon_Y} \tag{165}$$

$$e_4 = \frac{(\epsilon_{a4} + 0.5\epsilon_Y)}{\epsilon_Y} \tag{166}$$

where ϵ_{a3} and ϵ_{a4} are the corner strain values and $0.5\epsilon_Y$ is the normal residual strain. The following symbols are used for defining the load types:

P = Axial load

U = Uniaxial bending moment

B = Biaxial bending moment

T = Torsional moment

Table 1 presents dimensionless yield loads for Tests 1 through 4. The first column in this table defines the load type for these tests named as PR1, UR1, BR1 and TR1, respectively. The first symbol in these names represents the load type, and the last two symbols, namely R1, represent flexurally pinned boundary conditions. The second column of the table shows the section orientation. For the PR1, UR1 and TR1 tests, the end plate orientation shown in Figure 16(a) is adopted. For the BR1 test, the end plate orientation is shown in Figure 16(b). The third column shows the dimensionless axial load. The dimensionless bending moment and torsional moment are shown in the fourth and fifth columns, respectively. The mid-span deflections are shown in the sixth and seventh columns. Finally, the angle of twist is shown in the last column. The angle of twist is measured at the bottom end of the member. The dimensionless yield load values for tests PR1, UR1, BR1 and TR1 are 0.604, 0.992, 0.686, and 0.980, respectively.

Table 2 summarizes nine combined axial load, biaxial bending and torsion test results named as PBTR11 through PBTR19. These tests were performed by first applying the axial load, followed by biaxial bending moments, and followed by a gradually increasing torsional moment up to the yield limit while the axial load and bending moments are kept constant. In this table, the second column shows the dimensionless axial load. The third and fourth columns show the dimensionless bending moment about the x-axis and y-axis, respectively. The yield load values for dimensionless torsional moment t defined in Equation 155 are found to be in the range from 0.296 to 0.707. These yield loads are 27.88% to 69.76% lower than the t value for torsional loading only represented by TR1 in Table 1. The results in Table 2 show that the presence of p, m_x, and m_y has a pronounced effect in reducing the t value at yield limit.

Table 3 presents nine combined axial load, uniaxial bending and torsion test results named as PUTR11 through PUTR19. These tests were carried out by first applying the axial load, followed by uniaxial bending moment, and followed by a gradually increasing torsional moment up to the yield limit while the axial load and uniaxial bending moment

are held constant. The yield load values for dimensionless torsional moment t ranged from 0.359 to 0.820. The t values for test PUTR1 are found to be 18.13% to 66.31% lower than the t value of TR1. However, the t values for test PUTR1 are 6.67% to 12.05% higher than those of PBTR1. The results in Table 3 show that the presence of p and m_x for PUTR1 has a lesser effect in reducing the t value at yield limit than the presence of p, m_x, and m_y for PBTR1.

Table 4 presents nine combined biaxial bending and torsion test results named as BTR11 through BTR19. These tests were conducted by first applying the resultant biaxial bending moment and holding it constant. This was followed by a gradually increasing torsional moment up to the yield. The yield load values for t values are found to be in the range from 0.369 to 0.841, which are, respectively, 14.14% to 62.39% lower than the t value of TR1. However, the t values for test BTR1 are 2.99% to 10.42% higher than those of PUTR1. Furthermore, the t values for test BTR1 are 13.61% to 19.61% higher than those of PBTR1. In this table, the results show that the presence of m_x and m_y for BTR1 has a lesser effect in reducing the t value at yield limit than those of PUTR1 and PBTR1.

Table 5 shows nine uniaxial bending and torsion test results named as UTR11 through UTR19. These tests were performed by first applying the uniaxial bending moment and held constant, and they were followed by a gradually increasing torsional moment up to the yield limit. The yield load values for t are found to be in the range from 0.388 to 0.924. The t values for test UTR1 were 5.75% to 60.42% lower than the t value of TR1. However, the t values for test UTR1 were 0.86% to 10.46% higher than those of BTR1. Also, the t values are 9.38% to 15.67% higher than those of PUTR1. Furthermore, the t values for test UTR1 were 20.30% to 23.60% higher than those of PBTR1. The results in Table 5 show that the presence of m_x has a lesser effect in reducing the t value at yield limit than those of PBTR1, PUTR1 and BTR1.

Table 6 presents nine combined axial load and torsion test results named as PTR11 through PTR19. The t values for test PTR1 ranged from 0.369 to 0.869. These tests were conducted by first applying the axial load and kept constant; this was followed by a gradually increasing torsional moment up to the yield limit. The t values were 11.34% to 62.33% lower than that of TR1. Also, the t values for test PTR1 were 4.83% to 8.69% lower than those of UTR1. However, the t values for test PTR1 were 0.14% to 4.81%

higher than those of BTR1. Furthermore, the t values for test UTR1 were 4.84% to 10.55 higher than those of PUTR1. Finally, the t values for PR1 were 13.80% to 19.72% higher than those of PBTR1. The results in Table 6 show that the presence of p for PTR1 has a lesser effect in reducing the t values than those of BTR1, PUTR1 and PBTR1. However, the presence of m_x for test UTR1 has a lesser effect in reducing the t value at the yield limit than the presence of p for test PTR1.

Table 7 summarizes the dimensionless torsional moment for the PBTR1, PUTR1, BTR1, UTR1, and PTR1 tests. The dimensionless torsional moment t values for tests PBTR1, PUTR1, BTR1, UTR1, and PTR1 were 0.756, 0.841, 0.953, 0.999, and 0.935, respectively. In this table, the results show that PBTR1 and PUR1 have the lowest and highest dimensionless torsional moment t values, respectively.

Figure 25 shows dimensionless axial compressive load p versus midspan strain e relation for test PR1. In this figure, the horizontal ordinate represents the dimensionless axial strain, and vertical ordinate represents the dimensionless applied axial compressive load. As seen in this figure, the elastic yield point is in the nonlinear region due to the presence of initial out-of-straightness and p-delta effects. The elastic yield point for test PR1 is determined based on yielding initiated at midspan.

Figure 26 shows dimensionless uniaxial bending moment m versus midspan strain e curve for test UR1. In this figure, the horizontal axis represents the dimensionless axial strain, and vertical axis represents the dimensionless applied uniaxial bending moment. As seen in Figure 26, the curve follows a linear path up to the elastic yield point. Figure 27 shows dimensionless biaxial bending moment m versus midspan strain e relation for test BR1. In this figure, the curve is also linear up to the elastic yield point. The elastic yield point for tests UR1 and BR1 are determined based on yielding initiated at midspan. However, the maximum strain values at the member top end are well beyond the yield strain value for ϵ_Y when yielding initiates at midspan. The maximum strain value at the top end was theoretically found to be at one of the cross-sectional corners or middle of the side

The angle of twist ψ versus dimensionless torsional moment t curve for test TR1 is shown in Figure 28. In this figure, the horizontal axis represents the angle of twist, and vertical ordinate represents the dimensionless applied torsional moment. As seen in Figure 28, the elastic yield point is clearly in the linear region. The respective angle of twist ψ

versus dimensionless torsional moment t relations for tests PBTR1, PUTR1, BTR1, UTR1 and PTR1 are shown in Figures 29-33. As seen in these figures, the elastic yield points are clearly in the nonlinear region due to the p-delta effects.

3.3.2 Ultimate Strength Test Results

The member boundary conditions given in Section 2.4.2 are adopted for the ultimate strength tests. Herein, the following symbols are used for defining the flexure boundary conditions:

R44 = Bottom end fixed; pinned about x, and fixed about y at top end

R41 = Bottom end fixed and top end pinned

R11 = Both bottom and top ends pinned

All maximum load values used are dimensionless and defined as follows:

$$p^* = \frac{P^*}{P_c} \tag{167}$$

$$m_x^* = \frac{M_x^*}{M_{cx}} \tag{168}$$

$$m_y^* = \frac{M_y^*}{M_{cy}} \tag{169}$$

$$t^* = \frac{T^*}{T_c} \tag{170}$$

in which P^*, M_x^*, M_y^*, and T^* are the applied axial load bending moment about the x and y axes and torsional moment, respectively; and P_c, M_{cx}, M_{cy} and T_c are given in Equations 156-159, respectively.

Table 8 presents dimensionless maximum loads for Tests 1 through 4. In this table, the first column defines the load type for these tests named as PR44, UR44, BR44, and TR44, respectively. The maximum load values for tests PR44, UR44, BR44, and TR44 are 0.848, 2.473, 1.792, and 1.103, respectively. The ratios between the maximum loads PR44, UR44, BR44, and PR44 and yield loads PR1, UR1, BR1, and TR1 presented in Table 1 are 1.40, 2.49, 2.61 and 1.12, respectively.

Figure 34 shows dimensionless axial compressive load p^* versus midspan strain e relation for test PR44. It is observed that the curve follows a nonlinear path due to a combination of p-delta effects and inelastic action. Figures 35 and 36 show dimensionless moment m^* versus midspan strain e curves for tests UR44 and BR44, respectively. As seen in these figures, the curve is linear up to the yield limit and follows a nonlinear path

thereafter. The angle of twist ψ versus dimensionless torsional moment t^* relation for test TR44 is shown in Figure 37. It is observed that the curve also follows a linear path initially in the elastic range; however, it becomes nonlinear thereafter.

Table 9 presents dimensionless maximum loads for Tests 1 through 6. The first column in this table defines the load type for these tests named as TPR44, TUR44, TBR44, TBR41, TBPR44 and TBPR41, respectively. The dimensionless maximum load values for tests TPR44, TUR44, TBR44, TBR41, TBPR44 and TBPR41 are 0.478, 1.719, 0.935, 0.935, 0.269 and 0.130, respectively. The results in Table 9 show that a member can still carry a load even after its full plastification due to torsion has occurred.

The midspan deflection v versus dimensionless axial load p^* curve for test TPR44 is shown in Figure 38. This test is performed by first applying the torsion until the member full plastification due to torsion is attained and kept constant, and it is followed by a gradually increasing axial load up to the maximum load. Figure 39 shows dimensionless axial p^* load versus midspan strain e for test TPR44. The p^* value for test TPR44 is 43.55% lower than the p^* value of PR44. It can now be concluded that a member under the combined action of axial and torsion loading can still carry an axial load value of 20.82% lower than the p value of PR1 presented in Table 1 after its full plastification due to torsion has occurred.

The midspan deflection u versus dimensionless uniaxial bending moment m^* curve for test TUR44 is shown in Figure 40. For this test, the torsion is first applied until the member full plastification due to torsion is reached and held constant and is followed by a gradually increasing uniaxial bending moment up to the maximum load. Figure 41 shows dimensionless uniaxial bending moment m^* versus midspan strain e curve for test TUR44. The m^* value for test TUR44 is 30.47% lower than the m^* value of UR44. It can now be concluded that a member subject to combined uniaxial bending moment and torsion can still carry up to a bending moment value of 42.31% higher than the m value of UR1 presented in Table 1 after its full plastification due to torsion is reached.

The respective midspan deflection versus dimensionless resultant biaxial bending moment curves for tests TBR44 and TBR41 are shown in Figures 42 and 43. For these tests, the torsion is first applied until the member full plastification due to torsion occurs and is held constant; this is followed by a gradually increasing biaxial bending moment up

to the maximum load. The m^* values for tests TBR44 and TBR41 are found to be the same, which is 47.82% lower than the m^* value of BR44. Figures 44 and 45 show the dimensionless resultant biaxial bending moment m^* versus midspan strain e curves for tests TBR44 and TBR41, respectively. It can now be concluded that a member subjected to torsional moment and biaxial bending moments can still carry a bending moment of 26.66% higher than the m value of UR1 presented in Table 1 after its full plastification due to torsion is attained.

The respective midspan deflection versus dimensionless maximum axial load for tests TBPR44 and TBPR41 are shown in Figures 46 and 47. For these tests, the torsion is first applied until the member full plastification due to torsion is reached and held constant, followed by applying 0.7 of the maximum biaxial bending moments obtained in tests TB44 and TB41 and also held constant. Finally, this is followed by a gradually increasing axial load up to the maximum load. Figures 48 and 49 show dimensionless axial load p^* versus midspan strain e for TBPR44 and TBPR41, respectively. The p^* value for tests TBPR44 and TBPR41 are 68.30% and 84.70% lower than the p^* value of PR44, respectively. The p^* value for tests TBPR44 and TBPR41 are 55.54% and 78.51% lower than the p value of PR1 presented in Table 1, respectively. It can now be concluded that a member subject to plastic torsional moment and 0.7 of the plastic biaxial bending moments can still carry a significant axial load even after its full plastification due to torsion has occurred. The p^* value for test TBPR44 is found to be 2.07 times larger than the p^* value of TBPR41.

The results for tests PBTR11 and PBTR44 are summarized in Table 10. The dimensionless torsional moment t^* values for test series PBTR11 are 0.996 and 0.881, respectively. The dimensionless torsional moment t^* values for test series PBTR44 are 0.927 and 0.814, respectively. The respective angle of twist ψ versus dimensionless torsional moment t^* relations for test series PBTR11 and PBTR44 are shown in Figures 50 and 51. For $p^* = 0.2$ and $m_x^* = m_y^* = 0.2$, the t^* value for test PBTR11 is 9.66% lower than the t^* value of TR44. For $p^* = 0.5$ and $m_x^* = m_y^* = 0.5$, the t^* value for test PBTR11 is 20.17% lower than the t^* value of TR44. For $p^* = 0.2$ and $m_x^* = m_y^* = 0.2$, the t^* value for test PBTR44 is 15.91% lower than the t^* value of TR44. For $p^* = 0.5$ and $m_x^* = m_y^* = 0.5$, the t^* value for test PBTR44 is 26.23% lower than the t^* value of TR44. In the laboratory,

it is observed that once the member axial or flexure strength is reached during the test, it cannot carry any more load at all.

3.3.3 Warping Strain Measurements

The strain gage locations for measuring warping strains is shown in Figure 52. Four strain, gauges are used at the edges to measure the warping strain values. Two of those are placed at a distance of two inches below the top end, and the other two are placed at the midspan as schematically shown in Figure 53. The results for tests TR44 and TBPR41 are presented in Table 11. In this table, the first column defines the normal strains named as ϵ_1, ϵ_2, ϵ_3, and ϵ_4, respectively. The second column in this table shows the maximum normal strain values. The third column of Table 11 shows the ratio between the maximum normal strain and yield normal strain. For test TR44, the percentage maximum warping strain values for ϵ_1, ϵ_2, ϵ_3, and ϵ_4 are 1.35%, 3.06%, 1.35%, and 5.52%, respectively. For test TBPR41, the percentage warping strain values obtained under the applied plastic torsional moment for ϵ_1, ϵ_2, ϵ_3, and ϵ_4 are 1.10%, 3.11%, 1.81%, and 6.82%, respectively. The results for PBTR44 are illustrated in Table 12. For PBTR44 with $p^* = m^* = 0.4$, the percentage maximum warping strain values for ϵ_1, ϵ_2, ϵ_3, and ϵ_4 are 0.40%, 1.10%, 1.55%, and 3.81%, respectively. For TBPR44 with $p^* = m^* = 0.6$, the percentage warping strain values for ϵ_1, ϵ_2, ϵ_3, and ϵ_4 are 1.51%, 4.26%, 2.21%, and 5.22% , respectively. It can now be concluded that the warping or longitudinal strains due to applied torsional moments are negligible.

CHAPTER 4

THEORY VERSUS EXPERIMENTS

This chapter presents numerical results based on the theoretical formulation presented in Chapter 2 as well as a comparison of theoretically predicted load-deflection and load-strain relations. Also, presented herein is a comparison of the yield and ultimate loads.

4.1 Yield Limit Analysis

The member initial uniaxial and biaxial crookedness functions are taken as L/1000. The residual stresses σ_{rt} and σ_{rc} values are taken as $0.5\sigma_y$ and $-0.2\sigma_y$. The following spring constants are adopted herein:

k_1 = 0.0 kip-in/rad

k_2 = 13,000 kip-in/rad

k_3 = 24,000 kip-in/rad

k_4 = 1 x 10^{10} kip-in/rad

in which k_1 = 0.0 kip-in/rad represents the nearly pinned condition, k_2 = 13,000 kip-in/rad and k_3 = 24,000 kip-in/rad represent two different degrees of partial restraints and k_4 = 1 x 10^{10} kip-in/rad simulates a nearly fixed condition. The spring constants are represented as follows:

R1 = k_1

R2 = k_2

R3 = k_3

R4 = k_4

The influence of p-delta effects, initial residual stress, bending shear stress, rotational end restraints, and load sequences on the yield torsional moment of torsionally loaded beam-columns is studied, respectively.

4.1.1 Combined Axial Load, Biaxial Bending and Torsion

Table 13 presents magnitude of p-delta, bending shear stress, and initial residual stress effects on the yield torsional moment of PBTR1. In this table, T_B and T_r represent the torsional moment for bending shear stress and residual stress, respectively. The fifth and

sixth columns in this table show the p-delta effects named as Pu and Pv. The seventh column of Table 13 shows the ratio between the torsional moment with bending shear stress and yield torsional moment for PBTR1. Finally, the last column shows the ratio between the torsional moment with residual stress and yield torsional moment for PBTR1. The calculated Pu and Pv values ranged from 0.02 k-in to 1.64 k-in and from 0 to 0.36 k-in, respectively. The results show that the predicted yield torsional moment decreased by 6.64% to 15.69% in the presence of initial residual stresses. However, in the presence of bending shear stresses, the predicted yield torsional moment increased by 3.24%. It is also found that the p-delta and initial residual stresses both have significantly greater effects on the yield torsional moment than does the bending shear stress. Table 14 presents magnitude of flexural end restraint effects on the yield torsional moment for PBTR1. In this table, T_{R2}, T_{R3} and T_{R4} represent the yield torsional moment for spring constants R2, R3 and R4 , respectively. The fifth column of this table shows the ratio between T_{R2} and the yield torsional moment for PBTR1. The sixth column in Table 14 shows the ratio between T_{R3} and the yield torsional moment for PBTR1. Finally, the ratio between T_{R4} and the yield torsional moment for PBTR1 is shown in the last column. It is found that the predicted yield torsional moment has decreased by 7.47% to 14.62% in the presence of R2. Also, in the presence of R3 the predicted yield torsional moment has decreased by 4.38% to 11.78%. Furthermore, the predicted yield torsional moment has decreased by 2.58% to 8.08% in the presence of R4. It can now be concluded that the flexural end restraints R2, R3, and R4 result in a substantial decrease in the yield torsional moment of PBTR1.

4.1.2 Combined Axial Load, Uniaxial Bending and Torsion

Table 15 presents magnitude of p-delta, bending shear stress, and initial residual stress effects on the yield torsional moment of PUTR1. In this table, the calculated p-delta values Pu ranged from 0.02 k-in to 1.64 k-in. It is found that the predicted yield torsional moment increased by 2.93% in the presence of bending shear stresses. However, the predicted yield torsional moment decreased by 9.74% to 20.32% in the presence of residual stresses. It can now be concluded that that the effects of p-delta and initial residual stresses are more pronounced on the yield torsional moment than the effect of bending shear stress. The magnitude of flexural end restraint effects on the yield torsional moment for PUTR1 are presented in Table 16. It is found in Table 16 that the predicted yield torsional moment

decreased by 8.46% to 16.65% in the presence of R2. It is also found that the predicted yield torsional moment decreased by 5.71% to 14.16% in the presence of R3. Furthermore, the predicted yield torsional moment decreased by 3.04% to 9.09% in the presence of R4. It can now be concluded that flexural end restraints R2, R3 and R4 have significant effects on decreasing the yield torsional moment for PUTR1.

4.1.3 Combined Biaxial Bending and Torsion

Table 17 presents bending shear stress and initial residual stress effects on the yield torsional moment of BTR1. The results in this table show that the predicted yield torsional moment has increased by 2.60% in the presence of bending shear stresses. However, the predicted yield torsional moment decreased by 11.87% to 23.19% in the presence of residual stresses. It can therefore be concluded that the residual stresses have major effects on decreasing the yield torsional moment for BTR1. The magnitude of flexural end restraint effects on the yield torsional moment for BTR1 is illustrated in Table 18. It is found that the predicted yield torsional moment decreased by 14.23% to 25.29% in the presence of R2. The predicted yield torsional moment also decreased by 12.02% to 23.40%. Furthermore, the predicted yield torsional moment decreased by 12.45% to 23.95% in the presence of R4. It can therefore be concluded that flexural end restraints R2, R3 and R4 have minor effects on decreasing the yield torsional moment for BTR1.

4.1.4 Combined Uniaxial Bending and Torsion

Table 19 presents bending shear stress and initial residual stress effects on the yield torsional moment of UTR1. In this table, the results show that the calculated yield torsional moment increased by 2.48% in the presence of bending shear stresses. However, the calculated yield torsional moment decreased by 22.36% to 35.33% in the presence of residual stresses. It can now be concluded that the residual stresses have pronounced effects on decreasing the yield torsional moment for UTR1. Table 20 presents magnitude of flexural end restraint effects on the yield torsional moment for UTR1. Results show that the predicted yield torsional moments decreased by 24.41% to 37.06% in the presence of R2. Also, in the presence of R3 the predicted yield torsional moment decreased by 22.59% to 35.57%. Furthermore, the predicted yield torsional moment decreased by 23.22% to

36.23% in the presence of R4. It can therefore be concluded that the flexural end restraints R2, R3 and R4 have minor effects on decreasing the yield torsional moment for UTR1.

4.1.5 Combined Axial Load and Torsion

Table 21 presents the magnitude of p-delta and initial residual stress effects on the yield torsional moment of PTR1. It is found that the calculated p-delta values *Pu* ranged from 0 to 0.50 k-in. It is also found that the yield torsional moment decreased by 13.74% to 26.79% in the presence of residual stresses. The magnitude of flexural end restraint effects is summarized in Table 22. The results in this table show that the predicted yield torsional moment decreased by 1.89% to 7.53% in the presence of R2. Also in this table, the predicted yield torsional moment decreased by 1.90% to 7.55% in the presence of R3. Furthermore, the predicted yield torsional moment decreased by -0.18% to 4.06% in the presence of R4. It can now be concluded that both the residual stresses and flexural end restraints R2, R3 and R4 have pronounced effects on decreasing the yield torsional moment for PTR1.

4.2 Comparisons of Experimental and Theoretical Results at Yield Limit

Tables 23-27 present the theoretical and experimental results for PBTR1, PUTR1, BTR1, UTR1 and PTR1, respectively. In these tables, the fourth column shows the predicted dimensionless torsional moment. The fifth column of these tables shows the experimental dimensionless torsional moment. Finally, the sixth column shows the ratio between the predicted and experimental results. For PBTR1, the ratios between the predicted and experimental torsional moments ranged from 1.04 to 1.09. Also for PUTR1, the ratios between the results from the theory and experiment ranged from 1.02 to 1.09. Furthermore, the ratios between predicted and experimental torsional moments are found to be in the range from 1.06 to 1.12 for BTR1. The ratios between the predicted and tested results are also found to be in the range from 1.06 to 1.10 for UTR1. Finally, the ratios between predicted and experimental results ranged from 1.05 to 1.10 for PTR1. It is found that the predicted results are in good agreement with the experimental results.

Table 28 shows the magnitude of p-delta effects for PBTR1, PUTR1, BTR1, UTR1 and PTR1. It is found that the p-delta effects reduce the yield torsional moments for PBTR1, PUTR1, and PTR1. The maximum p-delta values are obtained for PBTR1 and PUTR1, and

the minimum p-delta value is obtained for PTR1. Table 29 presents the magnitude of beading shear stress effects for PBTR1, PUTR1, BTR1, UTR1, and PTR1. It is found that the beading shear stress does not have a significant effect on the yield torsional moment capacity. The maximum bending shear stress value is obtained for PBTR1, and the minimum bending shear stress value is obtained for PTR1. The magnitude of residual stress effects for PBTR1, PUTR1, BTR1, UTR1, and PTR1 are presented in Table 30. It is found that the effect of the initial residual stress can reduce the yield torsional moment capacity. The residual stresses are maximum and minimum for PTR1 and UTR1, respectively.

Tables 31-33 summarize the magnitude of flexural end restraint effects for PBTR1, PUTR1, BTR1, UTR1, and PTR1, respectively. The results show that the effects of flexural end restraints can reduce the yield torsional moment capacity. The partial end restraints are maximum and minimum for PTR1 and UTR1, respectively.

Figure 54 shows the dimensionless axial compressive load versus midspan strain relations for PR1. In this figure, the symbol "Theo" represents the predicted values from theoretical analysis. The curves are only matching in the linear region. However, at the yield point the strain value from the experiment is 5.66% higher than that of the predicted value.

Figures 55 and 56 show the dimensionless bending moment versus midspan strain curves for the UR1 and BR1 tests, respectively. For these figures, the curves are perfectly matching at the yield point. Figure 57 shows the angle of twist versus dimensionless torsional moment relations for TR1. The two curves are perfectly matching in the linear region. However, the experimental yield torsional moment and angle of twist are 1.55% and 1.62% higher than those of the predicted values.

Figures 58-62 show the dimensionless interaction curves for PBTR1, PUTR1, BTR1, UTR1, and PTR1, respectively. The horizontal axis represents the dimensionless normal stress, and the vertical axis represents the dimensionless shear stress. It is observed that the predicted yield interactions are almost the same as those of yield experimental curves.

4.3 Inelastic Stiffness Degradation Curves

A total of nine nodes along the length L was found to be adequate for the study presented herein. Node 9 or top end cross-section is found to be the most stressed cross-section. The inelastic member behavior is explained in the following sub-sections for a

variety of applied load types. All results are given in the dimensionless forms as follows. The dimensionless determinant of the member inelastic stiffness is defined as:

$$d = \frac{D}{D_0} \tag{171}$$

in which D is the determinant of the inelastic stiffness matrix given in Equation 149 and D_0 is the value of D at zero loading. The dimensionless axial compressive load is defined as:

$$p_{in} = \frac{P_{in}}{P_c} \tag{172}$$

where P_{in} is the applied axial load and P_c is given in Equation 156.

The dimensionless bending moment about the x-axis is defined as:

$$m_{x(in)} = \frac{M_{x(in)}}{M_{cx}} \tag{173}$$

In Equation 173, $M_{x(in)}$ is the applied bending moment about the x-axis and M_{cx} is given in Equation 157. The dimensionless bending moment about the y-axis is defined as:

$$m_{y(in)} = \frac{M_{y(in)}}{M_{cy}} \tag{174}$$

in which $M_{y(max)}$ is the applied bending moment about the y-axis and M_{cy} is given in Equation 158. The dimensionless torsional moment is defined as:

$$t_{in} = \frac{T_{in}}{T_c} \tag{175}$$

where T_{in} is the applied torsional moment and T_c is given in Equation 158. For R44 boundary type cases, the loading types are similar in nature to R11.

4.3.1 For Centrally Loaded Imperfect Column

Figure 63 shows dimensionless determinant d versus axial load p_{in} curve for column PR11. In this figure, the curve follows a mildly descending linear path from A to B. At point B, yielding commences at column midspan. From B to C, the curve follows a linear descending path as yielding increases and a nonlinear path CD thereafter ending at p_{max} corresponding to zero value of d. It is observed that path AC corresponds to the column bilinear behavior and CD corresponds to nearly exponential loss of stiffness. It is found that 74.33% of the column strength is in the bilinear range AC of the d versus axial load p_{in}.

Figure 64 shows dimensionless determinant d versus axial load p_{in} curve for column PR44. The curve for column PR44 is similar in nature to the column PR11 curve. It is found that 67% of the column strength is in the bilinear range. Figure 65 shows stiffness degradation curves for columns PR11 and PR44. In this figure, E and F represent the last points of the bilinear range. It is found that the peak dimensionless axial load for column PR44 is 6.16% higher than that of column PR11. It can now be concluded that column PR44 is stiffer than column PR11.

4.3.2 For Uniaxially Loaded Beam-Column

Figure 66 shows dimensionless determinant d versus bending moment $m_{x(in)}$ about the x-axis curve for beam-column PUR11. In this figure, $p_{in} = 0.5$ is first applied and held constant, followed by a gradually increasing bending moment about the x-axis until the dimensionless determinant reaches zero. As seen in this figure, the curve follows a linear, straight path from G to H and a nonlinear, descending path HI thereafter. It is found that 27.32% of the beam-column strength is in the linear range.

Figure 67 shows dimensionless determinant d versus bending moment $m_{x(in)}$ about the x-axis curve for beam-column PUR44. It is found that 40% of the beam-column strength is in the linear range. Figure 68 shows stiffness degradation curves for beam-columns PUR11 and PUR44. The last points of the linear range are represented by J and K. The peak dimensionless bending moment about the x-axis for beam-column PUR44 is 9.56% higher than that of beam-column PUR11. It can therefore be concluded that beam-column PUR44 is stiffer than beam-column PUR11.

4.3.3 For Biaxially Loaded Beam-Column

Figure 69 shows dimensionless determinant d versus bending moment $m_{y(in)}$ about the y-axis curve for beam-column PBR11. In this figure, $p_{in} = 0.5$ is first applied, followed by $m_{x(in)} = 0.5$ and followed by a gradually increasing bending moment about the y-axis until d reaches nearly zero while $p_{in} = 0.5$ and $m_{x(in)} = 0.5$ are held constant. It is found that the stiffness has decreased appreciably. The corner elemental areas for cross sectional Node 9 for beam-column PBR11 is shown in Figure 70. In this figure, the terms ϵ_1, ϵ_2, ϵ_3, and ϵ_4 represent the strain values for the four corners, which are found to be 0.0066, −0.0061, 0.0009, and −0.0002, respectively.

Figure 71 shows dimensionless determinant d versus bending moment $m_{y(in)}$ about the y-axis curve for beam-column PBR44. It is found that 18% of the beam-column strength is in the linear range. The corner elemental areas for cross sectional Node 9 for PBR44 are shown in Figure 72. The values for ϵ_1, ϵ_2, ϵ_3, and ϵ_4 are 0.0063, −0.0056, −0.0002, and −0.0012, respectively. Figure 73 shows stiffness degradation curves for beam-columns PBR11 and PBR44. The symbols L and M represent the last points in the linear range. The peak dimensionless bending moment about the y-axis for beam-column PBR11 is found to be 23.00% lower than that of beam-column PBR44. It can now be concluded that beam-column PBR11 is weaker than beam-column PBR44.

4.3.4 For Biaxially Loaded Beam-Column with Applied Torsion

Figure 74 shows dimensionless determinant d versus the torsional moment t_{in} curve for member PBTR11. In this figure, $p_{in} = 0.5$ is first applied, followed by $m_{x(in)} = m_{y(in)} = 0.5$, and followed by a gradually increasing torsional moment until the dimensionless determinant reaches zero while $p_{in} = 0.5$ and $m_{x(in)} = m_{y(in)} = 0.5$ are held constant. As seen in Figure 74, the curve is nonlinear throughout. Figure 75 shows the corner elemental areas for the four corners for member PBTR11. The strain values for terms ϵ_1, ϵ_2, ϵ_3, and ϵ_4 are found to be 0.0031, −0.0055, 0.0069, and 0.0062, respectively. The strain values for ϵ_1 and ϵ_2 have decreased by 53.03% and 9.84%, respectively. However, the strain values for ϵ_3 and ϵ_4 have increased by 86.96% and 96.77%, respectively.

Figure 76 shows dimensionless determinant d versus torsional moment t_{in} curve for member PBTR44. It is found that the stiffness has also decreased appreciably. Figure 77 shows the corner elemental areas for the four corners for member PBTR44. The strain values for terms ϵ_1, ϵ_2, ϵ_3, and ϵ_4 are 0.0034, −0.0038, 0.0023, and 0.0017, respectively. It is found that the strain values for ϵ_1 and ϵ_2 have decreased by 46.03% and 32.14%, respectively. However, the strain values for ϵ_3 and ϵ_4 have increased by 91.30% and 29.41%, respectively. Figure 78 shows stiffness degradation curves for members PBTR11 and PBTR44. As seen in this figure, the maximum dimensionless torsional moment for member PBTR11 is 24.26% higher than that of member PBTR44. It can now be concluded that member PBTR11 is stiffer than member PBT44.

4.3.5 For Torsionally Loaded Imperfect Member

Figure 79 shows the dimensionless determinant versus torsional moment curve for pure torsion loading. In this figure, the curve follows a linear, straight path from N to R and a descending, nonlinear path RS thereafter ending at t_{max} corresponding to $d = 0.0005$. It is found that 79% of the member strength is in the linear range.

4.4 Ultimate Strength of Members

Figure 80 shows dimensionless interaction curves for PTR11, UTR11, and BTR11. The curve for UTR11 is found to be on the conservative side of both the BTR11 and PTR11 curves. The maximum dimensionless torsional moment values for PTR11, UTR11, and BTR11 are 0.400, 0.312, and 0.337, respectively, as presented in Table 34. The maximum dimensionless torsional moment values for PUTR11 and PBTR11 are found to be 0.766 and 0.707, respectively, as presented in Table 35.

Figure 81 shows dimensionless interaction curves for PTR44, UTR44, and BTR44. In this figure, all curves are similar in nature. The maximum dimensionless torsional moment values for PTR44, UTR44, and BTR44 are 0.436, 0.450, and 0.446, respectively, as presented in Table 36. The maximum dimensionless torsional moment values for PUTR44 and PBTR44 are found to be 0.893 and 0.885, respectively, as presented in Table 37.

Figure 82 shows dimensionless interaction curves for PTR11 and PTR44. As seen in this figure, PTR11 is everywhere on the conservative side of PTR44. The maximum dimensionless torsional moment value for PTR44 is 8.31% higher than that of PTR11. Figure 83 shows dimensionless interaction curves for UTR11 and UTR44. In this figure, UTR11 is everywhere on the conservative side of UTR44. The maximum dimensionless torsional moment value for UTR44 is 30.55% higher than that of UTR11. Figure 84 shows dimensionless interaction curves for BTR11 and BTR44. In this figure, BTR11 is everywhere on the conservative side of BTR44. It is found that the maximum dimensionless torsional moment value for BTR44 is 24.32% higher than that of BTR11.

For biaxially loaded beam-columns with cross-sectional orientation shown in Figure 16(b) and having pinned end conditions, the terms M_{Bx0}, M_{By0}, and M_{TyL} are taken as zero. However, the finite integral procedure is used to numerically calculate the induced end moments M_{Bx0}, M_{By0}, and M_{TyL} using Equations 142-145 for biaxially loaded beam-

column with mixed pinned and fixed conditions. Figure 85 shows the dimensionless applied bending moment versus the induced bending moments. The maximum dimensionless induced moment values for M_{Bx0}, M_{By0}, and M_{TyL} are 0.724, 0.862, and 0.985, respectively. It is found that the induced moments , M_{Bx0}, M_{By0}, and M_{TyL}, are 40.39%, 48.09%, and 54.96% lower than the maximum applied bending moment M_{TxL}, respectively.

4.5 Comparisons of Experimental and Theoretical Results at Ultimate Strength

Figure 86 shows the dimensionless axial load versus midspan strain curves for PR44. The maximum strain value from the experimental test is found to be 3.61% higher than that of the predicted value. Figure 87 shows the dimensionless uniaxial bending moment versus midspan strain curves for UR44. The maximum strain value from experiment is observed to be 6.31% higher than that of the predicted one. Figure 88 shows the dimensionless resultant biaxial bending moment versus midspan strain curves for BR44. The predicted maximum strain value is also observed to be 5.14% lower than that of the experimental one. Figure 89 shows the angle of twist versus dimensionless torsional moment relations. The predicted maximum torsional moment value is observed to be 2.32% higher than that of the experimental result. However, the angle of twist from experiment is observed to be 2.51% higher than that of the predicted value.

Figure 90 shows the dimensionless axial compressive load versus midspan strain curves for TPR44. The maximum strain value from experiment is observed to be 4.49% higher than that of the predicted value. Figure 91 shows the dimensionless uniaxial bending moment versus midspan strain relations for TUR44. The predicted maximum strain value for TUR44 is found to be 16.53% higher than that of the experimental value.

Figure 92 shows the dimensionless resultant biaxial bending moment versus midspan strain relations for TBR44. The maximum strain value from experiment for TBR44 is observed to be 13.61% higher than that of the predicted value. Figure 93 shows the dimensionless resultant biaxial bending moment versus midspan strain relations for TBR41. The maximum strain value from experiment for TBR41 is found to be 16.09% higher than that of the predicted one.

Figure 94 shows the dimensionless axial compressive load versus midspan strain relations for TBPR44. The maximum strain value from experiment is also observed to be 3.82% higher than that of the predicted one. Figure 95 shows the dimensionless axial compressive load versus midspan strain relations for TBPR41. The predicted maximum strain value is found to be 7.29% higher than that of the test value.

Figure 96 shows the angle of twist versus dimensionless torsional moment relations for PBTR44. In this figure, the two curves are perfectly matching throughout. The experimental torsional moment values were 0.5% to 1.73% higher than those of the predicted ones. Figure 97 shows the angle of twist versus dimensionless torsional moment relations for PBTR11. The experimental torsional moment value is found to be 0.5% higher than that of the predicted result for both test series. Figures 98 and 99 show the dimensionless interaction curves for PBTR11and PBTR44, respectively. It is observed that good agreement is reached between the tested and predicted results.

Table 38 presents the maximum dimensionless load values for PR44, UR44, BR44, TR44, TPR44, TUR44, TBR44, TBR41, TBPR44, TBPR41, PBTR11, and PBTR44. The ratios between predicted and experimental results for PR44, UR44, BR44, and TR44 are 0.94, 1.01, 0.89, and 1.02, respectively. The ratio between predicted and tested results for TPR44 and TUR44 are 1.05 and 0.85, respectively. The ratios between the resuls from the theory and experiment for TBR44 and TBR41 are 0.83 and 0.83, respectively. The ratios between predicted and tested results for TBPR44 and TBPR41 are 1.04 and 0.93, respectively.

Table 39 presents the maximum dimensionless load values for PBTR11 and PBTR44. For PBTR11 with $p^* = m^* = 0.2$, the ratio between predicted and experimental results is 0.99. For PBTR11 with $p^* = m^* = 0.5$, the ratio between the results from the theory and experiment is also 0.99. For PBTR44 with $p^* = m^* = 0.4$, the ratio between predicted and experimental results is 0.98. Finally, the ratio between predicted and tested results is 0.99 for PBTR44 with $p^* = m^* = 0.6$.

CHAPTER 5

THRUST-MOMENT-TORSION INTERACTION RELATIONS

Presented in this chapter are a number of new yield and ultimate strength interaction relations for biaxially loaded beam-columns with applied torsion.

5.1 Yield Limit Load-Moment-Torsion Interaction Relationships

In order to develop yield load-moment-torsion interaction relationships, the normal stress σ and the shear stress τ at any given point on a cross section can be expressed in the following dimensionless forms:

$$\frac{\sigma}{\sigma_c} = \frac{P}{P_c} + \frac{M_x}{M_{cx}} + \frac{M_y}{M_{cy}} \tag{176}$$

$$\frac{\tau}{\tau_c} = \frac{T}{T_c} \tag{177}$$

In these expressions, P, M_x, M_y, and T are the applied axial load, bending moment about x and y axes, and torsional moment, respectively. The terms P_c, M_c, M_c, T_c, σ_c, and τ_c were previously defined in Equations 156 through 161. Bresler (63) and Parme et al. (64) used a two-segment linear and load contour approximation approaches to curve fit. In this dissertation, bilinear and trilinear approximation approaches are used to curve fit the experimental dimensionless interactions for PBTR1 shown in Figure 58 as well as an approximation with an exponent α, and a combination of the two are presented.

5.1.1 Biaxial Loading Interaction Expression with Torsion at Yield Limit

Keeping the experimental dimensionless normal stress the same as in Equation 176 and applying an exponent α to the dimensionless shear stress given in Equation 177, a new dimensionless torsion term is introduced here in the beam-column interaction expression corresponding to yield limit as follows:

$$\left(\frac{P}{P_c} + \frac{M_x}{M_{cx}} + \frac{M_y}{M_{cy}}\right) + \left(\frac{T}{T_c}\right)^{\alpha} \leq 1 \tag{178}$$

To account for the presence of residual stresses, the relationship between σ and τ is expressed as $\sigma^2 + \alpha^2\tau^2 = {\sigma_Y}^2$, where α is approximated as follows :

$$\alpha = larger\ of \begin{cases} \sqrt{\frac{(\sigma_Y^2 - \sigma_{rc}^2)}{\tau_c^2}} \\ \sqrt{\frac{(\sigma_Y^2 - \sigma_{rmax}^2)}{\tau_c^2}} \\ \sqrt{\frac{(\sigma_Y^2)}{\tau_c^2}} \end{cases} \quad (179)$$

in which σ_{rmax} is the larger of the absolute value of σ_{rc} and σ_{rt}. This definition of α is also used throughout this chapter.

5.1.2 Bilinear Yield Limit Interaction Expressions for Biaxial Loading and Torsion

Figure 100 shows experimental dimensionless interaction curve and a bilinear approximation using lines AB and BC for PBTR1. In this figure, the ordinates $\frac{\sigma}{\sigma_c}$ and $\frac{\tau}{\tau_c}$ are defined in Equations 176 and 177. The bilinear expressions are as follows:

$$\frac{6}{9}\left(\frac{P}{P_c} + \frac{M_x}{M_{cx}} + \frac{M_y}{M_{cy}}\right) + \frac{T}{T_c} \le 1 \qquad \text{if } \frac{T}{T_c} > 0.4 \quad (180a)$$

$$\left(\frac{P}{P_c} + \frac{M_x}{M_{cx}} + \frac{M_y}{M_{cy}}\right) + \frac{1}{4}\frac{T}{T_c} \le 1 \qquad \text{if } \frac{T}{T_c} \le 0.4 \quad (180b)$$

In these expressions, P, M_x, and M_y are the applied axial load and biaxial bending moments about the x and y axis, respectively.

5.1.3 Yield Limit Interaction Expressions with Exponent α

Combining the linear expressions of these two segments with an exponent α approximation approach,

$$\frac{6}{9}\left(\frac{P}{P_c} + \frac{M_x}{M_{cx}} + \frac{M_y}{M_{cy}}\right) + \left(\frac{T}{T_c}\right)^{\alpha} \le 1 \qquad \text{if } \frac{T}{T_c} > 0.4 \quad (181a)$$

$$\left(\frac{P}{P_c} + \frac{M_x}{M_{cx}} + \frac{M_y}{M_{cy}}\right) + \frac{1}{4}\left(\frac{T}{T_c}\right)^{\alpha} \le 1 \qquad \text{if } \frac{T}{T_c} \le 0.4\,. \quad (181b)$$

In Expressions 181a and 181b, the α value is calculated based on Equation 179.

5.1.4 Trilinear Yield Limit Interaction Expressions for Biaxial Loading and Torsion

Figure 101 shows an experimental dimensionless interaction curve and trilinear approximation using three lines, EF, FG and GH, for PBTR1. The trilinear expressions are as:

$$\frac{1}{4}\left(\frac{P}{P_c}+\frac{M_x}{M_{cx}}+\frac{M_y}{M_{cy}}\right)+\frac{T}{T_c} \le 1 \qquad \text{if } \frac{T}{T_c} \ge 0.9 \tag{182a}$$

$$\frac{5}{8}\left(\frac{P}{P_c}+\frac{M_x}{M_{cx}}+\frac{M_y}{M_{cy}}\right)+\frac{5T}{6T_c} \le 1 \qquad \text{if } 0.6 < \frac{T}{T_c} < 0.9 \tag{182b}$$

$$\left(\frac{P}{P_c}+\frac{M_x}{M_{cx}}+\frac{M_y}{M_{cy}}\right)+\frac{1}{3}\frac{T}{T_c} \le 1 \qquad \text{if } \frac{T}{T_c} \le 0.6 \tag{182c}$$

In these equations, P_c, M_{cx}, M_{cy}, and T_c are previously defined in Section 3.3.1.

5.1.5 Discussion for Yield Limit Analysis

Figure 102 shows experimental dimensionless interaction relationships between dimensionless normal and shear stresses corresponding to the initiation of yielding for PBTR1 and those based on Expression 178 named as BLIET with various α values. For $\frac{T}{T_c} < 0.5$ and α = 2.5, the interaction curve is close to the experimental curve and on the convervative side for its remaining portion. Figure 103 shows experimental dimensionless interaction relationships between dimensionless normal and shear stresses corresponding to the initiation of yielding for PBTR1 and those based on Expression 180 named as Bilinear. For $\frac{T}{T_c} > 0.4$, the interaction curve is close to the experimental curve. Figure 104 shows experimental dimensionless interaction relationships between dimensionless normal and shear stresses corresponding to the initiation of yielding for PBTR1 and those based on Expressions 181 named as IEE with various α values. For $0.82 \le \frac{T}{T_c} \le 0.4$, the experimental curve is conservative of all curves and close for $\frac{T}{T_c} \le 0.4$. It can now be concluded that α should then be taken between 1.2 and 2 to be on the conservative side everywhere. Figure 105 shows experimental dimensionless interaction relationships between dimensionless normal and shear stresses corresponding to the initiation of yielding for PBTR1 and those based on Expression 182 named as Trinilear. The trilinear interactions clearly represent a better approximation overall. Figure 106 shows

experimental dimensionless interaction and those based on Expression 180 and Expressions 178, 181, and 82 with $\alpha = 2$.

In summary, the accuracy of piecewise linear approximations depend on how closely it can approximate the experimental curve. As seen in Figure 106, the trilinear interaction expressions represent a better approximation. Thus, the trilinear interaction expressions can be used if a piecewise-linear approximation is desired. BLIET is more conservative than IEE and results in a better curve fit as shown in Figure 106.

5.1.6 Analysis Example

A beam-column with a W21x48 in. section, 12 feet long and a yield stress of 50 ksi is subjected to an axial factored live load of 150 kips and factored live bending moments of magnitudes 45 k-in., and 10 k-in., respectively, about the x and y axes as shown in Figures 1 and 5. Determine the value of the maximum service torsional moment that the member can be subjected to at its bottom end corresponding to the yield limit.

SOLUTION

Since $\frac{P}{\phi_c P_n} = 0.410$, use AISC-LFRD H1-1a as follows:

$\frac{P}{\phi_c P_n} + \frac{8}{9}\left(\frac{M_x}{\phi_b M_{nx}} + \frac{M_y}{\phi_b M_{ny}}\right) \leq 1$ gives $0.752 < 1$. Thus, the member is stable as a beam-column under the given loads.

Since the interaction expressions developed herein are based on yield limit, one should use the service loads. The self-weight of W21x48 is equal to 48 lb/ft. Using the following AISC-LFRD:

$Q_c = 1.2Q_D + 1.6Q_L$

where Q_D and Q_L are the service dead and live load, respectively. Using Equation 179, α is found to be 1.816. Finally, Expression 178 gives T = 13.571 k-in; Expression 180a gives T = 16.086 k-in since $\frac{T}{T_c} > 0.4$; Expression 181(a) gives T = 23.104 k-in since $\frac{T}{T_c} > 0.4$; and Expression 182(c) gives T = 18.367 k-in since $\frac{T}{T_c} < 0.6$. One should use the smallest T value since it leads to the smallest interaction expression value.

5.2 Beam-Column Stability Check without Torsion for International Specifications

Interaction Expressions 176 through 177 are developed based on the assumption that no member instability occurs for the given loads. The following beam-column stability checks are based on the following eight international steel design specifications. In this section, the values for the applied axial compressive load and bending moments about the x and y axes are taken as 0.9 of the yield loads. Also, the terms P_{max}, M_{xmax}, and M_{ymax} represent the factored maximum axial load and bending moments about the x and y axis, respectively. Furthermore, CS, OM, and LTB refer to cross sectional, overall member, and lateral-torsional buckling, respectively.

5.2.1 AS4100 Specification

The beam-column interaction expressions given by Standards Association of Australia (AS4100) are given as follows (65):

For doubly symmetric compact I cross-section, the section capacity check is given by:

$$\left(\frac{M_{rx}^{*}}{\phi M_{rx}}\right)^{\gamma_s} + \left(\frac{M_{ry}^{*}}{\phi M_{ry}}\right)^{\gamma_s} \leq 1 \tag{183a}$$

For other cross-sections, the section capacity check is given by:

$$\left(\frac{P_r}{\phi P_s} + \frac{M_{rx}}{\phi M_{sx}} + \frac{M_{ry}}{\phi M_{sy}}\right) \leq 1 \tag{183b}$$

where:

$$\gamma = 1.4 + \frac{P_r}{\phi P_s} \leq 2 \tag{184}$$

$$M_{rx} = 1.18 M_{sx}\left[1 - \frac{P_r}{\phi P_s}\right] \leq M_{sx} \tag{185}$$

$$M_{ry} = 1.19 M_{sx}\left[1 - \left(\frac{P_r}{\phi P_s}\right)^2\right] \leq M_{sy} \tag{186}$$

For a biaxially loaded beam-column, the overall member capacity is given by:

$$\left(\frac{M_{rx}^{*}}{\phi M_{rx}}\right)^{1.4} + \left(\frac{M_{ry}^{*}}{\phi M_{iy}}\right)^{1.4} \leq 1 \tag{187}$$

where M_{rx}^{*}, M_{ry}^{*}, P_r, M_{rx}, and M_{ry} are the applied loads; M_{rx} is the lesser of the factored in-plane moment capacity reduced by axial force and the out-of-plane moment capacity reduced by axial force; M_{iy} is the factored in-plane moment capacity; M_{sx} and M_{sy} are the factored nominal section moment capacities about the x and y axes, respectively; P_s is the nominal section capacity for axial load; and ϕ is the resistance factor for compression and bending. The results for beam-column stability check for HSS7x7x0.375, HRS8x6x0.375, and W8x31 cross-sections with the length of 12 feet are presented in Table 40 before torsion is applied. It is found that the stability checks are satisfactory since the members are stable.

5.2.2 AIJ Specification

The beam-column interaction expressions in Design Standard for Steel Structures, Architectural Institute of Japan (AIJ) are given as follows (65):

For H-shaped section, the section capacity check is given by:

$$\left(\frac{M_{1x}}{M_{px1}}\right)^2 + \frac{M_{1y}}{M_{py1}} \leq 1 \tag{188}$$

For members without buckling, the overall member capacity is given by:

$$\frac{P_1}{\phi_p P_y} + 0.85\,\frac{M_{1x}}{\phi_p M_{px}} + 0.85\,\frac{M_{1y}}{\phi_p M_{py}} \leq 1 \tag{189a}$$

For members with buckling, the overall member capacity is given by:

$$\frac{P_1}{\phi_c P_{uy}} + 0.85\,\frac{M_{1x}}{\phi_b M_{ux}} + 0.85\,\frac{M_{1y}}{\phi_p M_{py}} \leq 1 \tag{189b}$$

in which P_1 is the applied axial load; M_{px1} and M_{py1} are the plastic moment under axial force and bending with respect to the strong and weak axis; P_y is the axial compressive capacity for yielding; M_{1x} and M_{1y} are the applied bending moment with respect to the strong and weak axes; M_{px} and M_{py} are the plastic moment capacity with respect to the strong and weak axes; M_{ux} is the moment capacity with respect to the strong axis; P_{uy} is the axial compressive capacity for buckling out of the plane of bending; ϕ_p is the resistance factor for tension; ϕ_c is the resistance factor for compression; and ϕ_b is the resistance factor for bending. The results for beam-column stability check for HSS7x7x0.375,

HRS8x6x0.375, and W8x31 cross-sections with the length of 12 feet before torsion is applied are summarized in Table 41. The stability check revealed that the beam-columns are stable under the given loads.

5.2.3 AISC-LFRD Specification

The beam-column interaction expressions in American Institute of Steel Construction Manual (AISC-LFRD) are as follows (66):

$$\frac{P_u}{\phi_c P_n} + \frac{8}{9}\left(\frac{M_{ux}}{\phi_b M_{nx}} + \frac{M_{uy}}{\phi_b M_{ny}}\right) \leq 1 \qquad \text{if } \frac{P_u}{\phi_c P_n} \geq 0.2 \tag{190a}$$

$$\frac{P_u}{2\phi_c P_n} + \left(\frac{M_{ux}}{\phi_b M_{nx}} + \frac{M_{uy}}{\phi_b M_{ny}}\right) \leq 1 \qquad \text{if } \frac{P_u}{\phi_c P_n} < 0.2 \tag{190b}$$

in which P_u is the applied compressive axial load; P_n is the factored axial compressive capacity; M_{ux} and M_{uy} are the applied bending moments about the strong and weak axes; and M_{nx} *and* M_{ny} are the factored moment capacity with respect to the x and y axes, respectively. The results for beam-column stability check for HSS7x7x0.375, HRS8x6x0.375, and W8x31 cross-sections with the length of 12 feet are given in Table 42 before the torsional moment is applied. The results showed that the members are stable as beam-columns given the applied loads.

5.2.4 BS 5950 Specification

The beam-column interaction expressions in British Standard Institution (BS 5950) are as follows (66).

For Cross-section capacity check:

$$\frac{F}{AP_y} + \frac{M_{Bx}}{M_{Bcx}} + \frac{M_{By}}{M_{Bcy}} \leq 1 \tag{191a}$$

For buckling resistance check:

$$\frac{F_c}{P_c} + \frac{m_x M_x}{P_Y Z_x} + \frac{m_y M_y}{P_Y Z_y} \leq 1 \tag{191b}$$

$$\frac{F_c}{P_{cy}} + \frac{m_{LT} M_{LT}}{M_b} + \frac{m_y M_y}{P_Y Z_y} \leq 1 \tag{191c}$$

in which F, M_{Bx}, and M_{By} are the applied compressive axial load and bending moments about the x and y axes, respectively; A is the cross-sectional area of section; P_y is the design strength; M_{Bcx} and M_{Bcy} are the bending moment capacities about the x and y axes, respectively; m_x and m_y are the equivalent uniform moment factors for the x and y axes, respectively, obtained from Table 26 of BS 5950; P_{cx} and P_{cy} are compressive resistance about the x and y axes, respectively; Z_x and Z_y are the elastic modulus about the x and y axes, respectively; m_{LT} is the equivalent uniform moment factor for y axis flexural buckling obtained from Table 18 of BS 5950; M_{LT} is the maximum major axis moment in the segment length L_x governing P_{cx}; and M_b is the buckling resistance moment. The results for beam-column stability check for HSS7x7x0.375, HRS8x6x0.375, and W8x31 cross-sections with the length of 12 feet are presented in Table 43 before the torsional moment is applied. The results in this table showed that the members are stable as beam-columns given the applied loads.

5.2.5 CSA Specification

The beam-column interaction expressions in accordance with the Canadian Standards Association (CSA) are given as follows (67).

For Class 1 and Class 2 sections of I-Shaped members:

$$\frac{P_f}{P_r} + 0.85\frac{U_x M_{fx}}{M_{rx}} + \beta\frac{U_y M_{fy}}{M_{ry}} \leq 1 \tag{192a}$$

For other classes and sections:

$$\frac{P_f}{P_r} + \frac{U_x M_{fx}}{M_{rx}} + \frac{U_y M_{fy}}{M_{ry}} \leq 1 \tag{192b}$$

In these expressions, P_f is the factored axial compressive load including P-delta effects as defined in CSA clause 8.4; P_r is the factored axial compression capacity for different limit states; M_{fx} and M_{fy} are the factored major and minor axes bending moments including P-delta effects as defined in clause 8.4; M_{rx} and M_{ry} are the factored major and minor axes flexural capacities for different limit states; the factor β is taken as 0.6 for cross section strength and calculated in accordance with CSA 18.8.2 for overall member strength; and U_x and U_y are two factors to account for the second-order effects due to the deformation of a member between its ends. The results for beam-column stability check for

HSS7x7x0.375, HRS8x6x0.375, and W8x31 cross-sections with the length of 12 feet before torsion is applied are given in Table 44. All sections are class 1. It is found that the members are stable as beam-columns given the applied loads.

5.2.6 Eurocode 3

The beam-column interaction expression of European code for the design of steel structures (Eurocode 3) is given as follows (65).

For cross-section strength, the conservative expression is given by:

$$\frac{P_{Sd}}{P_p} + \frac{M_{x.Sd}}{M_{Nx}} + \frac{M_{y.Sd}}{M_{Ny}} \leq 1 \tag{193a}$$

For class 1 and 2 cross-sections, the overall member strength is given by:

$$\frac{P_{Sd}}{\chi_{min} A f_y} + \frac{k_x M_{x.Sd}}{W_{pl,x} f_y} + \frac{k_y M_{y.Sd}}{W_{pl,y} f_y} \leq 1 \tag{193b}$$

For class 1 and 2 cross-sections where the lateral-torsional buckling is relevant:

$$\frac{P_{Sd}}{\chi_y A f_y} + \frac{k_{LT} M_{x.Sd}}{\chi_{LT} W_{pl,x} f_y} + \frac{k_y M_{y.Sd}}{W_{pl,y} f_y} \leq 1 \tag{193c}$$

where:

$$M_{Nx} = 1.56 M_{pl,x}(1-n)(0.6+n) \quad \text{Rolled I or H section} \tag{194}$$

$$M_{Ny} = 1.11 M_{pl,y}(1-n) \quad \text{Rolled I or H section} \tag{195}$$

$$M_{Nx} = M_{Ny} = 1.11 M_{pl}(1-n) \quad \text{Square hollow section} \tag{196}$$

$$M_{Nx} = \frac{M_{pl,x}(1-n)}{(0.5 + \frac{ht}{A})} \quad \text{Rectangular hollow section} \tag{197}$$

$$M_{Ny} = M_{Ny} = 1.33 M_{pl,y}(1-n) \quad \text{Rectangular hollow section} \tag{198}$$

$$k_y = 1 - \frac{\mu_y P_{Sd}}{\chi_y A f_y} \quad \text{but } k_y \leq 1.5 \tag{199}$$

$$k_{LT} = 1 - \frac{\mu_{LT} P_{Sd}}{\chi_z A f_y} \quad \text{but } k_{LT} \leq 1.0 \tag{200}$$

in which:

$$\mu_y = \overline{\lambda}_y(2\beta_{My} - 4) + \frac{W_{pl,y}}{W_{el,y}} - 1 \qquad \text{but } \mu_y \leq 0.90 \tag{201}$$

$$\mu_{LT} = 0.15(\overline{\lambda}_x 2\beta_{M,LT} - 1) \qquad \text{but } \mu_{LT} \leq 0.90 \tag{202}$$

in which $P_{Sd}$is the applied axial load; P_p is the factored axial compressive capacity; $M_{x.Sd}$ and $M_{y.Sd}$ are the applied bending moments about the x and y axes, respectively; M_{Nx} and M_{Ny} are the factored design plastic moment resistances reduced due to the axial load P about the x and y axes, respectively; $M_{pl,x}$ and $M_{pl,y}$ are the factored plastic moment capacities; k_x and k_y are the modification factors; χ_x and χ_y are the reduction factors for column buckling about the x and y axes; $W_{pl,x}$ is the plastic section modulus; $W_{pl,y}$ is the elastic section modulus; β_{My} and β_{LT} are the equivalent moment factors accounting for the non-uniformity of the moment diagram; $\overline{\lambda}_x$ and $\overline{\lambda}_y$ are the dimensionless slenderness ratios about the x and y axes, respectively; and χ_{LT} is the reduction factor for lateral-torsional beam buckling. The results for beam-column stability check for HSS7x7x0.375, HRS8x6x0.375, and W8x31 cross-sections with the length of 12 feet before torsion is applied are summarized in Table 45. Based on the stability check, it is found that the sections are satisfactory since the members are not unstable.

5.2.7 GBJ Specification

The beam-column interaction expressions in the specification for the design of steel structures, namely, People's Republic of China National Standard (GBJ), are expressed as follows (65).

For cross-sectional capacity:

$$\frac{P_N}{Af} \mp \frac{M_{x.N}}{\gamma_x W_{1xf}} \mp \frac{M_{y.N}}{\gamma_x W_{1yf}} \leq 1 \tag{203a}$$

For symmetrical I-sections or box sections, the overall member strength capacity is given by:

$$\frac{P_N}{c_x Af} + \frac{\beta_{mx} M_{x.N}}{\gamma_x W_{1xf}(1-0.8\frac{P}{P_{Ex}})} + \frac{\beta_{ty} M_{y.N}}{c_{by} W_{1yf}} \leq 1 \tag{203a}$$

$$\frac{P_N}{c_y A f} + \frac{\beta_{tx} M_{x.N}}{c_{bx} W_{1xf}} + \frac{\beta_{my} M_{y.N}}{\gamma_y W_{1yf}(1-0.8\frac{P}{P_{Ey}})} \leq 1 \quad (203b)$$

where P_N, $M_{x.N}$, and $M_{y.N}$ are the factored applied loads; β_{mx}, β_{my} ; β_{tx} and β_{ty} are the equivalent moment factors; γ_x and γ_y are the plastic adaption coefficients; P_{Ex} and P_{Ey} are the Euler buckling loads about the strong and weak axes; A is the cross sectional area; f is the design normal strength of steel; $W_{1x}$and W_{1x} are the section modulie about the x and y axes, respectively, with respect to the maximum compressive stress; c_x and c_y are the strength reduction factors of centrally compressed members bent about the strong axis and weak axis; and c_{bx} and c_{by} are the strength reduction factors of laterally unsupported beams subjected to uniform bending about the strong axis and the axis. The results for beam-column stability check for HSS7x7x0.375, HRS8x6x0.375, and W8x31 cross-sections with the length of 12 feet before the torsional moment is applied are given in Table 46. It is found that the members are stable even in the presence of an applied torsional moment.

5.2.8 SNiP Specification

The beam-column interaction expressions in Russian Steel Structures (SNiP) are given as follows (66):

$$\frac{N}{\phi_{exy} A} \leq R_y \gamma_c \quad (204a)$$

For In-plane stability check:

$$\frac{N}{\phi_e A} \leq R_y \gamma_c \quad (204b)$$

For Out-plane stability check:

$$\frac{N}{c_{\varphi_y} A} \leq R_y \varphi_c \quad (204c)$$

where:

$$\phi_{exy} = \phi_{ey}(0.6c^{\frac{1}{3}} + 0.4c^{\frac{1}{4}}) \quad (205)$$

in which N is the calculated value for axial load; R_y is the yield stress; γ_c is the resistance factor, A is the cross sectional area; φ_y is the buckling coefficient; c is the coefficient that is determined from Equation 192 depending on the magnitude of eccentricity m_y; and ϕ_{ey} is determined in relation to non-dimensionless slenderness $\overline{\lambda}_y$ and modified relative eccentricity $m_{ef,y}$ and utilizing Equation 191. The terms $\overline{\lambda}_y$ and $m_{ef,y}$ are defined as:

$$\overline{\lambda} = \lambda\sqrt{\frac{R_y}{E}} \tag{206}$$

$$m_{ef} = \eta m \tag{207}$$

in which λ is the greatest slenderness of a member; η is the coefficient in relation to section shape; and m is the relative eccentricity. The results for beam-column stability check for HSS7x7x0.375, HRS8x6x0.375, and W8x31 cross-sections with the length of 12 feet are presented in Table 47. The results in this table show that the sections are adequate.

5.3 Analytical Basis for Proposed Beam-Column Interaction Expressions

The proposed beam-column interaction expression presented in this dissertation is based on the outcome of a rigorous analysis of beam-columns including both second-order effects and elasto-plastic behavior. The analysis involves a finite integral solution of a system of nonlinear governing differential equations for the beam-column problem while also accounting for member initial out-of-straighness and residual stresses.

5.3.1 Proposed Beam-Column Interaction Expression

The member initial uniaxial and biaxial crookedness functions are taken as L/1000. The residual stresses σ_{rt} and σ_{rc} for hollow rectangular and I-shaped are shown in Figures 4 and 5, respectively. Based on the results of analysis performed on HSS7x7x0.375, HRS8x6x0.375, and W21x48, the following expression is obtained:

$$\left(\frac{P}{P_n}\right)^{\frac{3}{5}\alpha_p} + \left(\frac{M_x}{M_{nx}}\right)^{\frac{3}{5}\beta_x} + \left(\frac{M_y}{M_{ny}}\right)^{\frac{3}{5}\beta_y} \leq 1 \tag{208a}$$

$$\left(\frac{P}{P_n}\right)^{\alpha_p} + \left(\frac{M_x}{M_{nx}}\right) + \left(\frac{M_y}{M_{ny}}\right) \leq 1 \tag{208b}$$

$$(\frac{P}{P_n}) + (\frac{M_x}{M_{nx}})^{\beta_x} + (\frac{M_y}{M_{ny}})^{\beta_y} \leq 1 \quad (208c)$$

where α_p, β_x, and β_y can be approximated as follows:

$$\alpha_p = \frac{P_Y}{P_c} \quad (209a)$$

$$\beta_x = \frac{M_{Yx}}{M_{cx}} \quad (209b)$$

$$\beta_y = \frac{M_{Yy}}{M_{cy}} \quad (209c)$$

The denominator terms on the right side of Equation 209 are defined separately for the hollow rectangular and I sections.

For the rectangular section shown in Figure 4:

$$P_c = A(\sigma_Y - 0.2\sigma_Y) \quad (210)$$

$$M_{cx} = S_x(\sigma_Y - 0.5\sigma_Y) \quad (211)$$

$$M_{cy} = S_y(\sigma_Y - 0.5\sigma_Y) \quad (212)$$

For the I section shown in Figure 5:

$$P_c = A(\sigma_Y - 0.3\sigma_Y) \quad (213)$$

$$M_{cx} = S_x(\sigma_Y - \sigma_{rmax}) \quad (214)$$

$$M_{cy} = S_y(\sigma_Y - \sigma_{rmax}) \quad (215)$$

. The terms P_n, M_{nx}, and M_{ny} in Expression 208 can be calculated based on one of the international specifications discussed in Section 5.2.1 through Section 5.2.8.

5.4 Comparison of Beam-Column Interaction Expressions

The results for international beam-column stability checks for HSS7x7x0.375, HRS8x6x0.375, and W8x31 cross-sections with the length of 12 feet and those based on Expressions 208a, 208b, and 208c are presented in Tables 48, 49, and 50, respectively. In these tables, λ and λprop represent the left-hand side of the international beam-column

interaction expressions given in Section 5.2 and proposed beam-column interaction expression given in Section 5.3, respectively. Table 48 gives the lowest ratios overall. A comparison of the international beam-column interaction expressions revealed that the nonlinear interaction expressions are more conservative than the linear ones. The international steel design specifications use two or more expressions to determine the load-carrying capacity of beam-columns. A new single beam-column interaction expression is formulated (Expression 208a) and presented in this dissertation with exponents that account for residual stress and initial out-of-straightness for hollow rectangular and I-shaped cross-sections.

5.4 Ultimate Load-Moment-Torsion Interaction Relationships

Applying the exponent α given by Equation 179 to the dimensionless shear stress and keeping the theoretical dimensionless normal stress the same, a new dimensionless torsion term is introduced in beam-column interaction expressions given in Sections 5.2 and 5.3 corresponding to ultimate strength. For the materially nonlinear or inelastic range P, M_x, M_y, and T are incremented until the ultimate values are obatined.

5.4.1 Including Torsion in AS4100 Beam-Column Expression at Ultimate Strength

Australia's AS4100 beam-column interaction expressions including a new dimensionless torsion term corresponding to ultimate strength are expressed as follows:

$$\left(\frac{M_x}{M_{rx}}\right)^{1.4} + \left(\frac{M_y}{M_{iy}}\right)^{1.4} + \left(\frac{T}{T_n}\right)^{\alpha} \leq 1 \tag{216a}$$

$$\left(\frac{P}{P_s} + \frac{M_x}{M_{sx}} + \frac{M_y}{M_{sy}}\right) + \left(\frac{T}{T_n}\right)^{\alpha} \leq 1 \tag{216b}$$

where:

$$\frac{\tau}{\tau_n} = \frac{T}{T_n} \tag{217}$$

$$\lambda_{AS} = \begin{cases} \left(\frac{M_x}{M_{rx}}\right)^{1.4} + \left(\frac{M_y}{M_{iy}}\right)^{1.4} \\ \left(\frac{P}{P_s} + \frac{M_x}{M_{sx}} + \frac{M_y}{M_{sy}}\right) \end{cases} \tag{218}$$

In Equation 217, τ_n is the shear strength; T is the applied torsion; and T_n is the torsional moment capacity. All terms in Equation 218 are previously defined in Section 5.2.1. The term α is given by Equation 179. The resistance reduction factors for axial load and bending moments should be taken as given by AS4100. However, the resistance reduction factor for torsion can tentatively be taken the same as the bending moment to be on the conservative side. Table 51 presents the results based on Expression 216 for HSS7x7x0.375, HRS8x6x0.375, and W8x31 cross-sections with the length of 12 feet. It is found that HRS8x6x0.375 is unstable for PBTR19, and both HSS7x7x0.375 and W8x31 are unstable for PBTR18. Figure 107 shows ultimate dimensionless interaction curves for the theory and HSS7x7x0.375, HRS8x6x0.375, and W8x31 based on Expression 216 with $\alpha = 2$, respectively. All curves are clearly conservative compared with the theoretical curve.

5.4.2 Including Torsion in AIJ Beam-Column Expression at Ultimate Strength

Japanese AIJ beam-column interaction expressions including the new dimensionless torsion are given as:

$$\frac{P}{P_y} + 0.85\frac{M_{1x}}{M_{px}} + 0.85\frac{M_{1y}}{M_{py}} + \left(\frac{T}{T_n}\right)^{\alpha} \leq 1 \tag{219a}$$

$$\frac{P}{P_{uy}} + 0.85\frac{M_{1x}}{M_{ux}} + 0.85\frac{M_{1y}}{M_{py}} + \left(\frac{T}{T_n}\right)^{\alpha} \leq 1 \tag{219b}$$

where:

$$\lambda_{AIJ} = \begin{cases} \frac{P}{P_y} + 0.85\frac{M_{1x}}{M_{px}} + 0.85\frac{M_{1y}}{M_{py}} \\ \frac{P}{P_{uy}} + 0.85\frac{M_{1x}}{M_{ux}} + 0.85\frac{M_{1y}}{M_{py}} \end{cases} \tag{220}$$

All terms in Equation 220 were previously defined in Section 5.2.2. The resistance reduction factors for axial load and bending moments should be taken as given by AIJ. However, the resistance reduction factor for bending can tentatively be used for the torsion to be on the conservative side. Table 52 presents the results based on Expression 219 for HSS7x7x0.375, HRS8x6x0.375, and W8x31 cross-sections with the length of 12 feet. Results in this table show that members W8x31, HSS7x7x0.375 and HRS8x6x0.375 become unstable for PBTR17. Figure 108 shows ultimate dimensionless interaction curves for the theory and HSS7x7x0.375, HRS8x6x0.375, and W8x31 based on Expression 219

with $\alpha = 2$, respectively. All curves are clearly on the conservative side of the theoretical curve.

5.4.3 Including Torsion in AISC-LFRD Beam-Column Expression at Ultimate Strength

American AISC-LFRD beam-column interaction expressions including the new dimensionless torsion corresponding to ultimate strength is obtained as

$$\frac{P_u}{\phi_c P_n} + \frac{8}{9}\left(\frac{M_{ux}}{\phi_b M_{nx}} + \frac{M_{uy}}{\phi_b M_{ny}}\right) + \left(\frac{T}{T_n}\right)^{\alpha} \leq 1 \qquad \text{if } \frac{P_u}{\phi_c P_n} \geq 0.2 \tag{221a}$$

$$\frac{P_u}{2\phi_c P_n} + \left(\frac{M_{ux}}{\phi_b M_{nx}} + \frac{M_{uy}}{\phi_b M_{ny}}\right) + \left(\frac{T}{T_n}\right)^{\alpha} \leq 1 \qquad \text{if } \frac{P_u}{\phi_c P_n} < 0.2 \tag{221b}$$

where:

$$\lambda_{AISC} = \begin{cases} \frac{P_u}{\phi_c P_n} + \frac{8}{9}\left(\frac{M_{ux}}{\phi_b M_{nx}} + \frac{M_{uy}}{\phi_b M_{ny}}\right) \\ \frac{P_u}{2\phi_c P_n} + \left(\frac{M_{ux}}{\phi_b M_{nx}} + \frac{M_{uy}}{\phi_b M_{ny}}\right) \end{cases} \tag{222}$$

All terms in Equation 222 are defined in Section 5.2.3. The resistance reduction factors for axial load and bending moments should be taken as given by AISC-LFRD. However, the resistance reduction factor for torsion can tentatively be taken as 0.9 to be on the conservative side. Table 53 presents the results based on Expression 221 for HSS7x7x0.375, HRS8x6x0.375, and W8x31 cross-sections with the length of 12 feet. In this table, W8x31 is unstable for PBTR16 and both HSS7x7x0.375 and HRS8x6x0.375 are unstable for PBTR17. Figure 109 shows ultimate dimensionless interaction curves for the theory and HSS7x7x0.375, HRS8x6x0.375, and W8x31 based on Expression 221 with $\alpha = 2$, respectively. All curves are clearly conservative compared with the theoretical curve.

5.4.4 Including Torsion in BS 5950 Beam-Column Expression at Ultimate Strength

British BS 5950 beam-column cross-sectional interaction expressions including the new dimensionless torsion corresponding to ultimate strength is obtained as

$$\frac{P}{AP_Y} + \frac{M_x}{M_{Bcx}} + \frac{M_y}{M_{Bcy}} + \left(\frac{T}{T_n}\right)^{\alpha} \leq 1 \tag{223}$$

where:

$$\lambda_{BS} = \begin{cases} \frac{P}{AP_Y} + \frac{M_x}{M_{Bcx}} + \frac{M_y}{M_{Bcy}} \end{cases} \quad (224)$$

All terms in Equation 224 are defined in Section 5.2.4. The resistance reduction factors for axial load and bending moments should be taken as given by BS 5950. However, the resistance reduction factor for torsion can tentatively be taken as 0.9 to be on the conservative side. Table 54 presents Expression 223 for HSS7x7x0.375, HRS8x6x0.375, and W8x31 cross-sections with the length of 12 feet. In this table, W8x31 is unstable for PBTR16, and both HSS7x7x0.375 and HRS8x6x0.375 become unstable for PBTR17. Figure 110 shows ultimate dimensionless interaction curves for the theory and HSS7x7x0.375, HRS8x6x0.375, and W8x31 based on Expression 223 with α = 2 respectively. All curves are conservative compared with the theoretical curve.

5.4.5 Including Torsion in CSA Beam-Column Expression at Ultimate Strength

Canadian beam-column interaction expressions with the new dimensionless torsion corresponding to ultimate strength is obtained as

$$\frac{P}{P_r} + 0.85\frac{U_x M_x}{M_{rx}} + \beta\frac{U_y M_y}{M_{ry}} + \left(\frac{T}{T_n}\right)^{\alpha} \leq 1 \quad (225a)$$

$$\frac{P}{P_r} + \frac{U_x M_x}{M_{rx}} + \frac{U_y M_y}{M_{ry}} + \left(\frac{T}{T_n}\right)^{\alpha} \leq 1 \quad (225b)$$

where:

$$\lambda_{CSA} = \begin{cases} \frac{P}{P_r} + 0.85\frac{U_x M_x}{M_{rx}} + \beta\frac{U_y M_y}{M_{ry}} \\ \frac{P}{P_r} + \frac{U_x M_x}{M_{rx}} + \frac{U_y M_y}{M_{ry}} \end{cases} \quad (226)$$

All terms in Equation 226 are defined in Section 5.2.5. The resistance reduction factors for axial load and bending moments should be taken as given by CSA. However, the resistance reduction factor for torsion can be tentatively taken as the same as the bending moment to be on the conservative side. The results based on Expression 225 for HSS7x7x0.375, HRS8x6x0.375, and W8x31 cross-sections with the length of 12 feet are presented in Table

55. In this table, W8x31, HSS7x7x0.375 and HRS8x6x0.375 are unstable for PBTR17. Figure 111 shows ultimate dimensionless interaction curves for the theory and HSS7x7x0.375, HRS8x6x0.375, and W8x31 based on Expressions 225 with $\alpha = 2$, respectively. All curves are clearly on the conservative side of the theoretical curve.

5.4.6 Including Torsion in Eurocode3 Beam-Column Expression at Ultimate Strength

European beam-column interaction expressions including the new dimensionless torsion corresponding to ultimate strength is obtained as:

$$\frac{P}{P_p} + \frac{M_x}{M_{Nx}} + \frac{M_y}{M_{Ny}} + \left(\frac{T}{T_n}\right)^{\alpha} \leq 1 \tag{227}$$

where:

$$\lambda_{\text{Euro}} = \left\{\frac{P}{P_p} + \frac{M_x}{M_{Nx}} + \frac{M_y}{M_{Ny}}\right. \tag{228}$$

The terms in Equation 228 are defined in Section 5.2.6. The resistance reduction factors for axial load and bending moments should be taken as given by Eurocode 3. However, the resistance reduction factor for the bending moment can tentatively also be used for torsion to be on the conservative side. The results based on Expression 227 for HSS7x7x0.375, HRS8x6x0.375, and W8x31 cross-sections with the length of 12 feet are presented in Table 56. In this table, W8x31 is unstable for PBTR16, and both HSS7x7x0.375 and HRS8x6x0.375 are unstable for PBTR17. Figure 112 shows ultimate dimensionless interaction curves for the theory and HSS7x7x0.375, HRS8x6x0.375, and W8x31 based on Expressions 227 with $\alpha = 2$ respectively. All curves are clearly conservative compared with the theoretical curve.

5.4.7 Including Torsion in GBJ Beam-Column Expression at Ultimate Strength

Chinese beam-column interaction expressions with the new dimensionless torsion corresponding to ultimate strength is obtained as:

$$\frac{P}{c_x A f} + \frac{\beta_{mx} M_x}{\gamma_x W_{1x} f\left(1 - 0.8\frac{P}{P_{Ex}}\right)} + \frac{\beta_{ty} M_y}{c_{by} W_{1y} f} + \left(\frac{T}{T_n}\right)^{\alpha} \leq 1 \tag{229a}$$

$$\frac{P}{c_y A f} + \frac{\beta_{tx} M_x}{c_{bx} W_{1xf}} + \frac{\beta_{my} M_y}{\gamma_y W_{1yf}(1-0.8\frac{P}{P_{Ey}})} + (\frac{T}{T_n})^{\alpha} \leq 1 \quad (229b)$$

where:

$$\lambda_{GBJ} = \begin{cases} \frac{P}{c_x A f} + \frac{\beta_{mx} M_x}{\gamma_x W_{1xf}(1-0.8\frac{P}{P_{Ex}})} + \frac{\beta_{ty} M_y}{c_{by} W_{1yf}} \\ \frac{P}{c_y A f} + \frac{\beta_{tx} M_x}{c_{bx} W_{1xf}} + \frac{\beta_{my} M_y}{\gamma_y W_{1yf}(1-0.8\frac{P}{P_{Ey}})} \end{cases} \quad (230)$$

All terms in Equation 230 are defined in Section 5.2.7. The resistance reduction factors for axial load and bending moments should be taken as given by GBJ. However, the resistance reduction factor for torsion can tentatively be taken as the larger of the reduction factors of axial load or bending moments on the conservative side. Table 57 presents the results based on Expression 229 for HSS7x7x0.375, HRS8x6x0.375, and W8x31 cross-sections with the length of 12 feet. In this table, all members become unstable for PBTR17. Figure 113 shows ultimate dimensionless interaction curves for the theory and HSS7x7x0.375, HRS8x6x0.375, and W8x31 based on Expression 229 with $\alpha = 2$, respectively. All curves are clearly conservative compared with the theoretical curve.

5.4.8 Including Torsion in SNiP Beam-Column Expression at Ultimate Strength

Russia's SNiP beam-column interaction expressions with the new dimensionless torsion corresponding to ultimate strength is obtained as:

$$\frac{P}{\phi_{exy} A R_y \gamma_c} + (\frac{T}{T_n})^{\alpha} \leq 1 \quad (231)$$

where:

$$\lambda_{SNiP} = \left\{ \frac{P}{\phi_{exy} A R_y \gamma_c} \right. \quad . \quad (232)$$

In Equation 232, P is the calculated axial load and all other terms are previously defined in Section 5.2.8. The resistance reduction factors for axial load and bending moments should be taken as given by SNiP. However, the reduction factor for torsion can tentatively be taken as the larger of the reduction factors of axial load or bending moments on the

conservative side. Table 58 presents the results based on Expression 231 for HSS7x7x0.375, HRS8x6x0.375, and W8x31 cross-sections with the length of 12 feet. In this table, W8x31 is unstable for PBTR15 and both HSS7x7x0.375 and HRS8x6x0.375 are unstable for PBTR16. Figure 114 shows ultimate dimensionless interaction curves for the theory and HSS7x7x0.375, HRS8x6x0.375, and W8x31 based on Expression 231 with α = 2, respectively. All cross-sectional curves are clearly conservative compared with the theoretical curve.

5.4.9 Biaxial Loading Interaction Expression with Torsion at Ultimate Strength

The biaxial loading interaction expressions with torsion at ultimate strength can be expressed as:

$$(\frac{P}{P_n})^{\frac{3}{5}\alpha_p} + (\frac{M_x}{M_{nx}})^{\frac{3}{5}\beta_x} + (\frac{M_y}{M_{ny}})^{\frac{3}{5}\beta_y} + (\frac{T}{T_n})^{\alpha} \leq 1 \tag{233}$$

where:

$$\lambda_{\text{BLIETU}} = \left\{(\frac{P}{P_n})^{\frac{3}{5}\alpha_p} + (\frac{M_x}{M_{nx}})^{\frac{3}{5}\beta_x} + (\frac{M_y}{M_{ny}})^{\frac{3}{5}\beta_y}\right. \tag{234}$$

All terms in Equation 234 are previously defined in Section 5.3. The resistance reduction factors for axial load, bending moments, and torsion can be taken as 0.9 in accordance with AISC-LFRD Specification. Table 59 presents the results based on Expression 233 for HSS7x7x0.375, HRS8x6x0.375, and W8x31 cross-sections with the length of 12 feet. In this table, W8x31 is unstable for PBTR16, and both HSS7x7x0.375 and HRS8x6x0.375 are unstable for PBTR17. Figure 115 shows ultimate dimensionless interaction curves for the theory and HSS7x7x0.375, HRS8x6x0.375, and W8x31 based on Expressions 233 with α = 2, respectively. All cross-sectional curves are clearly on the conservative side of the theoretical curve.

5.4.9 Discussion for Ultimate Strength Analysis

In Section 5.4, interaction expressions from Australia, Japan, the U.S., Great Britain, Canada, Europe, China, and Russia were modified to include torsion. These curves can also be compared in Figures 116-118 to the curve based on Expression 233 with α = 2 for PBTR1 formulated in Section 5.4.9. Figures 116-118 show theoretical dimensionless

torsion versus λ curves for HSS7x7x0.375, HRS8x6x0.375, and W8x31 cross-sections, respectively. As seen in these figures, all curves are on the conservative side of the theoretical curve. Also, SNiP is the least conservative for Figures 116 through 118. Furthermore, AS4100 and CSA are the most conservative for Figures 116-117 and Figure 118, respectively. Table 60 presents the results based on the modified interaction expressions formulated in Sections 5.4.1 through 5.4.9 for HSS7x7x0.375, HRS8x6x0.375, and W8x31. In this table, all interaction expressions are satisfactory for PBTR15 given the cross-sections. For PBTR16, all interaction expressions are satisfactory for both HSS7x7x0.375 and HRS8x6x0.375. However, the interaction expressions from Europe, Great Britain, the U.S., and BLIETU with dimensionless applied torsion are not satisfied for W8x31. All interaction expressions formulated in Sections 5.4.1 through 5.4.9 are satisfactory from PBTR11 through PBTR15. It can therefore be concluded that the general load-moment-torsion interaction expressions developed in this investigation can be applied to various cross sections with other material properties.

5.4.10 Analysis Example

A beam-column with a W21x48 in. section, 12 feet long and a yield stress of 50 ksi is subjected to an axial factored live load of 150 kips and factored live bending moments of magnitudes 45 k-in., and 10 k-in., respectively, about the x and y axes as shown in Figures 1 and 5. Determine the value of the maximum torsional moment that the member can be subjected to at its bottom end corresponding to the ultimate strength.

SOLUTION

The member is found to be stable in Section 5.1.6. Using Equation 179, α is found to be 1.816. Finally, the values for expressions formulated in Section 5.3 are as follows.

AS4100:

Expression 216 gives T = 25.297 k-in.

AIJ:

Expression 219 gives T = 10.969 k-in.

AISC-LFRD:

Expression 221 gives T = 16.715 k-in.

BS5950:

Expression 223 gives T = 12.425 k-in.

CSA:

Expression 225 gives T = 17.806 k-in.

Eurocode3:

Expression 227 gives T = 19.299 k-in.

GBJ:

Expression 229 gives T = 14.828 k-in.

SNiP:

Expression 229 gives T = 3.235 k-in.

BLIETU:

Expression 233 gives T = 17.434 k-in.

In this example, SNiP and AS4100 give the lowest and highest values for torsional moment, respectively.

CHAPTER 6

CONCLUSIONS AND FUTURE RESEARCH

6.1 Conclusions

Based on the results from the experimental and theoretical study of the inelastic behavior and strength of steel beam-columns with applied torsion presented in this dissertation, the main conclusions are summarized as follows.

1. For the experimental study requiring the application of a torsional moment, a new torsion application apparatus is developed and worked well when integrated into a biaxial bending test setup.
2. The experimental behavior of steel beam-columns with applied torsion is in good agreement with the predicted behavior based on the finite integral solution of the materially nonlinear governing differential equations.
3. The presence of axial load and bending moments results in a substantial reduction of member torsional capacity at yield limit as well as the ultimate member strength.
4. The member initial crookedness and residual stresses significantly decrease the torsional moment capacity at yield limit as well as the ultimate strength in the presence of axial load and bending moments.
5. Flexural partial end restraints decrease the torsional moment capacity at yield limit for the beam-columns analyzed.
6. A member fully plastified in torsion can still carry a significant axial load as well as bending moment.
7. Based on both experimental and theoretical results, a new load-moment-torsion yield limit interaction expression is developed.
8. Using the materially nonlinear analysis, a new load-moment-torsion ultimate strength interaction is formulated.
9. Modifications are developed for the beam-column interaction expressions from Australia, Canada, China, Great Britain, Japan, Russia, U.S., and those in Eurocode to include the effect of applied torsion.

6.2 Future Research

Future studies can include the development of load-moment-torsion interaction relations for members with singly-symmetric and unsymmetric cross sections. The effect of fire conditions on various interaction expressions also needs to be studied.

LIST OF REFERENCES

1. Ketter, R. C., "Stability of Beam-Columns above the Elastic Limit", *Proc. ASCE*, Vol.81, No.692, October 1955.

2. Galambos, T.V. and R.L. Ketter., "Columns Under Combined Bending and Thrust", Proceedings. ASCE, Vol. 85, EM2, 1959.

3. Mason, R. E., G.P. Fisher and G. Winter., "Eccentrically Loaded Hinged Steel Columns", ASCE, Vol. 84, EM4, 1958.

4. Milner, H. R., "The Elastic Plastic Stability of Stanchions Bent about Two Axes", Ph.D. Dissertation, Imperial College, University of London, December 1965.

5. Razzaq, Z., "Theoretical and Experimental Investigation of Biaxially Loaded Rectangular Tubular Columns", *M.S. Thesis*, University of Windsor, Windsor, Ontario, Canada, 1968.

6. Marshall, P. J. and Ellis, J. S., "The Ultimate capacity of Biaxially Loaded Box Steel Columns", *The Royal Military College of Canada*, Kingston, Ontario, Canada, February 1969.

7. Syal, I. C. and Sharma, S. S., "Elastic Behavior of Biaxially Loaded Steel Columns",*Journalof Structural Division*, ASCE, Vol.96, No. ST3, Proc Paper 7143, March 1970, pp. 469-486.

8. Sakda, S. and Chen W.F., "Analysis of Biaxially Loaded Columns", Fritz Engineering Laboratory Report No.331.12, September 1970.

9. Razzaq, Z., and McVinnie, W. W., "Rectangular Tubular Steel Columns Loaded Biaxially," *Journal of Structural Mechanics*, Vol, X, No. 4, 1982.

10. Razzaq, Z., and McVinnie, W. W., "Theoretical and Experimental Behavior of Biaxially Loaded Inelastic Columns," *Journal of Structural Mechanics*, Vol. 14, No. 3, March, 1986.

11. Darbhamulla, S. P., "Nonproportionally Loaded Steel Beam-Column and Flexibly-Connected Nonsway Frames," Ph.D. Dissertation, Old Dominion University, May, 1990.

12. Eidan, S. A., "Inelastic Stability of Nonproportionally Loaded Steel Sway Beam-Columns and Space Frames," Ph.D. Dissertation, Old Dominion University, 1992.

13. Zhao, Yanhong., "Thermo-Elasto-Plastic Behavior of Biaxially Loaded Steel Beam-Columns Including Those From World Trade Center", Ph.D. Dissertation, Old Dominion University, 2013.

14. Saint-Venant, Memoire sur la Torsion des prismes, Memoires des Savants Etrangers, XIV, 1855, pp. 233-560.
15. A, Nadai., "Z. Angew", *Math Mechanik* 3, 1923, pp. 442.

16. Timoshenko, S. P., "Einige Stabilitaetsprobleme der Elastizitaestheorie", *In Collected Papers of Stephen P. Timoshenko*, McGraw-Hill, New York, 1953, pp.1-50.

17. Timoshenko, S. P., "Sur la Stabilite des Systemes Elastiques", *In Collected Papers of Stephen P. Timoshenko*, McGraw-Hill, New York, 1953, pp.92-224.

18. Donnell, L.H., "Stability of Thin-Walled Tubes under Torsion," *Naca-Report*, No.479, 1935.

19. Burgoyne, C.J. and Brown, E.H., "Nonuniform Elastic Torsion", Int.J.Mech.Sci, Vol.36, No. 1, 1994, pp. 23-38

20. Chen. Chu., "The effect of initial twist on the torsional rigidity of thin prismatical bars and tubular members", *US National Congres of Applied Mechanics*, Vol 1, 1951, pp.265-269.

21. Ellis, J. S., Jury, E.J. and Kirk, D.W., "Torsional Behavior of Rectangular Hollow Sections," *Journal of Constructional Steel Research*, No.59, 2003, pp. 641-663.

22. Marshall, J., "Derivation of Torsional Formulas for Multiply Connected Thick-Walled Rectangular Sections", *Journal of Applied Mechanics*, Vol.2, No.37, 1970, pp. 399-402.

23. Carey, G.J.JR., "An investigation of plastic torsion in circular prismatic bars with a concentric or eccentric hole using the sand-heap analogy," *Master*. Thesis, Graduate School of the Agriculture and Mechanical College of Texas, May 1963.

24. Vlasov, V. Z., "Thin-Walled Elastic Beams", 2nd ed., Israel Program for Scientific Translation, Jerusalem, 1961.

25. Wagner, H.,"Verdrehung und Knickung von offenen Profilen (Torsion and buckling of open sections)", NACA TM 807, 1936.

26. Abramyan, B.L., "Torsion and Bending of Prismatic Rods of Hollow Rectangular Sections", *National Advisory Committee for Aeronautics*, TM 1319, November 1951.

27. Estabrooks, B. G. and Grondin, G. Y., "Combined Bending and Torsion of Steel I-Shaped Beams", Structural Engineering Report No.276, January 2008.

28. Nuttall, H., and Gaydon, F.A.,"On the Combined Bending and Twisting of Beams of Various Sections", *Journal of the Mechanics and Physics of Solids*, Vol 6, 1957, pp.17-26.

29. Ishikawa, H., "Elasto-Plastic Stress Analysis of Prismatic Bar under Combined Bending and Torsion", *ZAMM*, Vol.53, No. 1, 1973, pp. 17-30.

30. Wiener, P.M., and Bathe, K.J., "On Elastic-Plastic Analysis of I-Beams in Bending and Torsion," *Computers and Structures*, Vol. 17, No. 5-6, 1983, pp. 711-718.

31. Kyungsik, K., and Chai. H. Y.," Ultimate Strength of Steel Rectangular Box Beams Subjected to Combined Action of Bending and Torsion," *Engineering Structures*, ASCE, Vol. 120, No. 12, December, 1994, pp. 3397-3417.

32. Hill, R., and Siebel, M.P.L., "On combined bending and twisting of thin tubes in the plastic range", *Philosophical Magazine*, Vol.42, No.330, 1951, pp.722-733.

33. Hill, R., and Siebel, M.P.L., "On the plastic distortion of solid bars by combined bending and twisting", *Journal of the Mechanics and Physics of Solids*, Vol.1, 1953, pp.207-214.

34. Iwegwu, E. O., "Plastic flexure and torsion," *Journal of the Mechanics and Physics of Solids*, Vol.8, 1960, pp.141-146.

35. Onat, E. T., and Shield, R.T., "Remarks on Combined Bending and Twisting of Thin Tubes in the plastic range", *J.appl.Mech*, Vol.20, 1953, pp.345-348.

36. Boulton, N. S., "Plastic Twisting and Bending of an I-Section in which the Warp is Restricted," *International Journal of Mechanical Sciences*, Vol.4, 1962, pp.491-502.

37. Dinno, K.S., and Merchant, W., "Procedure for Calculating the Plastic Collapse of I-Sections under bending and torsion",*The Structural Engineer*, Vol.43, No. 7, 1965, pp. 219-221.

38. Razzaq, Z., and Galambos, V. T., "Biaxial Bending Tests with or without Torsion," *Journal of Structural Engineering*, ASCE, Vol. 105, No. 11, 1979b, pp. 2187-2202.

39. Trahair, N.S. and Bill, S., "Elastic Biaxial Bending and Torsion of Thin-Walled Members", Thin-Walled Structures, No. 9, 1990, pp. 269-307

40. Strelbytska, O. I., and Evseyenko, G.I., "Double bending with torsion of thin-walled bars beyond the elastic limit elastic limit," *Dopovidi Akademii nauk URSR*, 1962, pp.1308-1312.

41. Shugyo, M., and Li, J. P, "Inelastic and Stability Analysis of Linearly Tapered Box Columns under Biaxial Bending and Torsion", *Report of the Faculty of Engineering*, Nagasaki University, Vol.25, No. 45, 1995, pp. 143-149.

42. Hodge, P.G, and Sankaranrayanan, R.,"The Determination of Safe Loads of Beams Subjected to Combined Twisting and Biaxial Bending moments", *Journal of Applied Mechanics*, Vol 26, No.3, 1959, pp.442-447.

43. Iwegwu, E. O., "Combined Plastic Bending and Torsion," *Journal of the Mechanics and Physics of Solids*, Vol.10, 1962, pp.277-282.

44. Avitzur, B., and Pan, J.Z., "Cylinder under Combined Axial and Torsion Load," *Int. J. Mach. Tool Des. Res.*, ASCE, Vol. 105, No. 11, November, 1979, pp. 2187-2202.

45. Mahendran, M., and Murray, N. W., "Ultimate Load Behaviour of Box-Columns under Combined loading of Axial Compression and Torsion," *Thin-Walled Structures*, Vol. 9, No. 1-4, 1990, pp. 91-120.

46. Wang, Y. H., Nie, J.G. and Fan, J.S., "Theoretical model and investigation of concrete filled steel tube columns under axial force-torsion combined action," *Thin-Walled Structures*, No.69, 2013, pp. 1-9.

47. Sved, G, and Brooks, D.S.,"Elastic-plastic Behaviour of a Round Bar Subjected to Axial Force and Torque",*Acta Technica*, Vol.50, 1965, pp. 337-351.

48. Feigen, M., "Inelastic Behavior under Combined Tension and Torsion", *U.S National Congress of Applied Mechanics*, Vol.2, 1954, pp.469-476.

49. MII, H., "Plastic Deformation of Light Metal Bars Strained with Combined Tension and Torsion", *Journal of the Society of Applied Mechanics of Japan*, Vol.3, 1950, pp.196-198.

50. Ono, Akimas., "Stress and Strain in Metals Undergoing Plastic Flow-Tube Wall Subjected to Axial Pull and Torque", *Comm*, Vol.29, No.9, 1953, pp.446-451.

51. Kitada. T., and Nakai. H.," Ultimate Strength of Box Stub Columns under Beams Combined Actions of Compression, Bending and Torsion," *Construction Steel Research*, , No. 13, 1989, pp. 153-168.

52. Timoshenko, S. P., "Sur la Stabilite des Systemes Elastiques", *In Collected Papers of Stephen P. Timoshenko*, McGraw-Hill, New York, 1953, pp.92-224.

53. Trahair, N.S., and Pi. Y. L.," Torsion, Bending and Buckling of Steel Beams," *Engineering Structures*, ASCE, Vol. 19, No. 5, 1997, pp. 372-377.

54. Bleich, F., and Bleich, H.,"Bending, Torsion and Buckling of Bars Composed of Thin Walls ", *IABSE Congress Report*, Vol.2, 1936.

55. Goodier, J.N., " Flexural Torsional Buckling of Bars of Open Section under Bending, Eccentric Thrust or Torsional Loads ", *Bulletin of the Engineering Experiment Station*, Vol.28, 1942.

56. Galambos, T.V., "Inelastic Lateral-Torsional Buckling of Eccentrically Loaded Wide-Flange Columns," Ph.D. Dissertation, Lehigh University, 1959,.University Microfilm Inc., Ann Arbor, Michigan.

57. Galambos, T. V., "Stability Design Criteria for Metal Structures", Fifth Edition, *John Wiley & Sons*, Inc., New York, 1998.

58. Razzaq, Z., and Calash, A. Y., "Imperfect Columns with Biaxial Partial Restraints," *Journal of Structural Engineering*, ASCE, Vol. 111, No. 4, April, 1985, pp. 758-776.

59. Von, M. (1913), " Mechanik der festen Körper im plastisch deformablen Zustand. Göttin," *Nachr. Math.* Phys., vol. 1, pp. 582–592.

60. Brown, P. T., and Trahair, N. S., "Finite Integral Solution of Differential Equation," *Civil Engineering Transactions*, Institution of Engineers, Australia, Vol. CE10, No. 2, October 1969.

61. Usami, T., and Galambos, T. V., "Eccentrically Loaded Single Angle Columns," Publications, *International Association for Bridge and Structural Engineering*, Vol. 31-II, Zurich, 1971.

62. Sanders, E. C., "Experimental Investigation of Steel Angle Column Buckling and Comparison to Seven International Design Specifications," Master Report, Old Dominion University, 2009.

63. Bresler, B. (1960), "Design criteria for reinforced columns under axial load and biaxial bending," *ACI Journal, Proceedings*, 57, 481-490. Disc., 1621-1638.

64. Parme, A.L., Nieves, J.M., Gouwens, A. (1966), "Capacity of reinforced rectangular columns subjected to biaxial bending," *ACI Journal, Proceedings*, 63, 911-923.

65. Beedle, S. Lynn., "Stability of Metal Structures A World View", Second Edition, Structural Stability Research Council, 1991.

66. AISC (2010), Specification for Structural Steel Buildings, ANSI/AISC 360-10, American Institute of Steel Construction, Chicago, IL, 2010.

67. CSA (2009), Design of Steel Structures, CSA S16.09, *Canadian Standards Association*, 5060 Spectrum Way, Suite 200, Mississauga, Ontario, Canada L4W5N6.

68. Eurocode 3 (2014), Design of Steel Structures Part 1.1 General Rules and Rules for Buildings, European Convention for Constructional Steelwork.

Table 1. Dimensionless yield loads, deflections and angle of twist

					Midspan Deflections		
Load Type	Section Orientation Shown in	p	m	t	u (in.)	v (in.)	ψ (rads.)
PR1	Fig.16(a)	0.604			-	0.303	-
UR1	Fig.16(a)		0.992		0.199	-	-
BR1	Fig.16(b)		0.686		0.096	0.093	-
TR1	Fig.16(a)			0.980	-	-	0.128

Table 2. Dimensionless loads and angle of twist for Test Series PBTR1

Test	p	m_x	m_y	t	ψ (rads.)
PBTR11	0.1	0.1	0.1	0.707	0.095
PBTR12	0.2	0.2	0.2	0.696	0.089
PBTR13	0.3	0.3	0.3	0.681	0.083
PBTR14	0.4	0.4	0.4	0.650	0.083
PBTR15	0.5	0.5	0.5	0.614	0.082
PBTR16	0.6	0.6	0.6	0.584	0.082
PBTR17	0.7	0.7	0.7	0.522	0.071
PBTR18	0.8	0.8	0.8	0.426	0.057
PBTR19	0.9	0.9	0.9	0.296	0.037

Table 3. Dimensionless loads and angle of twist for Test Series PUTR1

Test	p	m_x	t	ψ (rads.)
PUTR11	0.1	0.1	0.802	0.110
PUTR12	0.2	0.2	0.790	0.107
PUTR13	0.3	0.3	0.769	0.107
PUTR14	0.4	0.4	0.739	0.105
PUTR15	0.5	0.5	0.698	0.096
PUTR16	0.6	0.6	0.645	0.090
PUTR17	0.7	0.7	0.559	0.073
PUTR18	0.8	0.8	0.484	0.066
PUTR19	0.9	0.9	0.330	0.038

Table 4. Dimensionless loads and angle of twist for Test Series BTR1

Test	m_x	m_y	t	ψ (rads.)
BTR11	0.1	0.1	0.841	0.111
BTR12	0.2	0.2	0.829	0.106
BTR13	0.3	0.3	0.807	0.102
BTR14	0.4	0.4	0.762	0.094
BTR15	0.5	0.5	0.732	0.097
BTR16	0.6	0.6	0.706	0.084
BTR17	0.7	0.7	0.604	0.081
BTR18	0.8	0.8	0.529	0.076
BTR19	0.9	0.9	0.369	0.050

Table 5. Dimensionless loads and angle of twist for Test Series UTR1

Test	m_x	t	ψ (rads.)
UTR11	0.1	0.924	0.118
UTR12	0.2	0.910	0.115
UTR13	0.3	0.886	0.115
UTR14	0.4	0.851	0.109
UTR15	0.5	0.804	0.106
UTR16	0.6	0.743	0.099
UTR17	0.7	0.663	0.091
UTR18	0.8	0.534	0.070
UTR19	0.9	0.388	0.051

Table 6. Dimensionless loads and angle of twist for Test Series PTR1

Test	p	t	ψ (rads.)
PTR11	0.1	0.869	0.115
PTR12	0.2	0.856	0.115
PTR13	0.3	0.809	0.110
PTR14	0.4	0.800	0.108
PTR15	0.5	0.734	0.099
PTR16	0.6	0.698	0.093
PTR17	0.7	0.605	0.087
PTR18	0.8	0.508	0.074
PTR19	0.9	0.369	0.053

Table 7. Dimensionless loads for different combined load types

Load Type	p	m_x	m_y	t
PBTR1	1.0	1.0	1.0	0.756
PUTR1	1.0	0.0	1.0	0.841
BTR1	0.0	1.0	1.0	0.953
UTR1	0.0	1.0	1.0	0.999
PTR1	1.0	0.0	0.0	0.935

Table 8. Dimensionless maximum loads, deflections and angle of twist

					Midspan Deflections		
Load Type	Section Orientation	p*	m*	t*	u (in.)	v (in.)	ψ (rads.)
PR44	Fig.16(b)	0.848			-	0.619	-
UR44	Fig.16(a)		2.473		0.528	-	-
BR44	Fig.16(b)		1.792		0.350	0.357	-
TR44	Fig.16(a)			1.103	-	-	0.205

Table 9. Dimensionless maximum loads and deflections

Load Type	Section Orientation	p*	m*	Midspan Deflections u (in.)	Midspan Deflections v (in.)
TPR44	Fig.16(a)	0.478		-	0.602
TUR44	Fig.16(a)		1.719	0.506	-
TBR44	Fig.16(b)		0.935	0.259	0.263
TBR41	Fig.16(b)		0.935	0.279	0.292
TBPR44	Fig.16(b)	0.269			0.797
TBPR41	Fig.16(b)	0.130			0.296

Table 10. Loads and angle of twist for Test Series PBTR11 and PBTR44

Test	p*	m^*_x	m^*_y	t*	ψ (rads.)
PBTR11	0.2	0.2	0.2	0.996	0.154
PBTR11	0.5	0.5	0.5	0.881	0.138
PBTR44	0.4	0.4	0.4	0.927	0.131
PBTR44	0.6	0.6	0.6	0.814	0.143

Table 11. Warping or longitudinal strains for Test Series TR44 and TBPR41

	Test			
	TR44		TBPR41	
Normal Strain	ϵ_{max} (in./in.)	$\lvert\epsilon_{max}/\epsilon_Y\rvert$ x 10^2	ϵ_{max} (in./in.)	$\lvert\epsilon_{max}/\epsilon_Y\rvert$ x 10^2
ϵ_1	-0.000027	1.35	-0.000022	1.10
ϵ_2	-0.000061	3.06	-0.000062	3.11
ϵ_3	-0.000027	1.35	-0.000036	1.81
ϵ_4	-0.000110	5.52	-0.000136	6.82

Table 12. Warping or longitudinal strains for Test Series PBTR44

	Test			
	TBPR44			
	$p^* = m^* = 0.4$		$p^* = m^* = 0.6$	
Normal Strain	ϵ_{max} (in/in)	$\lvert\epsilon_{max}/\epsilon_Y\rvert$ x 10^2	ϵ_{max} (in/in)	$\lvert\epsilon_{max}/\epsilon_Y\rvert$ x 10^2
ϵ_1	-0.000008	0.40	-0.000003	0.15
ϵ_2	-0.000022	1.10	-0.000085	4.26
ϵ_3	-0.000031	1.56	-0.000044	2.21
ϵ_4	-0.000076	3.81	-0.000104	5.22

Table 13. P-delta effects, T_B , and T_r for Test Series PBTR1 (with $u_o = v_o = L/1000$)

Test	p	m_x	m_y	Pu (kip-in)	Pv (kip-in)	T_B/T_c	T_r/T_c
PBTR11	0.1	0.1	0.1	0.019	0.003	1.034	0.934
PBTR12	0.2	0.2	0.2	0.076	0.012	1.034	0.916
PBTR13	0.3	0.3	0.3	0.172	0.029	1.034	0.902
PBTR14	0.4	0.4	0.4	0.308	0.054	1.034	0.889
PBTR15	0.5	0.5	0.5	0.485	0.089	1.034	0.877
PBTR16	0.6	0.6	0.6	0.705	0.135	1.034	0.867
PBTR17	0.7	0.7	0.7	0.969	0.193	1.034	0.858
PBTR18	0.8	0.8	0.8	1.280	0.267	1.034	0.850
PBTR19	0.9	0.9	0.9	1.640	0.358	1.034	0.843

Table 14. T_{R2} , T_{R3} and T_{R4} for Test Series PBTR1 (with $u_o = v_o = L/1000$)

Test	p	m_x	m_y	T_{R2}/T_c	T_{R3}/T_c	T_{R4}/T_c
PBTR11	0.1	0.1	0.1	1.046	1.046	1.027
PBTR12	0.2	0.2	0.2	1.061	1.062	1.038
PBTR13	0.3	0.3	0.3	1.075	1.075	1.048
PBTR14	0.4	0.4	0.4	1.088	1.088	1.056
PBTR15	0.5	0.5	0.5	1.099	1.099	1.064
PBTR16	0.6	0.6	0.6	1.109	1.109	1.071
PBTR17	0.7	0.7	0.7	1.118	1.118	1.077
PBTR18	0.8	0.8	0.8	1.126	1.126	1.083
PBTR19	0.9	0.9	0.9	1.133	1.133	1.088

Table 15. Pu, T_B , and T_r for Test Series PUTR1 (with u_o = L/1000; v_o = 0)

Test	p	m_x	Pu	T_B/T_c	T_r/T_c
PUTR11	0.1	0.1	0.019	1.030	9.737
PUTR12	0.2	0.2	0.076	1.030	11.732
PUTR13	0.3	0.3	0.172	1.030	13.455
PUTR14	0.4	0.4	0.308	1.030	14.960
PUTR15	0.5	0.5	0.485	1.030	16.286
PUTR16	0.6	0.6	0.705	1.030	17.464
PUTR17	0.7	0.7	0.969	1.030	18.518
PUTR18	0.8	0.8	1.280	1.030	19.466
PUTR19	0.9	0.9	1.640	1.030	20.324

Table 16. T_{R2} , T_{R3} and T_{R4} for Test Series PUTR1 (with u_o = L/1000; v_o = 0)

Test	p	m_x	m_y	T_{R2}/T_c	T_{R3}/T_c	T_{R4}/T_c
PUTR11	0.1	0.1	0.1	0.943	0.943	0.970
PUTR12	0.2	0.2	0.2	0.927	0.927	0.958
PUTR13	0.3	0.3	0.3	0.913	0.913	0.948
PUTR14	0.4	0.4	0.4	0.901	0.901	0.939
PUTR15	0.5	0.5	0.5	0.890	0.890	0.932
PUTR16	0.6	0.6	0.6	0.881	0.881	0.925
PUTR17	0.7	0.7	0.7	0.873	0.873	0.919
PUTR18	0.8	0.8	0.8	0.865	0.865	0.914
PUTR19	0.9	0.9	0.9	0.859	0.858	0.909

Table 17. T_B , and T_r for Test Series BTR1

Test	m_x	m_y	T_B/T_c	T_r/T_c
BTR11	0.1	0.1	1.027	0.881
BTR12	0.2	0.2	1.027	0.860
BTR13	0.3	0.3	1.027	0.842
BTR14	0.4	0.4	1.027	0.826
BTR15	0.5	0.5	1.027	0.811
BTR16	0.6	0.6	1.027	0.799
BTR17	0.7	0.7	1.027	0.787
BTR18	0.8	0.8	1.027	0.777
BTR19	0.9	0.9	1.027	0.768

Table 18. T_{R2} , T_{R3} and T_{R4} for Test Series BTR1

Test	p	m_x	m_y	T_{R2}/T_c	T_{R3}/T_c	T_{R4}/T_c
BTR11	0.1	0.1	0.1	0.880	0.880	0.875
BTR12	0.2	0.2	0.2	0.859	0.858	0.854
BTR13	0.3	0.3	0.3	0.841	0.840	0.835
BTR14	0.4	0.4	0.4	0.825	0.824	0.819
BTR15	0.5	0.5	0.5	0.810	0.810	0.805
BTR16	0.6	0.6	0.6	0.798	0.797	0.792
BTR17	0.7	0.7	0.7	0.786	0.786	0.780
BTR18	0.8	0.8	0.8	0.776	0.775	0.770
BTR19	0.9	0.9	0.9	0.767	0.766	0.760

Table 19. T_B , and T_r for Test Series UTR1

Test	m_x	T_B/T_c	T_r/T_c
UTR11	0.1	1.025	0.776
UTR12	0.2	1.025	0.753
UTR13	0.3	1.025	0.732
UTR14	0.4	1.025	0.713
UTR15	0.5	1.025	0.697
UTR16	0.6	1.025	0.683
UTR17	0.7	1.025	0.669
UTR18	0.8	1.025	0.658
UTR19	0.9	1.025	0.647

Table 20. T_{R2} , T_{R3} and T_{R4} for Test Series UTR1

Test	p	m_x	m_y	T_{R2}/T_c	T_{R3}/T_c	T_{R4}/T_c
UTR11	0.1	0.1	0.1	1.290	1.292	1.302
UTR12	0.2	0.2	0.2	1.331	1.333	1.344
UTR13	0.3	0.3	0.3	1.369	1.371	1.383
UTR14	0.4	0.4	0.4	1.404	1.406	1.419
UTR15	0.5	0.5	0.5	1.437	1.439	1.453
UTR16	0.6	0.6	0.6	1.468	1.470	1.484
UTR17	0.7	0.7	0.7	1.497	1.499	1.514
UTR18	0.8	0.8	0.8	1.524	1.526	1.542
UTR19	0.9	0.9	0.9	1.549	1.552	1.568

Table 21. T_B , and T_r for Test Series PTR1 (with u_o = L/1000; v_o = 0)

Test	p	Pu	T_r/T_c
PTR11	0.1	0.001	13.739
PTR12	0.2	0.015	16.773
PTR13	0.3	0.026	17.991
PTR14	0.4	0.072	20.641
PTR15	0.5	0.118	22.152
PTR16	0.6	0.181	23.499
PTR17	0.7	0.262	24.708
PTR18	0.8	0.365	25.799
PTR19	0.9	0.495	26.788

Table 22. T_{R2} , T_{R3} and T_{R4} for Test Series PTR1 (with u_o = L/1000; v_o = 0)

Test	p	m_x	m_y	T_{R2}/T_c	T_{R3}/T_c	T_{R4}/T_c
PTR11	0.1	0.1	0.1	0.981	0.981	1.002
PTR12	0.2	0.2	0.2	0.967	0.967	0.984
PTR13	0.3	0.3	0.3	0.962	0.962	0.981
PTR14	0.4	0.4	0.4	0.951	0.950	0.974
PTR15	0.5	0.5	0.5	0.944	0.944	0.971
PTR16	0.6	0.6	0.6	0.938	0.938	0.967
PTR17	0.7	0.7	0.7	0.933	0.933	0.964
PTR18	0.8	0.8	0.8	0.929	0.929	0.962
PTR19	0.9	0.9	0.9	0.925	0.924	0.959

Table 23. Experimental and predicted results for Test Series PBTR1

Test	p	m_x	m_y	t_{theo}	t_{exp}	t_{theo}/t_{exp}
PBTR11	0.1	0.1	0.1	0.738	0.707	1.04
PBTR12	0.2	0.2	0.2	0.727	0.696	1.04
PBTR13	0.3	0.3	0.3	0.707	0.681	1.04
PBTR14	0.4	0.4	0.4	0.680	0.650	1.05
PBTR15	0.5	0.5	0.5	0.642	0.614	1.05
PBTR16	0.6	0.6	0.6	0.593	0.584	1.02
PBTR17	0.7	0.7	0.7	0.530	0.522	1.02
PBTR18	0.8	0.8	0.8	0.445	0.426	1.05
PBTR19	0.9	0.9	0.9	0.323	0.296	1.09

Table 24. Experimental and predicted results for Test Series PUTR1

Test	p	m_x	t_{theo}	t_{exp}	t_{theo}/t_{exp}
PUTR11	0.1	0.1	0.820	0.802	1.023
PUTR12	0.2	0.2	0.808	0.790	1.023
PUTR13	0.3	0.3	0.787	0.769	1.023
PUTR14	0.4	0.4	0.756	0.739	1.023
PUTR15	0.5	0.5	0.714	0.698	1.023
PUTR16	0.6	0.6	0.660	0.645	1.023
PUTR17	0.7	0.7	0.589	0.559	1.053
PUTR18	0.8	0.8	0.495	0.484	1.023
PUTR19	0.9	0.9	0.359	0.330	1.089

Table 25. Experimental and predicted results for Test Series BTR1

Test	m_x	m_y	t_{theo}	t_{exp}	t_{theo}/t_{exp}
BTR11	0.1	0.1	0.929	0.841	1.104
BTR12	0.2	0.2	0.915	0.829	1.104
BTR13	0.3	0.3	0.891	0.807	1.104
BTR14	0.4	0.4	0.856	0.762	1.124
BTR15	0.5	0.5	0.809	0.732	1.104
BTR16	0.6	0.6	0.747	0.706	1.059
BTR17	0.7	0.7	0.667	0.604	1.104
BTR18	0.8	0.8	0.560	0.529	1.059
BTR19	0.9	0.9	0.407	0.369	1.104

Table 26. Experimental and predicted results for Test Series UTR1

Test	m_x	t_{theo}	t_{exp}	t_{theo}/t_{exp}
UTR11	0.1	0.97	0.924	1.055
UTR12	0.2	0.96	0.910	1.055
UTR13	0.3	0.93	0.886	1.055
UTR14	0.4	0.90	0.851	1.055
UTR15	0.5	0.85	0.804	1.055
UTR16	0.6	0.78	0.743	1.055
UTR17	0.7	0.70	0.663	1.055
UTR18	0.8	0.59	0.534	1.100
UTR19	0.9	0.43	0.388	1.100

Table 27. Experimental and predicted results for Test Series PTR1

Test	p	t_{theo}	t_{exp}	t_{theo}/t_{exp}
PTR11	0.1	0.915	0.869	1.053
PTR12	0.2	0.900	0.856	1.051
PTR13	0.3	0.887	0.809	1.097
PTR14	0.4	0.840	0.800	1.049
PTR15	0.5	0.794	0.734	1.081
PTR16	0.6	0.733	0.698	1.049
PTR17	0.7	0.654	0.605	1.081
PTR18	0.8	0.550	0.508	1.081
PTR19	0.9	0.399	0.369	1.082

Table 28. p-delta effects for different combined load types (with $u_o = v_o = L/1000$)

Load Type	p	m_x	m_y	Pu	Pv
PBT	0.9	0.9	0.90	1.640	0.358
PUT	0.9	-	0.90	1.640	-
BT	-	0.9	0.90	-	-
UT	-	-	0.90	-	-
PT	0.9	-	-	0.495	-

Table 29. Bending shear stress effects for different combined load types

Load Type	p	m_x	m_y	T_B/T_{R1}
PBT	0.9	0.9	0.90	1.034
PUT	0.9	-	0.90	1.030
BT	-	0.9	0.90	1.027
UT	-	-	0.90	1.025
PT	0.9	-	-	1.000

Table 30. Residual stress effects for different combined load types

Load Type	p	m_x	m_y	T_r/T_{R1}
PBT	0.9	0.9	0.90	0.843
PUT	0.9	-	0.90	0.797
BT	-	0.9	0.90	0.768
UT	-	-	0.90	0.647
PT	0.9	-	-	0.862

Table 31. Effects of R2 for different combined load types

Load Type	p	m_x	m_y	T_{R2}/T_{R1}
PBT	0.9	0.9	0.90	0.882
PUT	0.9	-	0.90	0.859
BT	-	0.9	0.90	0.767
UT	-	-	0.90	0.645
PT	0.9	-	-	0.925

Table 32. Effects of R3 for different combined load types

Load Type	p	m_x	m_y	T_{R3}/T_{R1}
PBT	0.9	0.9	0.90	0.882
PUT	0.9	-	0.90	0.858
BT	-	0.9	0.90	0.766
UT	-	-	0.90	0.644
PT	0.9	-	-	0.924

Table 33. Effects of R4 for different combined load types

Load Type	p	m_x	m_y	T_{R4}/T_{R1}
PBT	0.9	0.9	0.90	0.919
PUT	0.9	-	0.90	0.909
BT	-	0.9	0.90	0.760
UT	-	-	0.90	0.638
PT	0.9	-	-	0.959

Table 34. Maximum torsional moments for PTR11, UTR11, and BTR11

Load Type	p_{max}	$m_{x(max)}$	$m_{y(max)}$	t_{max}
PTR11	0.900	-	-	0.400
UTR11	-	-	0.900	0.312
BTR11	-	0.900	0.900	0.337

Table 35. Maximum torsional moments for PUT11 and PBTR11

Load type	p_{max}	$m_{x(max)}$	$m_{y(max)}$	t_{max}
PUTR11	0.500	-	0.500	0.766
PBTR11	0.500	0.500	0.500	0.707

Table 36. Maximum torsional moments for PTR44, UTR44, and BTR44

Load Type	p_{max}	$m_{x(max)}$	$m_{y(max)}$	t_{max}
PTR44	0.900	-	-	0.436
UTR44	-	-	0.900	0.450
BTR44	-	0.900	0.900	0.446

Table 37. Maximum torsional moments for PUT44 and PBTR44

Load type	p_{max}	$m_{x(max)}$	$m_{y(max)}$	t_{max}
PUTR44	0.500	-	0.500	0.893
PBTR44	-	0.500	0.500	0.885

Table 38. Results for TPR44, TUR44, TBR44, TBR41, TBPR44, and TBPR41

Load Type	p^*_{exp}	m^*_{exp}	t^*_{exp}	p^*_{theo}	m^*_{theo}	t^*_{theo}	p^*_{theo}/p^*_{exp}	m^*_{theo}/m^*_{exp}	t^*_{theo}/t^*_{exp}
PR44	0.848			0.800			0.944		
UR44		2.473			2.500			1.011	
BR44		1.792			1.588			0.886	
TR44			1.103			1.129			1.024
TPR44	0.478			0.501			1.047		
TUR44		1.719			1.468			0.854	
TBR44		0.935			0.772			0.826	
TBR41		0.935			0.795			0.851	
TBPR44	0.269			0.279			1.040		
TBPR41	0.130			0.120			0.927		
PBTR11			0.996			0.991			0.995
PBTR11			0.881			0.876			0.995
PBTR44			0.927			0.911			0.983
PBTR44			0.814			0.810			0.995

Table 39. Test and predicted results for Test Series PBTR11 and PBTR44

Test	p^*	m^*_x	m^*_y	t^*_{theo}	t^*_{exp}	t^*_{theo}/t^*_{exp}
PBTR11	0.2	0.2	0.2	0.991	0.996	0.995
PBTR11	0.5	0.5	0.5	0.876	0.881	0.995
PBTR44	0.4	0.4	0.4	0.911	0.927	0.983
PBTR44	0.6	0.6	0.6	0.810	0.814	0.995

Table 40. AS4100 Stability Checks without Torsion

AS4100			
CS Strength	HSS7x7x0.375	HSS8x6x0.375	W8x31
P=	119.250	119.250	95.760
M_x=	13.023	13.950	24.063
M_y=	13.023	11.786	8.111
L (in) =	144.000	144.000	144.000
Expression 183	0.548	0.547	0.148
OM Strength Expression 187	0.801	0.799	0.848

Table 41. AIJ Stability Checks without Torsion

AIJ	HSS7x7x0.375	HSS8x6x0.375	W8x31
P=	119.250	119.250	95.760
M_x=	13.023	13.950	24.063
M_y=	13.023	11.786	8.111
L (in) =	144.000	144.000	144.000
Expression 189	0.698	0.724	0.861

Table 42. AISC-LFRD Stability Checks without Torsion

AISC-LFRD	HSS7x7x0.375	HSS8x6x0.375	W8x31
P=	119.250	119.250	95.760
M_x=	13.023	13.950	24.063
M_y=	13.023	11.786	8.111
L (in) =	144.000	144.000	144.000
Expression 190	0.609	0.628	0.703

Table 43. BS 5950 Stability Checks without Torsion

BS 5950			
CS Check	HSS7x7x0.375	HSS8x6x0.375	W8x31
P=	119.250	119.250	95.760
M_x=	13.023	13.950	24.063
M_y=	13.023	11.786	8.111
L (in) =	144.000	144.000	144.000
Expression 191a	0.493	0.492	0.538
In-plane 'Buckling' Expression 191b	0.592	0.643	0.765
Out-plane Buckling Expression 191c	-	0.645	0.780

Table 44. CSA Stability Checks without Torsion

CSA			
CS Strength	HSS7x7x0.375	HSS8x6x0.375	W8x31
P=	119.250	119.250	95.760
M_x=	13.023	13.950	24.063
M_y=	13.023	11.786	8.111
L (in) =	144.000	144.000	144.000
Expression 192	0.548	0.547	0.505
OM Strength Expression 192	0.660	0.690	0.675
LTB Check Expression 192		0.659	0.669

Table 45. Eurocode 3 Stability Checks without Torsion

Eurocode 3			
CS Strength	HSS7x7x0.375	HSS8x6x0.375	W8x31
P=	119.250	119.250	95.760
M_x=	13.023	13.950	24.063
M_y=	13.023	11.786	8.111
L (in) =	144.000	144.000	144.000
Expression 193a	0.517	0.517	0.558
OM Strength Expression 193b	0.490	0.514	0.574
LTB Check Expression 193c	-	0.515	0.662

Table 46. GBJ Checks without Torsion

GBJ			
CS Strength	HSS7x7x0.375	HSS8x6x0.375	W8x31
P=	119.250	119.250	95.760
M_x=	13.023	13.950	24.063
M_y=	13.023	11.786	8.111
L (in) =	144.000	144.000	144.000
Expression 203a	0.466	0.465	0.506
OM Strength Expression 203b	0.675	0.703	0.796

Table 47. SNiP Stability Checks without Torsion

SNiP	HSS7x7x0.375	HSS8x6x0.375	W8x31
P=	119.250	119.250	95.760
M_x=	13.023	13.950	24.063
M_y=	13.023	11.786	8.111
L (in) =	144.000	144.000	144.000
Expression 204	0.807	0.804	0.814

Table 48. Stability Check for International Codes and Expression 208a

Stability Check	HSS7x7x0.375			HRS8x6x0.375			W8x31		
	λ	λ_{Prop}	λ_{prop}/λ	λ	λ_{Prop}	λ_{prop}/λ	λ	λ_{Prop}	λ_{prop}/λ
Australia	0.801	0.742	0.926	0.799	0.756	0.947	0.848	0.852	1.004
Canada	0.548	0.568	1.038	0.69	0.614	0.89	0.675	0.751	1.113
China	0.675	0.62	0.918	0.703	0.626	0.891	0.796	0.775	0.973
Europe	0.517	0.518	1.002	0.514	0.558	1.085	0.662	0.799	1.206
Japan	0.698	0.642	0.919	0.724	0.689	0.951	0.861	0.872	1.012
Great Britain	0.592	0.531	0.898	0.643	0.602	0.936	0.78	0.776	0.994
Russia	0.807	0.736	0.913	0.804	0.728	0.906	0.814	0.823	1.011
US	0.609	0.556	0.913	0.628	0.594	0.945	0.703	0.787	1.119

Table 49. Stability Check for International Codes and Expression 208b

Stability Check	HSS7x7x0.375			HRS8x6x0.375			W8x31		
	λ	λ_{Prop}	λ_{prop}/λ	λ	λ_{Prop}	λ_{prop}/λ	λ	λ_{Prop}	λ_{prop}/λ
Australia	0.548	0.725	1.323	0.547	0.722	1.32	0.612	0.718	1.173
Canada	0.66	0.541	0.82	0.69	0.568	0.823	0.675	0.614	0.91
China	0.675	0.593	0.879	0.703	0.621	0.883	0.796	0.666	0.837
Europe	0.517	0.481	0.93	0.514	0.503	0.979	0.662	0.66	0.997
Japan	0.698	0.609	0.872	0.724	0.643	0.888	0.861	0.731	0.849
Great Britain	0.592	0.514	0.868	0.643	0.563	0.876	0.78	0.654	0.838
Russia	0.807	0.764	0.947	0.804	0.761	0.947	0.814	0.745	0.915
US	0.609	0.529	0.869	0.628	0.548	0.873	0.703	0.652	0.927

Table 50. Stability Check for International Codes and Expression 208c

Stability Check	HSS7x7x0.375			HRS8x6x0.375			W8x31		
	λ	λ_{Prop}	λ_{prop}/λ	λ	λ_{Prop}	λ_{prop}/λ	λ	λ_{Prop}	λ_{prop}/λ
Australia	0.548	0.7	1.278	0.547	0.698	1.276	0.612	0.659	1.077
Canada	0.66	0.513	0.777	0.69	0.541	0.784	0.675	0.553	0.819
China	0.675	0.533	0.79	0.703	0.56	0.796	0.796	0.571	0.717
Europe	0.517	0.458	0.886	0.514	0.481	0.935	0.662	0.582	0.88
Japan	0.698	0.587	0.841	0.724	0.62	0.857	0.861	0.667	0.774
Great Britain	0.592	0.479	0.809	0.643	0.53	0.824	0.78	0.571	0.732
Russia	0.807	0.764	0.948	0.804	0.761	0.947	0.814	0.745	0.915
US	0.609	0.5	0.821	0.628	0.52	0.827	0.703	0.573	0.816

Table 51. Expression 216 for HSS7x7x0.375, HSS8x6x0.375 and W8x31

AS4100	p^*	m^*_x	m^*_y	Expression 216		
				HSS7x7x0.375	HSS8x6x0.375	W8x31
PBTR11	0.1	0.1	0.1	0.021	0.016	0.025
PBTR12	0.2	0.2	0.2	0.068	0.053	0.078
PBTR13	0.3	0.3	0.3	0.140	0.112	0.158
PBTR14	0.4	0.4	0.4	0.242	0.194	0.266
PBTR15	0.5	0.5	0.5	0.383	0.304	0.403
PBTR16	0.6	0.6	0.6	0.575	0.448	0.575
PBTR17	0.7	0.7	0.7	0.840	0.637	0.787
PBTR18	0.8	0.8	0.8	1.218	0.888	1.048
PBTR19	0.9	0.9	0.9	1.790	1.236	1.372

Table 52. Expression 219 for HSS7x7x0.375, HSS8x6x0.375 and W8x31

AIJ	p^*	m^*_x	m^*_y	Expression 219		
				HSS7x7x0.375	HSS8x6x0.375	W8x31
PBTR11	0.1	0.1	0.1	0.128	0.117	0.128
PBTR12	0.2	0.2	0.2	0.266	0.246	0.270
PBTR13	0.3	0.3	0.3	0.414	0.387	0.427
PBTR14	0.4	0.4	0.4	0.571	0.539	0.598
PBTR15	0.5	0.5	0.5	0.738	0.704	0.784
PBTR16	0.6	0.6	0.6	0.915	0.879	0.985
PBTR17	0.7	0.7	0.7	1.101	1.067	1.200
PBTR18	0.8	0.8	0.8	1.297	1.267	1.429
PBTR19	0.9	0.9	0.9	1.503	1.478	1.673

Table 53. Expression 221 for HSS7x7x0.375, HSS8x6x0.375 and W8x31

AISC-LFRD	p^*	m^*_x	m^*_y	Expression 221		
				HSS7x7x0.375	HSS8x6x0.375	W8x31
PBTR11	0.1	0.1	0.1	0.130	0.119	0.131
PBTR12	0.2	0.2	0.2	0.271	0.250	0.276
PBTR13	0.3	0.3	0.3	0.420	0.393	0.436
PBTR14	0.4	0.4	0.4	0.580	0.547	0.610
PBTR15	0.5	0.5	0.5	0.749	0.713	0.799
PBTR16	0.6	0.6	0.6	0.929	0.891	1.003
PBTR17	0.7	0.7	0.7	1.117	1.081	1.221
PBTR18	0.8	0.8	0.8	1.316	1.282	1.453
PBTR19	0.9	0.9	0.9	1.524	1.496	1.700

Table 54. Expression 223 for HSS7x7x0.375, HSS8x6x0.375 and W8x31

BS 5950	p^*	m^*_x	m^*_y	Expression 223		
				HSS7x7x0.375	HSS8x6x0.375	W8x31
PBTR11	0.1	0.1	0.1	0.137	0.125	0.139
PBTR12	0.2	0.2	0.2	0.284	0.261	0.293
PBTR13	0.3	0.3	0.3	0.440	0.410	0.462
PBTR14	0.4	0.4	0.4	0.607	0.570	0.645
PBTR15	0.5	0.5	0.5	0.783	0.741	0.842
PBTR16	0.6	0.6	0.6	0.968	0.925	1.054
PBTR17	0.7	0.7	0.7	1.164	1.120	1.281
PBTR18	0.8	0.8	0.8	1.369	1.327	1.522
PBTR19	0.9	0.9	0.9	1.584	1.546	1.778

Table 55. Expression 225 for HSS7x7x0.375, HSS8x6x0.375 and W8x31

CSA	p^*	m^*_x	m^*_y	Expression 225		
				HSS7x7x0.375	HSS8x6x0.375	W8x31
PBTR11	0.1	0.1	0.1	0.122	0.113	0.109
PBTR12	0.2	0.2	0.2	0.255	0.238	0.232
PBTR13	0.3	0.3	0.3	0.396	0.374	0.369
PBTR14	0.4	0.4	0.4	0.548	0.523	0.521
PBTR15	0.5	0.5	0.5	0.709	0.683	0.688
PBTR16	0.6	0.6	0.6	0.880	0.855	0.869
PBTR17	0.7	0.7	0.7	1.061	1.038	1.065
PBTR18	0.8	0.8	0.8	1.252	1.234	1.275
PBTR19	0.9	0.9	0.9	1.452	1.441	1.500

Table 56. Expression 227 for HSS7x7x0.375, HSS8x6x0.375 and W8x31

Eurocode 3	p	m_x	m_y	Expression 227		
				HSS7x7x0.375	HSS8x6x0.375	W8x31
PBTR11	0.1	0.1	0.1	0.137	0.125	0.139
PBTR12	0.2	0.2	0.2	0.284	0.261	0.293
PBTR13	0.3	0.3	0.3	0.440	0.410	0.462
PBTR14	0.4	0.4	0.4	0.607	0.570	0.645
PBTR15	0.5	0.5	0.5	0.783	0.741	0.842
PBTR16	0.6	0.6	0.6	0.968	0.925	1.054
PBTR17	0.7	0.7	0.7	1.164	1.120	1.281
PBTR18	0.8	0.8	0.8	1.369	1.327	1.522
PBTR19	0.9	0.9	0.9	1.584	1.546	1.778

Table 57. Expression 229 for HSS7x7x0.375, HSS8x6x0.375 and W8x31

GBJ	p^*	m^*_x	m^*_y	Expression 229		
				HSS7x7x0.375	HSS8x6x0.375	W8x31
PBTR11	0.1	0.1	0.1	0.122	0.112	0.117
PBTR12	0.2	0.2	0.2	0.256	0.238	0.248
PBTR13	0.3	0.3	0.3	0.403	0.378	0.394
PBTR14	0.4	0.4	0.4	0.562	0.533	0.555
PBTR15	0.5	0.5	0.5	0.734	0.702	0.730
PBTR16	0.6	0.6	0.6	0.919	0.886	0.920
PBTR17	0.7	0.7	0.7	1.118	1.085	1.124
PBTR18	0.8	0.8	0.8	1.331	1.300	1.342
PBTR19	0.9	0.9	0.9	1.558	1.532	1.576

Table 58. Expression 231 for HSS7x7x0.375, HSS8x6x0.375 and W8x31

SNiP	p^*	m^*_x	m^*_y	Expression 231		
				HSS7x7x0.375	HSS8x6x0.375	W8x31
PBTR11	0.1	0.1	0.1	0.082	0.081	0.067
PBTR12	0.2	0.2	0.2	0.175	0.173	0.148
PBTR13	0.3	0.3	0.3	0.276	0.278	0.244
PBTR14	0.4	0.4	0.4	0.388	0.394	0.354
PBTR15	0.5	0.5	0.5	0.509	0.522	0.479
PBTR16	0.6	0.6	0.6	0.641	0.661	0.618
PBTR17	0.7	0.7	0.7	0.781	0.813	0.772
PBTR18	0.8	0.8	0.8	0.932	0.976	0.940
PBTR19	0.9	0.9	0.9	1.092	1.151	1.123

Table 59. Expression 233 for HSS7x7x0.375, HSS8x6x0.375 and W8x31

BLIETU	p^*	m^*_x	m^*_y	Expressions 233		
				HSS7x7x0.375	HSS8x6x0.375	W8x31
PBTR11	0.1	0.1	0.1	0.158	0.154	0.154
PBTR12	0.2	0.2	0.2	0.291	0.284	0.309
PBTR13	0.3	0.3	0.3	0.427	0.419	0.476
PBTR14	0.4	0.4	0.4	0.570	0.563	0.655
PBTR15	0.5	0.5	0.5	0.722	0.716	0.847
PBTR16	0.6	0.6	0.6	0.884	0.880	1.054
PBTR17	0.7	0.7	0.7	1.055	1.055	1.274
PBTR18	0.8	0.8	0.8	1.237	1.242	1.509
PBTR19	0.9	0.9	0.9	1.428	1.440	1.758

Table 60. Expressions 216-233 for HSS7x7x0.375, HSS8x6x0.375 and W8x31

	HSS7x7x0.375	HRS8x6x0.375	W8x31
PBTR15	$p^* = m^*_x = m^*_y = 0.5$		
Australia	0.735	0.660	0.734
Canada	0.709	0.683	0.688
China	0.734	0.702	0.730
Europe	0.783	0.741	0.842
Japan	0.738	0.704	0.784
Great Britain	0.783	0.741	0.842
Russia	0.509	0.522	0.479
US	0.749	0.713	0.799
BLIETU	0.722	0.716	0.847
PBTR16	$p^* = m^*_x = m^*_y = 0.6$		
Australia	0.882	0.793	0.881
Canada	0.880	0.855	0.869
China	0.919	0.886	0.920
Europe	0.968	0.925	1.054
Japan	0.915	0.879	0.985
Great Britain	0.968	0.925	1.054
Russia	0.641	0.661	0.618
US	0.929	0.891	1.003
BLIETU	0.884	0.880	1.054

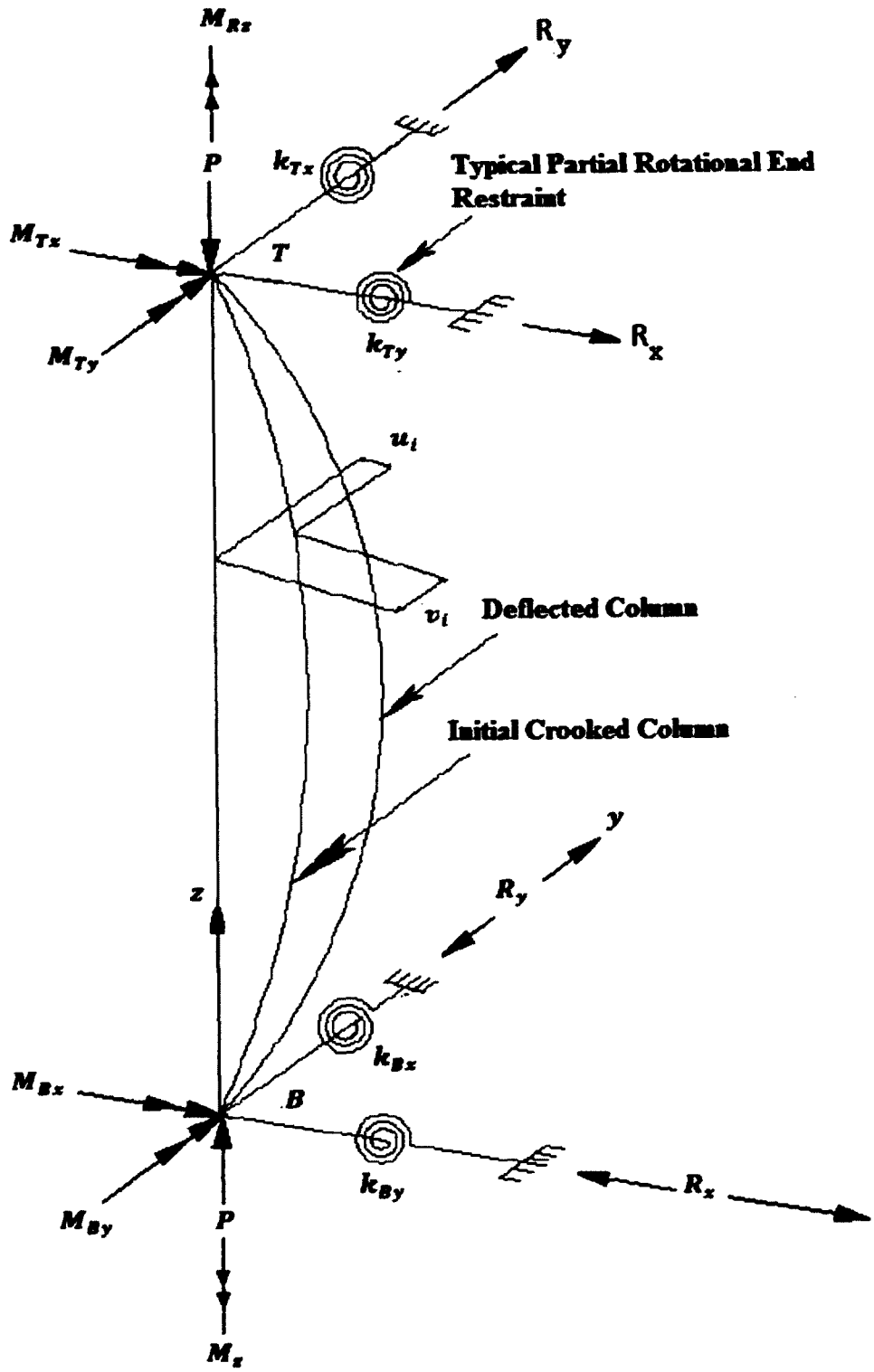

Figure 1. Torsionally loaded imperfect beam-column

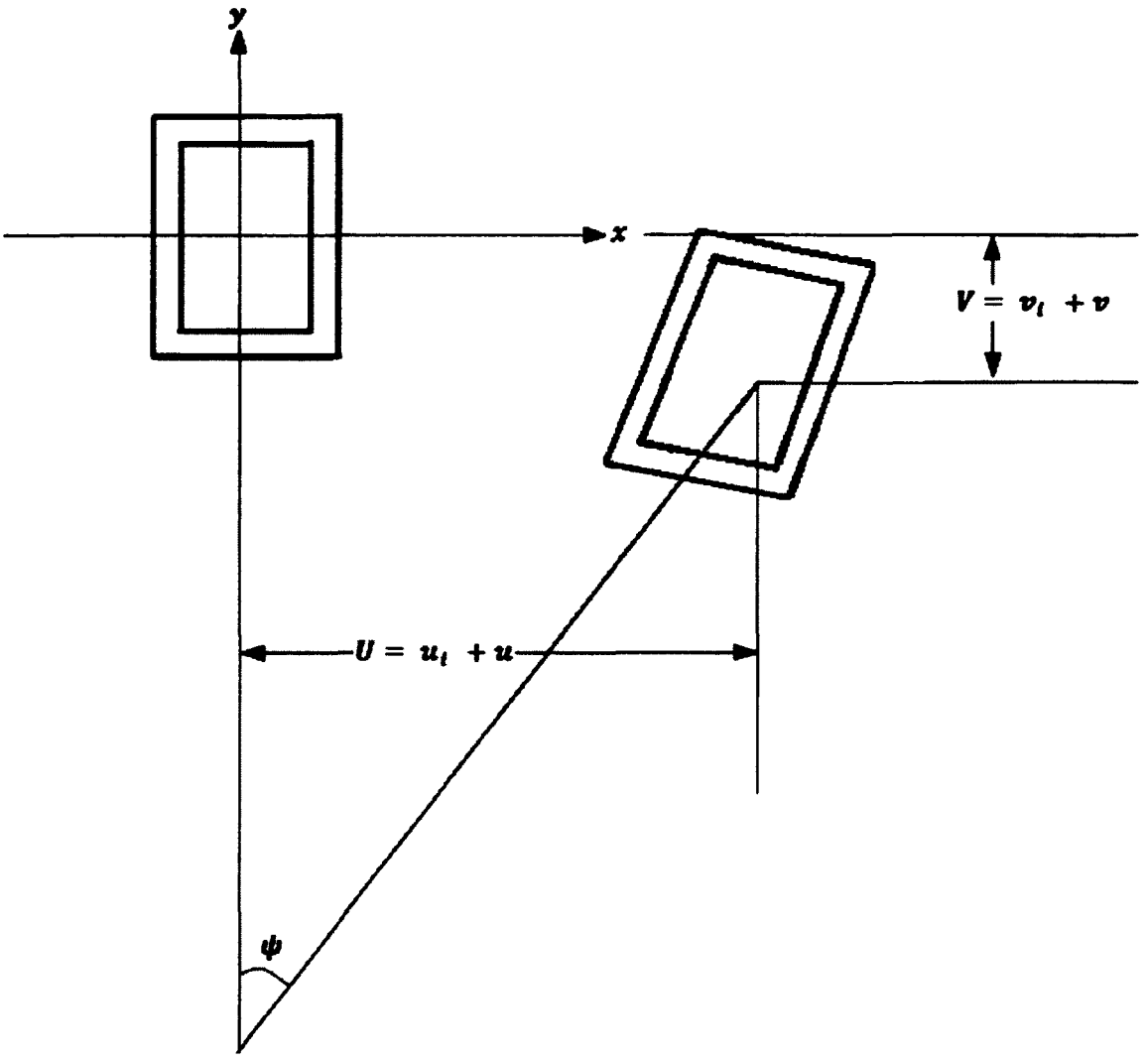

Figure 2. Total displacements U, V and ψ

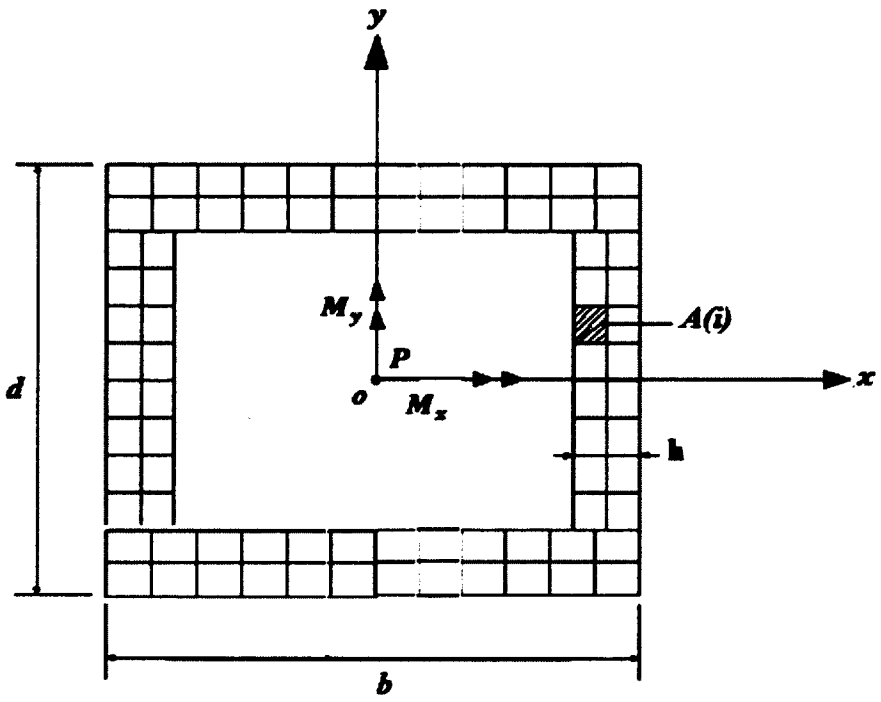

Figure 3. Discretized hollow rectangular section with applied loads P, M_x and M_y

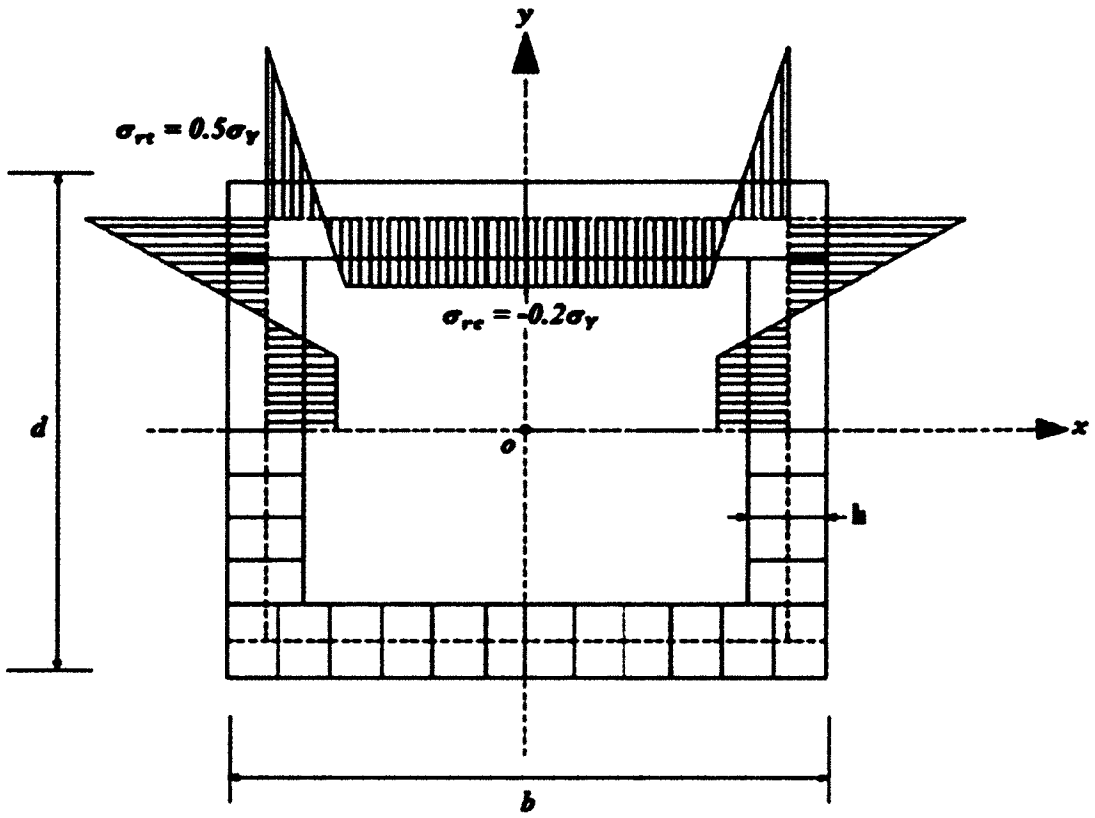

Figure 4. Residual stress distribution

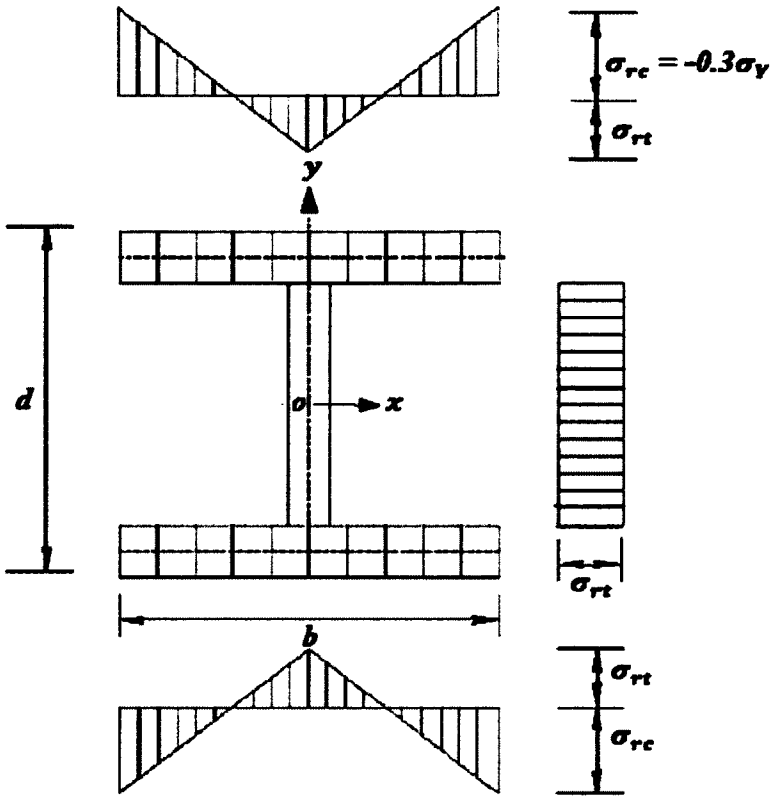

Figure 5. I-section with residual stress distribution

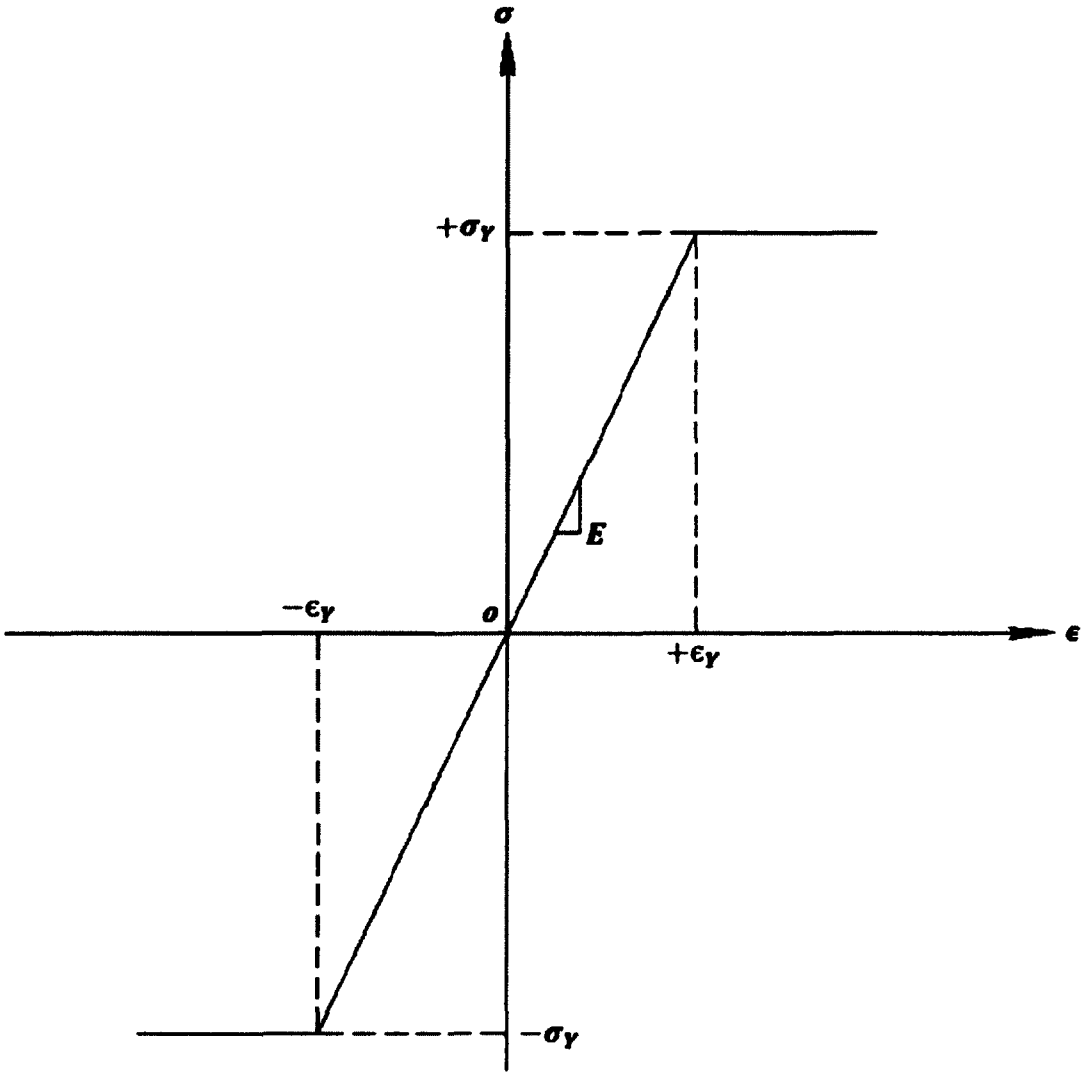

Figure 6. Material normal stress-strain relationship

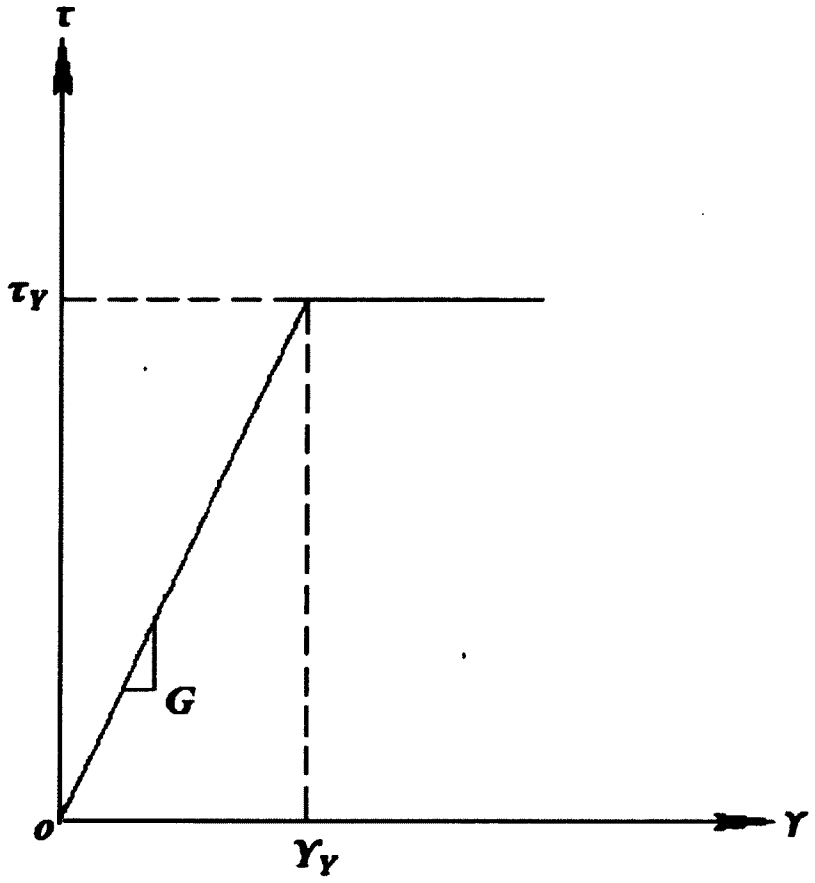

Figure 7. Material shear stress- shear strain relationship

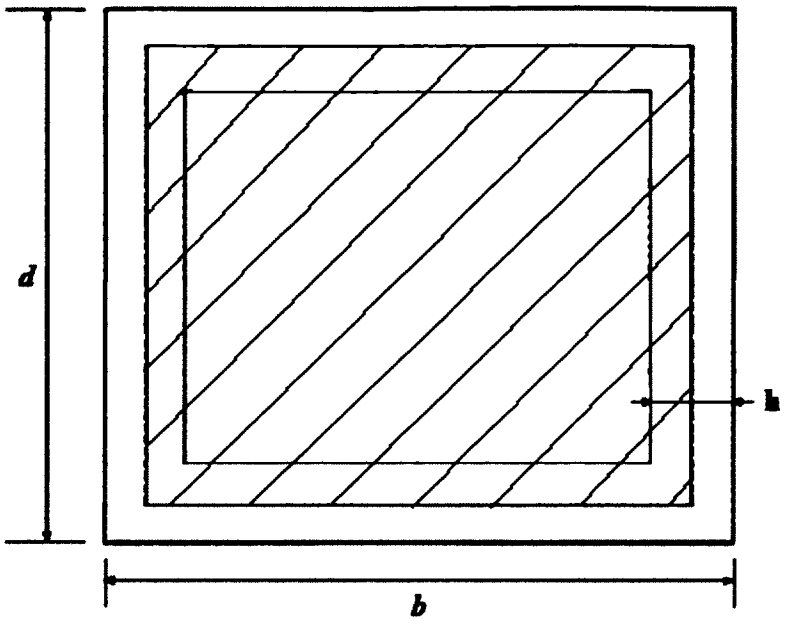

Figure 8. Definition of A_E

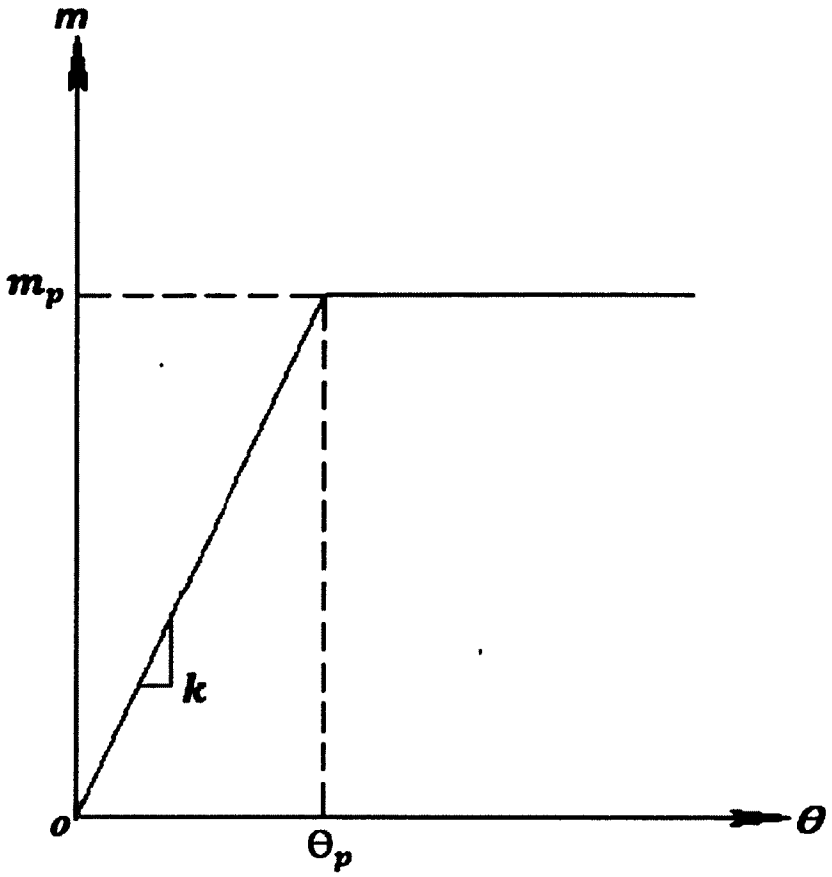

Figure 9. Moment-rotation relationship

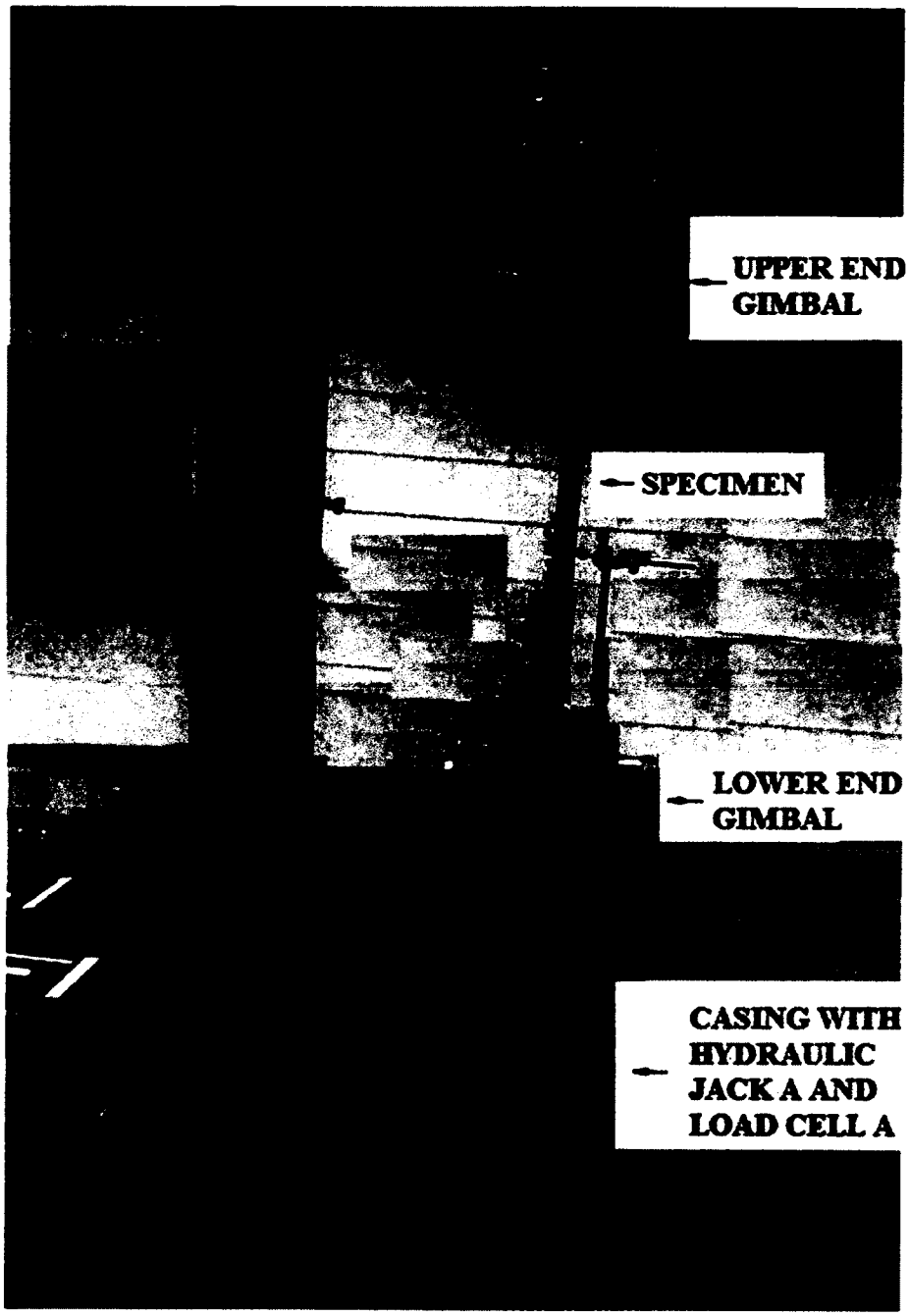

Figure 10. Axial load test set up

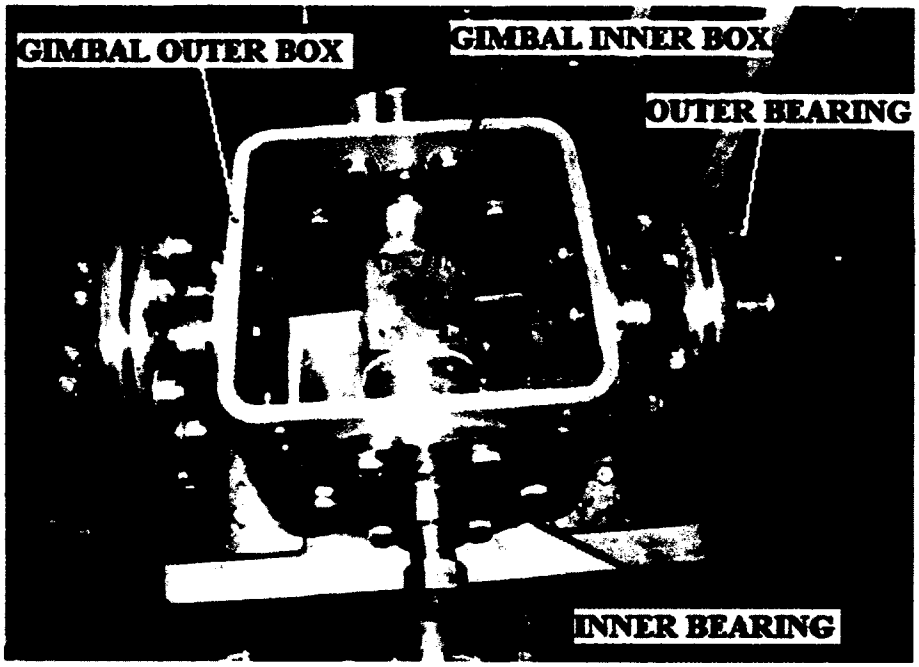

Figure 11. Lower end gimbal

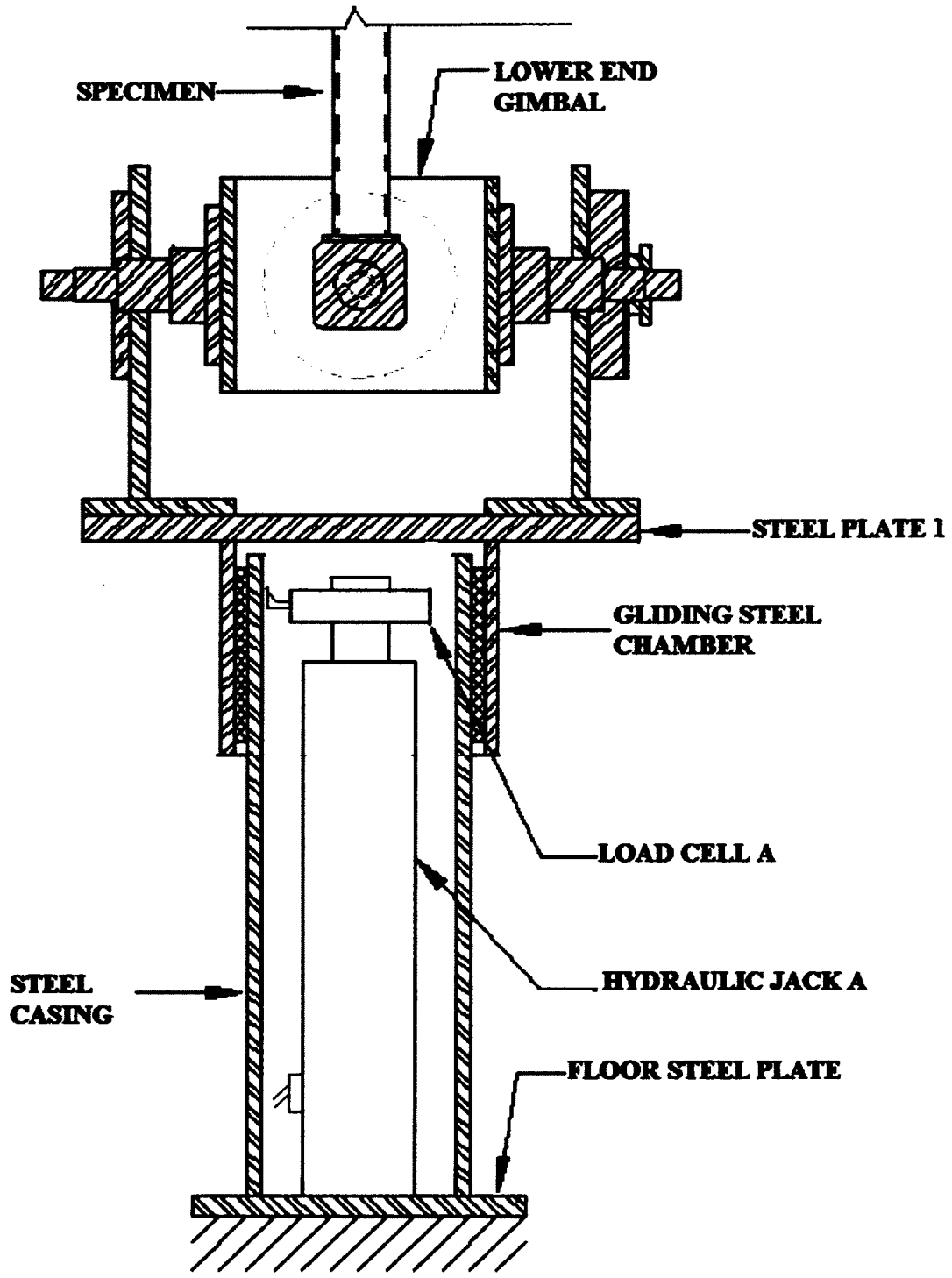

Figure 12. Schematic of lower portion of setup for axial load and bending tests

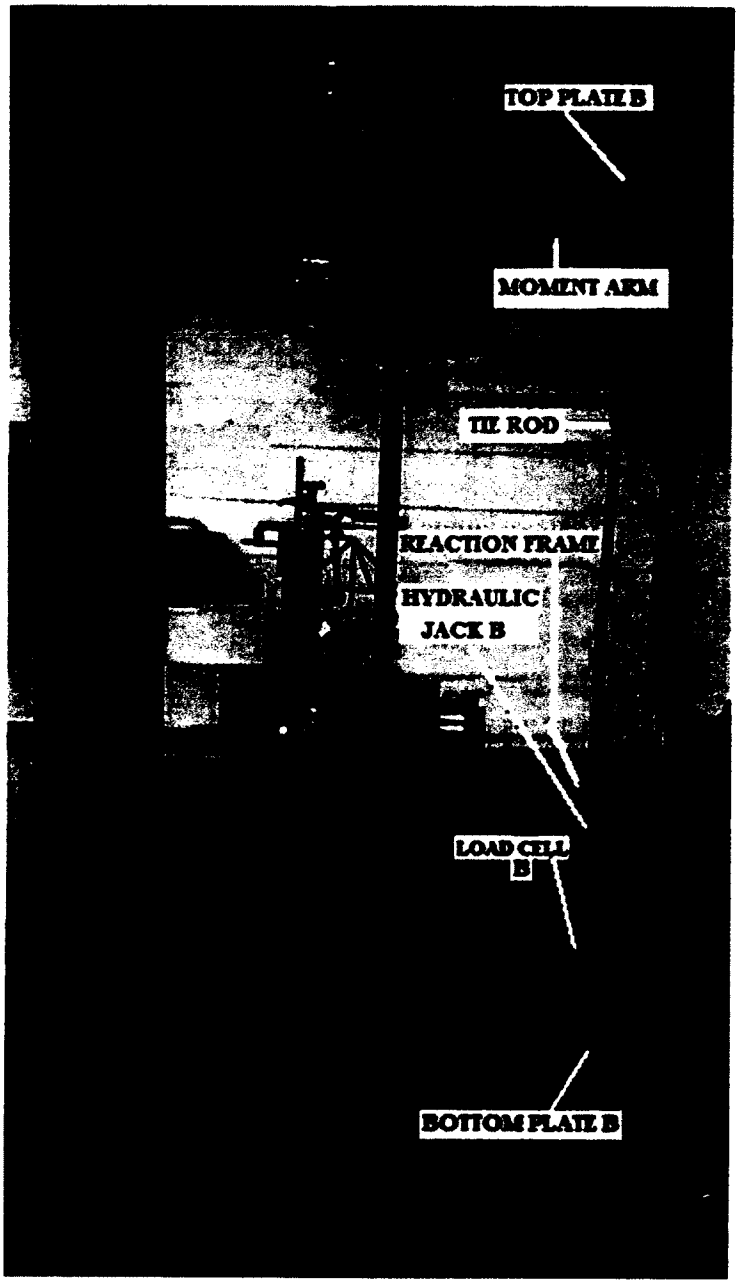

Figure 13. Combined axial and bending test set up

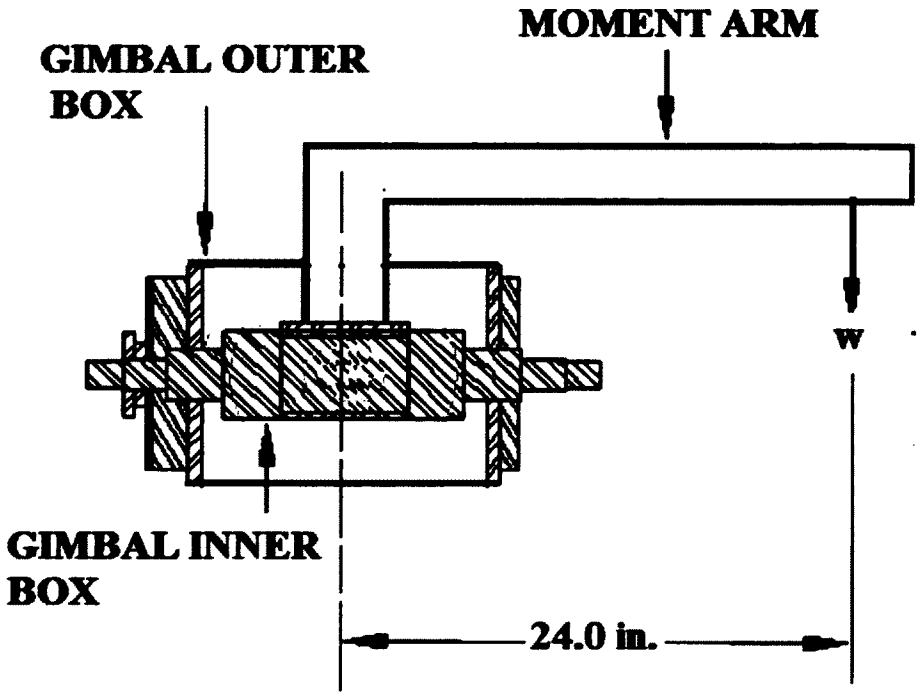

Figure 14. Schematic of upper end gimbal with moment arm

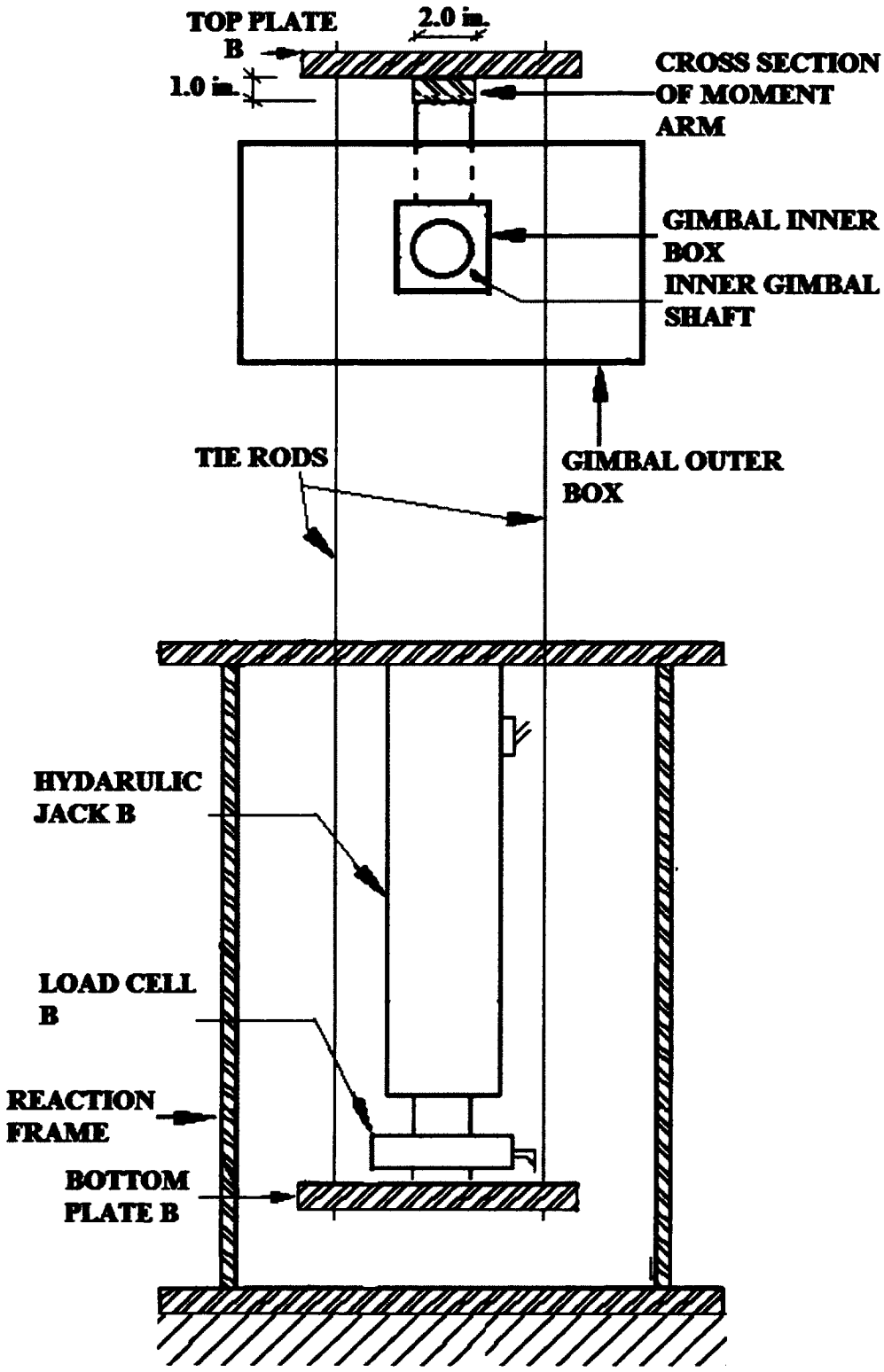

Figure 15. Schematic of bending device

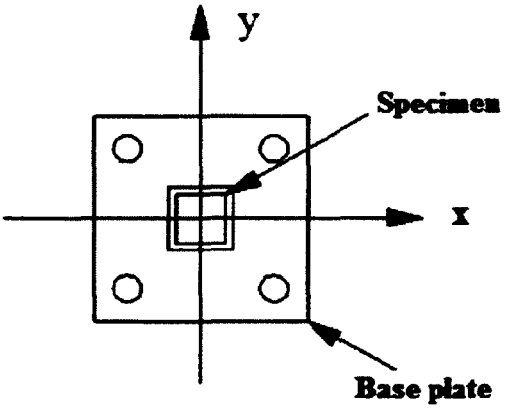

a) Axial compression, uniaxial bending and Torsion tests

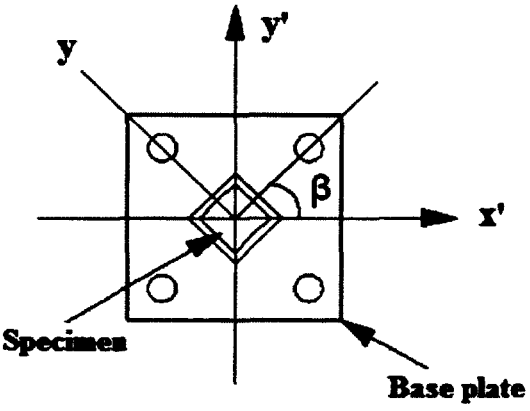

b) Biaxial bending test

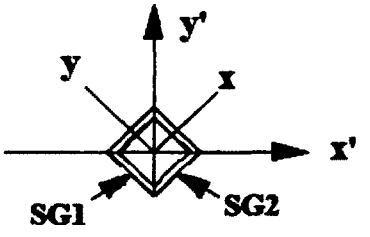

c) Midspan strain gauge locations

Figure 16. Test specimen end plate details and strain gauge locations

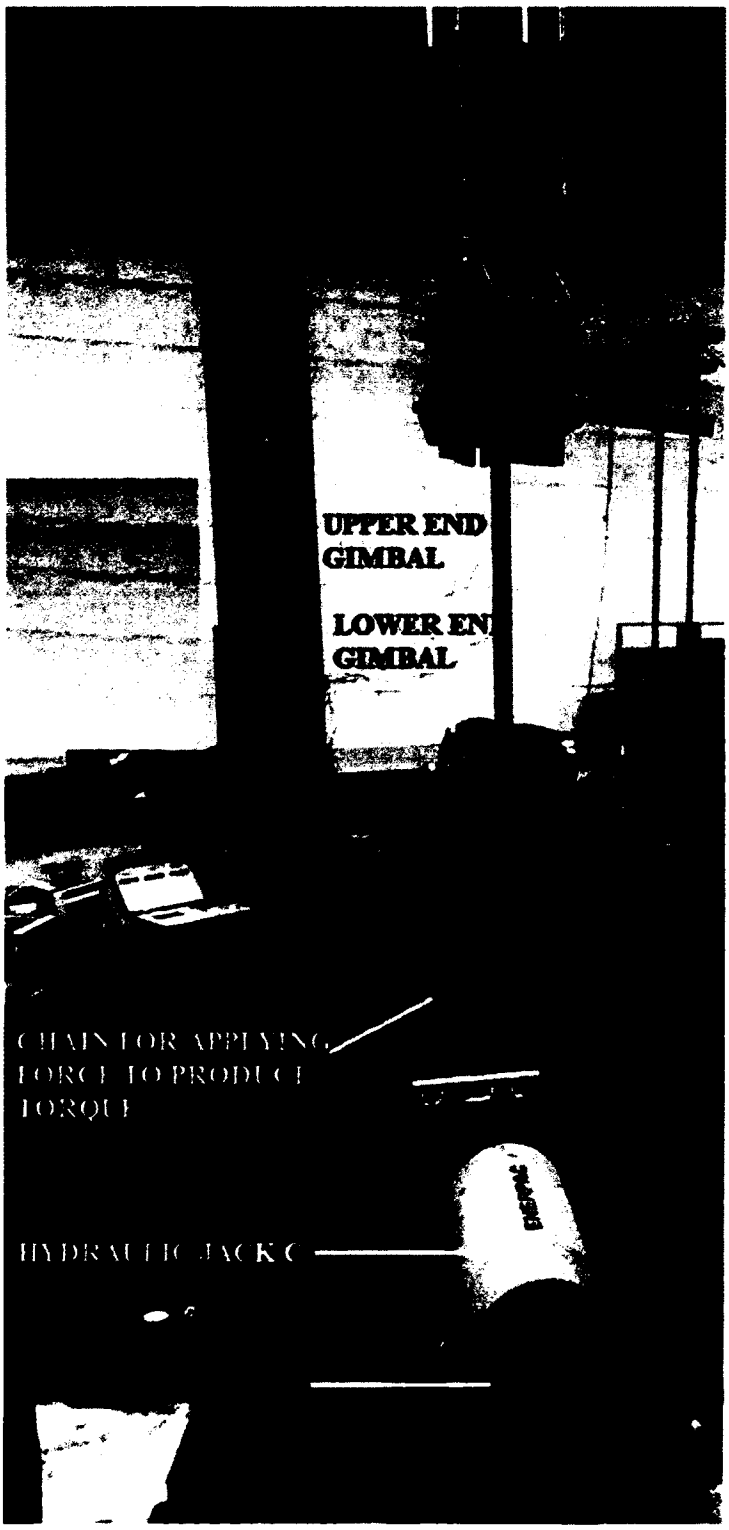

Figure 17. Combined axial, bending and torsion test set up

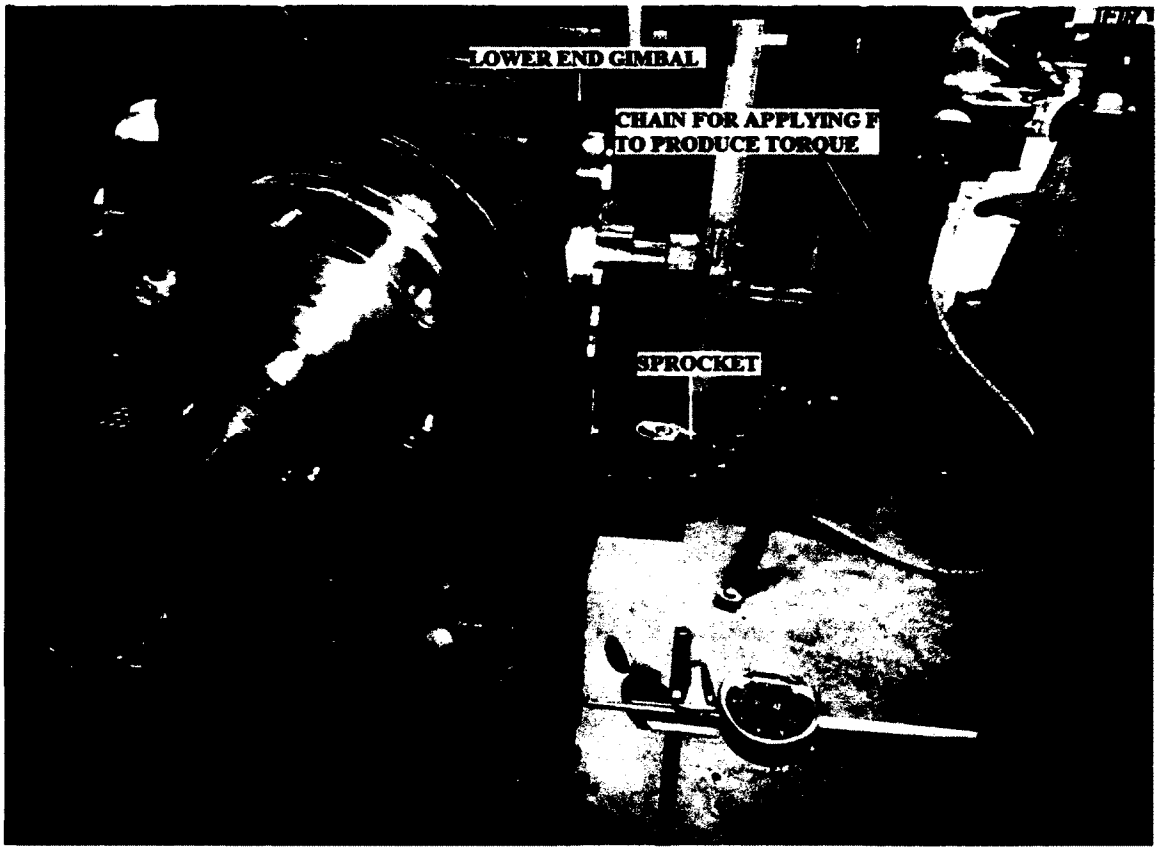

Figure 18. Test set up to apply force F with eccentricity e* to produce torque

Figure 19. Test set up with steel balls in circular groove

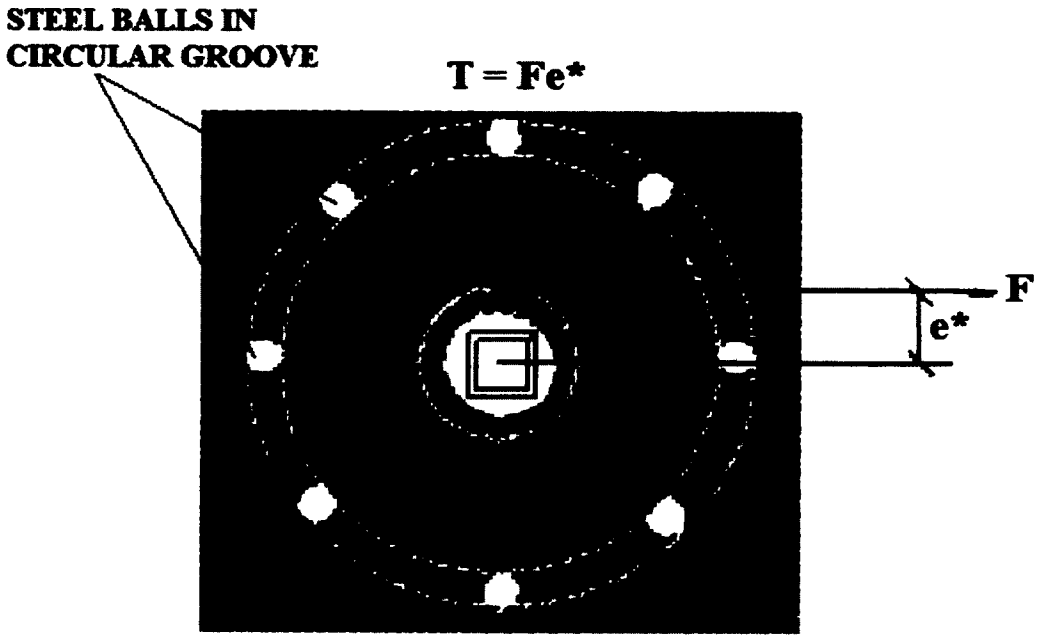

Figure 20. Schematic of test set up to apply F with eccentricity e* to produce torque

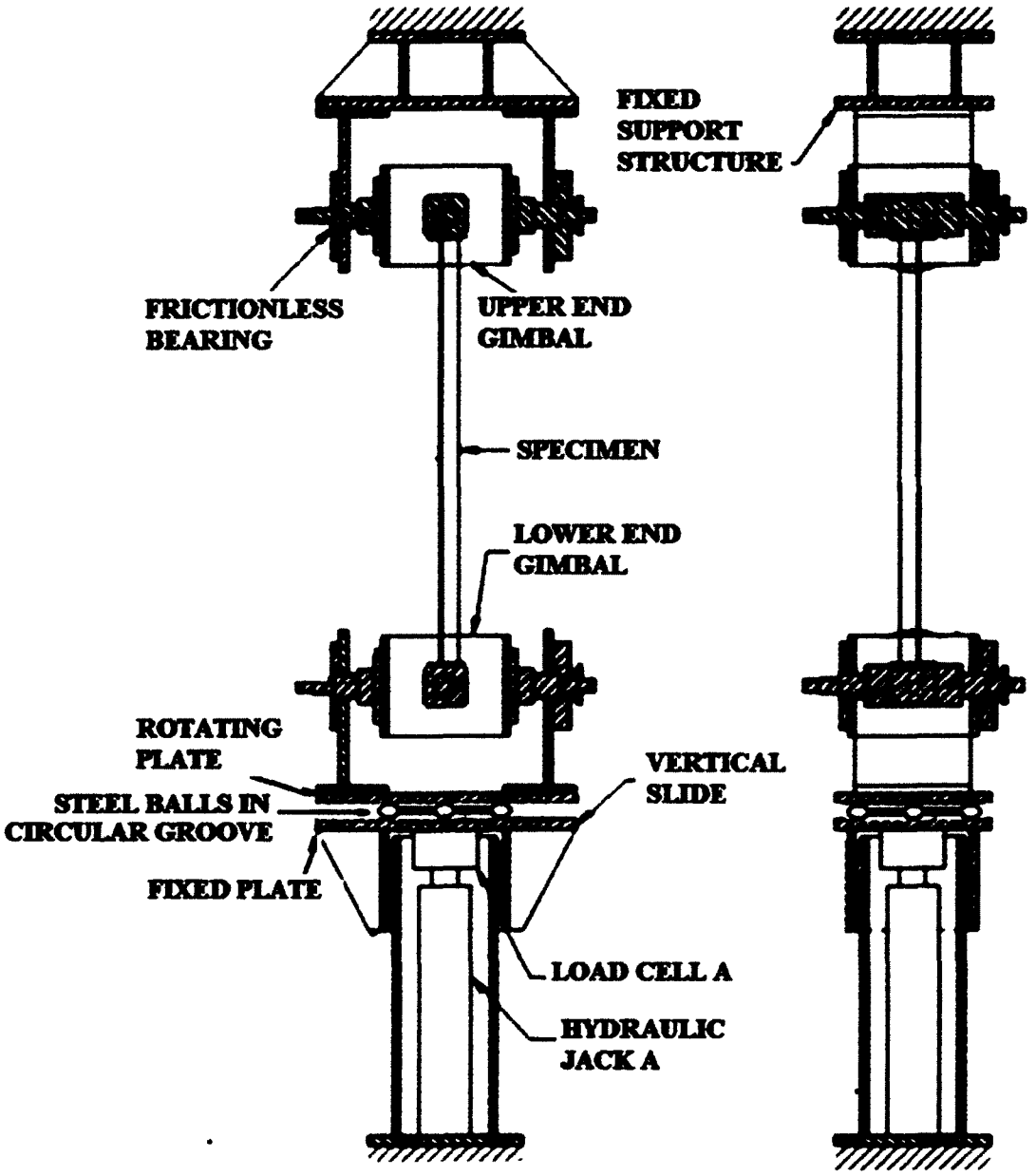

Figure 21. Schematic of a portion of apparatus modified to apply torque

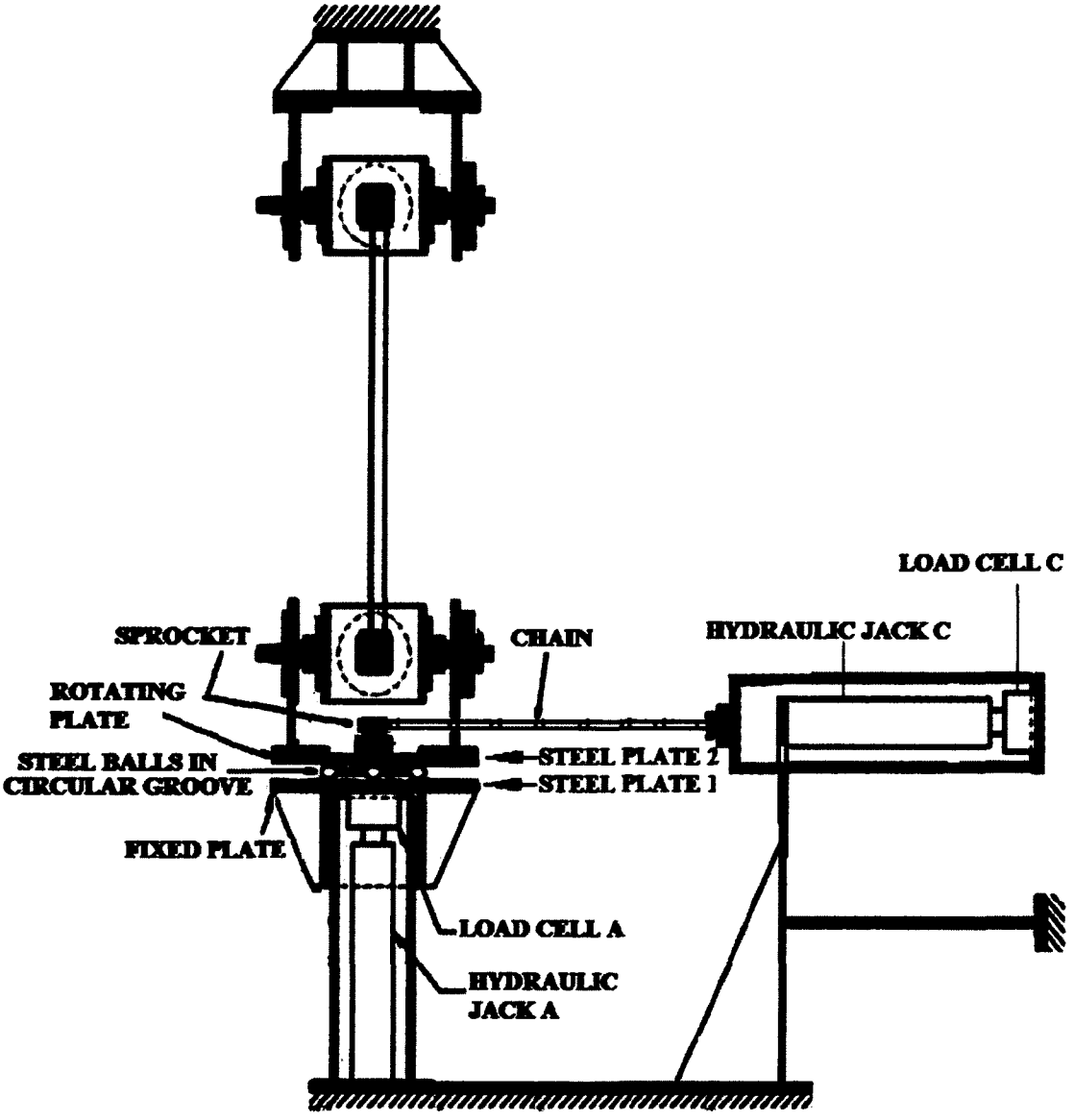

Figure 22. Schematic of a portion of apparatus with torque device

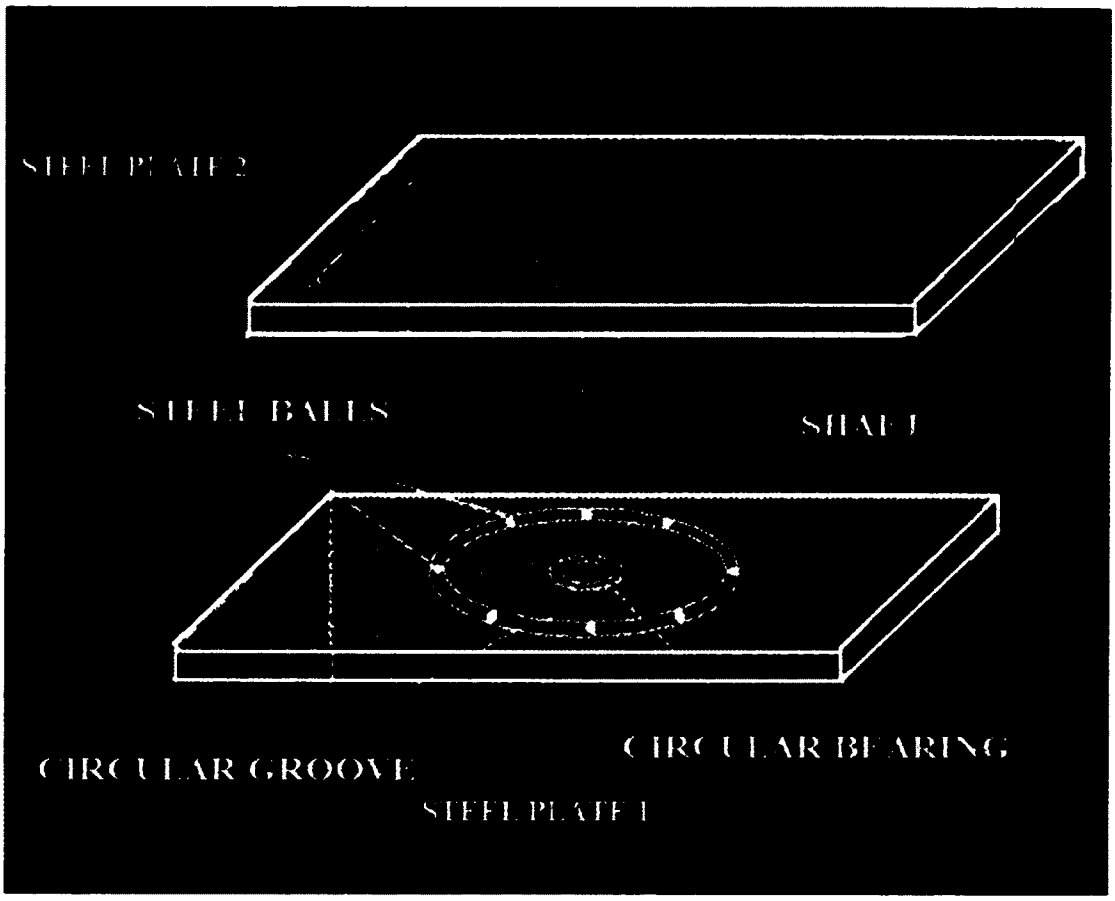

Figure 23. Steel Plates 1 and 2 for torque assembly below lower end gimbal

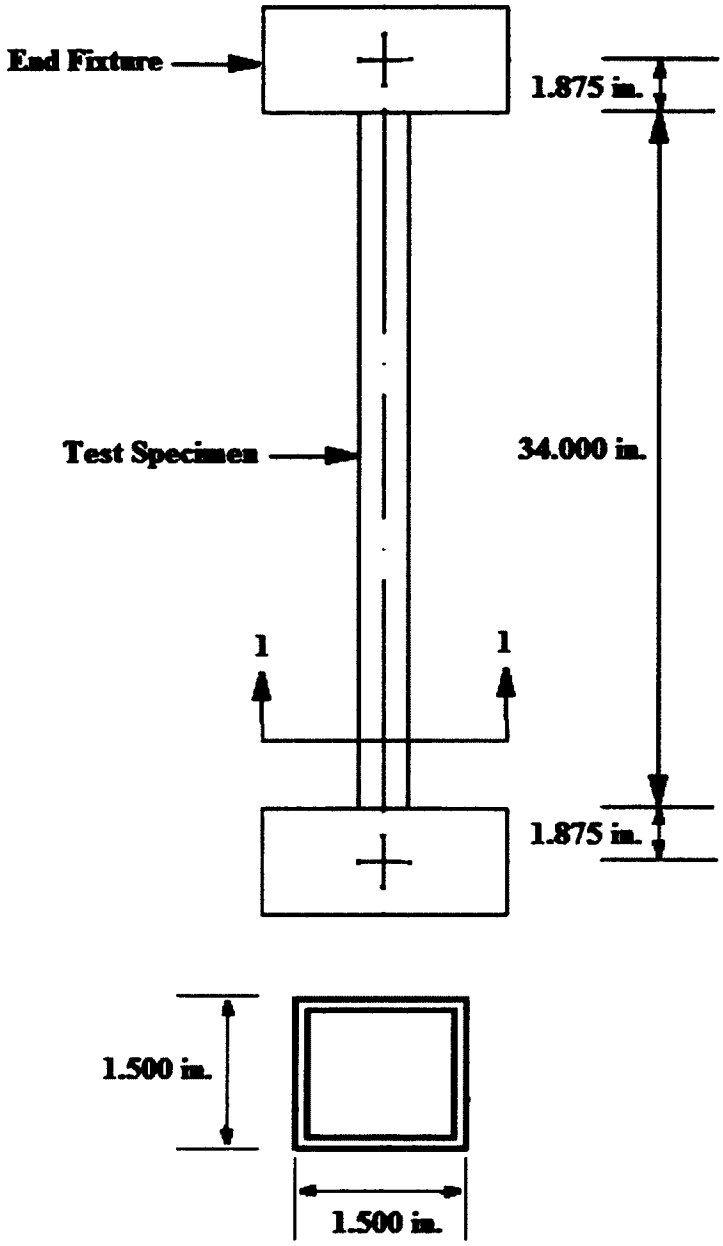

Figure 24. Schematic of specimen and its cross section

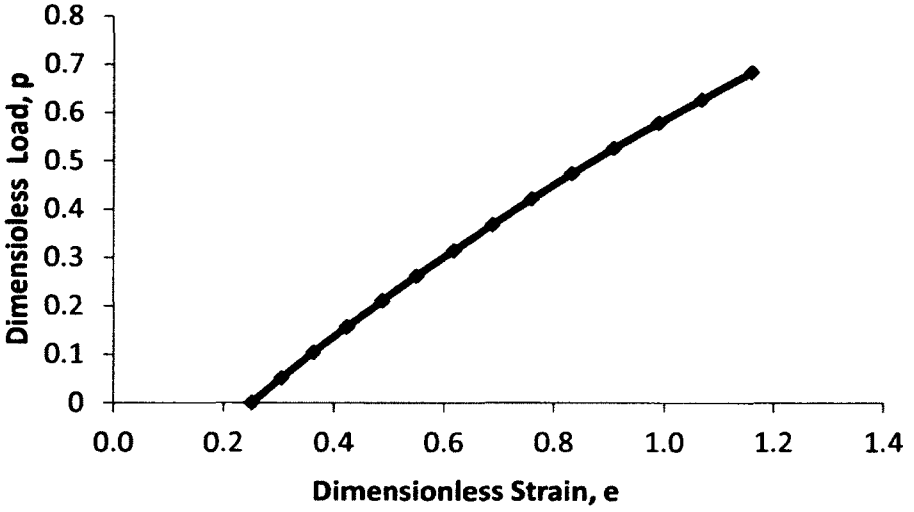

Figure 25. Dimensionless p-e curve up to yield for PR1

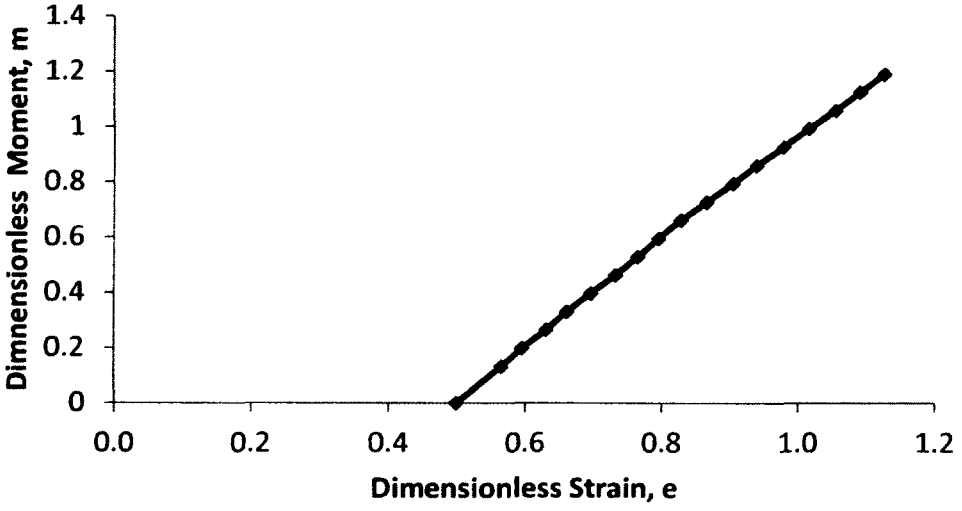

Figure 26. Dimensionless m-e curve up to yield for UR1

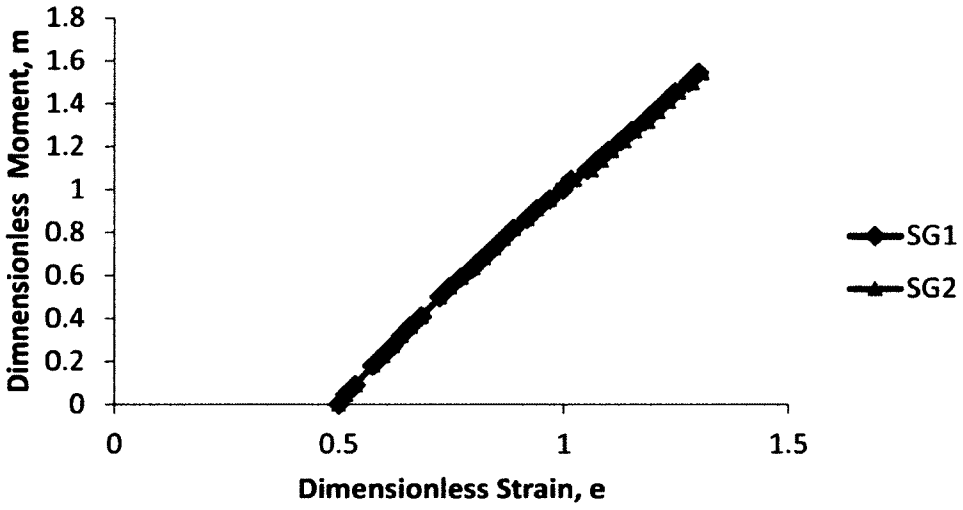

Figure 27. Dimensionless m-e curves up to yield for BR1

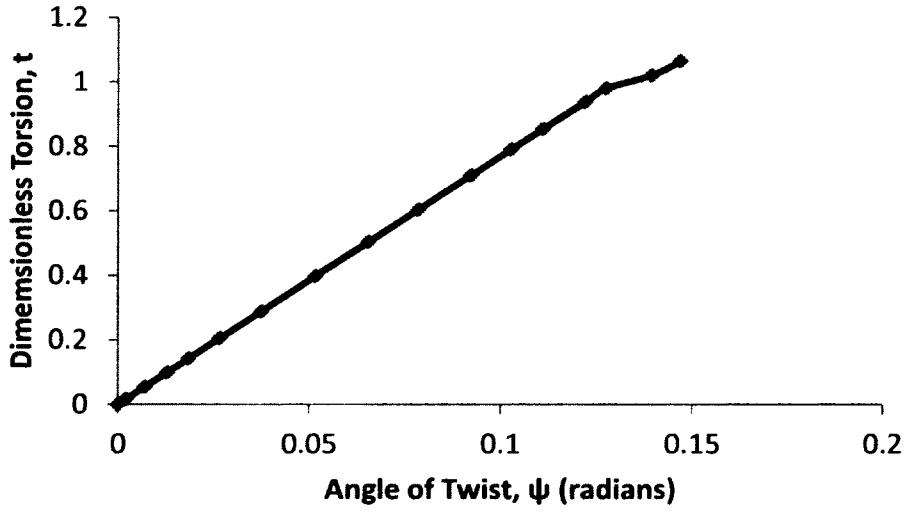

Figure 28. Dimensionless t-ψ curve up to yield curve for TR1

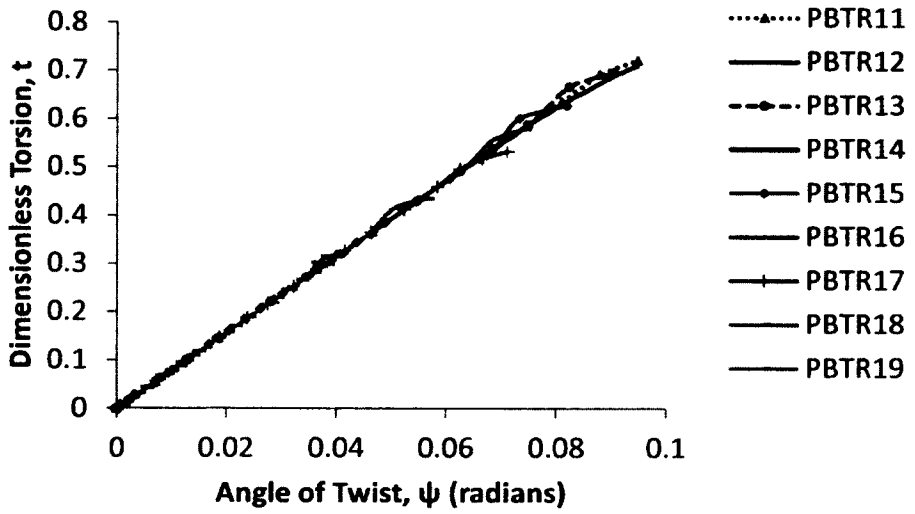

Figure 29. Dimensionless t-ψ curves for Test Series PBTR1

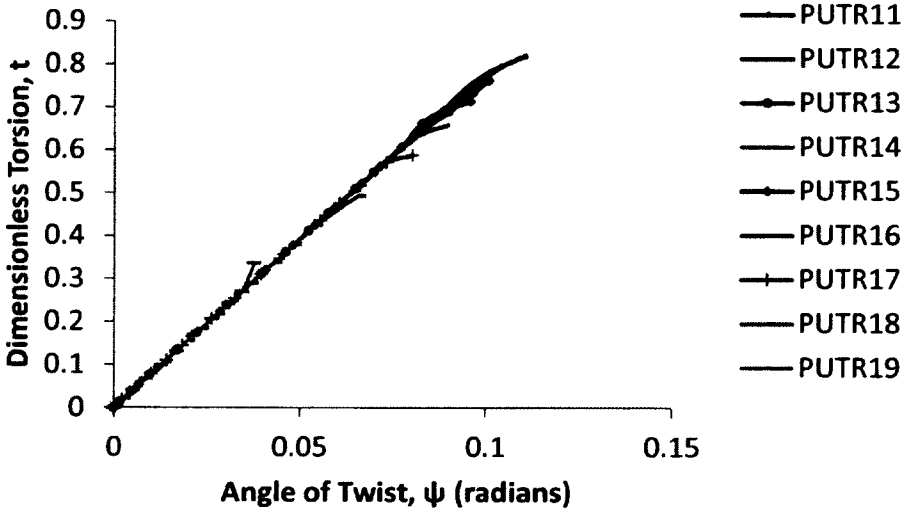

Figure 30. Dimensionless t-ψ curves for Test Series PUTR1

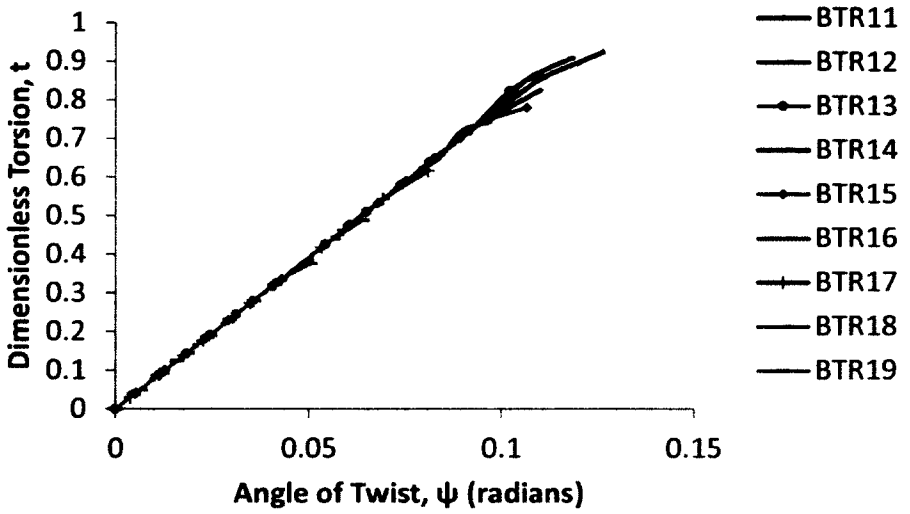

Figure 31. Dimensionless t-ψ curves for Test Series BTR1

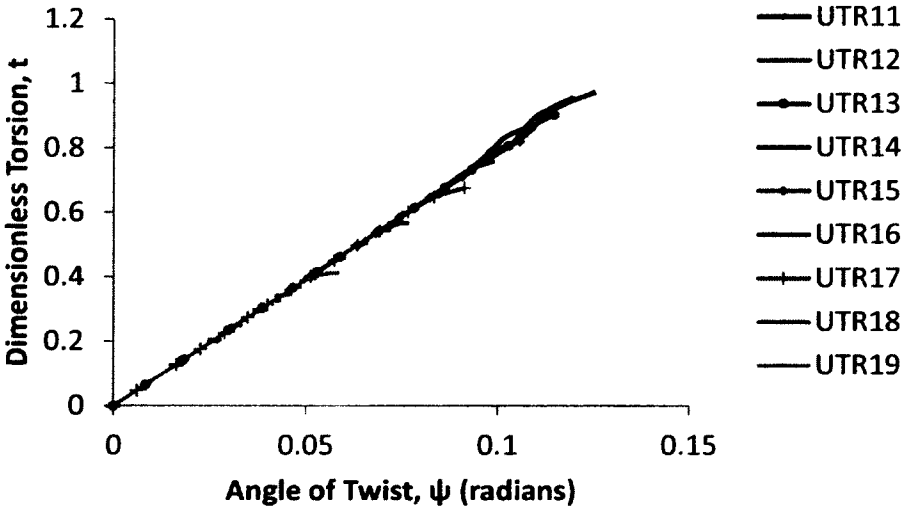

Figure 32. Dimensionless t-ψ curves for Test Series UTR1

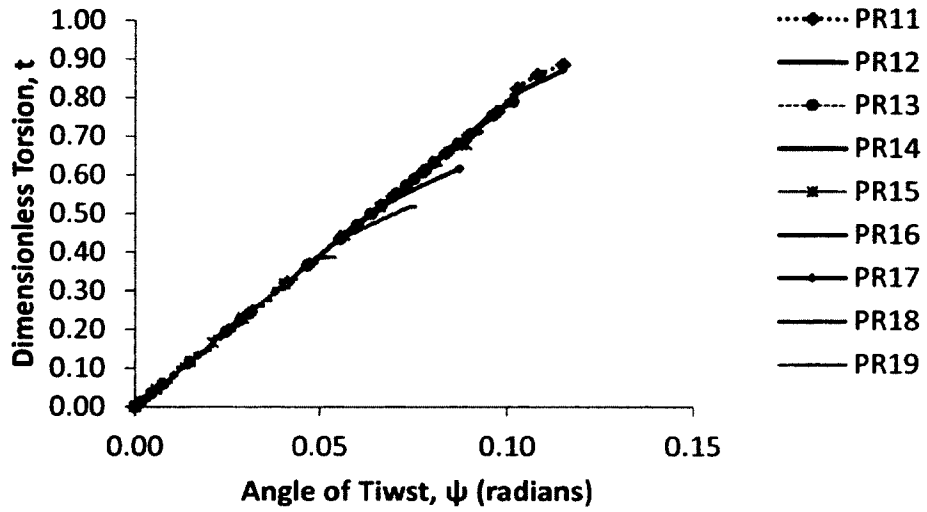

Figure 33. Dimensionless t-ψ curves with constant P for PTR1

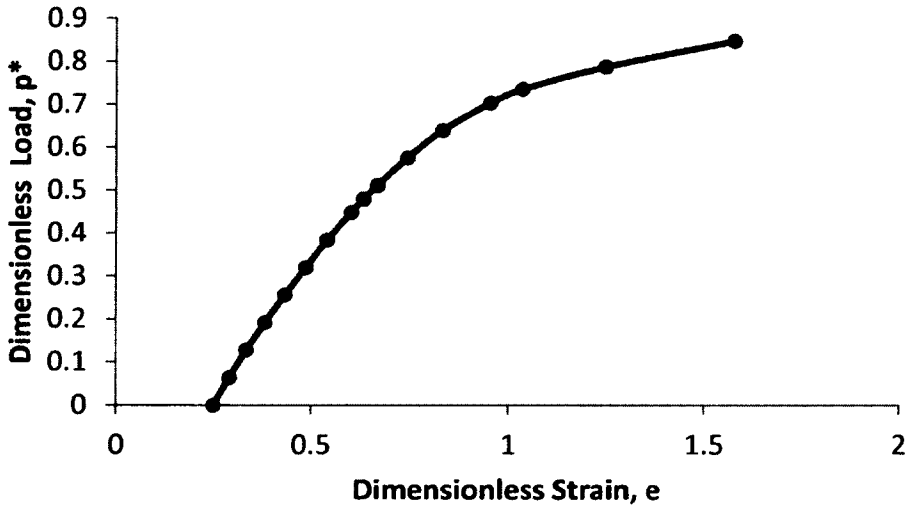

Figure 34. Dimensionless p*-e curve up to collapse for PR44

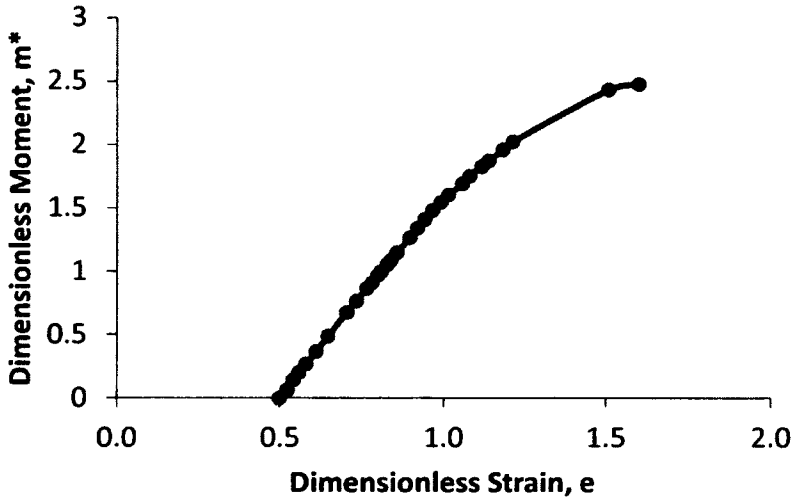

Figure 35. Dimensionless m*-e curve up to collapse for UR44

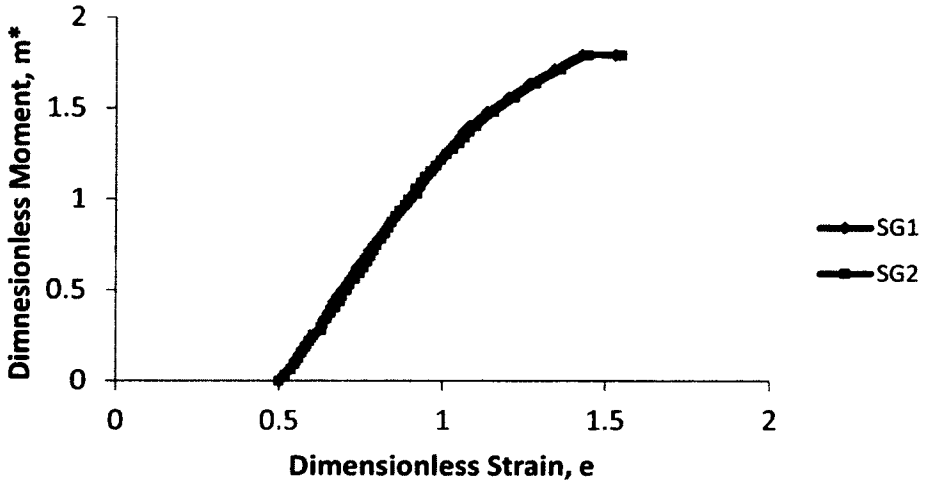

Figure 36. Dimensionless m*-e curves up to collapse for BR44

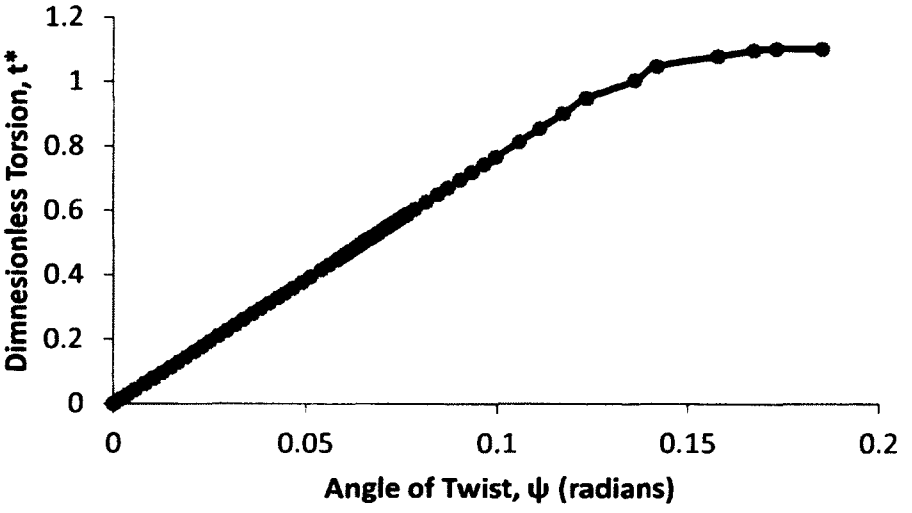

Figure 37. Dimensionless t*-ψ curve up to collapse for TPR44

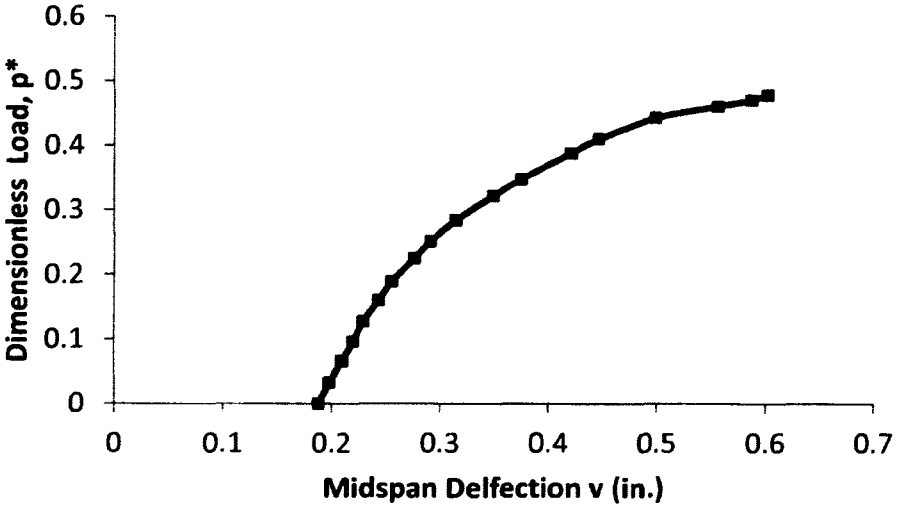

Figure 38. Dimensionless p*-v curve for TPR44

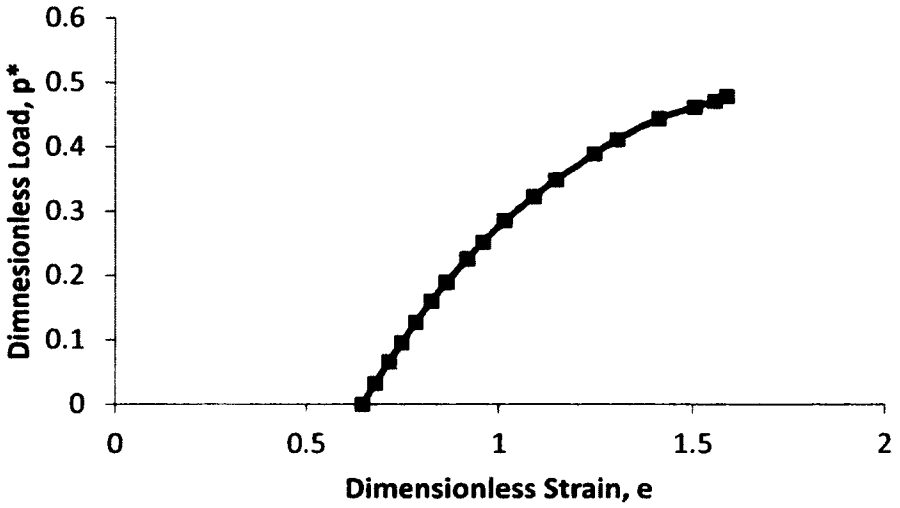

Figure 39. Dimensionless p*-e curve for TPR44

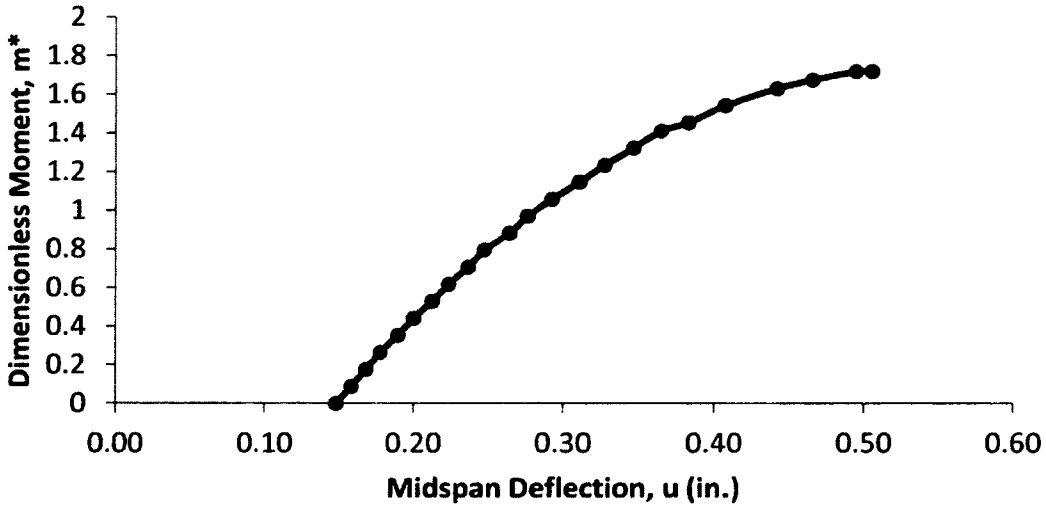

Figure 40. Dimensionless m*-u curve for TUR44

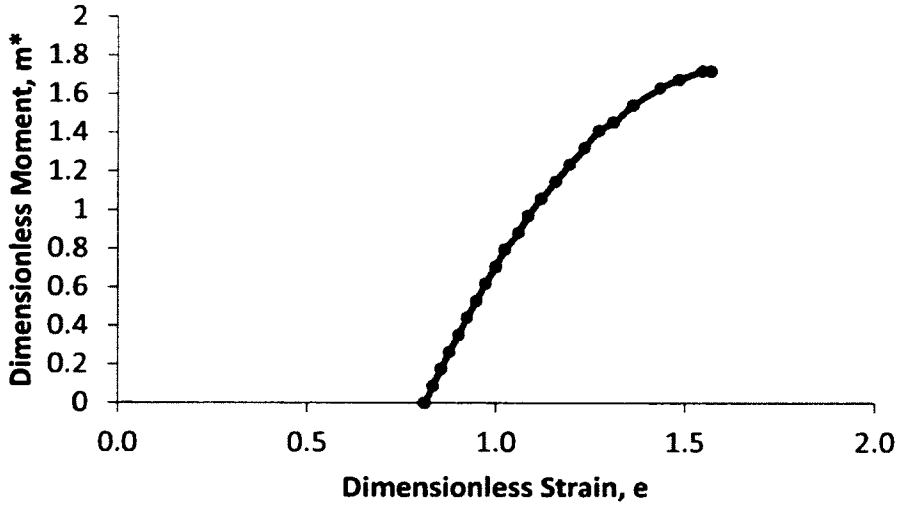

Figure 41. Dimensionless m*-e curve for TUR44

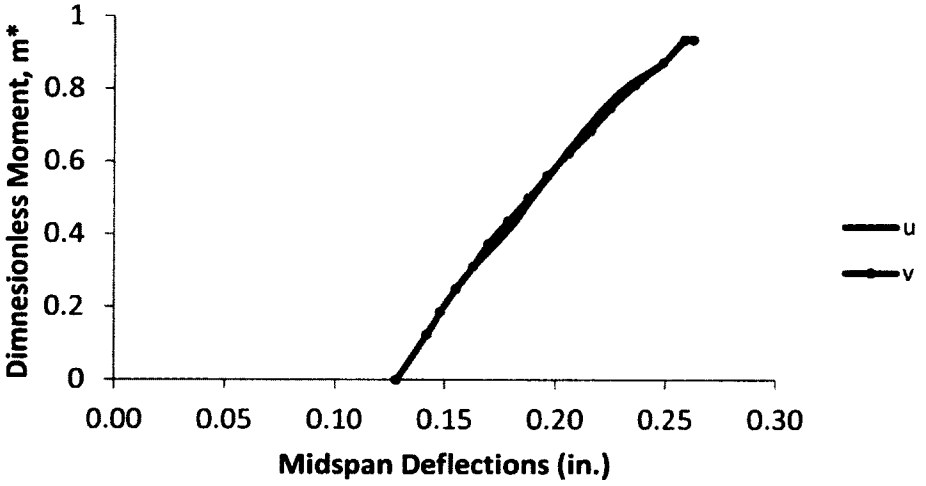

Figure 42. Dimensionless m*-deflection curves for TBR44

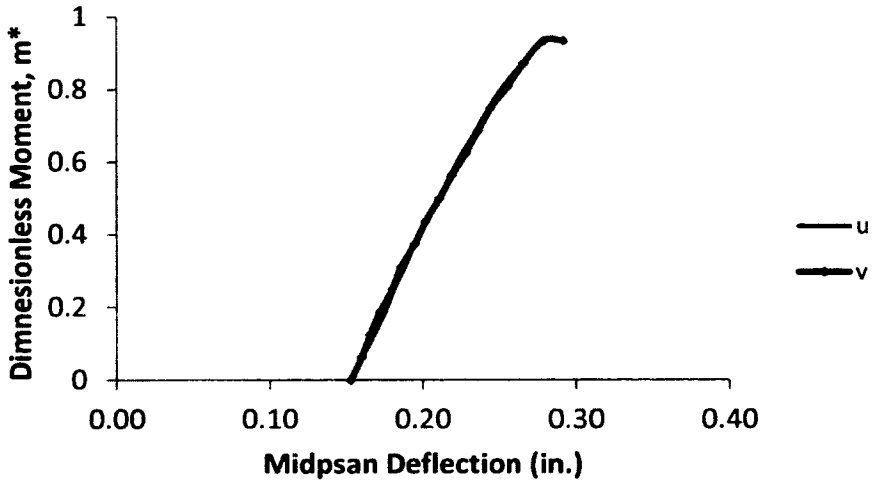

Figure 43. Dimensionless m*-deflection curves for TBR41

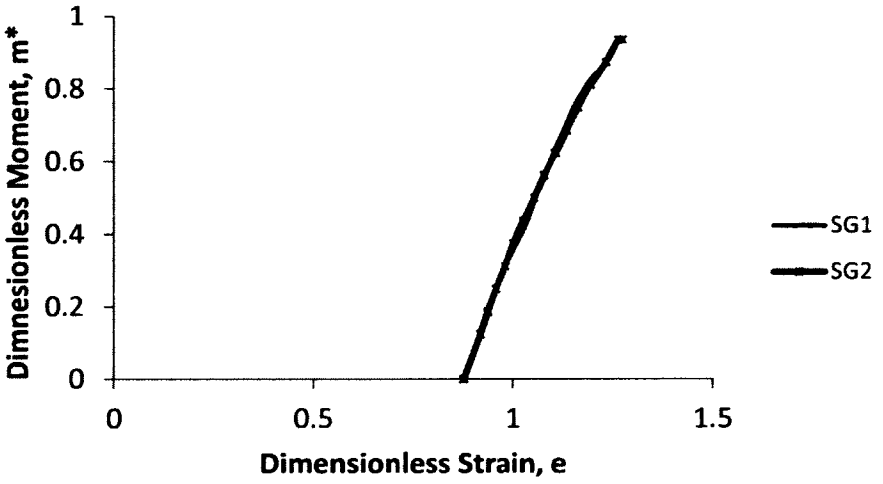

Figure 44. Dimensionless m*-e curves for TBR44

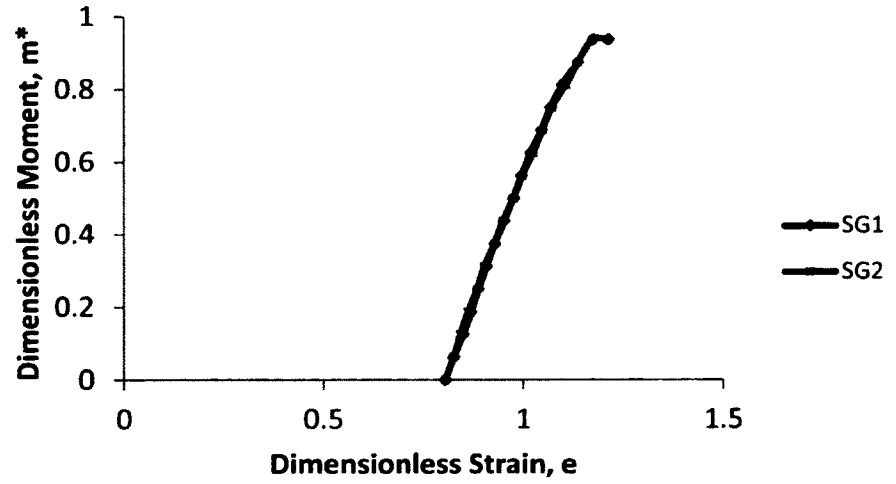

Figure 45. Dimensionless m*-e curves for TBR41

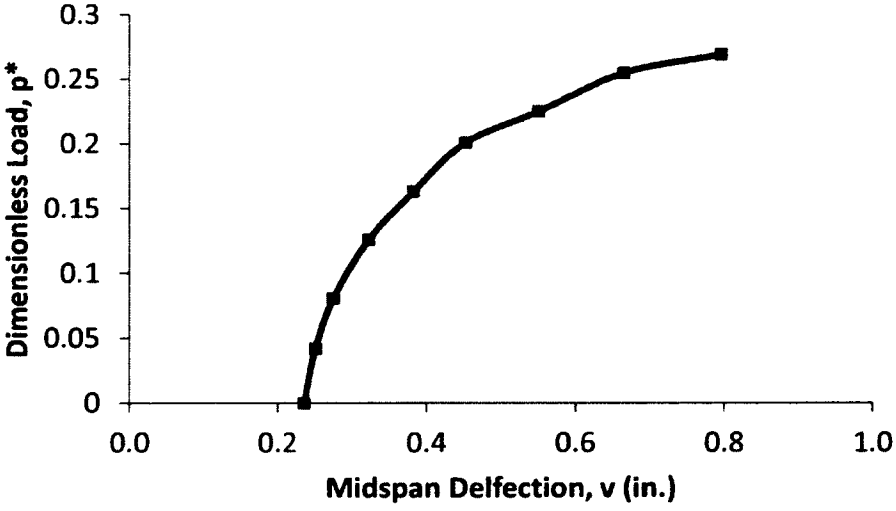

Figure 46. Dimensionless p*-v curve for TBPR44

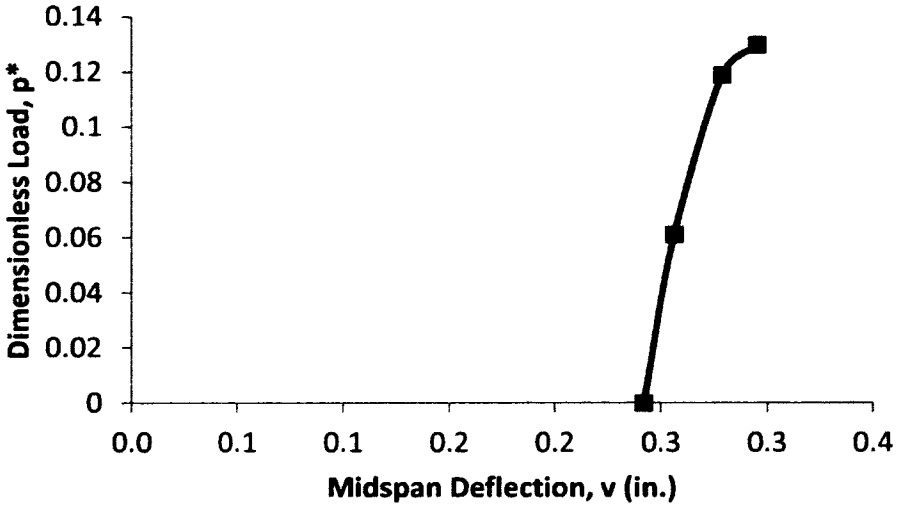

Figure 47. Dimensionless p*-v curve for TBPR41

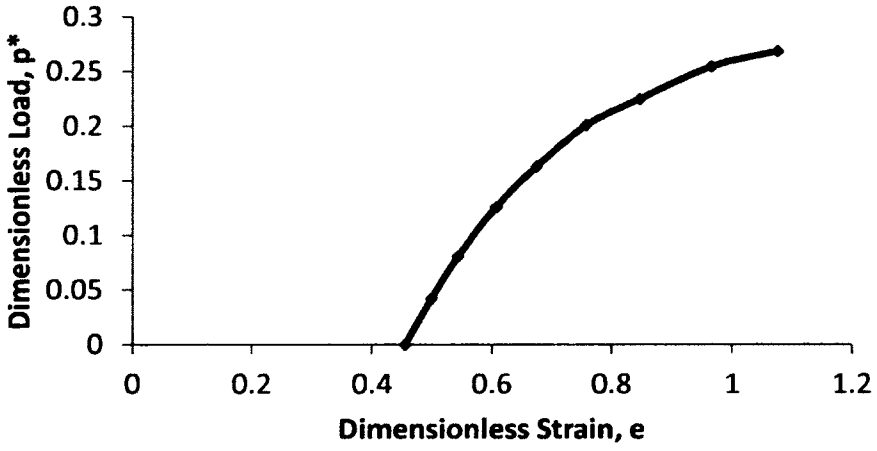

Figure 48. Dimensionless p*-e curve for TBPR44

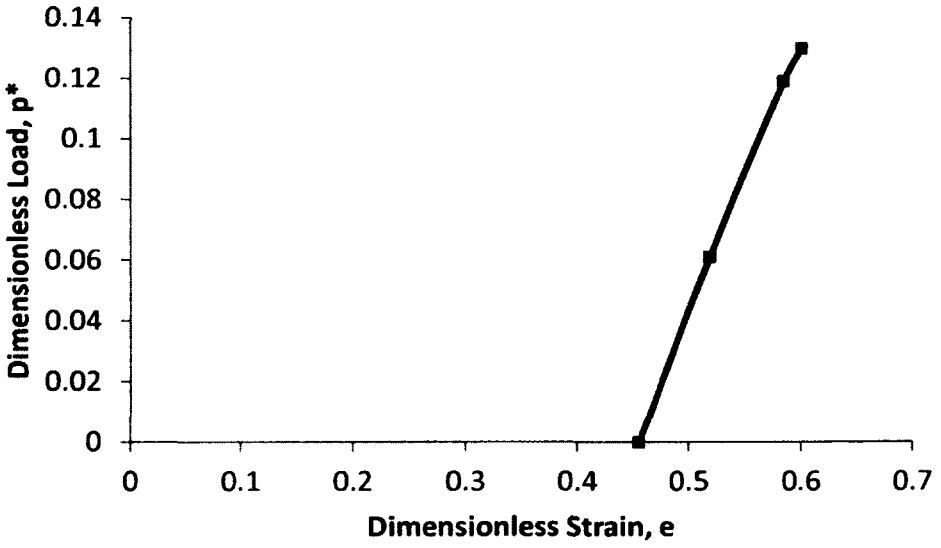

Figure 49. Dimensionless p*-e curve for TBPR41

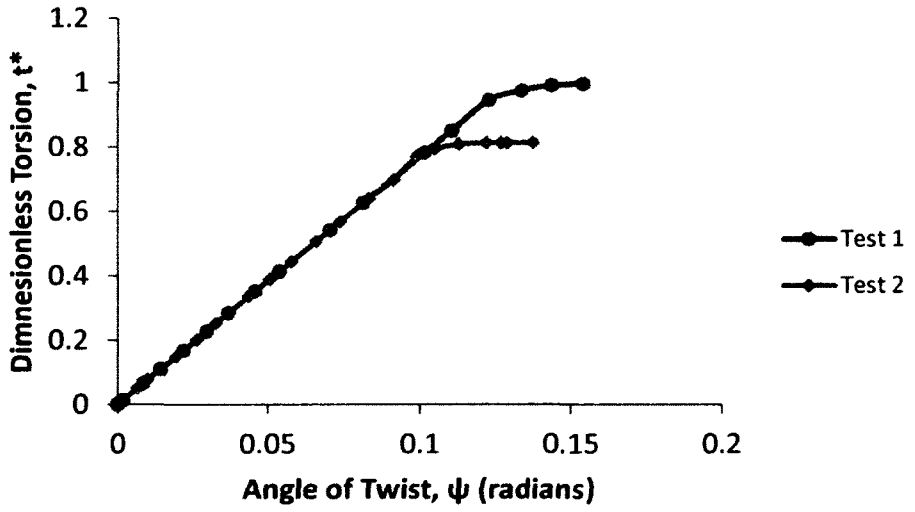

Figure 50. Dimensionless t*-ψ curves for Test Series PBTR11

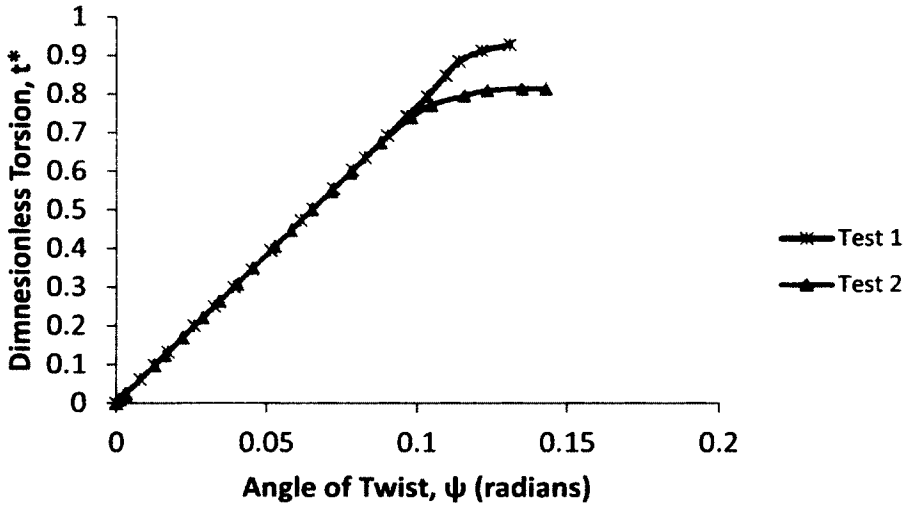

Figure 51. Dimensionless t*-ψ curves for Test Series PBTR44

Figure 52. Strain gage locations for measuring warping strains

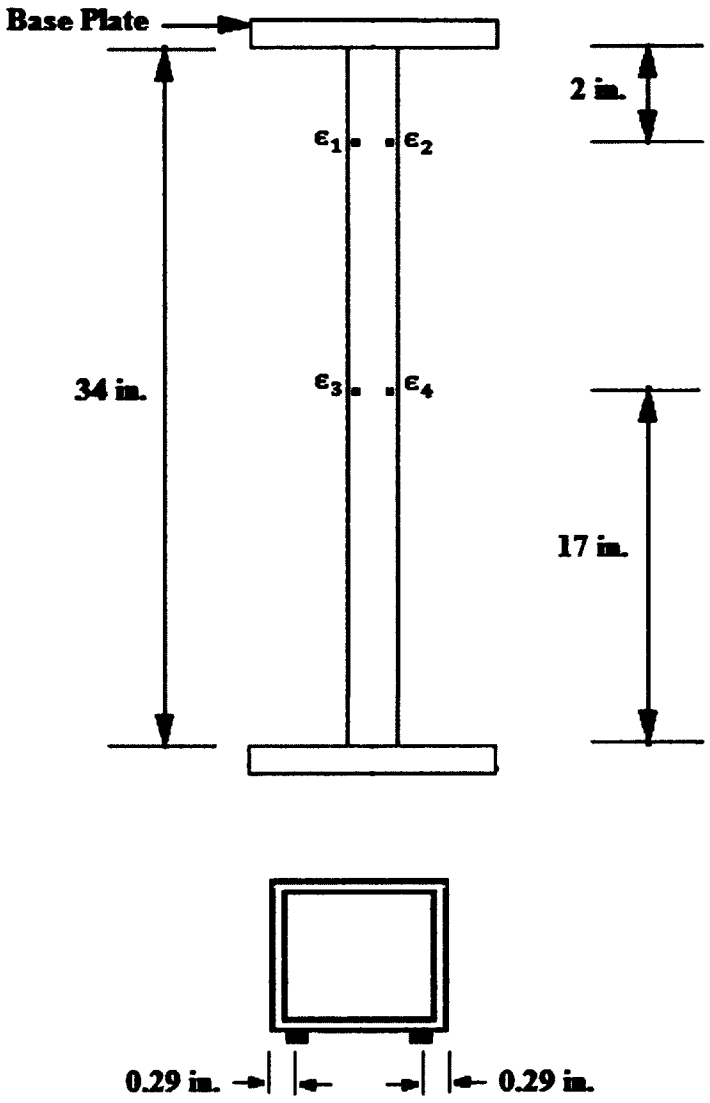

Figure 53. Schematic of specimen with strain gages to measure the warping strains

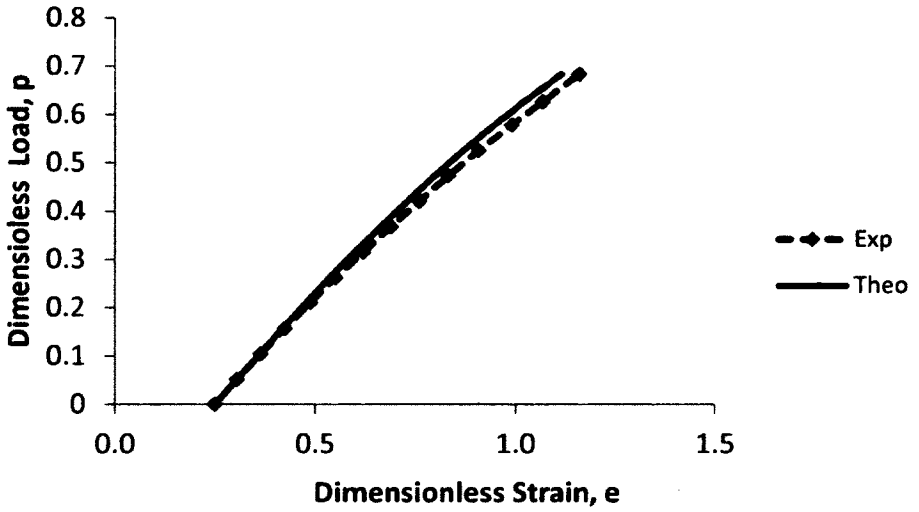

Figure 54. Dimensionless experimental and predicted p-e curves for PR1

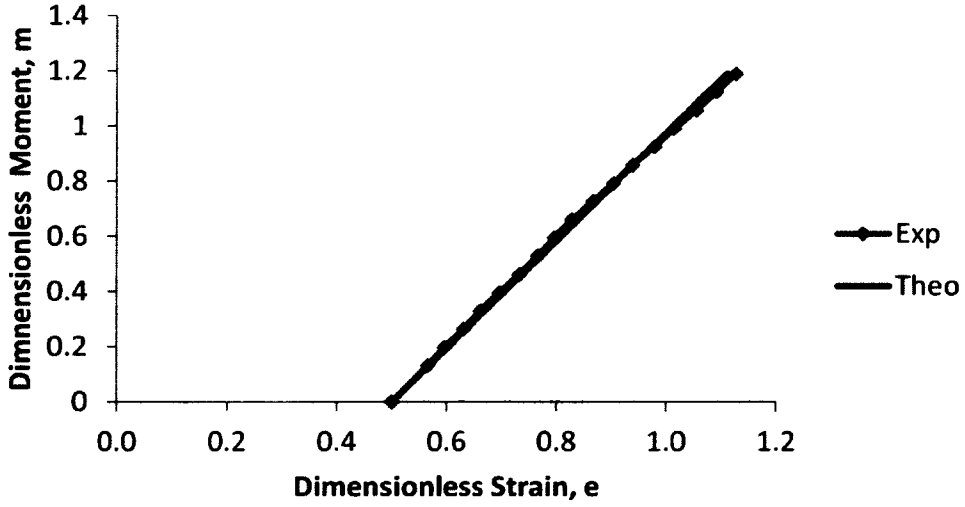

Figure 55. Dimensionless experimental and predicted m-e curves for UR1

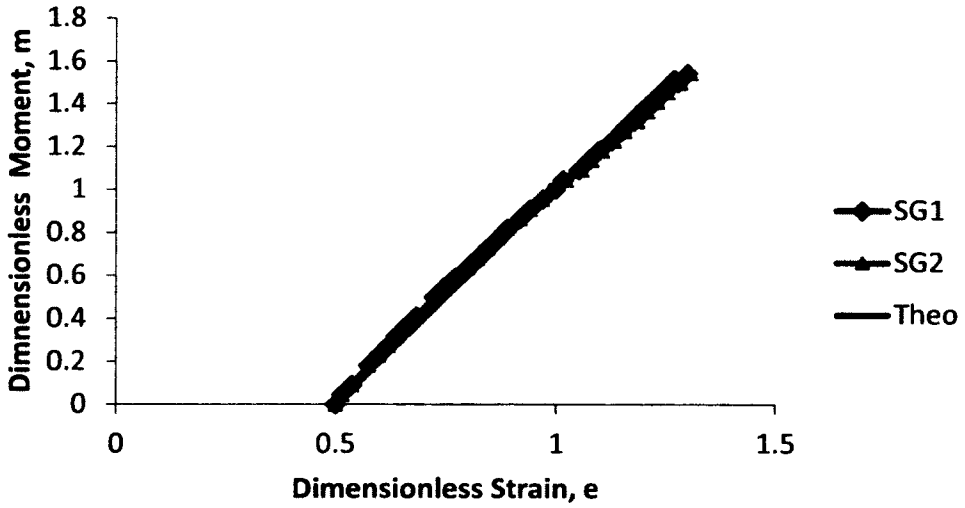

Figure 56. Dimensionless experimental and predicted m-e curves for BR1

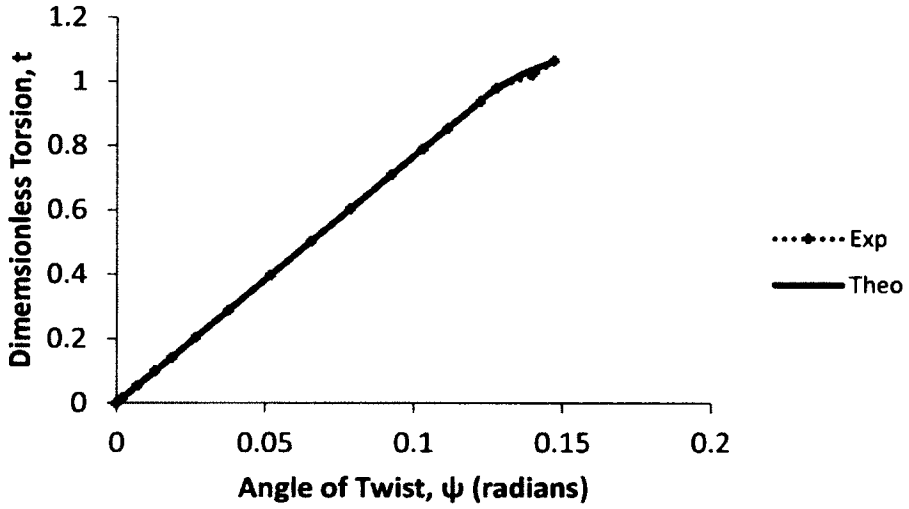

Figure 57. Dimensionless experimental and predicted t- ψ curves for TR1

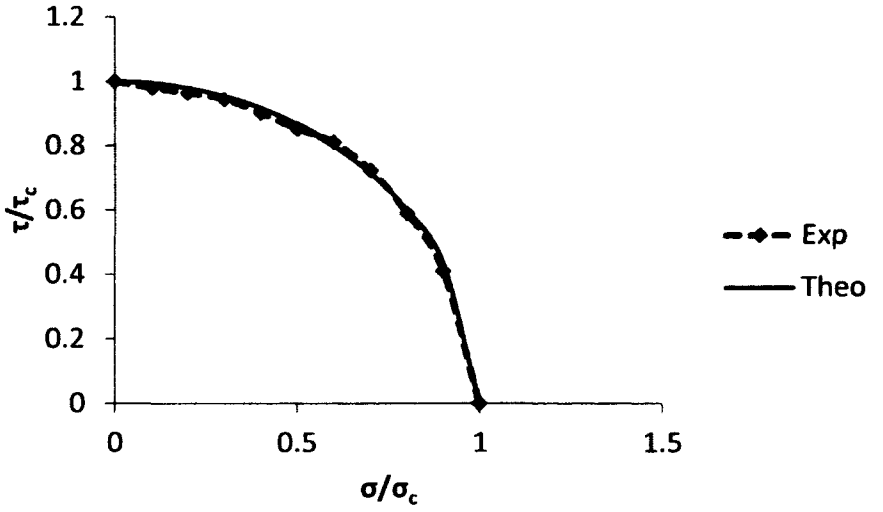

Figure 58. Comparisons of dimensionless interaction curves for PBTR1

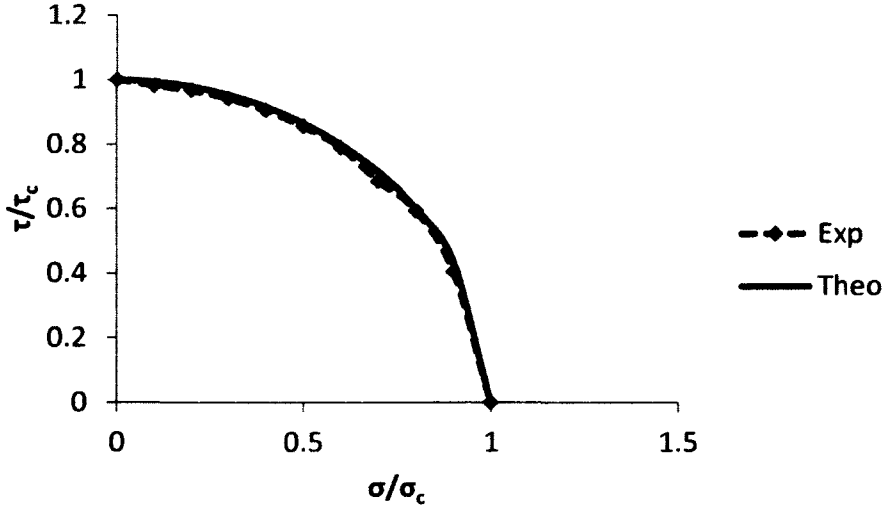

Figure 59. Comparisons of dimensionless interaction curves for PUTR1

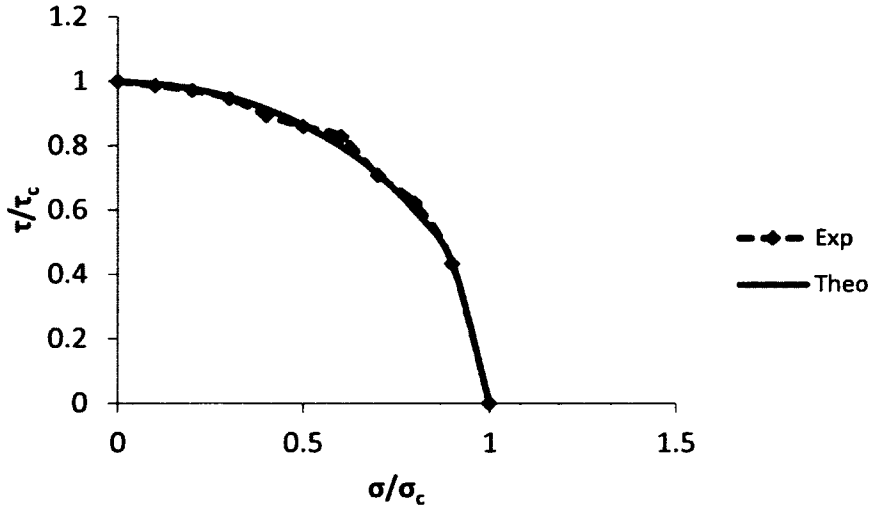

Figure 60. Comparisons of dimensionless interaction curves for BTR1

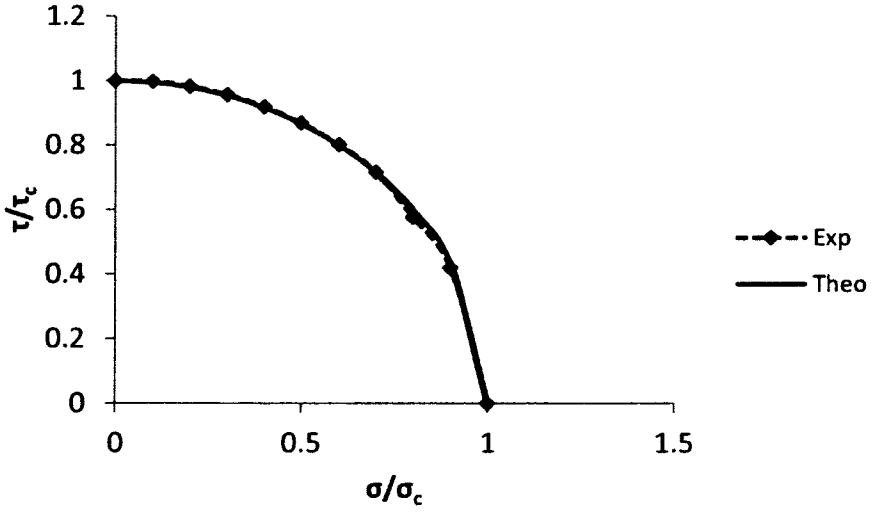

Figure 61. Comparisons of dimensionless interaction curves for UTR1

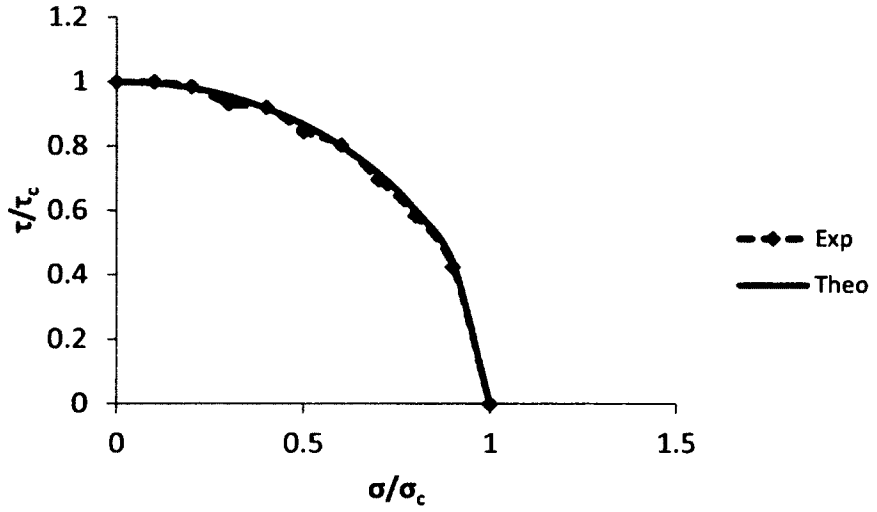

Figure 62. Comparisons of dimensionless interaction curves for PTR1

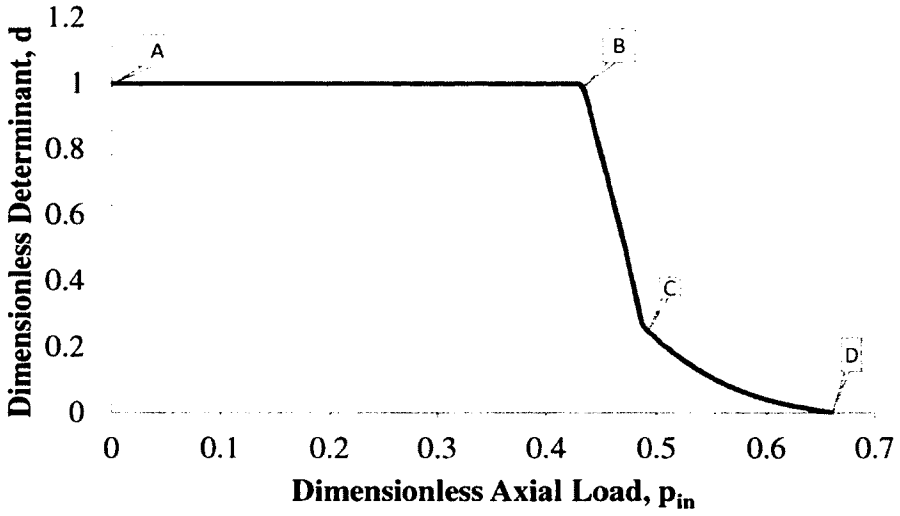

Figure 63. Dimensionless d-p_{in} curve for PR11

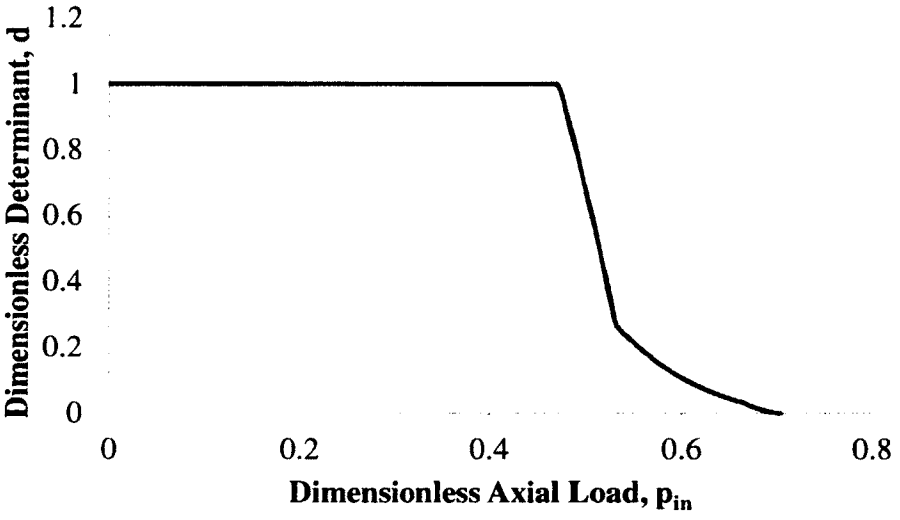

Figure 64. Dimensionless d-p_{in} curve for PR44

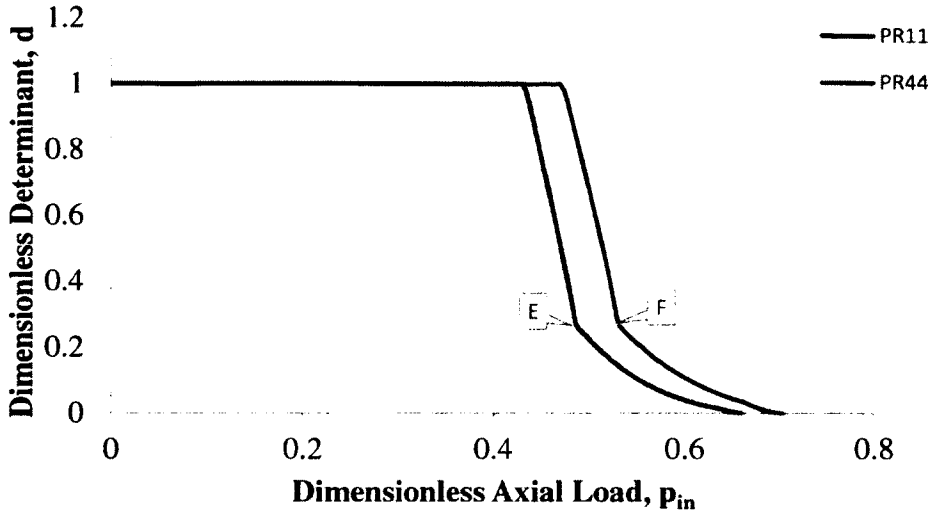

Figure 65. Dimensionless d-p_{in} curves for PR11 and PR44

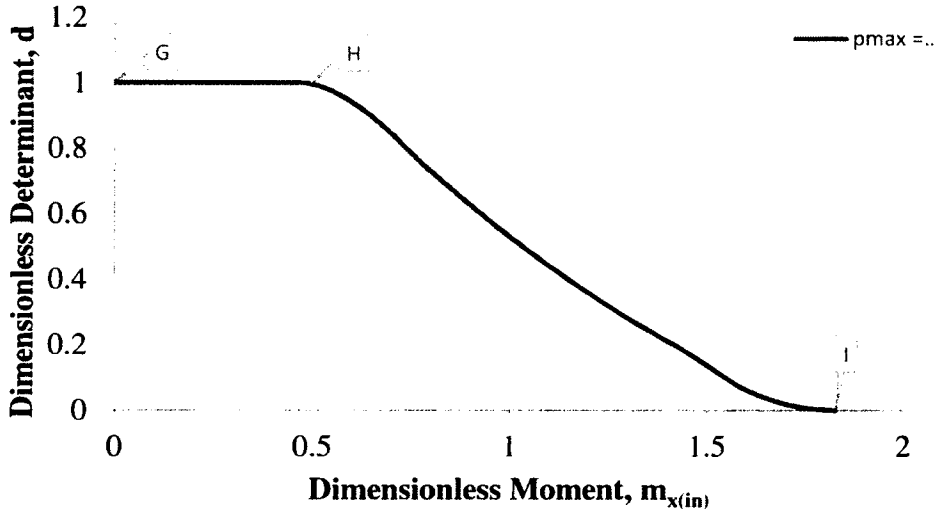

Figure 66. Dimensionless d-$m_{x\,(in)}$ curve for PUR11 with constant p_{in} value

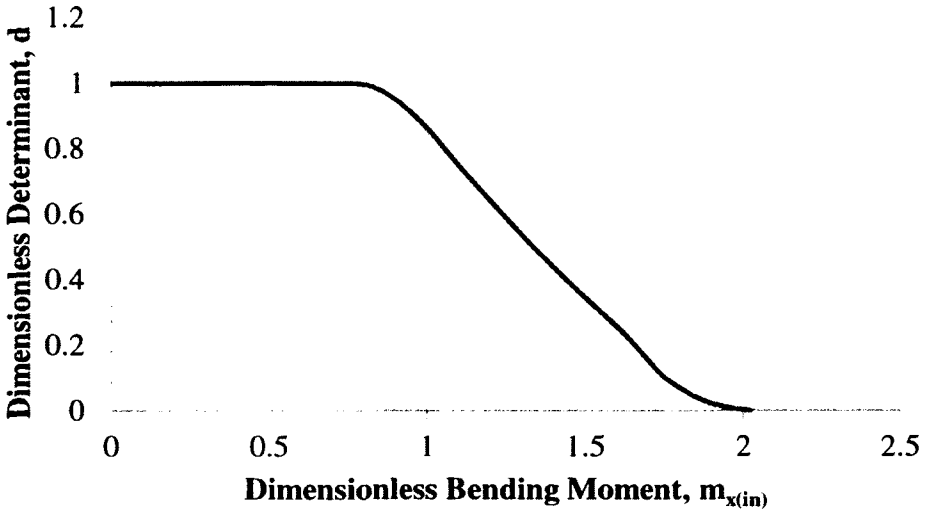

Figure 67. Dimensionless d-$m_{x\,(in)}$ curve for PUR44 with constant p_{in} value

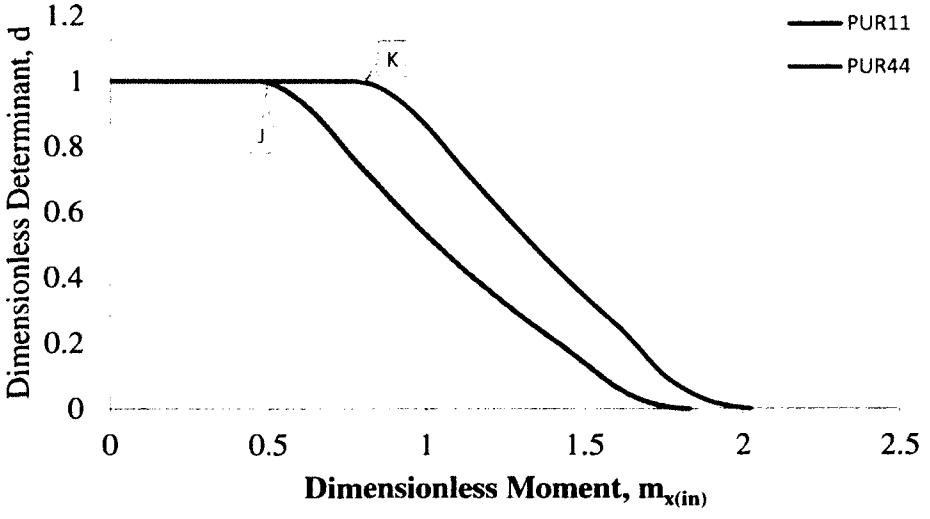

Figure 68. Dimensionless d-$m_{x\,(in)}$ curves for PUR11 and PUR44

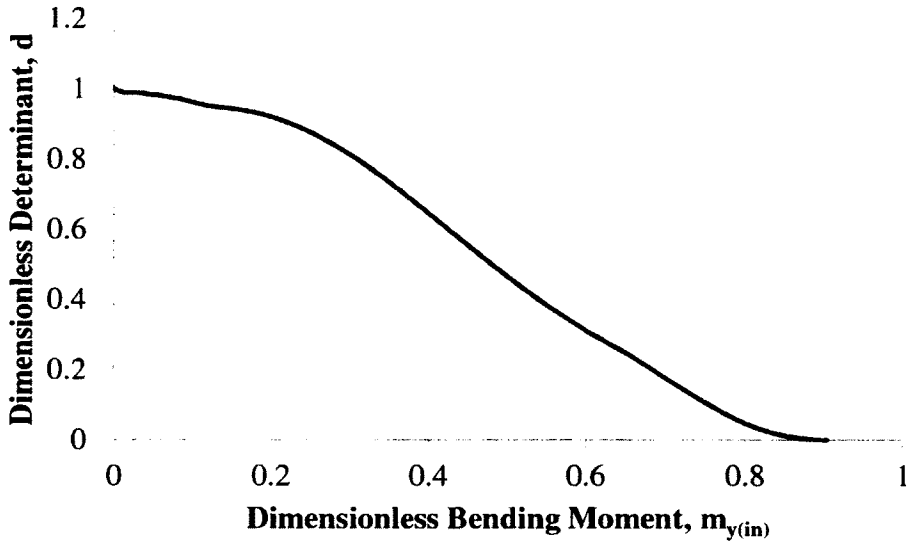

Figure 69. Curve for PBR11 with constant p_{in} and $m_{x\,(in)}$ values

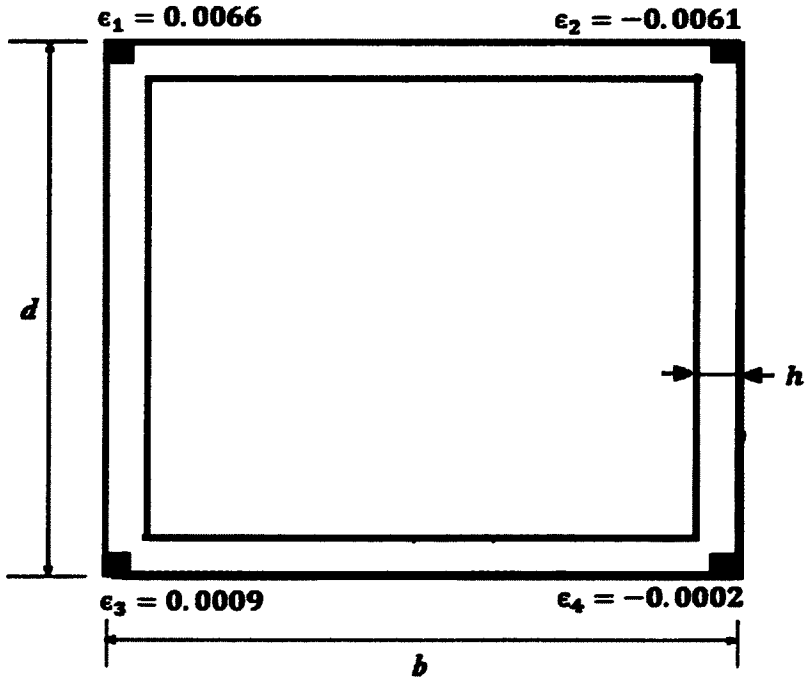

Figure 70. Corner elemental areas for PBR11 at Node 9

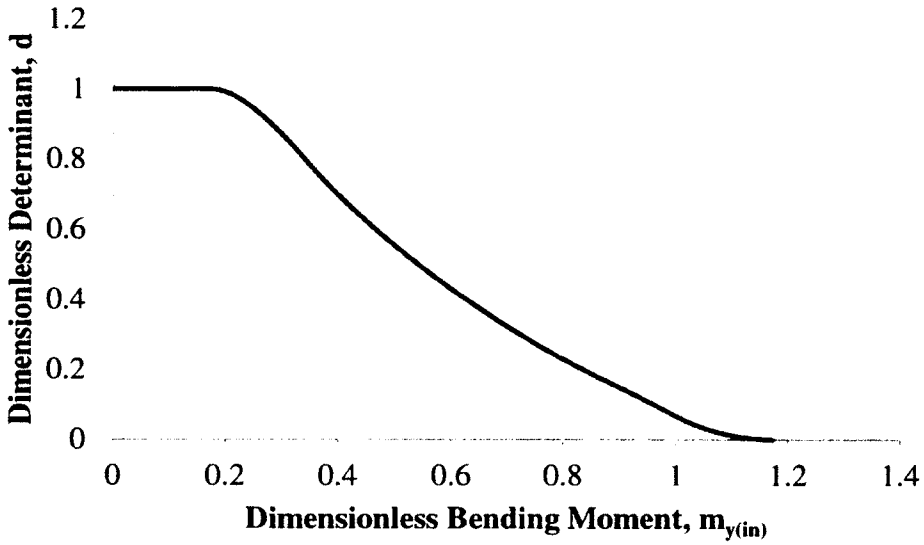

Figure 71. Curve for PBR44 with constant p_{in} and $m_{x\,(in)}$ values

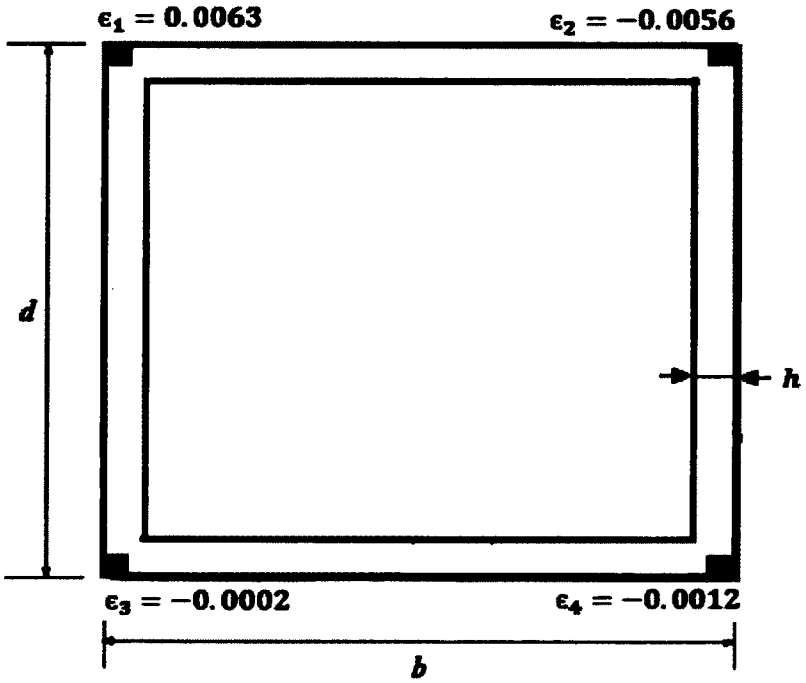

Figure 72. Corner elemental areas for PBR44 at Node 9

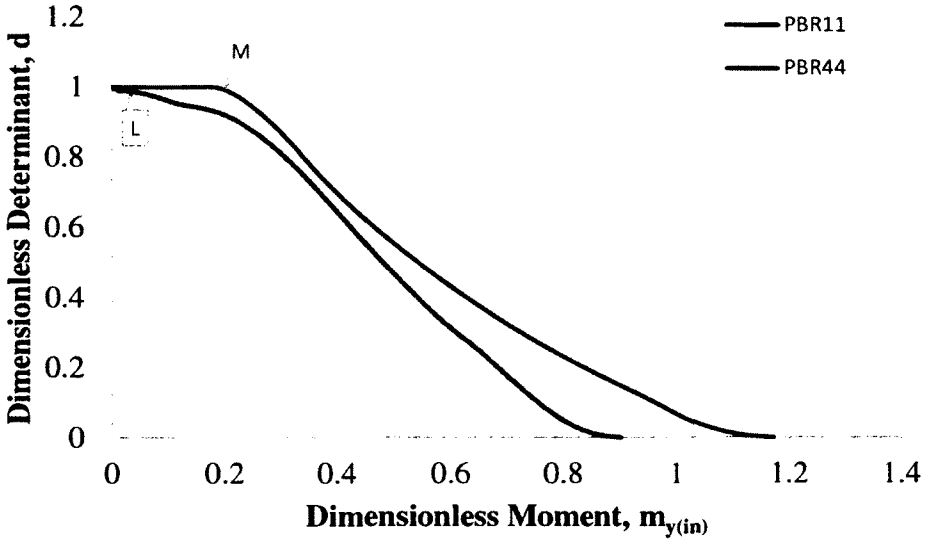

Figure 73. Dimensionless d-$m_{y\,(in)}$ curves for PBR11 and PBR44

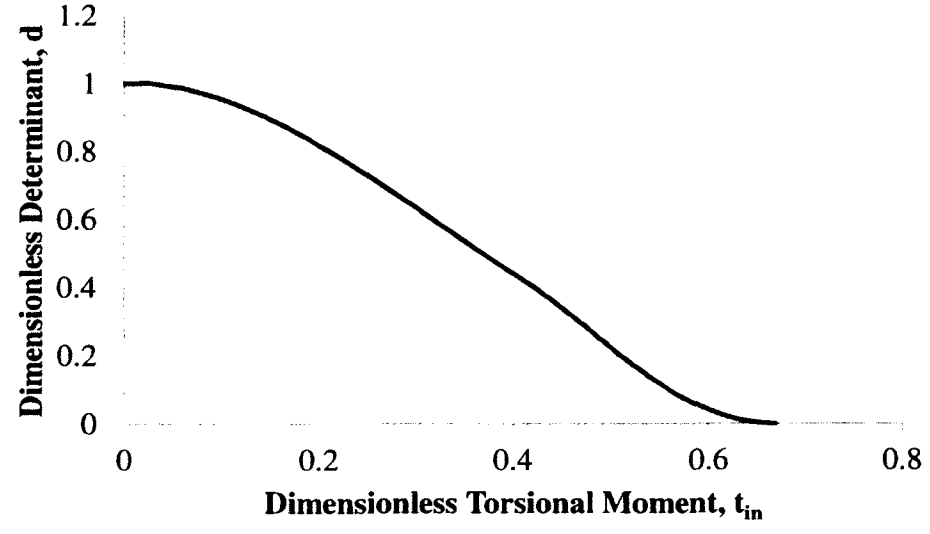

Figure 74. Curve for PBTR11 with constant p_{in}, $m_{x\,(in)}$, and $m_{y\,(in)}$ values

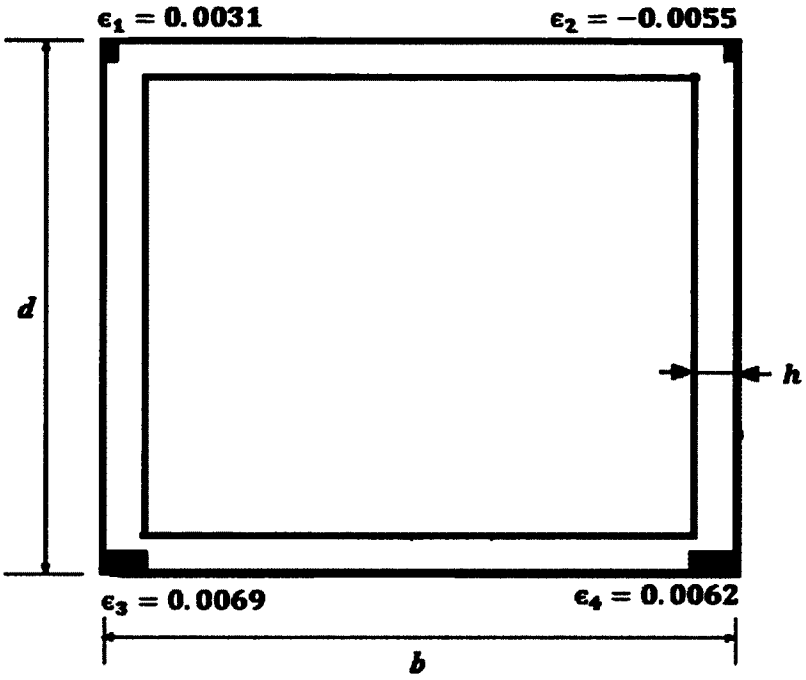

Figure 75. Corner elemental areas for PBTR11 at Node 9

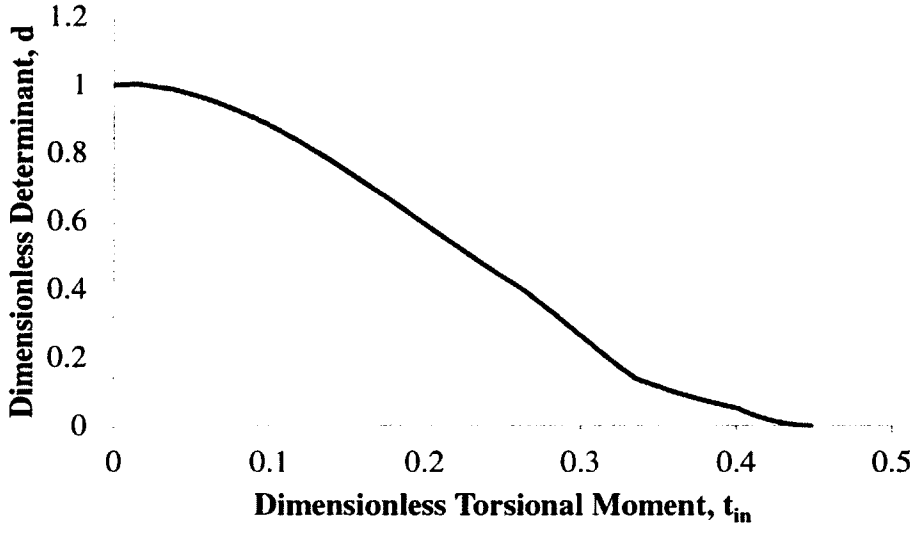

Figure 76. Curve for PBTR44 with constant p_{in}, $m_{x\,(in)}$, and $m_{y\,(in)}$ values

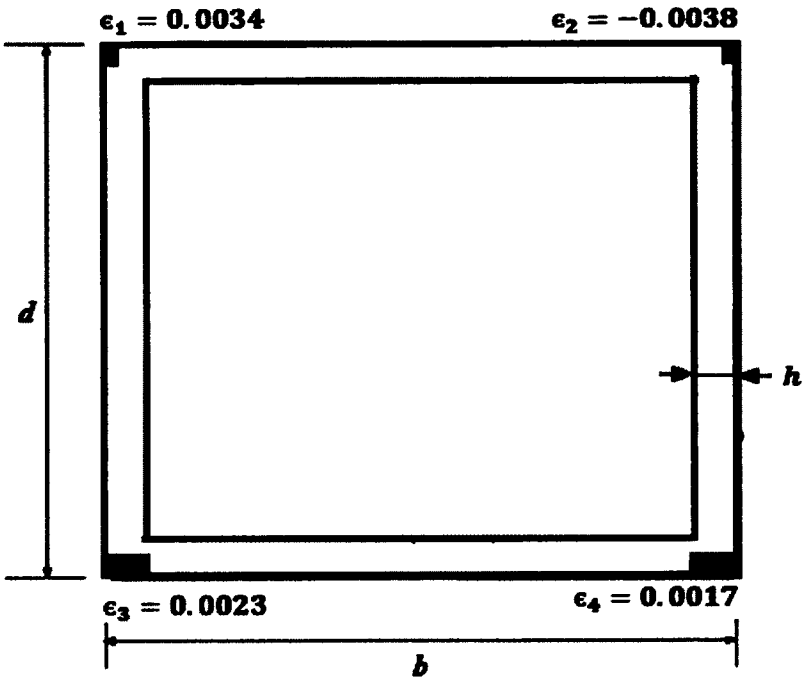

Figure 77. Corner elemental areas for PBTR44 at Node 9

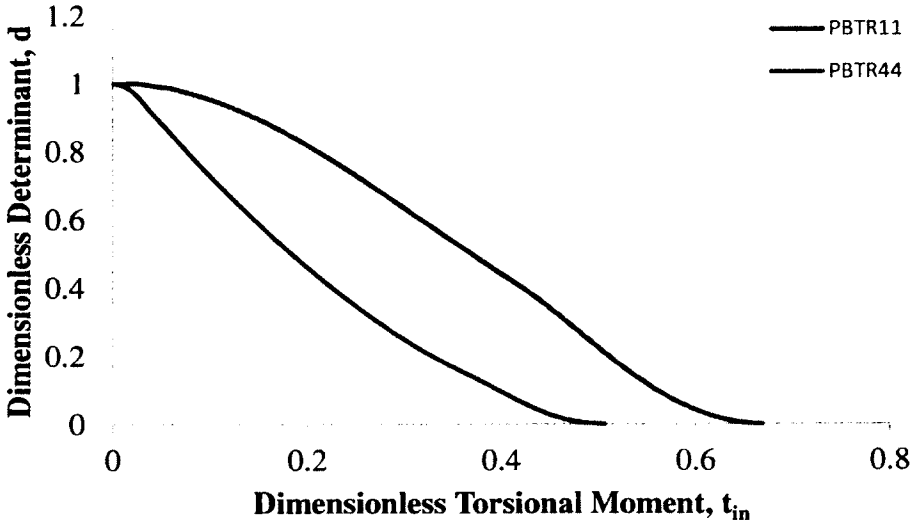

Figure 78. Dimensionless d-t_{in} curves for PBTR11 and PBTR44

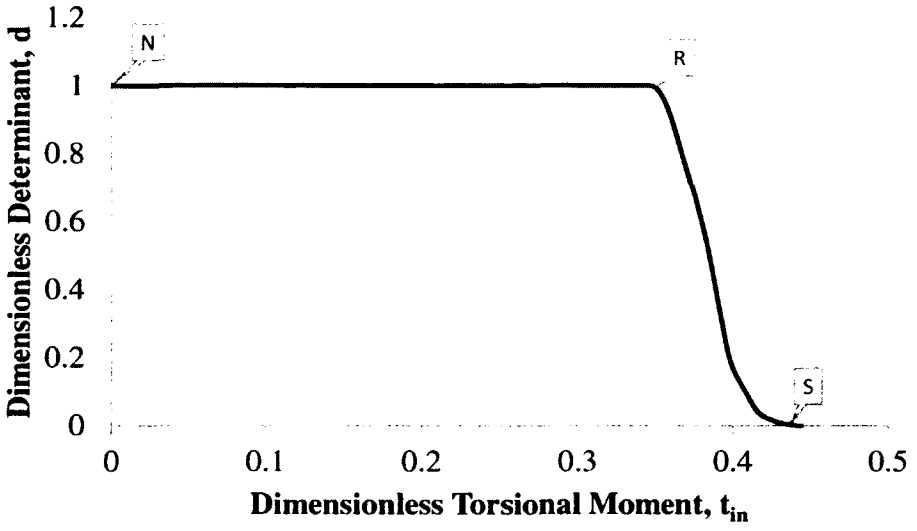

Figure 79. Dimensionless d-t_{in} curve for torsion loading only

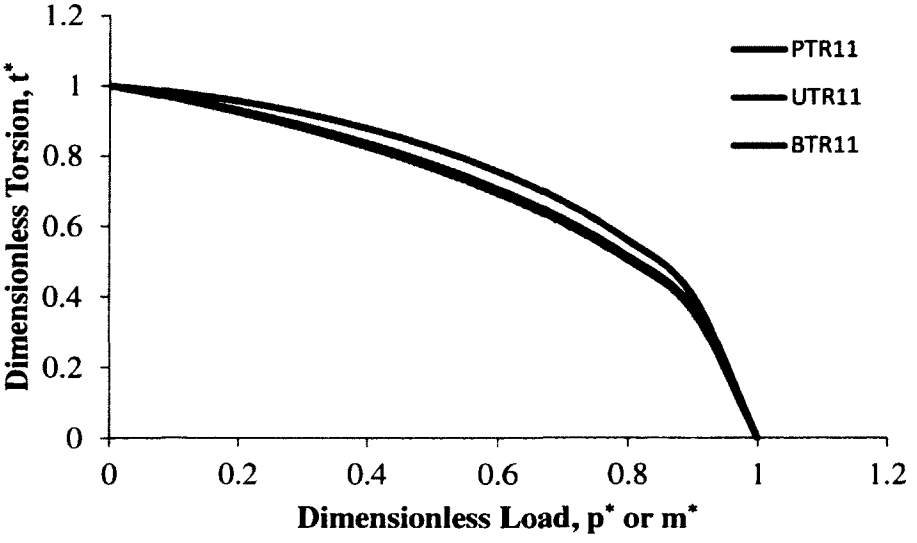

Figure 80. Dimensionless curves for PTR11, UTR11, and BTR11

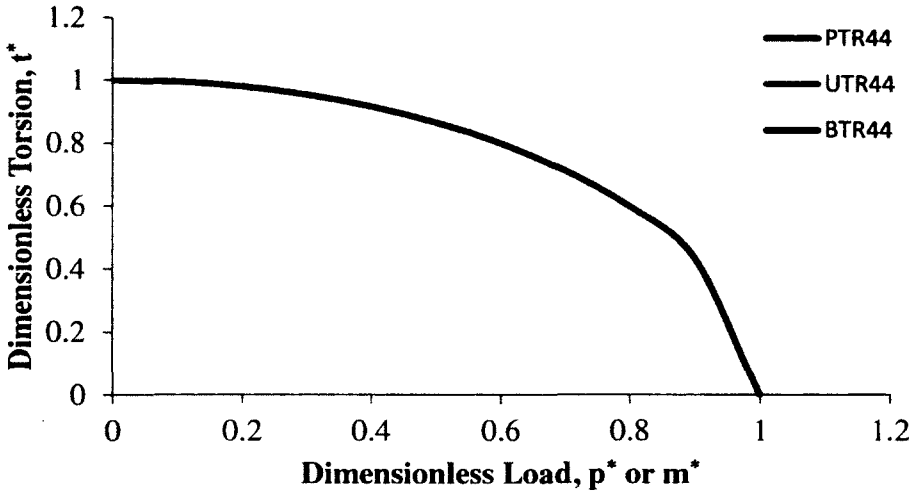

Figure 81. Dimensionless curves for PTR44, UTR44, and BTR44

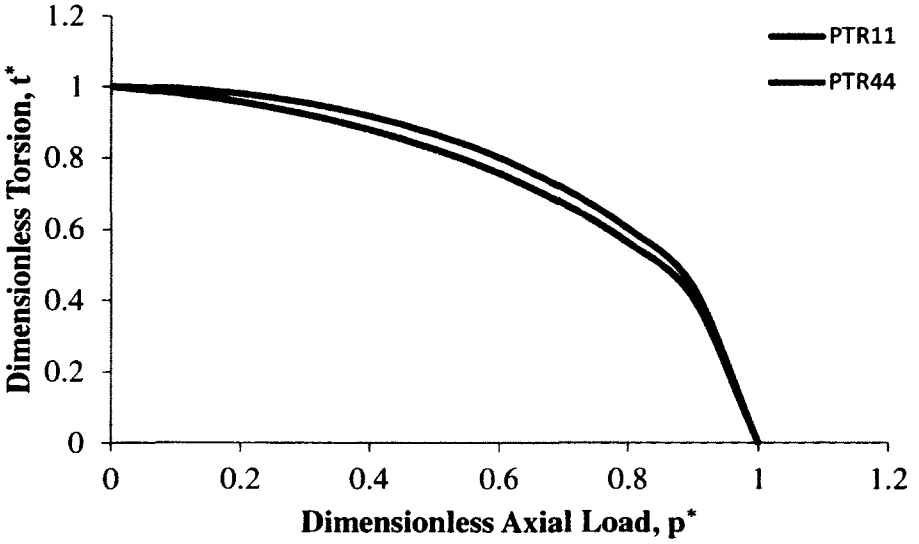

Figure 82. Dimensionless curves for PTR11 and PTR4

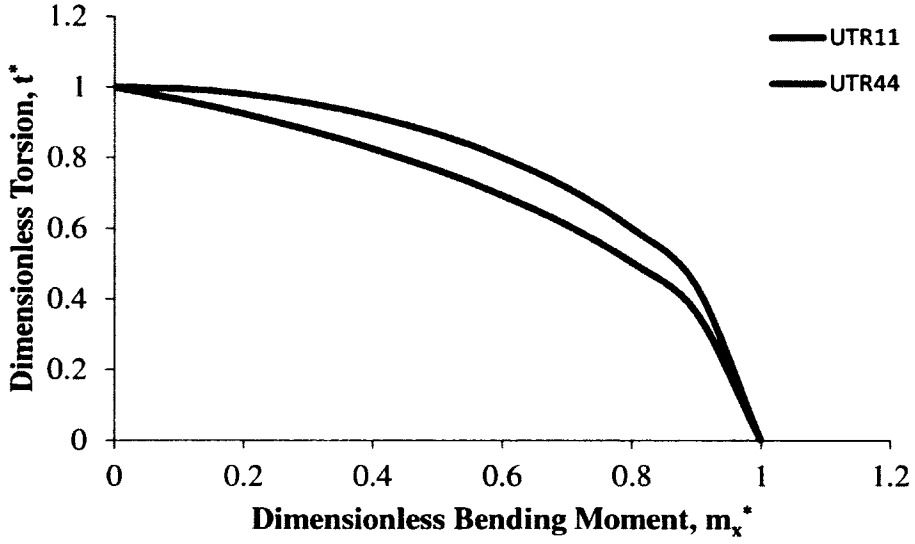

Figure 83. Dimensionless curves for UTR11 and UTR44

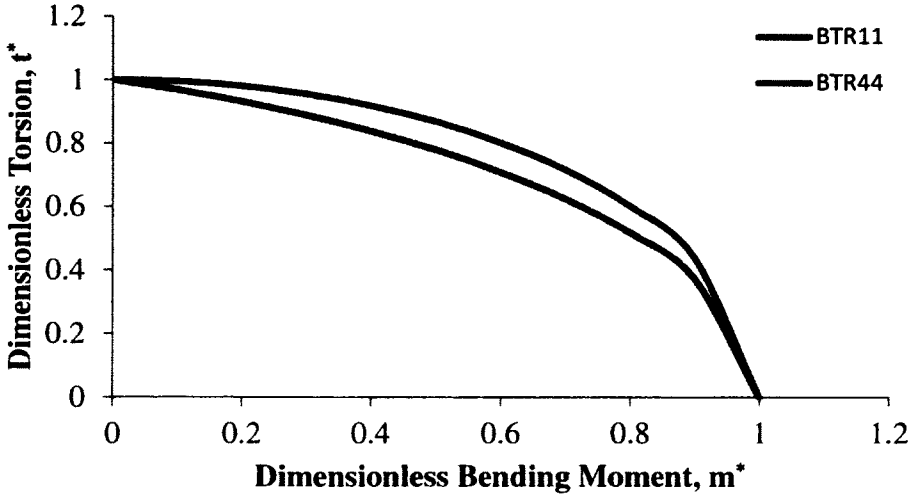

Figure 84. Dimensionless curves for BTR11 and BTR44

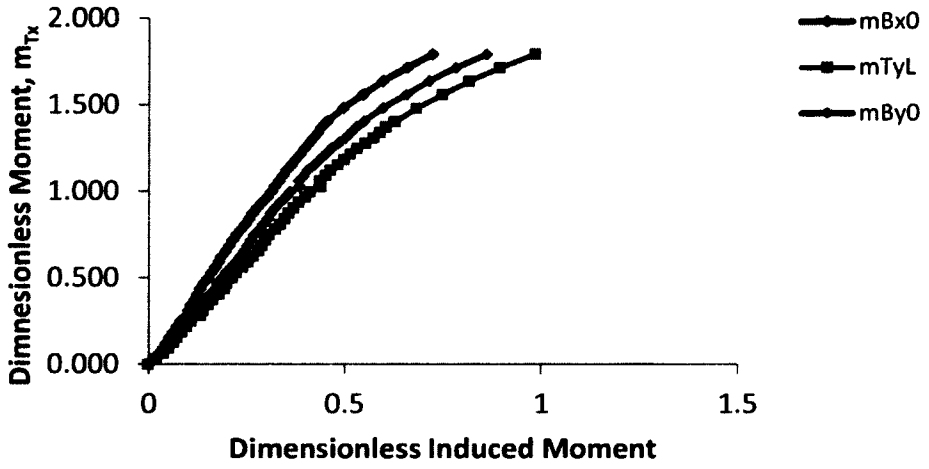

Figure 85. Dimensionless applied and Induced Moment Curves for BR44

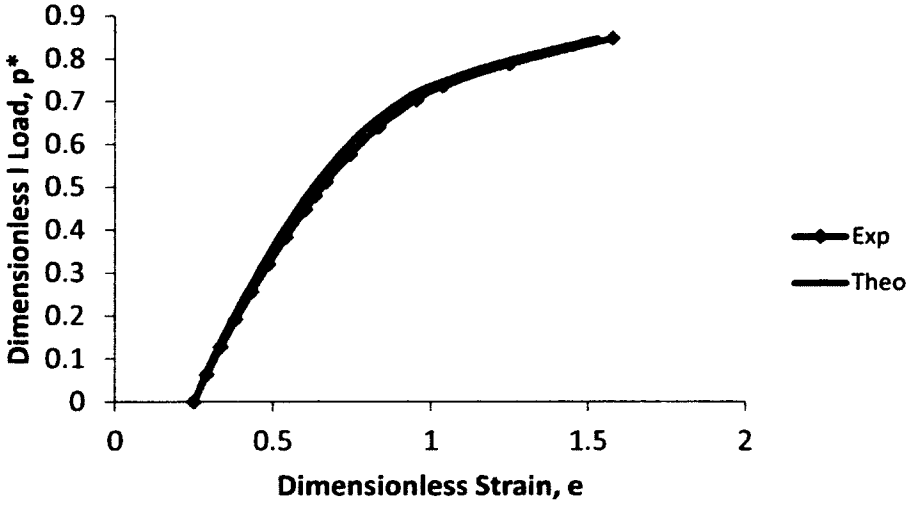

Figure 86. Dimensionless experimental and predicted p*-e curves for PR44

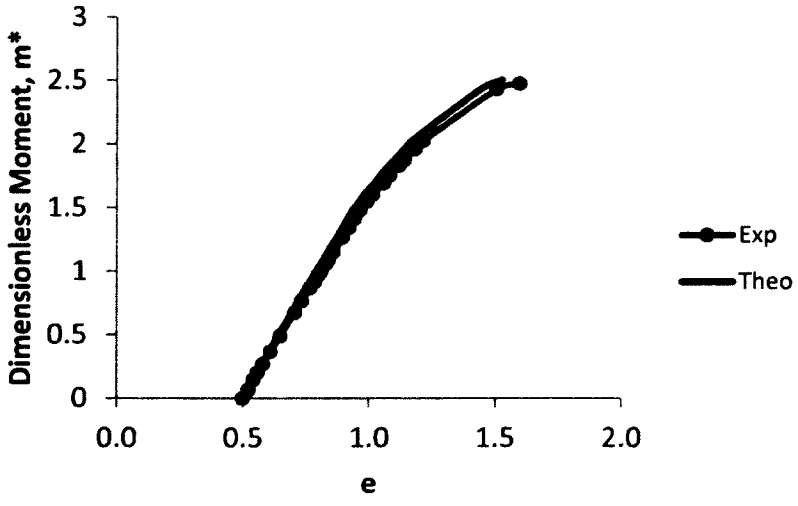

Figure 87. Dimensionless experimental and predicted m*-e curves for UR44

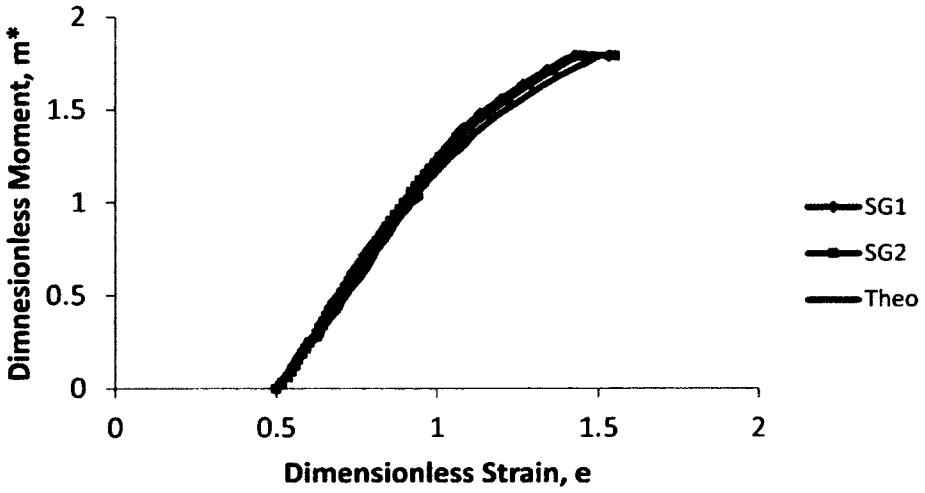

Figure 88. Dimensionless experimental and predicted m*-e curves for BR44

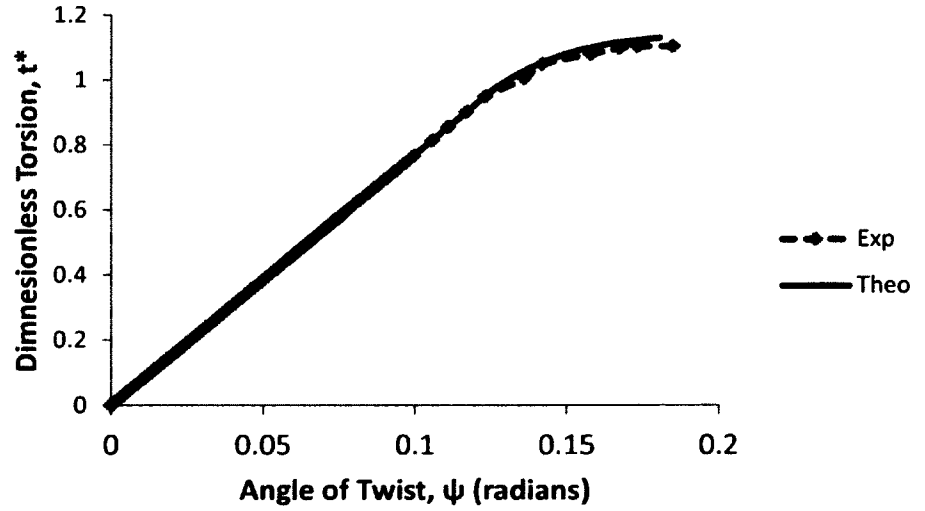

Figure 89. Dimensionless experimental and predicted t*-ψ curves for TR44

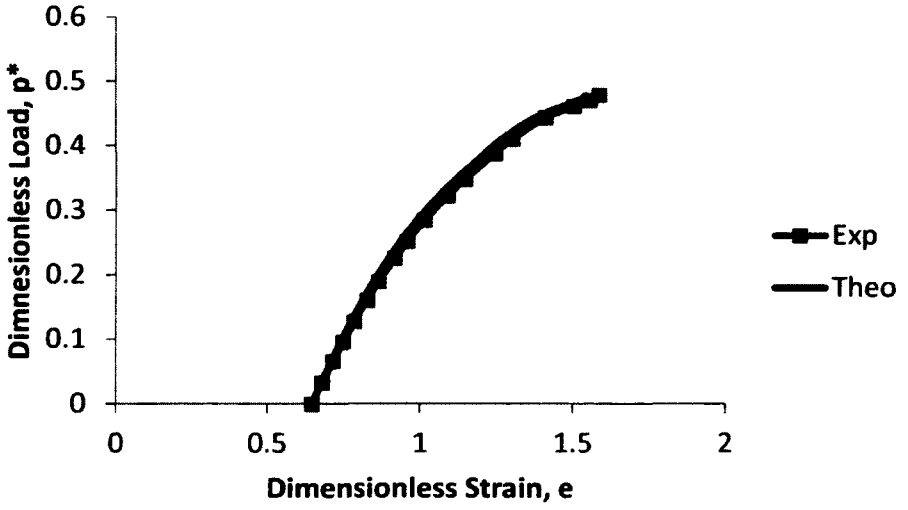

Figure 90. Dimensionless experimental and predicted p*-e curves for TPR44

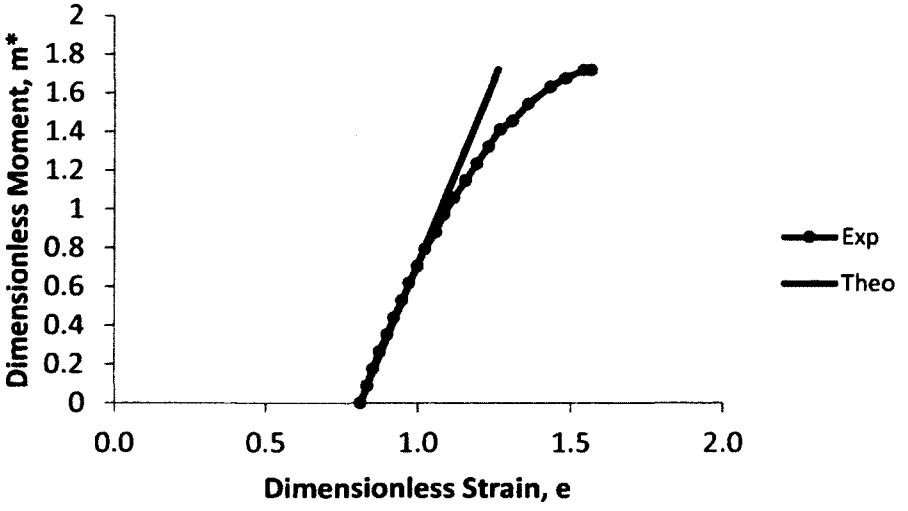

Figure 91. Dimensionless experimental and predicted m*-e curves for TUR44

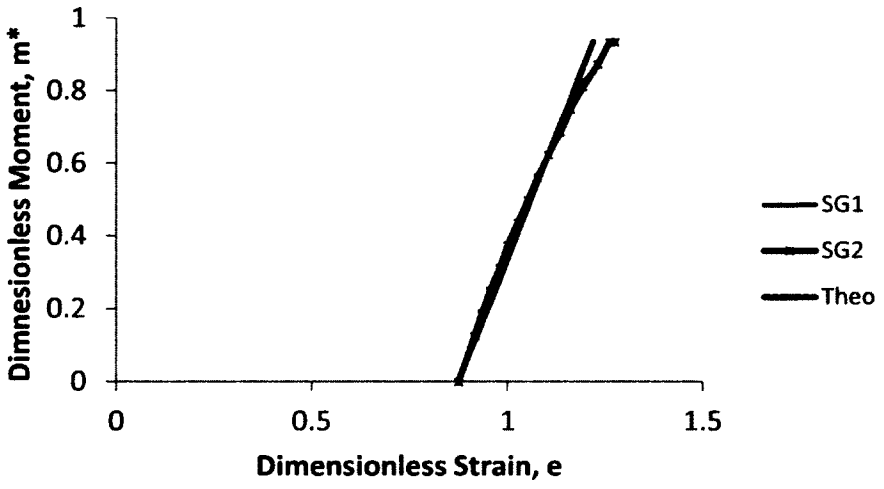

Figure 92. Dimensionless experimental and predicted m*-e curves for TBR44

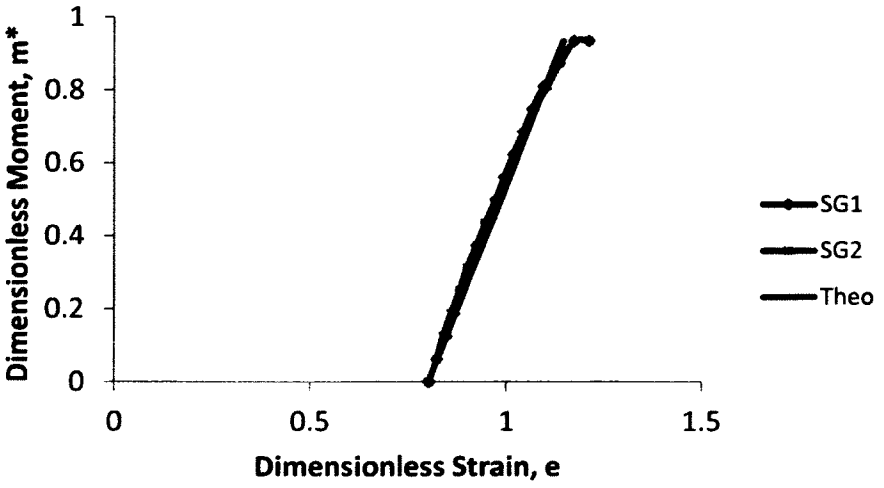

Figure 93. Dimensionless experimental and predicted m*-e curves for TBR41

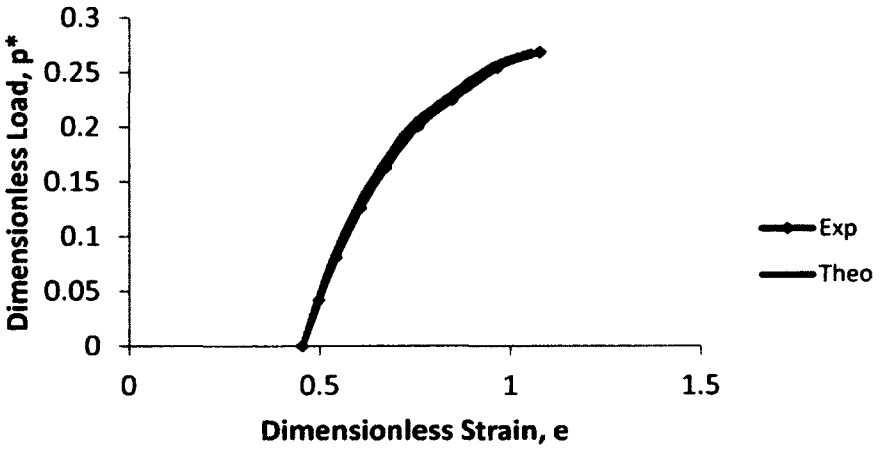

Figure 94. Dimensionless experimental and predicted p*-e curves for TBPR44

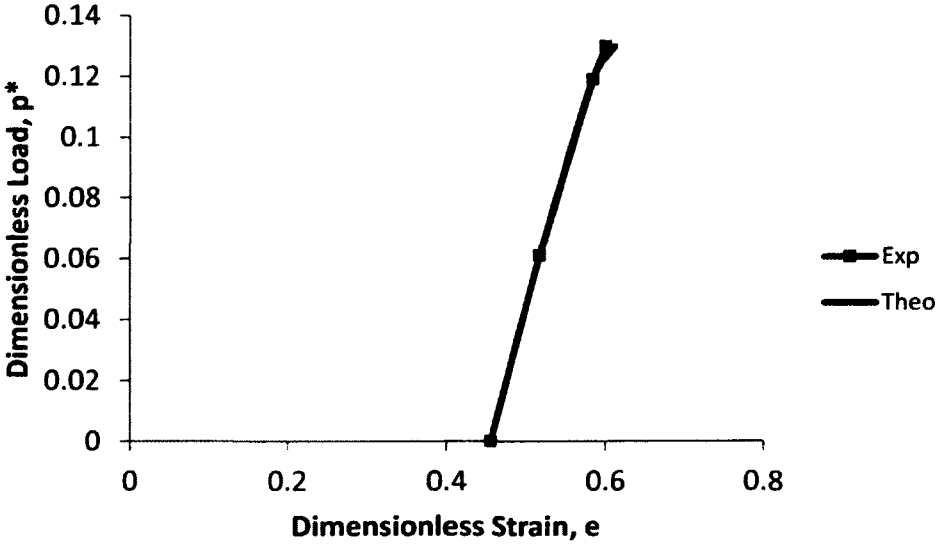

Figure 95. Dimensionless experimental and predicted p*-e curves for TBPR41

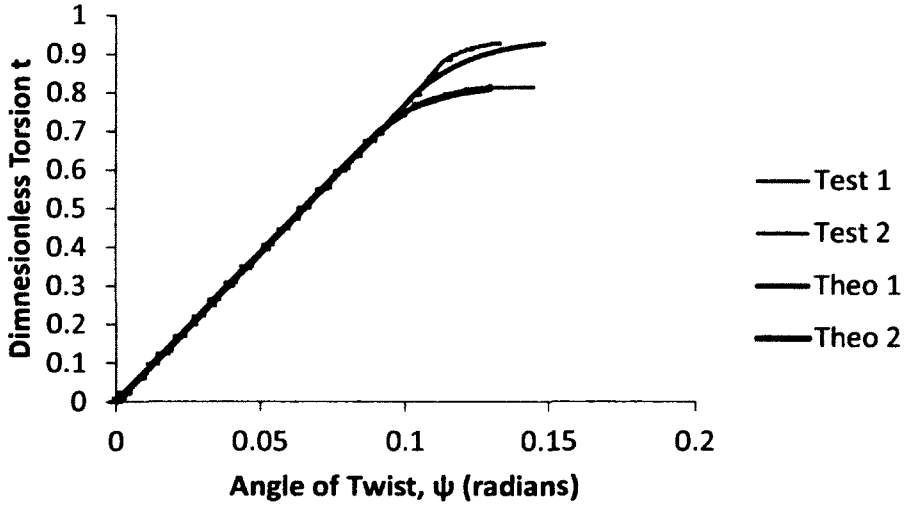

Figure 96. Dimensionless experimental and predicted t-ψ curves for PBTR44

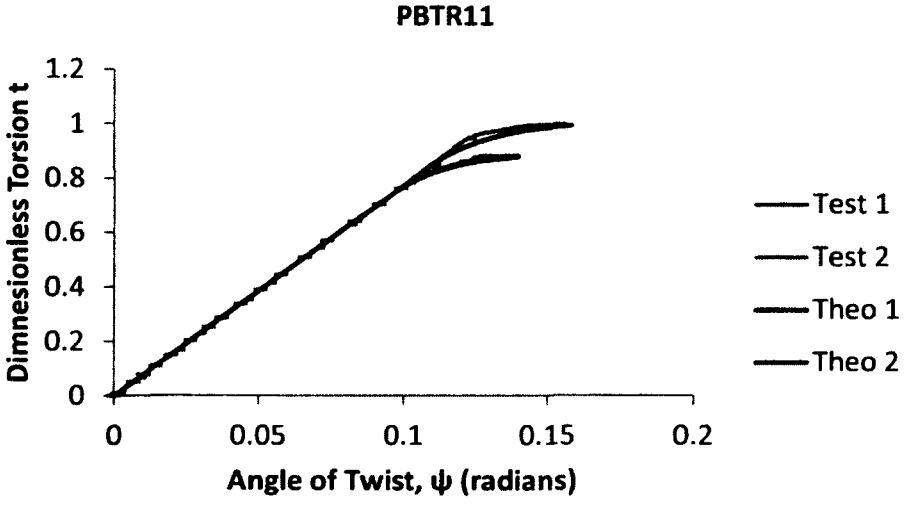

Figure 97. Dimensionless experimental and predicted t-ψ curves for PBTR11

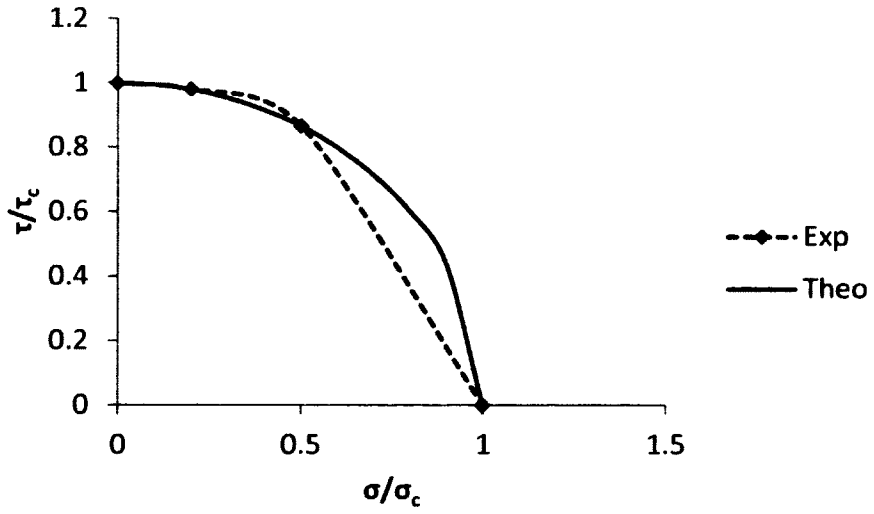

Figure 98 Dimensionless interaction curves for Test Series PBTR11

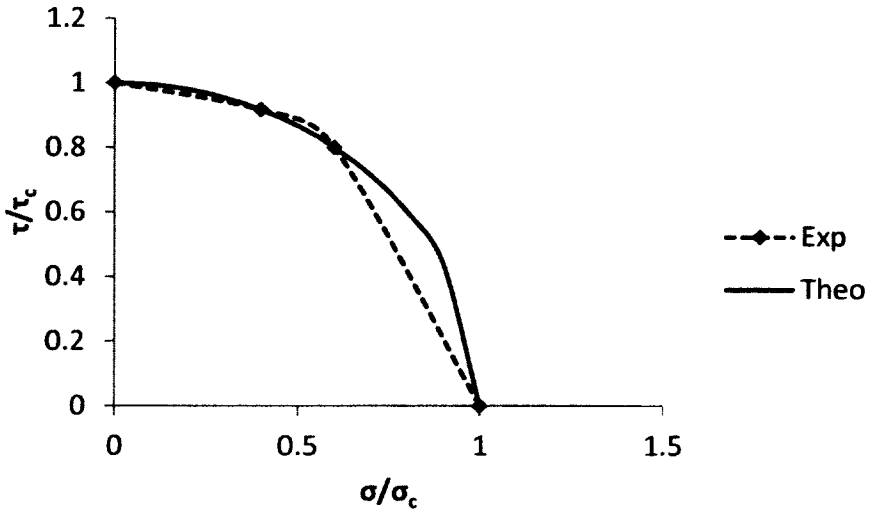

Figure 99. Dimensionless interaction curves for Test Series PBTR44

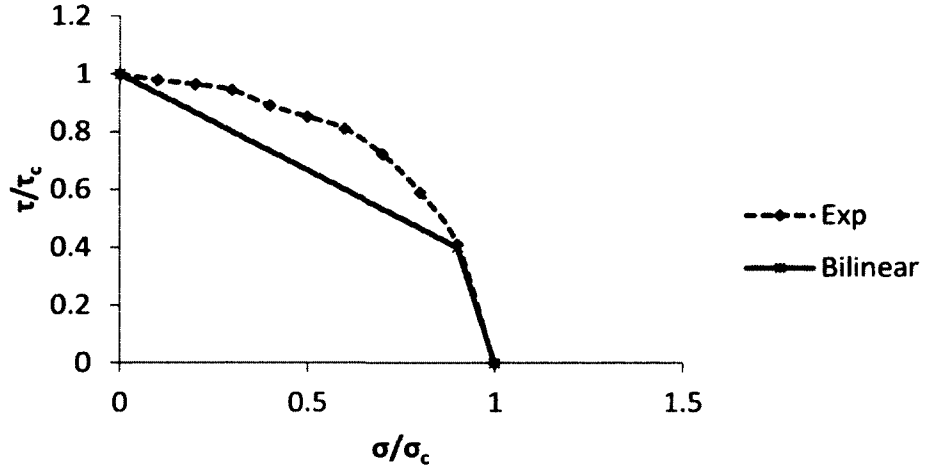

Figure 100. Bilinear approximation approach for Test Series PBTR1

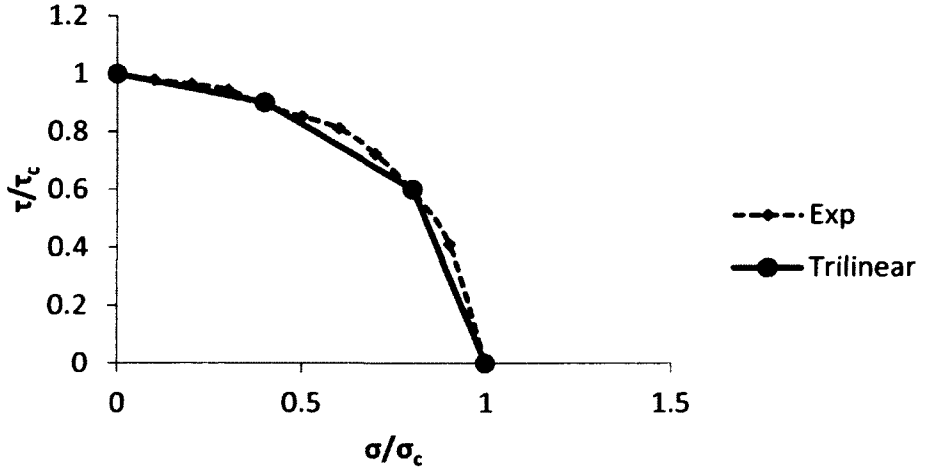

Figure 101. Trilinear approximation approach for Test Series PBTR1

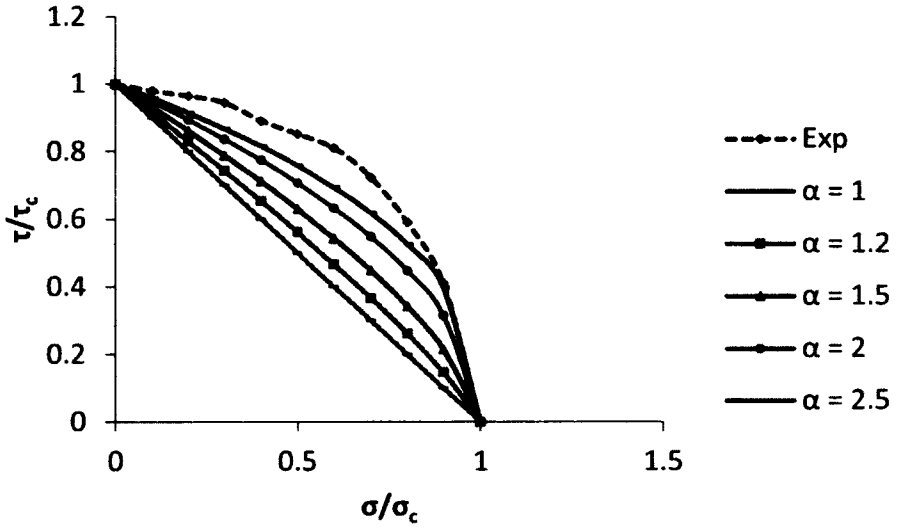

Figure 102. Expression 178 with different α values curves for Test Series PBTR1

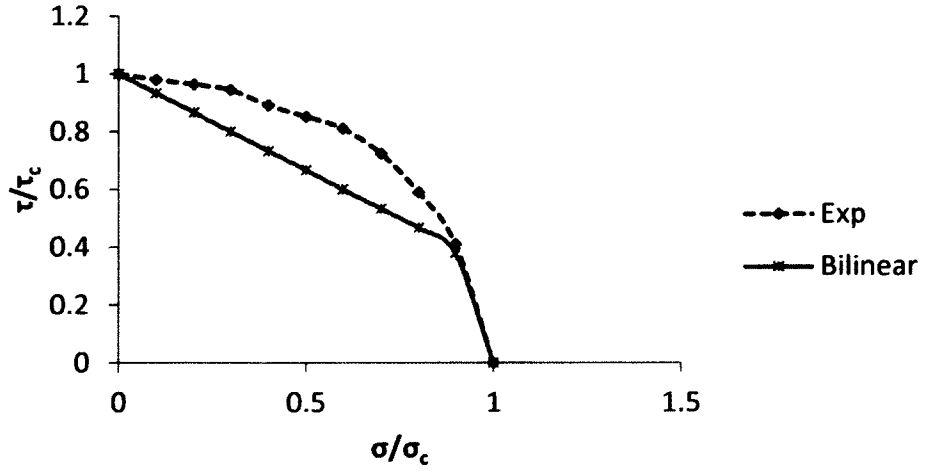

Figure 103. Bilinear curve for Test Series PBTR1

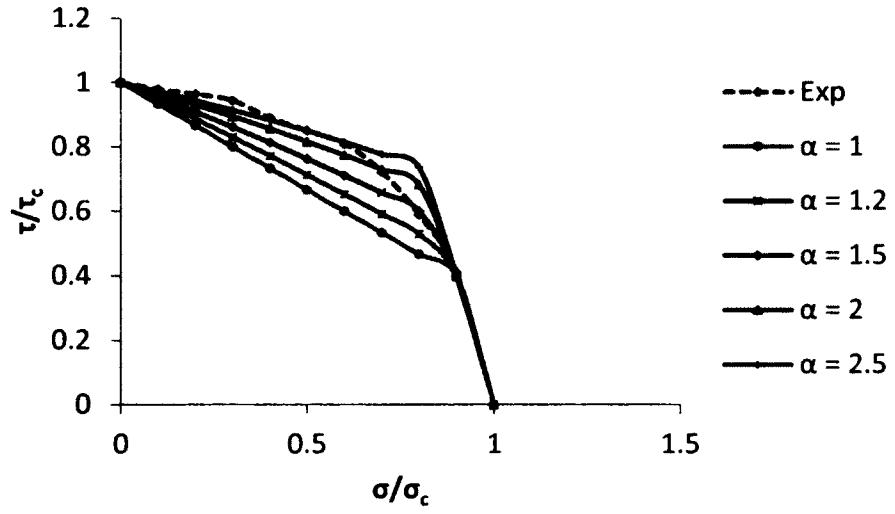

Figure 104. Expression 181 with different α values curves for Test Series PBTR1

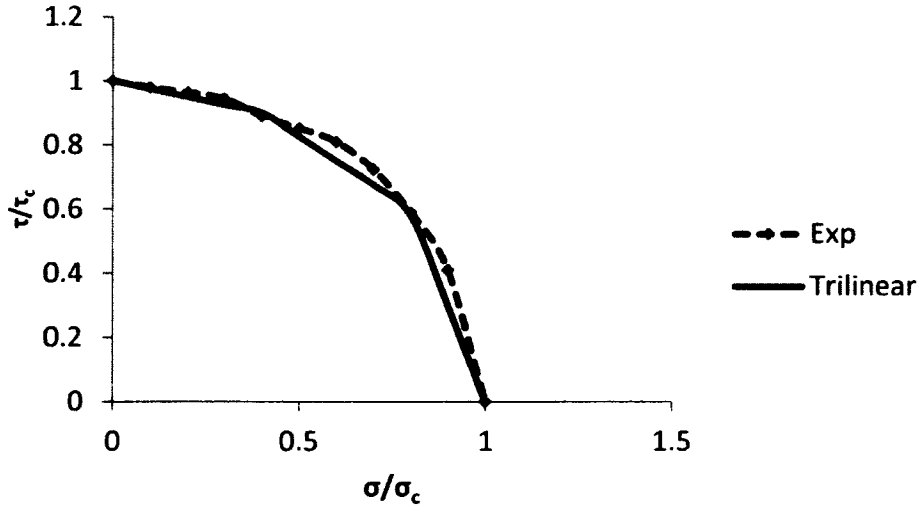

Figure 105. Trinilear curve for Test Series PBTR1

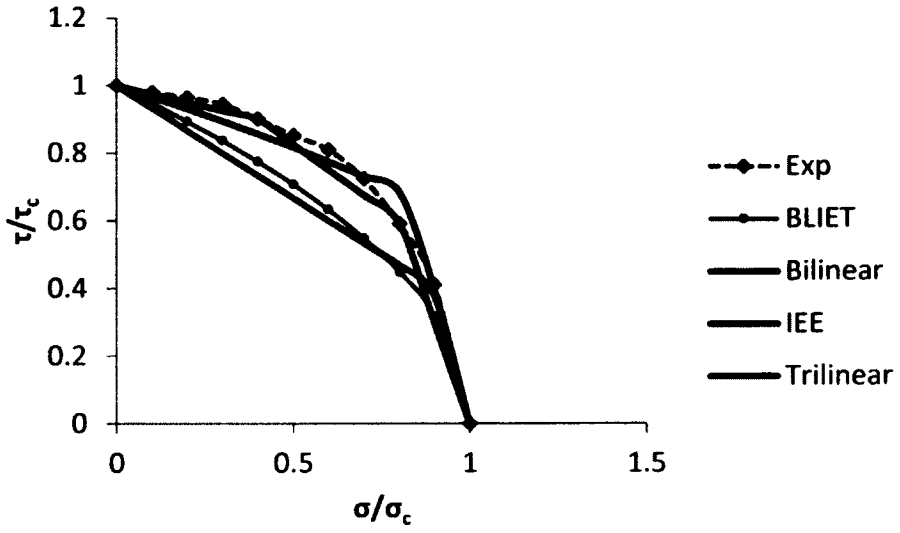

Figure 106. BLIET, Bilinear, IEE and Trilinear curves for PBTR1

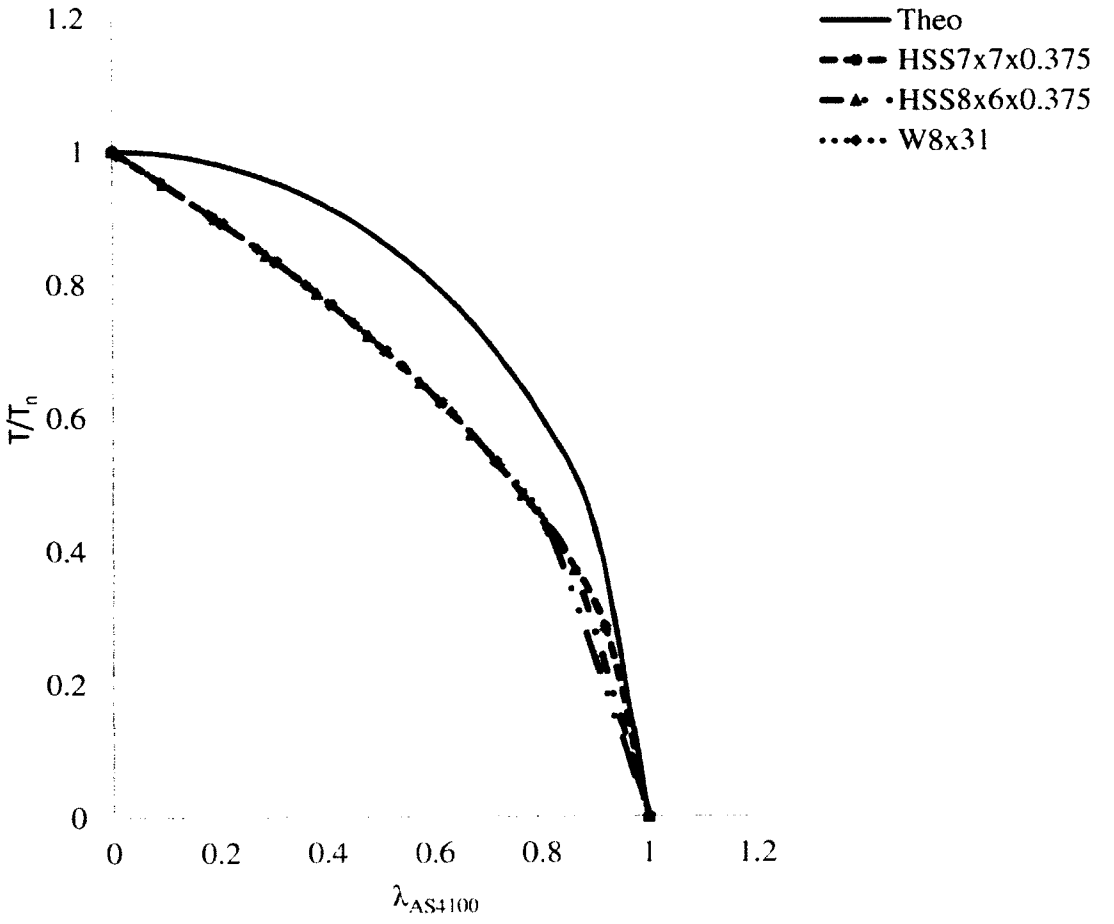

Figure 107. Expression 216 with α = 2 curves for PBTR1

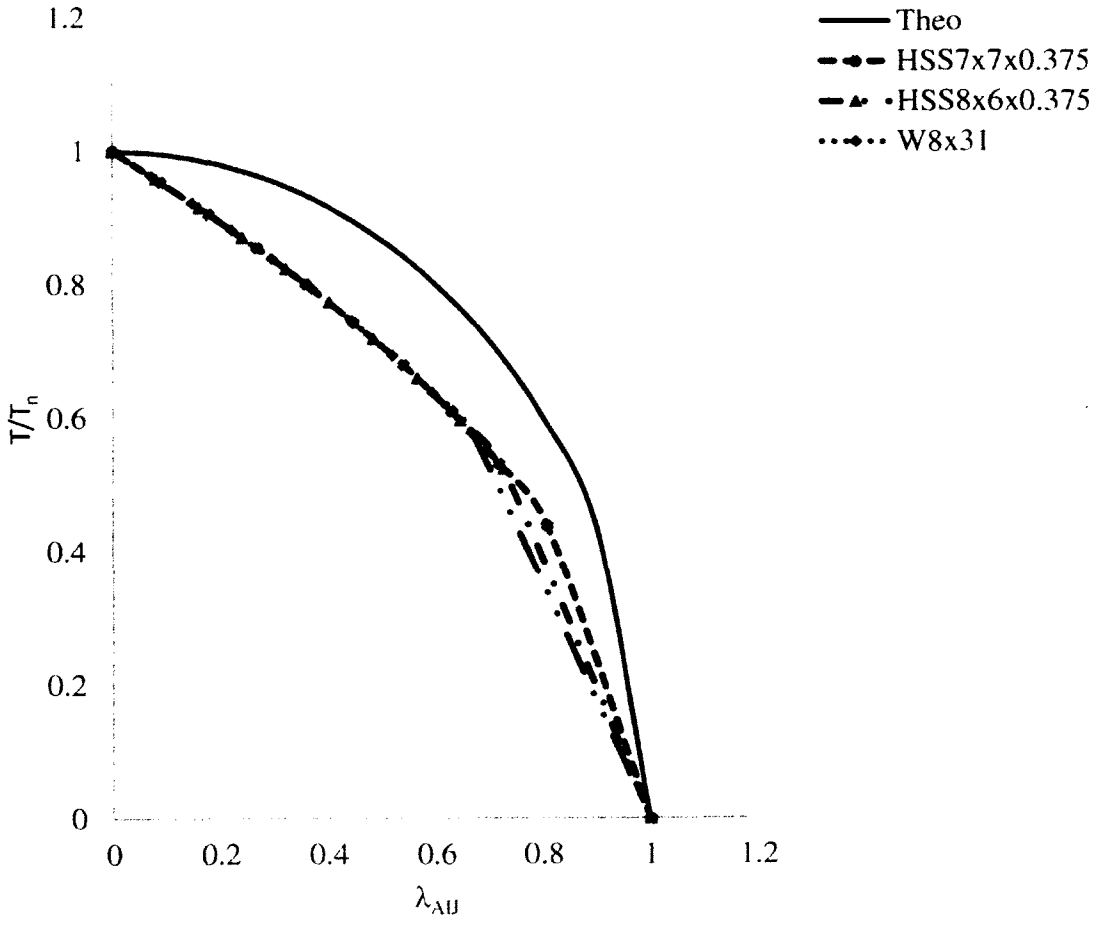

Figure 108. Expression 219 with α = 2 curves for PBTR1

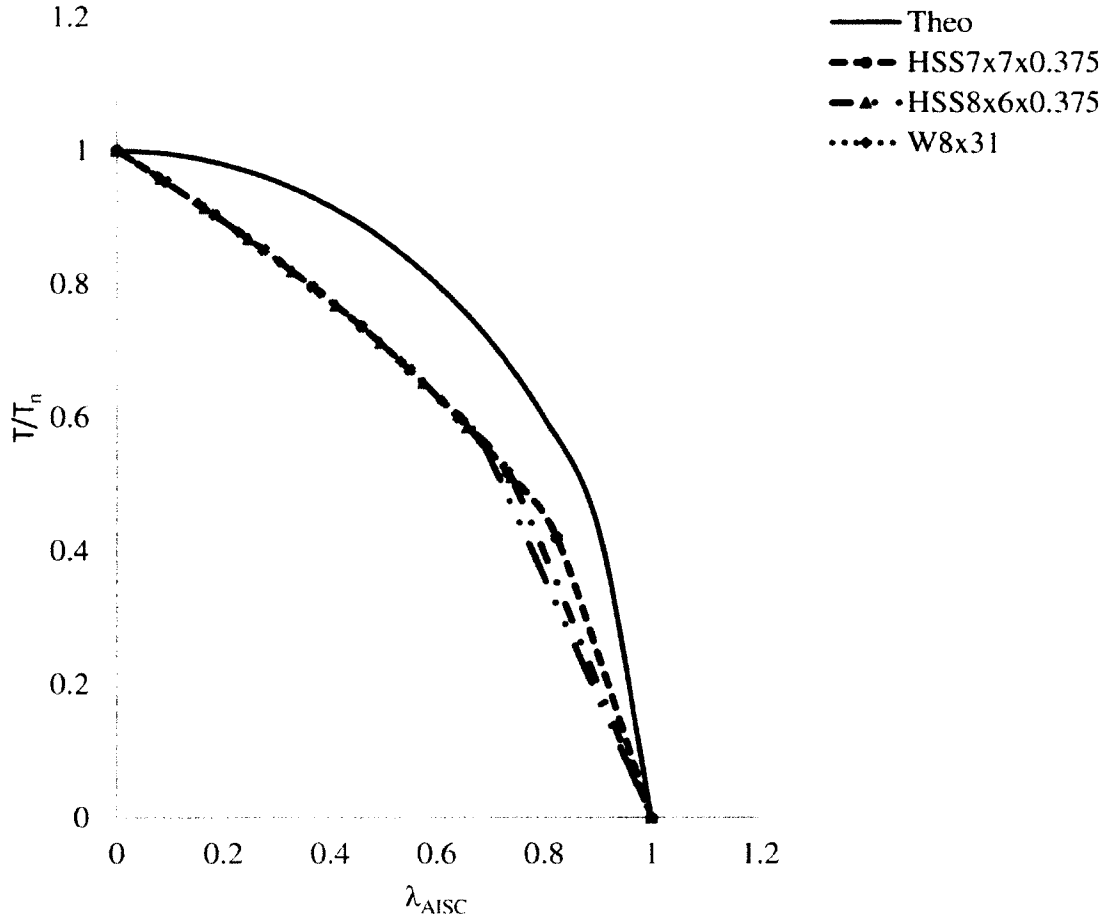

Figure 109. Expression 221 with $\alpha = 2$ curves for PBTR1

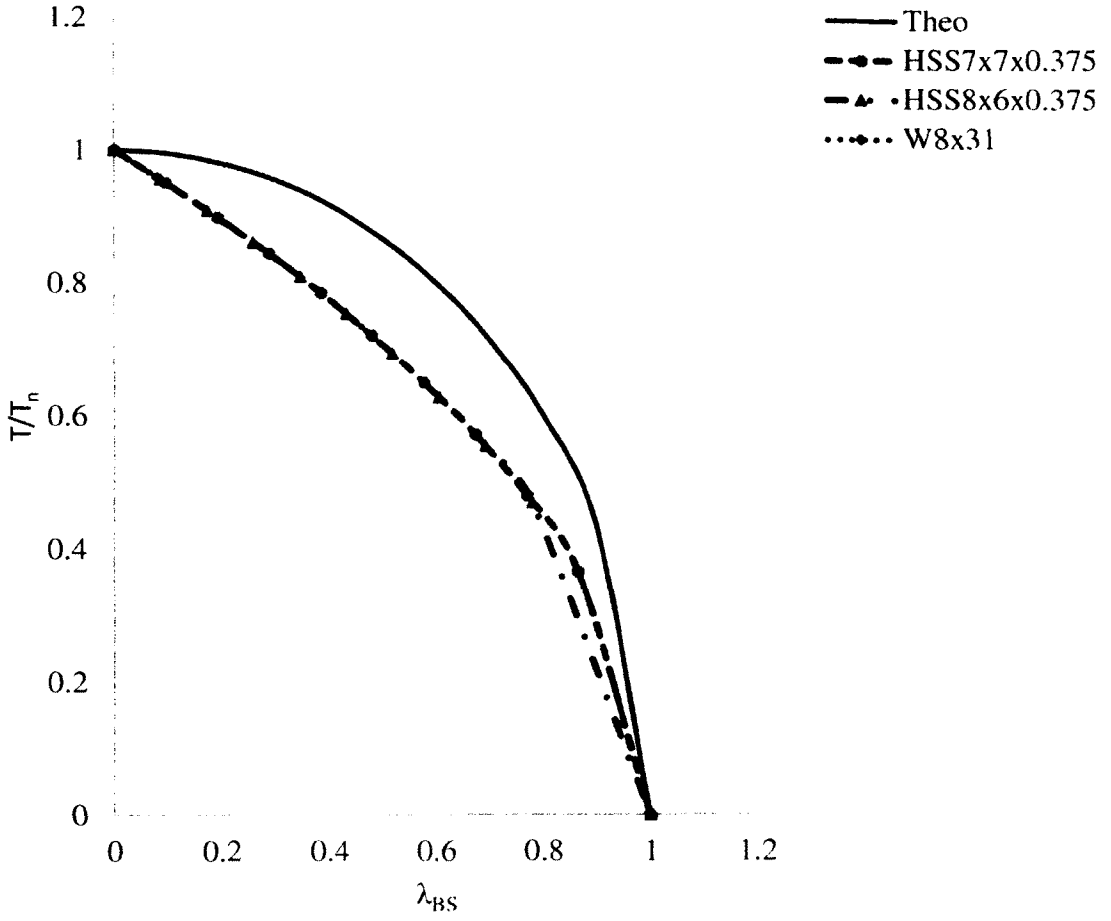

Figure 110. Expression 223 with α = 2 curves for PBTR1

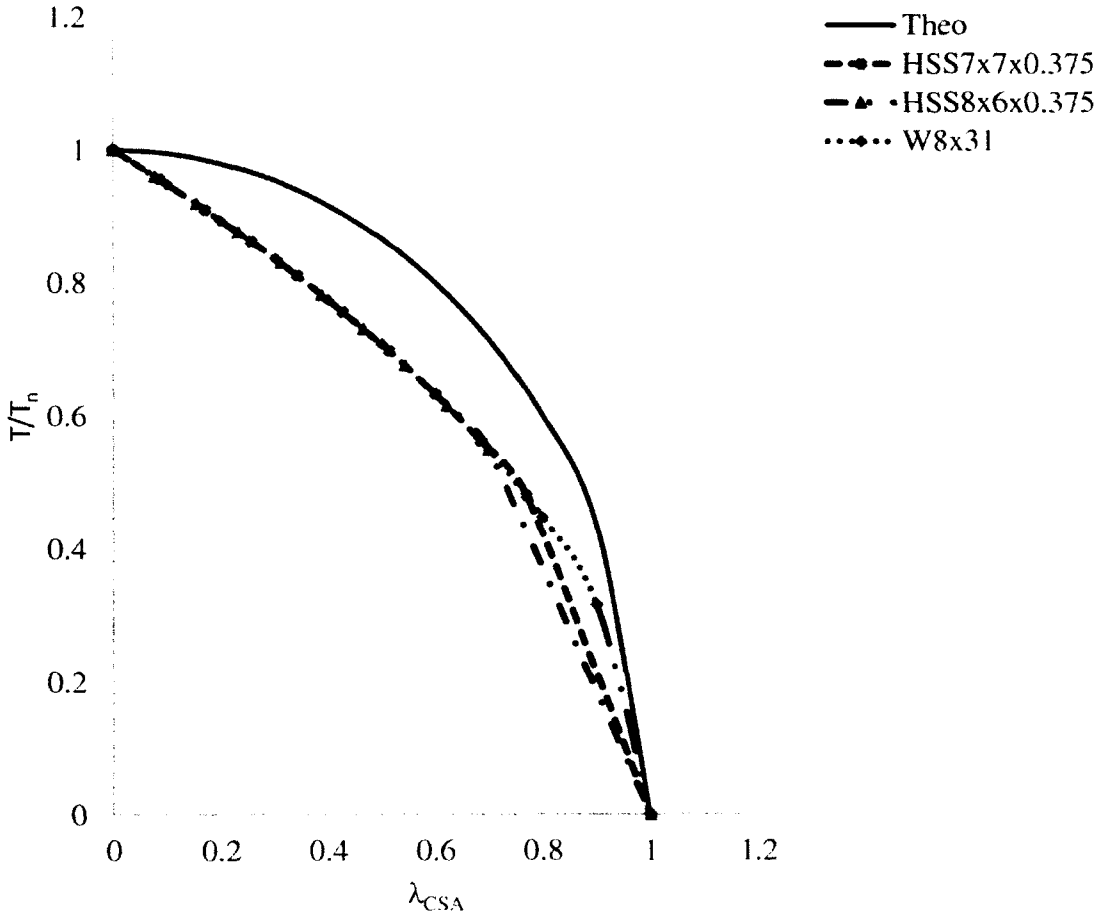

Figure 111. Expression 225 with $\alpha = 2$ curves for PBTR1

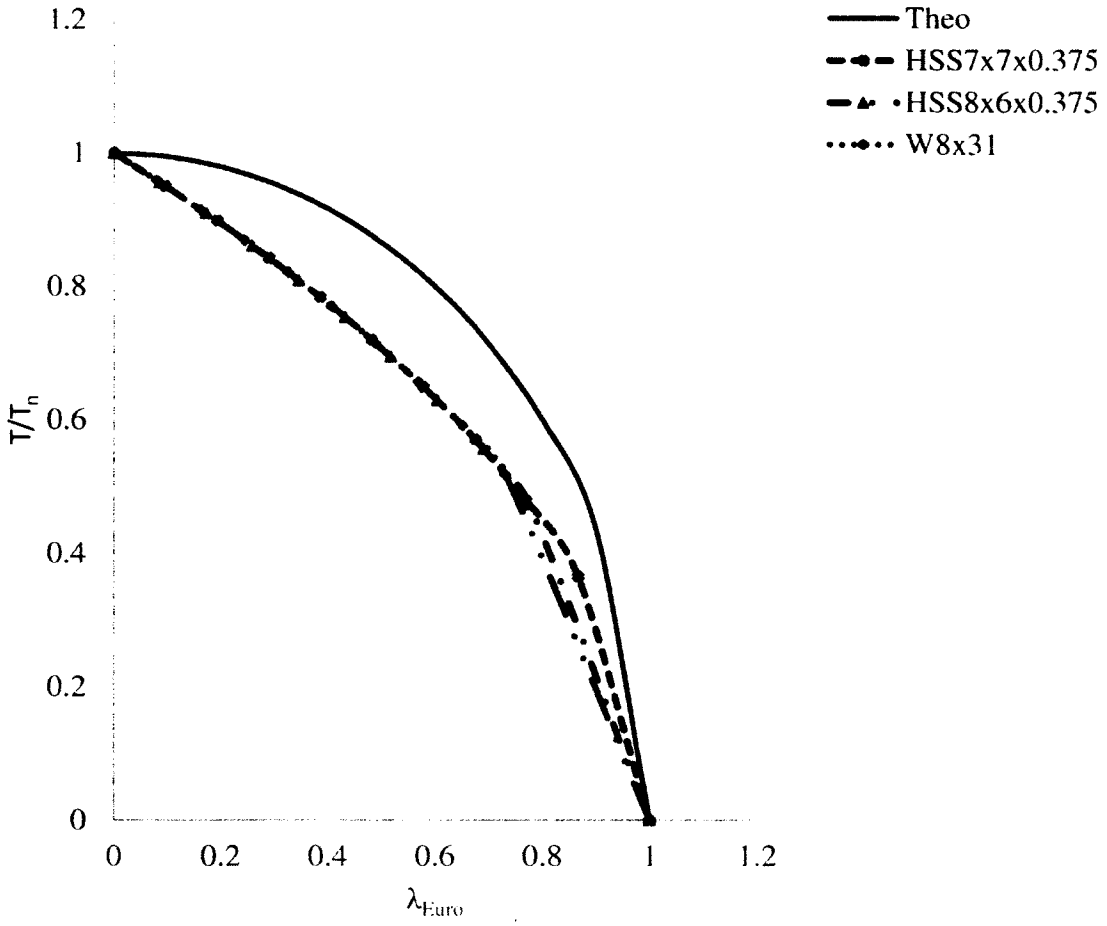

Figure 112. Expression 227 with $\alpha = 2$ curves for PBTR1

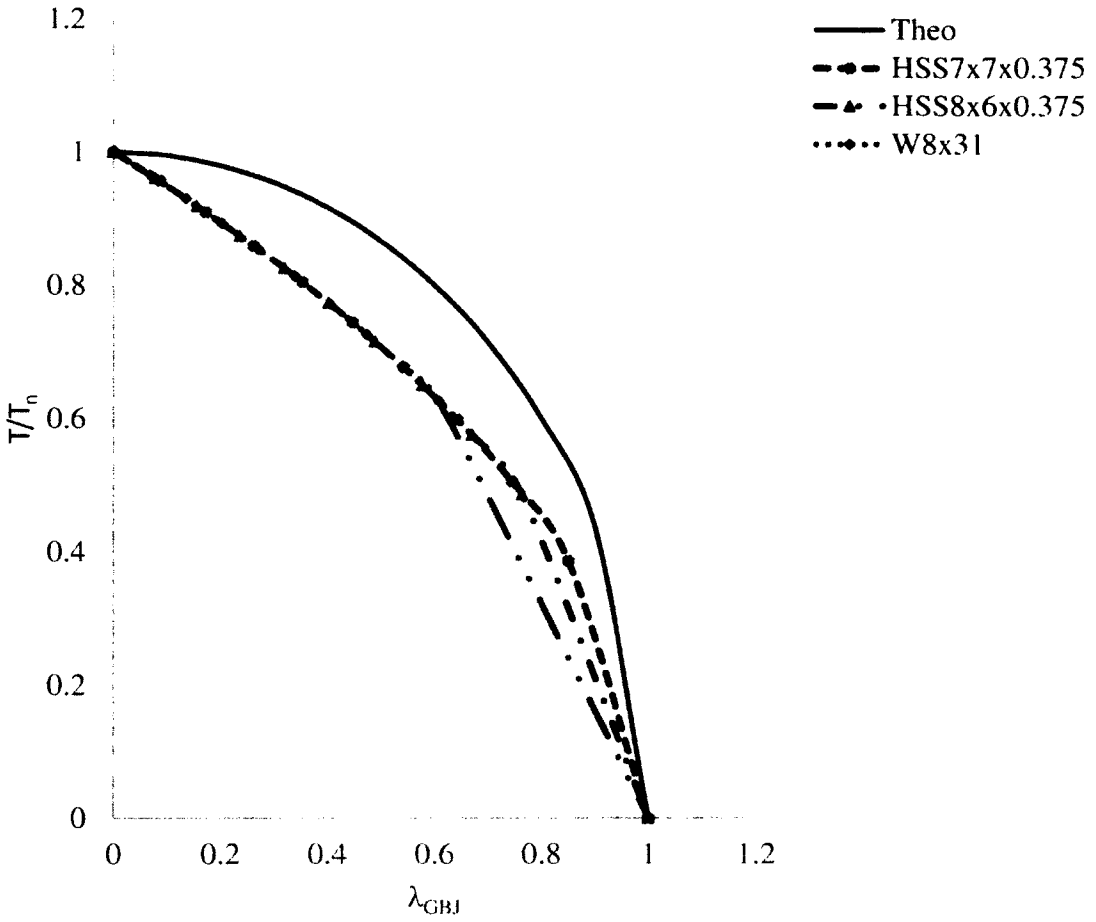

Figure 113. Expression 229 with α = 2 curves for PBTR1

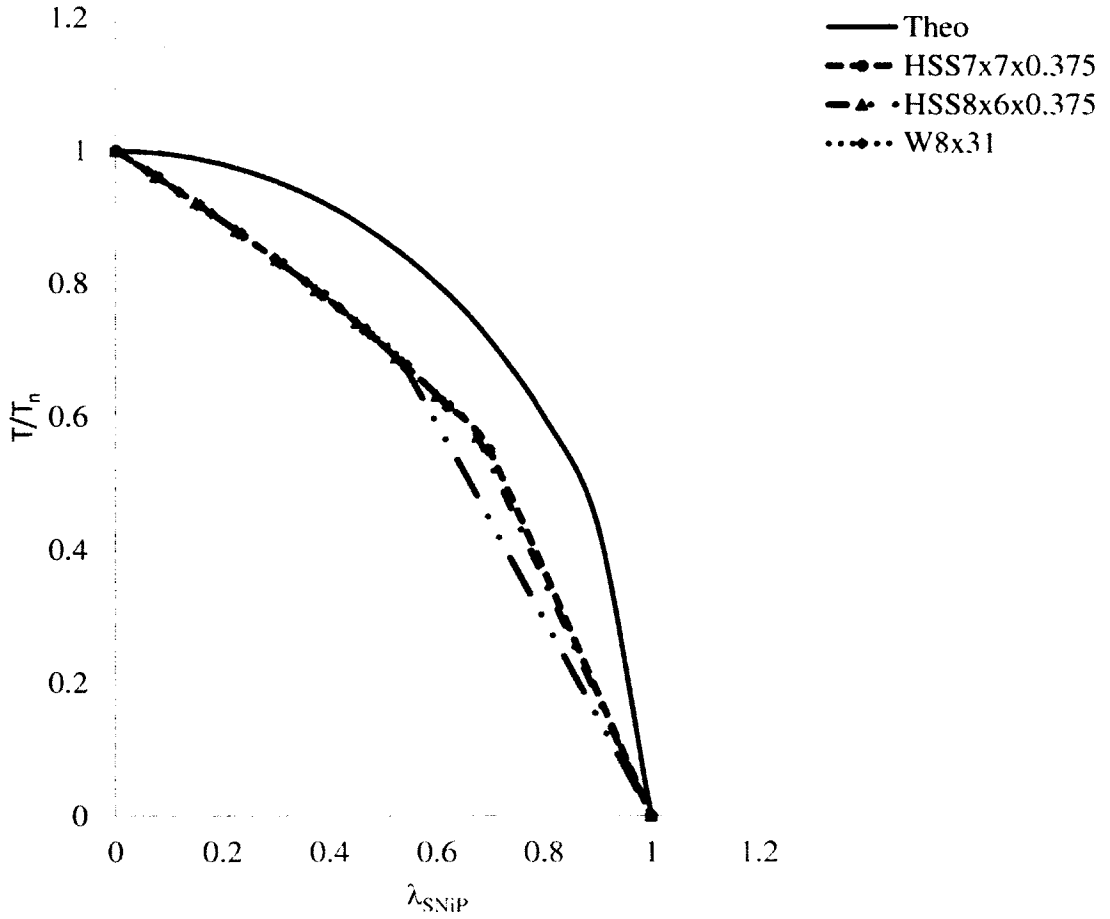

Figure 114. Expression 231 with α = 2 curves for PBTR1

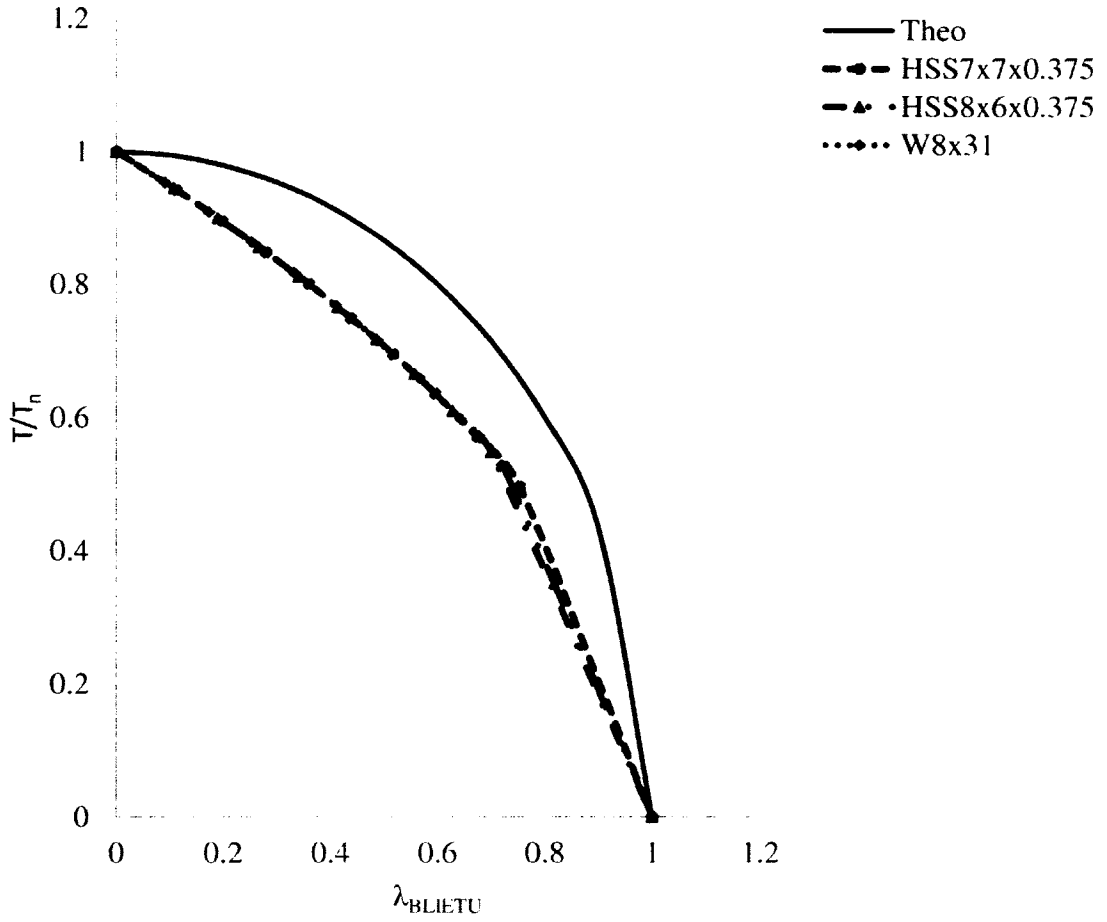

Figure 115. Expression 233 with α = 2 curves for PBTR1

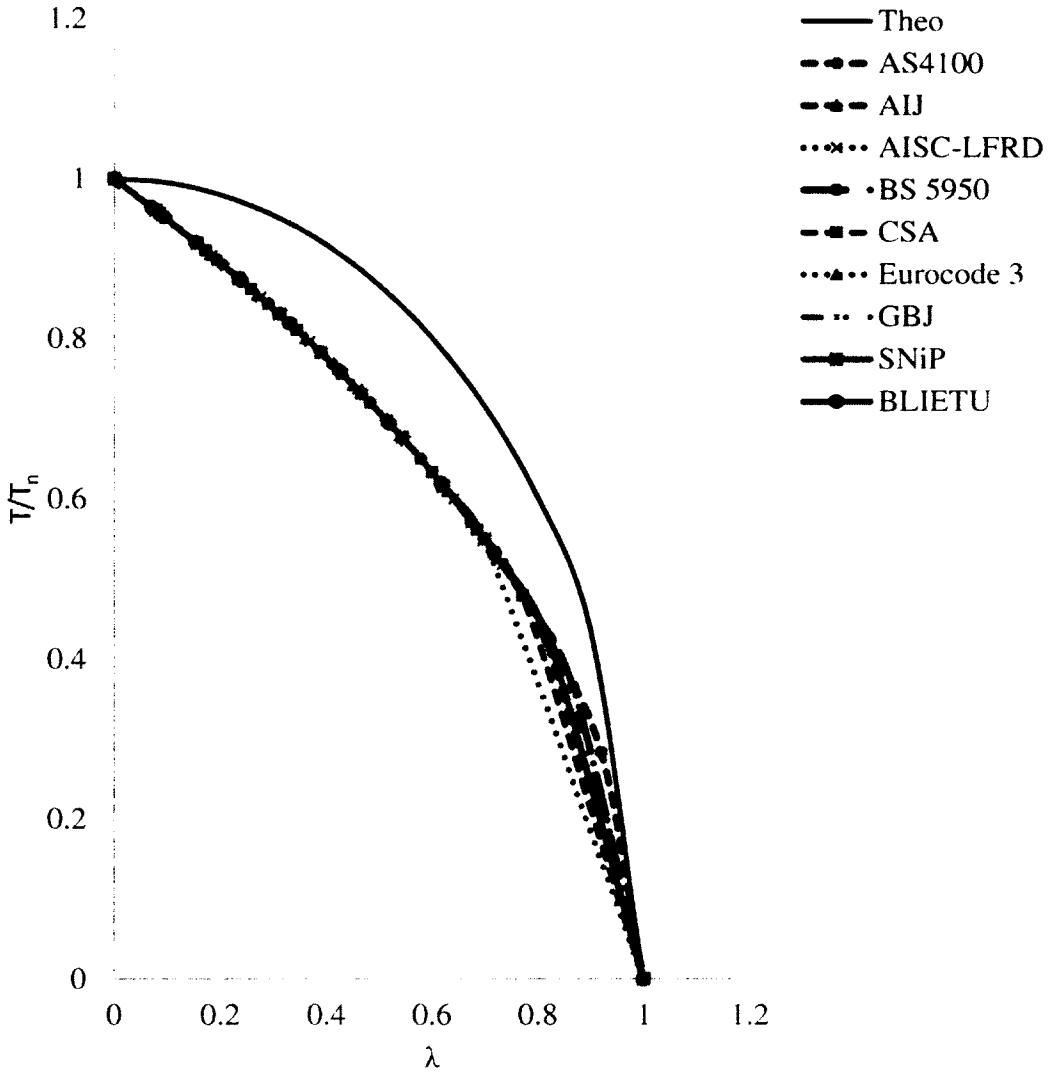

Figure 116. Dimensionless curves with α = 2 for PBTR1 with HSS7x7x0.375 for various countries

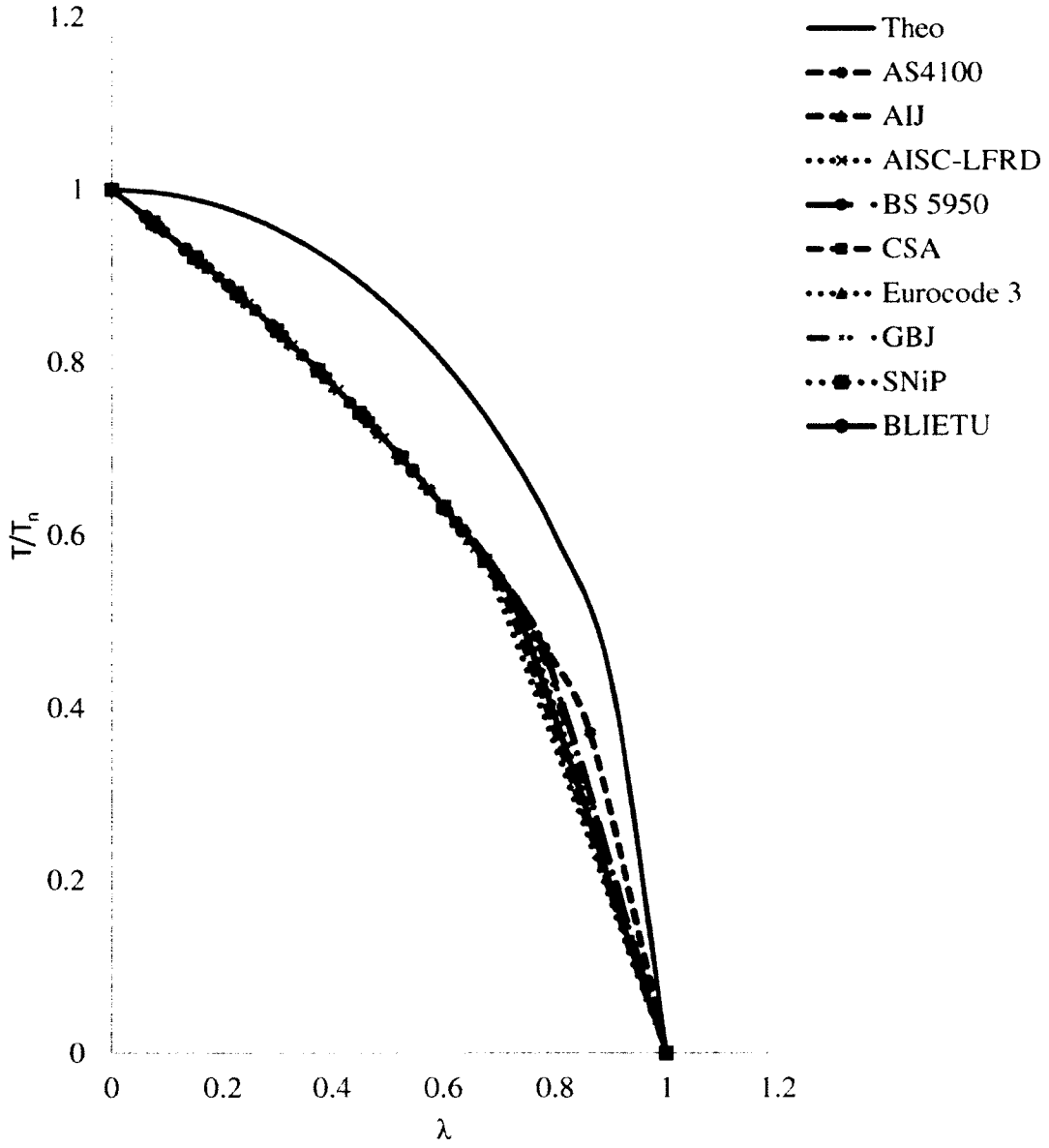

Figure 117. Dimensionless curves with α = 2 for PBTR1 with HRS8x6x0.375 for various countries

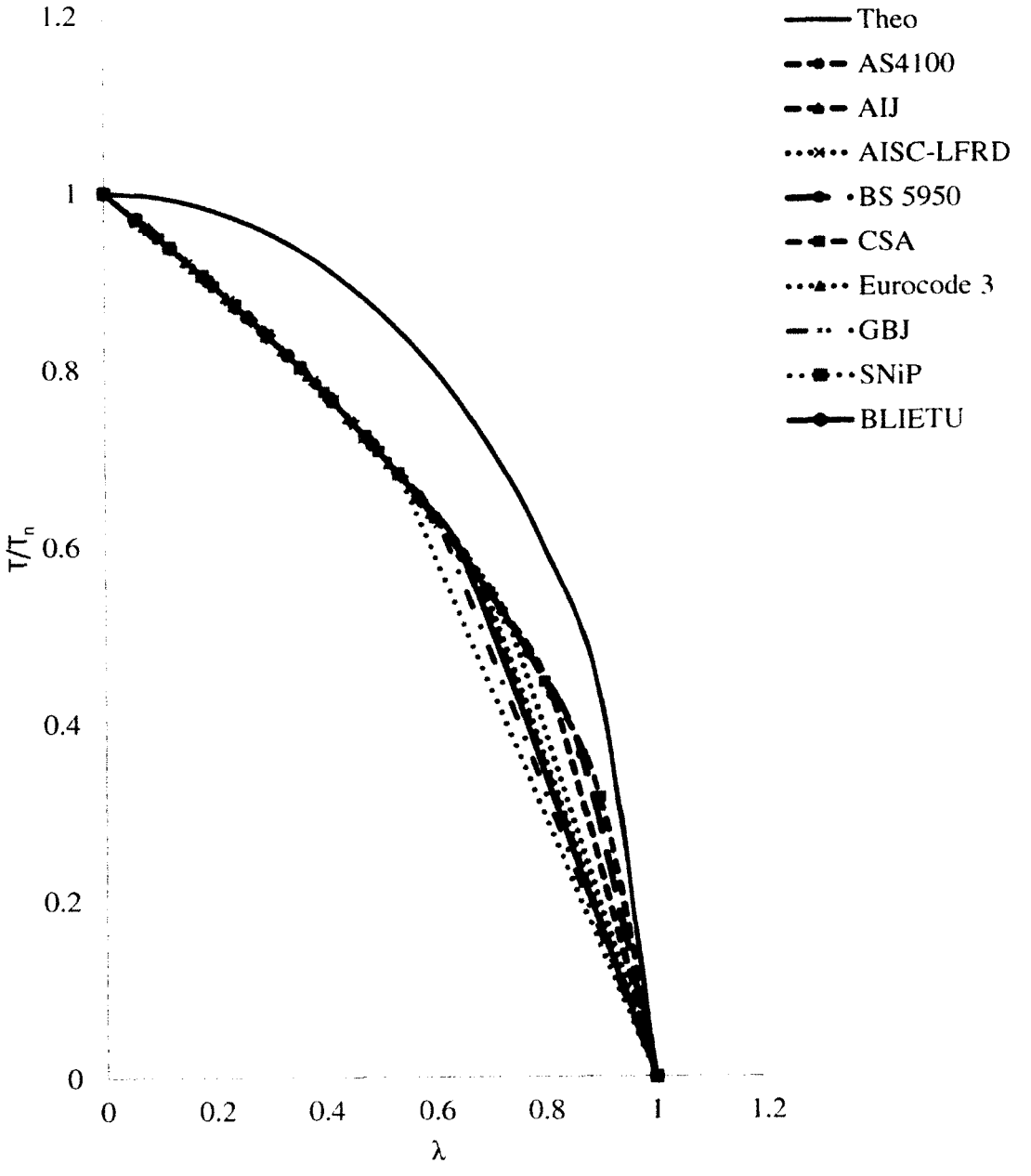

Figure 118. Dimensionless curves with α = 2 for PBTR1 with W8x31 for various countries

APPENDIX A: Finite Integral Derivation

Let the variation of a function f over an interval be $z_j < z < z_{j+1}$ such that $z_{j+1} - z_j = h$, is approximated by a parabola:

$$f = a\,z^2 + b\,z + c \tag{A1}$$

and let it be fitted to three adjacent values of f. Thus, it is found that:

$$\int_{z_i}^{z_{i+1}} f\,dz = \frac{h}{12}(5\,f_i + 8\,f_{i+1} - f_{i+2}) \tag{A2}$$

$$\int_{z_i}^{z_{i+2}} f\,dz = \frac{h}{12}(4\,f_i + 16\,f_{i+1} + 4\,f_{i+2}) \tag{A3}$$

for an integral defined by:

$$l_i = \int_0^{ith} f\,dz \tag{A4}$$

The matrix equation formed by Equations A2-A3 can be written as follows:

$$\{l_i\} = \frac{h}{12}[N]\{f\} \tag{A5}$$

where :

$$\{l\} = \{l_0\ l_1\ l_2 \dots \dots \dots l_n\}^T \tag{A6}$$

$$\{f\} = \{f_0\ f_1\ f_2 \dots \dots \dots f_n\}^T \tag{A7}$$

and N is a square matrix of size $n + 1$ defined by:

$$[N] = \begin{bmatrix} 0 & 0 & 0 & 0 & 0 & 0 & \cdot & \cdot & \cdot \\ 5 & 8 & -1 & 0 & 0 & 0 & \cdot & \cdot & \cdot \\ 4 & 16 & 4 & 0 & 0 & 0 & \cdot & \cdot & \cdot \\ 4 & 16 & 9 & 8 & -1 & 0 & \cdot & \cdot & \cdot \\ 4 & 16 & 8 & 16 & 4 & 0 & \cdot & \cdot & \cdot \\ 4 & 16 & 8 & 16 & 9 & 8 & \cdot & \cdot & \cdot \\ \cdot & \cdot & \cdot & \cdot & \cdot & \cdot & \cdot & \cdot & \cdot \\ \cdot & \cdot & \cdot & \cdot & \cdot & \cdot & \cdot & \cdot & \cdot \\ \cdot & \cdot & \cdot & \cdot & \cdot & \cdot & \cdot & \cdot & \cdot \end{bmatrix} \tag{A8}$$

Let the function l be equal to f and approximated by a series of parabolas; the second integral m of the function is given by:

$$m_i = \int_0^{ith} l\,dz = \int_0^{ith}\int_0^{ith} f\,dz\,dz \tag{A9}$$

Equation 71 can be approximated by:

$$\{m\} = \left(\frac{h}{12}\right)^2 [N]^2\{f\} \tag{A10}$$

Therefore, the following integrals for the function F are obtained:

$$F_i'' = \int_0^{ith} F'''' \, dz \tag{A11}$$

$$F_i' = \int_0^{ith} \int_0^{ith} F'''' \, dz \, dz \tag{A12}$$

$$F_i = \int_0^{ith} \int_0^{ith} \int_0^{ith} F'''' \, dz \, dz \, dz \tag{A13}$$

These equations can be approximated, respectively, as follows:

$$\{F''\} = \frac{h}{12}[N]\{F''''\} \tag{A14}$$

$$\{F'\} = \left(\frac{h}{12}\right)^2 [N]^2\{F''''\} \tag{A15}$$

$$\{F\} = \left(\frac{h}{12}\right)^3 [N]^3\{F''''\} \tag{A16}$$

Here, $[N]^2$ = [N] [N] and $[N]^3$ = [N] [N] [N].

APPENDIX B: Finite Integral Formulation

The lower order derivatives of the dependent variables u, v, and ψ are expressed as follows:

$$u_i'' = \frac{h}{12}[N]\{u_i'''\} \tag{B1}$$

$$u_i' = \left(\frac{h}{12}\right)^2 [N]^2\{u_i'''\} - \left(\frac{h}{12}\right)^3 \frac{1}{L}\left[N_n^{(3)}\right]\{u_i'''\} \tag{B2}$$

$$u_i = \left(\frac{h}{12}\right)^3 [N]^3\{u_i'''\} - \left(\frac{h}{12}\right)^3 \frac{1}{L}\{z\}\left[N_n^{(3)}\right]\{u_i'''\} \tag{B3}$$

$$v_i'' = \frac{h}{12}[N]\{v_i'''\} \tag{B4}$$

$$v_i' = \left(\frac{h}{12}\right)^2 [N]^2\{v_i'''\} - \left(\frac{h}{12}\right)^3 \frac{1}{L}\left[N_n^{(3)}\right]\{v_i'''\} \tag{B5}$$

$$v_i = \left(\frac{h}{12}\right)^3 [N]^3\{v_i'''\} - \left(\frac{h}{12}\right)^3 \frac{1}{L}\{z\}\left[N_n^{(3)}\right]\{v_i'''\} \tag{B6}$$

$$\psi_i'' = \frac{h}{12}[N]\{\psi_i'''\} - \left(\frac{h}{12}\right)^2 \frac{1}{L}\left[N_n^{(2)}\right]\{\psi_i'''\} \tag{B7}$$

$$\psi_i' = \left(\frac{h}{12}\right)^2 [N]^2\{\psi_i'''\} - \left(\frac{h}{12}\right)^2 \frac{1}{L}\{z\}\left[N_n^{(2)}\right]\{\psi_i'''\} \tag{B8}$$

$$\psi_i = \left(\frac{h}{12}\right)^3 [N]^3\{\psi_i'''\} + \left(\frac{L}{2} - \frac{z^2}{2L}\right)\left(\frac{h}{12}\right)^2\left[N_n^{(2)}\right]\{\psi_i'''\} - \left(\frac{h}{12}\right)^3\left[N_n^{(3)}\right]\{\psi_i'''\} \tag{B9}$$

The solutions for $u'(0)$, $u(L)$, are given as:

$$u'(0) = -\left(\frac{h}{12}\right)^3 \frac{1}{L}\left[N_n^{(3)}\right]\{u_i'''\} \tag{B10}$$

$$u'(L) = \left(\frac{h}{12}\right)^2\left[N_n^{(2)}\right]\{u_i'''\} - \left(\frac{h}{12}\right)^3 \frac{1}{L}\left[N_n^{(3)}\right]\{u_i'''\} \tag{B11}$$

The equations for terms $v'(0)$, *and* $v'(L)$ are similar in nature with $u'(0)$, *and* $u'(L)$.

The solutions for $\psi(L)$ and $\psi'(L)$ are expressed as below:

$$\psi(L) = -\left(\frac{h}{12}\right)^3\left[N_n^{(3)}\right]\{\psi_i'''\} \tag{B12}$$

$$\psi'(L) = \left(\frac{h}{12}\right)^2 [N]^2\{\psi_i'''\} - \left(\frac{h}{12}\right)^2\left[N_n^{(2)}\right]\{\psi_i'''\} \tag{B13}$$

in which, $[N_n^{(2)}]$ is the last row of the matrix product $[N]^2$, and $\left[N_n^{(3)}\right]$is the last row of the matrix product$[N]^3$.

APPENDIX C: N-Matrix Expressions

The N matrix is defined as follows:

$$[N_1] = \frac{h}{12}[N] \tag{C1}$$

$$[N_2] = \left(\frac{h}{12}\right)^2 [N]^2 - \left(\frac{h}{12}\right)^3 \frac{1}{L}\left[N_n^{(3)}\right] \tag{C2}$$

$$[N_3] = \left(\frac{h}{12}\right)^3 [N]^3 - \left(\frac{h}{12}\right)^3 \frac{1}{L}\{z\}\left[N_n^{(3)}\right] \tag{C3}$$

$$[N_4] = \frac{h}{12}[N] - \left(\frac{h}{12}\right)^2 \frac{1}{L}\left[N_n^{(2)}\right] \tag{C4}$$

$$[N_5] = \left(\frac{h}{12}\right)^2 [N]^2 - \left(\frac{h}{12}\right)^2 \frac{1}{L}\{z\}\left[N_n^{(2)}\right] \tag{C5}$$

$$[N_6] = \left(\frac{h}{12}\right)^3 [N]^3 - \left(\frac{h}{12}\right)^3 \left[N_n^{(3)}\right] \tag{C6}$$

$$[N_7] = \left(\frac{L}{2} - \frac{z^2}{2L}\right)\left(\frac{h}{12}\right)^2 \left[N_n^{(2)}\right] \tag{C7}$$

$$[N_8] = -\left(\frac{h}{12}\right)^3 \frac{1}{L}\left[N_n^{(3)}\right] \tag{C8}$$

$$[N_9] = \left(\frac{h}{12}\right)^2 \left[N_n^{(2)}\right] - \left(\frac{h}{12}\right)^3 \frac{1}{L}\left[N_n^{(3)}\right] \tag{C9}$$

APPENDIX D: Computer Program

```
%August 05 2015

clear; clc;

% Input Data: Enter these values; Areas in inch^2 and stresses in ksi.
A        = 1.5;                                    %Width in inches,
along xP. (P is for prime.)
B        = 1.5;                                    %Depth in inches,
along yP.
tf       = 0.125;                                     %Flange thickness
in inches.
tw       = 0.125;                                     %Web thickness in
inches.
NA       = 228;                                    %Number of layers
along width, along xP.
NB       = 228;                                    %Number of layers
along Depth, along yP.
v1       = 0;                                     %Distance of the
outer edge of vertical plate from left side. Limit for v1 = 0 to B/2-
tw.
v2       = 0;                                     %Distance of the
outer edge of vertical plate from right side. limit for v2 = 0 to B/2-
tw.
L        = 34;                                    %Length (in).
E        = 29599;                                 % Modulus of
elasticity (ksi.)
G        = 11200;                                  % Shear molulus of
elasticity
sigma    = 59;                                    % Normal yield stress
(ksi).
sigma1   = 30;                                    % Shear yield stress
(ksi).
kB1x      = 0;                                    % Spring stiffness
constant (k-in/rad) at end B about x-axis (nearly pinned condition).
kB1y      = 0;                                    % Spring stiffness
constant (k-in/rad) at end B about y-axis (nearly pinned condition.
kB2x     = 13000;                                 % Spring stiffness
constant (k-in/rad) at end B about x-axis (partial restraint
condition).
kB2y     = 13000;                                 % Spring stiffness
constant (k-in/rad) at end B about y-axis (partial restraint
condition).
kB3x     = 24000;                                 % Spring stiffness
constant (k-in/rad) at end B about x-axis (partial restraint
condition).
kB3y     = 24000;                                 % Spring stiffness
constant (k-in/rad) at end B about y-axis (partial restraint
condition).
kB4x     = 10^10;                                 % Spring stiffness
constant (k-in/rad) at end B about x-axis (nearly fixed condition).
kB4y     = 10^10;                                 % Spring stiffness
constant (k-in/rad) at end B about y-axis (nearly fixed condition).
```

```
kT1x      = 0;                                          % Spring stiffness
constant (k-in/rad) at end T about x-axis (nearly pinned condition).
kT1y      = 0;                                          % Spring stiffness
constant (k-in/rad) at end T about y-axis (nearly pinned condition.
kT2x = kT2y    = 13000;                                      % Spring
stiffness constant (k-in/rad) at end T about x-axis (partial restraint
condition).
kT3x = kT3y    = 24000;                                      % Spring
stiffness constant (k-in/rad) at end T about x-axis (partial restraint
condition).
kT4x      = 10^10;                                      % Spring stiffness
constant (k-in/rad) at end T about x-axis (nearly fixed condition).
kT4y      = 10^10;                                      % Spring stiffness
constant (k-in/rad) at end T about y-axis (nearly fixed condition).
uoi       = L/1000;                                     % Initial crookdness,
uoi = voi.

N square matrix of size 9
%Input Loading Data:
%Input Loading Data: for tangent stiffness program.
NA        = 228;                                     %Number of layers along
flange width and web depth.
NB        = 228;                                      %Number of layers
along flange and web thickness.
iter      = 100;                                    %Max. No. of iterations
of while loop to match internal and external actions.
DeoA      = 0.00001;                                %Starting strains value;
Axial strain to calculate intial values of stiffness matrix.
del_P     = 0.5;                                    %Load increment for
axial load application.
del_Mx    = 0.1;                                     %Interval for external
Mx
del_My    = 0.1;                                     %Increment for
external My

%Calculated Inputs; Based on the values given above.
As2       = A*B-(A-2*tw)*(B-2*tf);                  %Area of section
calculated from dimensions given.
Sx = A*B^3/(6*B)-(A-2*tw)*(B-2*tf)^3/(6*d);     %Elastic section modulus
about x axis.
Sy = B*A^3/(6*A)-(B-2*tf)*(A-2*tw)^3/(6*b);     %Elastic section modulus
about y axis.
Zx = A*B^2/4-(A-2*tw)*(B-2*tf)^2/(4);           %Plastic section modulus
about x axis.
Zy = B*A^2/4-(B-2*tf)*(A-2*tw)^2/(4);           %Plastic section modulus
about y axis.
fy        = sqrt((fym)^2-3*(tauy^2));           %Yeild strength.
ey        = fy/Es;                              %Yield strain.
Py        = fy*As2;                             %Axial yield load. Used
for normalizing P.
Mpy       = Zy*fy;                              %Plastic My. Used for
normalizing My.
Mpx       = Zx*fy;                              %Plastic Mx. Used for
normalizing Mx.
Mpz       = tauy*2*tf*AE;                                %Plastic Mx. Used
for normalizing Mx.
```

```
delAs1  = (b*tf)/(NA*NB);                    %Elemental area in top
flange.
delAs2  = (b*tf)/(NA*NB);                    %Elemental area in
bottom flange.
delAs3  = ((D-2*tf)*tw)/(NA*NB);             %Elemental area in left
web.
delAs4  = ((D-2*tf)*tw)/(NA*NB);             %Elemental area in
right web.

for i = 1:NA;
        for j = 1:NB;


Bxxp1(i,j) = ( (a11p1(i,j))*a22p1(i,j) -
a12p1(i,j)*a21p1(i,j) )/a11p1(i,j);
Bxyp1(i,j) = ( (a11p1(i,j))*a23p1(i,j) -
a21p1(i,j)*a13p1(i,j) )/a11p1(i,j);
Bxwp1(i,j) = ( (a11p1(i,j))*a24p1(i,j) -
a21p1(i,j)*a14p1(i,j) )/a11p1(i,j);
Byxp1(i,j) = ( (a11p1(i,j))*a32p1(i,j) -
a12p1(i,j)*a31p1(i,j) )/a11p1(i,j);
Byyp1(i,j) = ( (a11p1(i,j))*a33p1(i,j) -
a13p1(i,j)*a31p1(i,j) )/a11p1(i,j);
Bywp1(i,j) = ( (a11p1(i,j))*a34p1(i,j) -
a14p1(i,j)*a31p1(i,j) )/a11p1(i,j);


        end

end


% Calculate a's for each element based on the strain in the
element.Plate II

a11p2  = E*Ae2;
a12p2  = E*Sxe2;      a21p2 = a12p2;
a13p2  = E*Sye2;      a31p2 = a13p2;
a22p2    = E*Ixe2;
a23p2    = zeros(ND,NB);
a24p2    = zeros(ND,NB);
a32p2    = zeros(ND,NB);
a33p2    = E*Iye2;
a34p2    = zeros(ND,NB);
a14p2    = zeros(ND,NB);


for i = 1:NB;
        for j = 1:NA;


Bxxp2(i,j) = ( (a11p2(i,j))*a22p2(i,j) -
a12p2(i,j)*a21p2(i,j) )/a11p2(i,j);
```

```
Bxyp2(i,j) = ( (a11p2(i,j))*a23p2(i,j) -
a21p2(i,j)*a13p2(i,j) )/a11p2(i,j);
Bxwp2(i,j) = ( (a11p2(i,j))*a24p2(i,j) -
a21p2(i,j)*a14p2(i,j) )/a11p2(i,j);
Byxp2(i,j) = ( (a11p2(i,j))*a32p2(i,j) -
a12p2(i,j)*a31p2(i,j) )/a11p2(i,j);
Byyp2(i,j) = ( (a11p2(i,j))*a33p2(i,j) -
a13p2(i,j)*a31p2(i,j) )/a11p2(i,j);
Bywp2(i,j) = ( (a11p2(i,j))*a34p2(i,j) -
a14p2(i,j)*a31p2(i,j) )/a11p2(i,j);

        end

end



% Calculate a's for each element based on the strain in the
element.Plate III

a11p3  = E*Ae3;
a12p3  = E*Sxe3;      a21p3 = a12p3;
a13p3  = E*Sye3;      a31p3 = a13p3;
a22p3    = E*Ixe3;
a23p3    = zeros(NB,ND);
a24p3    = zeros(NB,ND);
a32p3    = zeros(NB,ND);
a33p3    = E*Iye3;
a34p3    = zeros(NB,ND);
a14p3    = zeros(NB,ND);


for i = 1:NA;
        for j = 1:NB;

Bxxp3(i,j) = ( (a11p3(i,j))*a22p3(i,j) -
a12p3(i,j)*a21p3(i,j) )/a11p3(i,j);
Bxyp3(i,j) = ( (a11p3(i,j))*a23p3(i,j) -
a21p3(i,j)*a13p3(i,j) )/a11p3(i,j);
Bxwp3(i,j) = ( (a11p3(i,j))*a24p3(i,j) -
a21p3(i,j)*a14p3(i,j) )/a11p3(i,j);
Byxp3(i,j) = ( (a11p3(i,j))*a32p3(i,j) -
a12p3(i,j)*a31p3(i,j) )/a11p3(i,j);
Byyp3(i,j) = ( (a11p3(i,j))*a33p3(i,j) -
a13p3(i,j)*a31p3(i,j) )/a11p3(i,j);
Bywp3(i,j) = ( (a11p3(i,j))*a34p3(i,j) -
a14p3(i,j)*a31p3(i,j) )/a11p3(i,j);

        end

end
```

```
% Calculate a's for each element based on the strain in the
element.Plate
% IV


a11p4  = E*Ae4;
a12p4  = E*Sxe4;      a21p4 = a12p4;
a13p4  = E*Sye4;      a31p4 = a13p4;
a22p4    = E*Ixe4;
a23p4    = zeros(ND,NB);
a24p4    = zeros(ND,NB);
a32p4    = zeros(ND,NB);
a33p4    = E*Iye4;
a34p4    = zeros(ND,NB);
a14p4    = zeros(ND,NB);

for i = 1:ND;
        for j = 1:NB;

Bxxp4(i,j) = ( (a11p4(i,j))*a22p4(i,j) -
a12p4(i,j)*a21p4(i,j) )/a11p4(i,j);
Bxyp4(i,j) = ( (a11p4(i,j))*a23p4(i,j) -
a21p4(i,j)*a13p4(i,j) )/a11p4(i,j);
Bxwp4(i,j) = ( (a11p4(i,j))*a24p4(i,j) -
a21p4(i,j)*a14p4(i,j) )/a11p4(i,j);
Byxp4(i,j) = ( (a11p4(i,j))*a32p4(i,j) -
a12p4(i,j)*a31p4(i,j) )/a11p4(i,j);
Byyp4(i,j) = ( (a11p4(i,j))*a33p4(i,j) -
a13p4(i,j)*a31p4(i,j) )/a11p4(i,j);
Bywp4(i,j) = ( (a11p4(i,j))*a34p4(i,j) -
a14p4(i,j)*a31p4(i,j) )/a11p4(i,j);

        end

end


a21P1 = sum(sum(a21p1));
a21P2 = sum(sum(a21p2));
a21P3 = sum(sum(a21p3));
a21P4 = sum(sum(a21p4));
a21P  = a21P1+a21P2+a21P3+a21P4;
a21 = a21P;

a31P1 = sum(sum(a31p1));
a31P2 = sum(sum(a31p2));
a31P3 = sum(sum(a31p3));
a31P4 = sum(sum(a31p4));
a31P  = a31P1+a31P2+a31P3+a31P4;
a31 = a31P;

BxxP1 = sum(sum(Bxxp1));
BxxP2 = sum(sum(Bxxp2));
BxxP3 = sum(sum(Bxxp3));
BxxP4 = sum(sum(Bxxp4));
```

```
BxxP  = BxxP1+BxxP2+BxxP3+BxxP4;
Bxx = ones(9,9);
Bxx = BxxP*Bxx;

BxyP1 = sum(sum(Bxyp1));
BxyP2 = sum(sum(Bxyp2));
BxyP3 = sum(sum(Bxyp3));
BxyP4 = sum(sum(Bxyp4));
BxyP  = BxyP1+BxyP2+BxyP3+BxyP4;
Bxy = ones(9,9);
Bxy = BxyP*Bxy;


ByyP1 = sum(sum(Byyp1));
ByyP2 = sum(sum(Byyp2));
ByyP3 = sum(sum(Byyp3));
ByyP4 = sum(sum(Byyp4));
ByyP  = ByyP1+ByyP2+ByyP3+ByyP4;
Byy = ones(9,9);
Byy = ByyP;

ByxP1 = sum(sum(Byxp1));
ByxP2 = sum(sum(Byxp2));
ByxP3 = sum(sum(Byxp3));
ByxP4 = sum(sum(Byxp4));
ByxP  = ByxP1+ByxP2+ByxP3+ByxP4;
Byx = ones(9,9);
Byx = ByxP*Byx;



% Finite Integral Matrice calculation.

N_1          = N^1;                                  % N_1= = N^1 = N.
N_2          = N^2;                                  % N_2= = N^2 = N*N.
Nn1          = repmat (N_1(9,:),9,1);                % Nn2=[Nn]^2 =  make
a 9x9 matrix with last row of N2.
Nn2          = repmat (N_2(9,:),9,1);                % Nn3=[Nn]^2 =  make
a 9x9 matrix with last row of N3.
h            = L/8;                                  % h is the interval.
z            = 0:h:L;

for k = 1:length(z);
    Nn1z(k,:)  = Nn1(k,:)*z(k);                      %
Nn2z(k,:)={z}/L[Nn]^2.
end

for k = 1:length(z);
    Nn2z(k,:)  = Nn2(k,:)*z(k);
end

N1           = h/12*N-(h/12)^2*(1/L)*Nn2;
N2           = (h/12)^2*N^2-(h/12)^2*(1/L)*Nn2z;
```

```
N3          = -(h/12)^2*(1/L)*Nn2;
N4          = (h/12)*Nn1-(h/12)^2*(1/L)*Nn2;

  for n = 1:length(P)
    for k = 1: length(z)
    q1(k,:) =   N4(k,:)*kT1x*(z(k)/L)';
    end
    Q1(:,:,n) = Bxx+A*P(1,n)*N2+q1*A;
end

for k = 1:length(T)
    Q2(:,:,k) = Bxy-A*T(1,k)*N1;
end


for n = 1:length(My)
for k = 1: length(z) %length(My)
    NN3 = N4;
    q3(k,:) =   NN3(k,:)*(z(k)/L)';    %Nine Q3's matrices. My(1,k)*
end
Q3(:,:,n) = A*My(1,n)*q3*N6 - A*P(1,n)*xo*N6;
end



for k = 1:length(T)
    Q4(:,:,k) = Byx+A*T(1,k)*N1;
end

for n = 1:length(P)
     for k = 1: length(z)
    q5(k,:) =   N4(k,:)*kT1y*(z(k)/L)';
    end
    Q5(:,:,n) = Byy+A*P(1,n)*N2+A*q5;
end


for n = 1:length(Mx)
    for k = 1: length(z)
    NN6 = N4;
    q6(k,:) =   NN6(k,:)*(z(k)/L)';
end
    Q6(:,:,n) = A*q6*Mx(1,n)*N6+ A*P(1,n)*xo*N6;
end

for n = 1:length(My)
     for k = 1: length(z)
    q7(k,:) = N1(k,:)*(z(k)/L)';
    end
    Q7(:,:,n) = q7*My(1,n)-N1*P(1,n)*xo-N2/L*My(1,n);
end

for n = 1:length(Mx)
     for k = 1: length(z)
```

```
    q8(k,:) = N1(k,:)*(z(k)/L)';
    end
    Q8(:,:,n) = q8*Mx(1,n)+N1*P(1,n)*yo-N2/L*Mx(1,n);
end

 Q9(:,:,n) = Cw-N5*Ct;

for n = 1:length(Mx)
    for k = 1:length(z)
        fex1(k,:) =-(z(k)/L)';
end
    Fex1(:,:,n) = -A*P(1,n)*uoi-A*Mx(1,n)*fex1-Sx*P(1,n);
end

for n = 1:length(My)
    for k = 1:length(z)
        fex2(k,:) =(z(k)/L)';
end
    Fex2(:,:,n) =-A*P(1,n)*uoi+A*My(1,n)*fex1-Sx*P(1,n);
end

for n = 1:length(T)
    for m = 1:length(z)
       fah(m,1) = T(n);
    end
    Fex3(:,:,n) = -fah;

Q = [Q1 Q2 Q3; Q4 Q5 Q6; Q7 Q8 Q9];
F = [Fex1; Fex2; Fex3];

delta(:,:,n)  = Q(:,:,n)\F(:,:,n) ;
% delta1 = delta(1:8,:);                          % delta 1 = v'''.
delta1 = delta(1:9,:);                            % delta 1 = v'''.
% delta2 = delta(9:16,:);                         % delta 1 = u'''.
delta2 = delta(10:18,:);                          % delta 1 = u'''.
% delta3 = delta(17:24,:);                        % delta 1 = phi''' or
triple prime of angle of twist.
delta3 = delta(19:27,:);                          % delta 1 = phi''' or
triple prime of angle of twist.

v1   = N1*delta1;                                 %v1   = v' .
u1   = N1*delta2;                                 %u1   = u' .
phi1 = N1*delta3;                                 %phi1 = phi' .

v   = N2*delta1;                                 %v   = v .
u   = N2*delta2;                                 %u  = u .
phi = N2*delta3;                                 %ph = phi .

% v   = N3*delta1;                                 %v   = v .
% u   = N3*delta2;                                 %u   = u .
% phi = (N6+N6)*delta3;                            %phi = phi .
end
```